Glass Unlocked

Designing an Additively Manufactured
Reversible Interlayer Connection
for Structural Use of Free-Form Glass Units

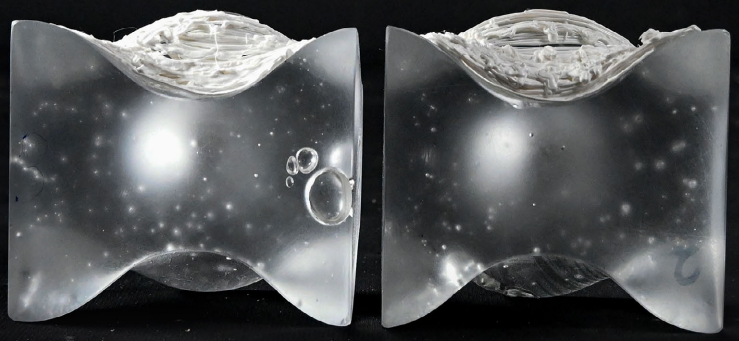

TU Delft

Glass Unlocked

Designing an Additively Manufactured Reversible Interlayer Connection for Structural Use of Free-Form Glass Units

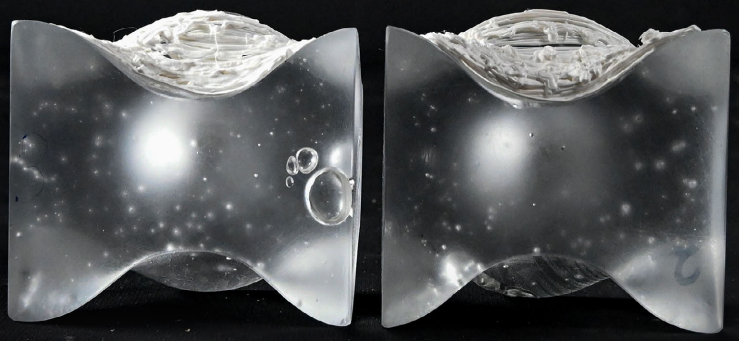

Eloy Constantijn van Kessel
4871073

Master of Science
Building Technology

Faculty: Architecture and the Built Environment

Project duration:
Nov 2024 – Jun 2025

First supervisor:
Dr. ir. Faidra Oikonomopoulou

Second supervisor:
Dr. Serdar Aşut

External delegate:
Ir. Henri van Bennekom

TU Delft

Acknowledgments

First of all, a big thank you to Dr. ir. **Faidra Oikonomopoulou**. Thank you for guiding me with a lot of enthusiasm throughout this thesis and coming up with so many ideas each time we spoke. The cast and 3d printed glass resources I was able to use really made my process a lot more fun and interesting. It was a pleasure working with you on this project!

Next, thank you to dr. **Serdar Aşut** for guiding me throughout this thesis and for setting me on the course of printing with the UR5 robot. Your feedback gave me a lot to think about in terms of robotic fabrication and practicalities.

A special thank you to 'DOTX system controls' and in particalur **Jelle Kalsbeek** who provided me with a lot of his time to discuss and come up with the robotic workflow discussed in this thesis. Not only this, but thank you very much for sponsoring the '5 axis slicer' needed to make this project successful. Your help has been very valuable for this thesis research.

Thank you to the MIT team, with whom we had bi-weekly meetings where I could show the progress I made. A special thank you to **Kaitlyn Becker** for your extensive expertise in the manufacturing of numerous materials. Your feedback has been very important for my learning curve. Another great thank you to **Daniel Massimino**, whose work has been partly the starting point of this thesis. The knowledge in structural glass and your way of conveying this knowledge has been great to see and learn from.

A big thanks to **Navid Vafa** who helped me set up the shear tests at Civil Engineering as well as making the results comprehensible.

Thank you to Ir. Arch. **Paul de Ruiter** for your many feedback on 3D printing and guidance. Furthermore, thank you for allowing me to use all of the equipment in the LAMA lab.

Henry Kiksen helped me with soldering the electrical wires needed to robotically print, thank you for this! Furthermore, thank you for fixing the many problems I encountered with the 3D printers and extruders...

Thank you to **Veronika Laszlo** for the enthusiasm and reassurance you brought at several stages in this thesis when things did not go to plan. Also, thank you for helping with resources needed to make the robot arm work.

Thanks to **Hans van Ginhoven** I had the opportunity to waterjet cut specimens needed for the research. I also thank you for the interest in the project and the fast responses I got when I asked you for something.

Thank you to **Wilfried Damen** for keeping an eye out when Faidra was unavailable so the shear tests could continue. I also thank you for the

feedback you gave me on the proposed test set-up and the help (and pictures) you offered during testing.

Thank you Mrs. ir. **Telesilla Bristogianni** for checking in with the proposed test set-up and for the numerous meetings we had with MIT where you gave your valuable feedback on the project.

Concluding, thank you to **Valérie Hayez** who made time to meet several times in the early stages to discuss the numerous possibilities in silicone available with an open mind.

This master thesis marks the end of a long period of studying at the TU Delft, I would like to thank all of the people who supported me throughout this period. Of course, my fellow students and friends who studied next to me through the years, who I had a lot of fun with and who I have been able to learn a lot from. Furthermore, thank you to all the people who I did not mention who have been a support in this long but fruitful period. Lastly, special thanks to my family for providing me with endless support and trust. Now, I hope you enjoy reading this thesis!

Abstract

To achieve true circularity, load-bearing glass structures need joinery systems that not only meet structural and aesthetic performance criteria but also support disassembly and recycling.

An iterative design approach was employed, starting with a comprehensive literature review of structural glass connections and proceeds through hands-on material trials. In adhesion experiments, polymers commonly used in Additive Manufacturing (AM) were evaluated for their warping, manufacturability and bond strength on glass substrates. Building on these insights, an iterative geometry optimisation phase refined a snap-fit interlocking design. This design was then mechanically tested and validated through a case study and prototype.

Key findings include the selection of PLA as a pragmatic interlayer material, balancing printability, minimal thermal warping, and sufficient stiffness, despite its low glass transition temperature (60 °C) and biodegradability. The resulting elastic averaging interlock is manufacturable (1 mm nozzle), resists thermal distortion, and self-aligns under preload. Mechanical validation of this interlock involved custom shear and compression tests, which demonstrated peak force transmission between F_{shear} = 1.77 kN and 6.13 kN under a starting preload of F_{normal} = 500 N. These forces correspond to effective friction coefficients of approximately mu = 1.060, exceeding typical friction values specified in Eurocode. An architectural case study of a compressive-only glass vault confirmed that service-level compressive stresses and wind-induced lateral loads remain within safe limits while allowing damage-free disassembly.

A robotic, non-planar AM workflow was developed to create a 1:2 interlayer prototype on osteomorphic shaped cast glass bricks. Using a 5-axis slicer and a UR5 robotic arm in combination with a custom extrusion end-effector and an Arduino microcontroller, the designed interlayers were AM but leave room for optimisation. This prototype showcased the adaptability of the approach to custom and complex geometries. Finally, heat-softening of the PLA interlayers enables clean separation and full material recovery, supporting a truly circular lifecycle for both glass and polymer components.

This proof-of-concept paves the way for scalable production of polymer interlayers for structural glass applications. It demonstrates that AM can play an important role in enabling reversible, high-performance structural glass assemblies, bringing circular construction one step closer.

Contents

1 Introduction

1.1 Background

Glass is and has long been an integral part of architecture and construction, primarily valued for its transparency and widely used in flat, two-dimensional applications such as windows, façades, and partitions. While its aesthetic and functional qualities have made glass omnipresent in the built environment, its production and end-of-life treatment pose significant sustainability challenges. Currently, the glass industry contributes approximately 95 million tonnes of CO2 emissions annually to the construction sector (Madhumitha Jaganmohan, 2024). Mostly driven by high-temperature processing and a lack of effective recycling strategies, especially in the architectural domain.

Although glass is theoretically 100% recyclable without quality loss, in practice, much of it is either downcycled or discarded (Oikonomopoulou, DeBrincat, & Fuhrmann, 2023). Most of what actually is recycled in a close-loop is exclusively internal and pre-consumer (e.g. offcuts and rejects during production). A major obstacle lies in how glass is used: traditional assemblies often involve permanent adhesives or laminates, which contaminate the material and prevent reuse. This is also problematic in the growing field of structural glass, where custom geometries and advanced manufacturing methods like casting and additive manufacturing (AM) are emerging as powerful techniques.

These new fabrication techniques offer more than just aesthetic flexibility; they also present an opportunity for circularity. Glass units made through casting or AM can, in theory, be shaped for easy disassembly and reuse. Furthermore, using these techniques, discarded glass, which would otherwise be sent to landfills, can be recycled into highly functional load bearing units (Stern, Townsend, Massimino, & Becker, 2024). However, the lack of reversible connection systems makes this potential difficult to realise in practice. The industry currently relies on adhesive-based connections that complicate disassembly and contaminate the glass, making recycling and reuse of the glass components nearly impossible.

To close the gap between design potential and the current state of joinery systems, there is a clear need for a system that enables both structural integrity and reversibility. This thesis addresses that need by focusing on the development of a reversible, 3D-printed or injection-moulded interlayer that allows glass components to be securely connected and easily disassembled without adhesives.

1.2 Problem Statement

1.2.1 Main Problem Statement

Current applications of cast glass in load-bearing glass structures often rely on bonded interfaces, which hinder reversibility and recyclability. The integration of free-form glass bricks into reversible structural assemblies requires a tailored approach that considers both geometry and mechanical interlock precision. Without such systems, the potential of cast glass as a sustainable structural material remains underused.

Sub-problems

1. Existing adhesive-based connections free-form glass structures contaminate glass, making recycling and reusing difficult.
2. Dry-stacked glass systems often lack the necessary structural integrity for complex geometries.
3. There is limited research into reversible, 3D-printed or injection-moulded interlayers for structural glass applications..

1.2.2 General objective

This research aims to develop a novel, reversible interlayer connection system tailored to the structural use of free-form cast glass units. The objective is to design, prototype, and evaluate a connection strategy that enables the assembly and disassembly of free-form glass geometries without the use of permanent adhesives or intrusive mechanical connectors. The approach uses a digital fabrication techniques, including additive manufacturing and parametric modeling, to create a system that aligns with the principles of circularity, precision, and aesthetics.

The intended outcome is a proof-of-concept system that not only meets the mechanical requirements for structural performance, but also facilitates reuse, modularity, and design flexibility. Through experimental validation and design iteration, the research contributes to the broader field of circular structural glass applications and offers a scalable model for future architectural implementations.

Sub-objectives

1. Identify materials suitable for reversible interlayers that are compatible with glass and suitable for additive manufacturing or injection moulding.
2. Develop interlayer geometries that provide both stability and disassembly.
3. Optimise the interface between the glass and the interlayer for strength and reversibility.
4. Test and evaluate the performance of the proposed interlayer system in terms of load-bearing capacity, ease of assembly/disassembly, and recyclability.

1.2.3 Final Products:

To design and test a prototype of a compressive-only, free-form glass structure (using either cast or AM glass components) that is self-supporting and demountable. Central to this is the development of a 3D-printed or injection moulded interlayer that locks the glass units together without permanent adhesives. This prototype would showcase the feasibility of the concept and its relevance for circular construction.

1.2.4 Boundary conditions

Material constraints

- The material must be suitable for AM or injection moulding

- The material must adhere to or interlock with glass without compromising recyclability
- The material must maintain structural integrity under normal environmental conditions (temperature, humidity, UV exposure) for several years.

Performance requirements

- The assembly system must provide sufficient structural strength for architectural applications.
- The connections must allow for easy disassembly without damaging the glass blocks.
- The system should maintain its performance for the intended lifespan of the structure (likely several decades).

Manufacturing and assembly

- The fabrication process must align with current additive manufacturing practices.
- The design should accommodate custom geometries and modular flexibility.

1.3 Research Questions

1.3.1 Main research question

How can an additive manufactured or injection-moulded interlayer be designed to create reversible connections between free-form glass components while maintaining structural integrity?

Sub-questions

1. Which materials are suitable for additive manufactured or injection-moulded interlayers in glass structures?
2. How can the geometry of the interlayer and glass units be optimised for both strength and disassembly?
3. What interface strategies between glass and interlayer ensure performance and reversibility?
4. How does the proposed system compare to existing methods in terms of mechanical behaviour?

2
Methodology and Approach

2.1 Research Design

An iterative research design approach is adopted that combines a literature review, computational design, experimental testing, and prototyping to investigate and validate a reversible interlayer system.

The research begins with a comprehensive literature review to establish the current state of knowledge. This contains a review of existing joinery systems in modular (glass) structures, joinery strategies in reversible design, and an investigation into material candidates for AM and injection moulding. Apart from materials, the last part will focus on surface treatment, interlocking geometries, and debonding mechanisms.

Informed by the literature study, two interlayer connection concepts are developed. Option 1, the Dry-Click, is evaluated against Option 2, the Direct-Print: an interlock using a robotic arm on to print on non-planar glass surfaces. Digital design tools are then employed to create and iterate interlayer geometries. Next, experimental testing of the chosen AM polymers is conducted to evaluate print quality, warping behaviour, and glass adhesion. Mechanical shear tests are performed to assess the strength, failure modes, and reliability of the interface.

The fabrication method of the proposed interlayer is discussed and validated in an architectural context through a case study. This case study will draw inspiration from the Glass Vault (see Figure 2.1). This project will serve as a basis and a similar looking compressive-only glass vault using the novel interlayer system will be designed. The final phase involves robotic fabrication of the interlayer on real glass bricks using a UR5 robotic arm, integrated via a custom robotic workflow. This prototype shows the feasibility of the concept of this master thesis.

Throughout the research, emphasis will be placed on the circular potential of the proposed system, including material recyclability, ease of disassembly, and potential for component reuse. The iterative loop between digital modelling, physical testing, and prototyping ensures that both theoretical performance and practical feasibility are evaluated.

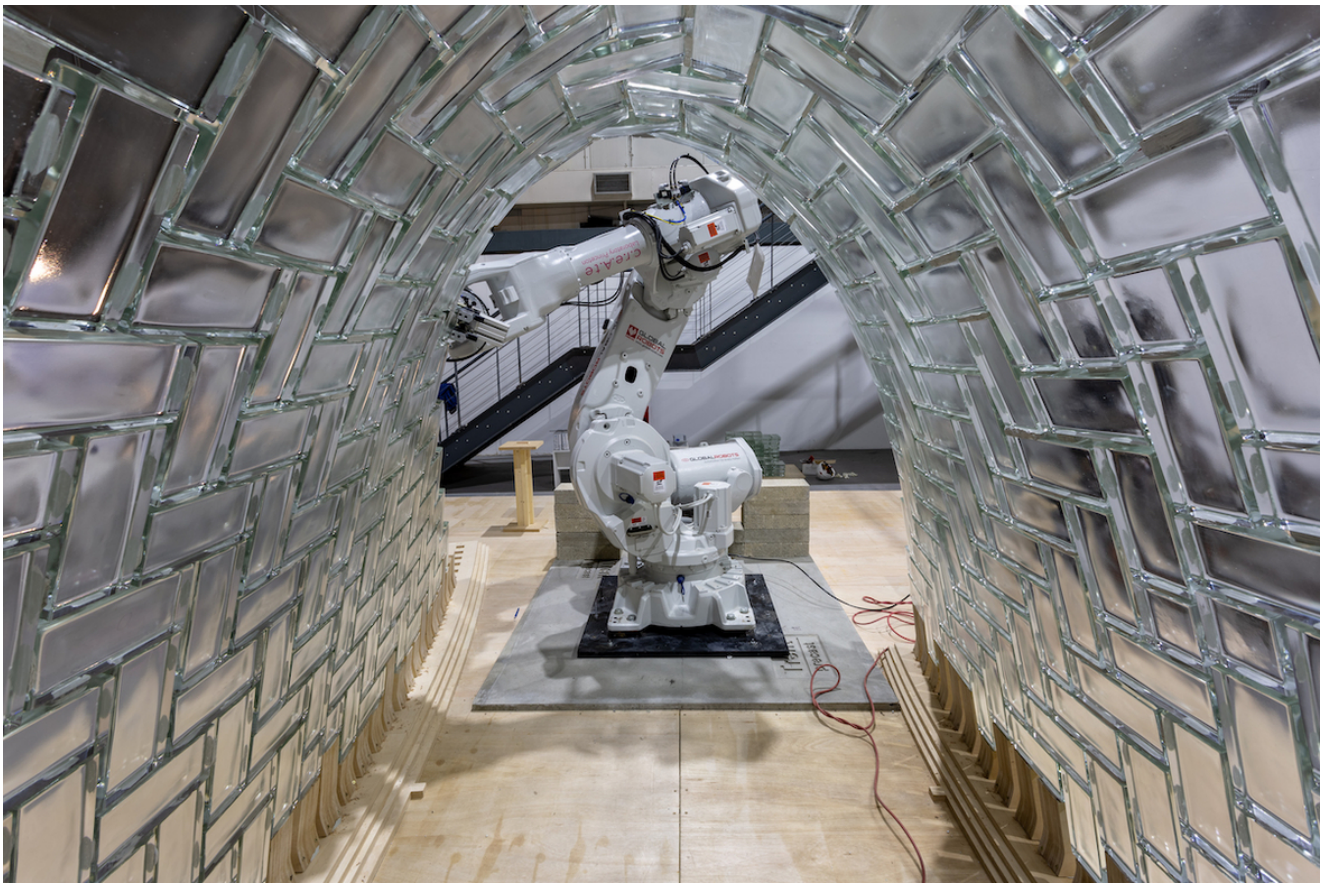

Figure 2.1: the Glass Vault case study, image by Maciej Grzeskowiak

2.2 Relevance

This project addresses critical challenges in sustainable architecture and circular construction practices. The glass industry currently contributes approximately 95 million tonnes of CO_2 emissions annually (Madhumitha Jaganmohan, 2024). Despite the theoretical recyclability of glass being 100% without degradation in quality, actual recycling rates remain limited due to contamination and irreversible bonding methods. This work aims to reduce environmental impact by enabling the reuse and recycling of glass components. The development of a reversible, structural interlayer system for structural glass assemblies responds to this disconnect between theoretical recyclability and practical implementation. By focusing on additive manufacturing (AM) techniques, this study investigates how these interlayers can enable the reuse and recycling of glass elements without compromising architectural freedom.

Professionally, this research bridges the gap between advanced manufacturing technologies and traditional construction methods. It provides architects and engineers with novel approaches to design adaptable and recyclable glass structures, potentially leading to more efficient and cost-effective building practices in the long term. An AM interlayer capable of forming dry, mechanical connections opens new opportunities for bespoke and reversible glass structures.

From a scientific perspective, the thesis contributes to several underexplored domains: the mechanical behaviour of AM polymer interfaces with glass; the integration of reversible designing into structural assemblies; and the (lack of) standardisation and performance data in the emerging field of 3D-printed and cast glass structures. Currently, the lack of performance data and design guidelines hinders the scalability of these innovations. By delivering experimentally validated prototypes and quantifying performance characteristics such as shear strength and ease of disassembly, this study supports the long-term objective of integrating these novel

techniques into mainstream construction practice.

This research aligns with broader societal and environmental imperatives to transition to a climate-neutral construction. Ultimately, the objective is to bring the glass industry one small step closer to this agreed upon goal.

3
Literature Study

3.1 Potential of Freeform AM and cast glass structures in architecture

3.1.1 Introduction

Glass has been a crucial element in architecture for a very long time, mainly due to its transparency and versatility. However, currently the glass industry faces significant environmental challenges, contributing approximately 95 million tonnes of CO2 emissions annually to the construction sector (Madhumitha Jaganmohan, 2024). In theory, glass is 100% recyclable, endlessly, and without loss of quality or purity. In reality, only a small percentage of glass is recycled. This is most common in the glass container industry; for example, in the US 31,8% of glass food and beverage packaging was recycled in 2018, with some states like California reaching 80% (GPI, n.d.). Recycling rates in Europe are at a much higher rate already, with the EU28 reaching an average glass container rate of 78% in 2019. The partnership 'Close the Glass Loop' aims to achieve a post-consumer glass container collection target of 90% by 2030, (close the glass loop, 2021). Other industries like automotive or architectural glass are either being downcycled or landfilled. Because of the specific wishes from the clients, once the glass enters the consumer market, the prospects of recycling become minimal (Oikonomopoulou, Ioannidis, Koniari, & Bristogianni, 2023). This is caused by multiple reasons, from contamination, optical requirements such as a foil, to difficulties in demountability. Despite these problems, efforts are being made to become a "net-zero" industry by 2050. In the recycling process, used glass is ground into cullet, which melts at a lower temperature and uses approximately 40 percent less energy than is required to make glass from raw materials. It also helps reduce the amount of solid waste that goes into landfill (Kamau, Stec, Tu, & Schlorke, 2021). Innovative recycling methods are being pursued; for example, studies are being done on crushed glass as a replacement for sand in concrete, supporting biodiversity by reducing the impact arising from sand extraction (Kamau et al., 2021). Other innovative fabrication methods such as additive manufacturing (AM) and glass casting are emerging as promising solutions to create free-form glass structures in architectural applications. Departing from traditional 2D float glass production, AM and casting techniques offer novel design flexibility and material efficiency. These methods enable the creation of complex geometries and customised shapes without the need for expensive tooling, reducing material waste and energy consumption (Stern et al., 2024). Due to the inherent high compressive strength of glass, typically between 800 and 1000 MPa, Saint Gobain Sekurit, n.d., glass can be used as load-bearing components. For example, a study by Massimino, Townsend, Folinus, Stern, and Becker (2024) shows how AM could create interlocking glass masonry units with optimised structural performance and minimal material use. Furthermore, these advanced fabrication methods offer the potential for circular construction practices. AM and cast glass components can be designed for easy disassembly and reuse, as well as recycled without performance degradation (Stern et al., 2024). By enabling the use of recycled glass in the production process, these techniques contribute to a more sustainable built environment and expand the possibilities for innovative and energy-efficient architectural designs. To get a better understanding of the potential of these manufacturing techniques, the following sub-chapters will delve deeper into the advantages, limitations, and applications of Additive Manufacturing and casting of glass.

3.1.2 Additive Manufactured Glass: Overview, Advantages, Limitations, and Applications

Overview

Additive Manufacturing (AM) of glass, enables design flexibility and allows for the creation of complex geometries that traditional methods could not achieve previously. It involves Fused Deposition modelling (FDM) of molten glass. FDM is a process where a molten material (in this case glass) is extruded layer-by-layer to create a three-dimensional object (see Figure 3.1). The development of glass AM has progressed through several iterations of specialised printers, each building upon the capabilities of its predecessor. The next sub-chapters will explain AM based on the development of these 3D printers, from G3DP1 to G3DP3.

G3DP1, developed in 2015 by MIT's Mediated Matter group, served as a proof of concept. It demonstrated the feasibility of creating optically transparent objects through layer-by-layer deposition of molten glass. The G3DP1 had a print volume of 250 x 250 x 300 mm, a reservoir size of 2.1 kg, and a flow rate of 2.2 kg/h.

Introduced in 2018, **G3DP2** was a significant advancement in glass AM technology. The G3DP2 system has a digitally integrated, three-zone thermal control system, in combination with a four-axis motion control system (Inamura, Stern, Lizardo, Houk, & Oxman, 2018). It enables large-scale production with improved speed and reliability, ensuring precision and consistency in glass products.

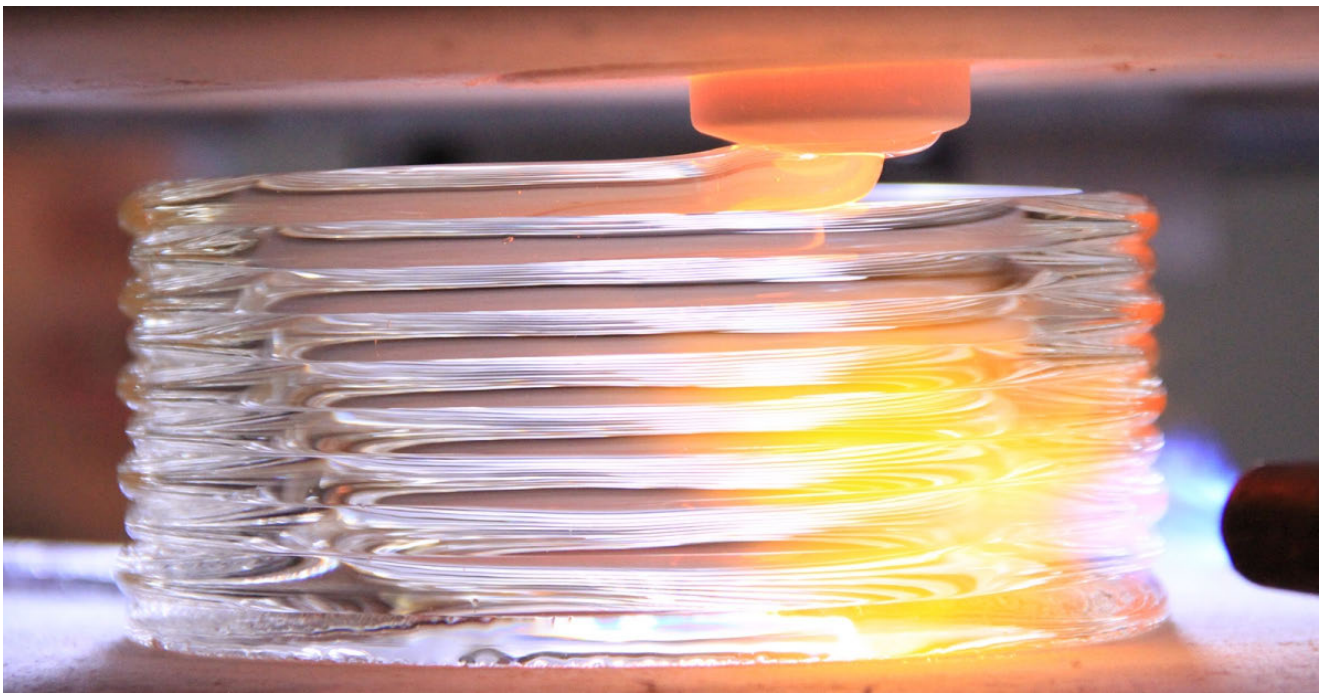

Figure 3.1: Fused Deposit Modelling of molten glass through nozzle, *Image credits: Markus Kayser*

The vertical thermal control module consists of the following three sub-systems: the Material Reservoir, the Nozzle Control, and the Build Chamber (see Figure 3.2). The Material Reservoir is a container made of alumina that holds and heats the molten soda lime glass to approximately 1090 °C. It acts as a kiln cartridge holding enough molten glass to print a single (architectural) component. The Nozzle Control is located just below the Material Reservoir and serves as an interface between the thermal and mechanical systems. It consists of an alumina nozzle and two-part thermal control mechanisms. The molten soda lime glass is funnelled through the nozzle into the last part (Figure 3.1), the 'Build Chamber': an electric kiln that operates at 480°C during printing, just below the annealing temperature of around 515 °C. This chamber provides

a controlled environment for the printed object, ensuring that the printed, cooling objects avoid thermal shock. This three-zone system allows for precise control over the glass temperature at each stage of the printing process, from melting to extrusion to annealing. This level of control is essential for maintaining consistent glass viscosity, ensuring print quality, and preventing defects caused by rapid temperature changes (Inamura et al., 2018). Another development in the G3DP2 is a four-axis motion control system, so apart from the X-, Y- and Z-axis, the printer involves an A-axis. Which is a precision rotary table providing rotational motion around the Z-axis This motion control system enables complex geometries and precise control over the orientation of the print nozzle relative to the print path. The G3DP2 had a print volume of 320 x 320 x 350 mm, a reservoir size of 25.5 kg, and a flow rate of 5.2 kg/h.

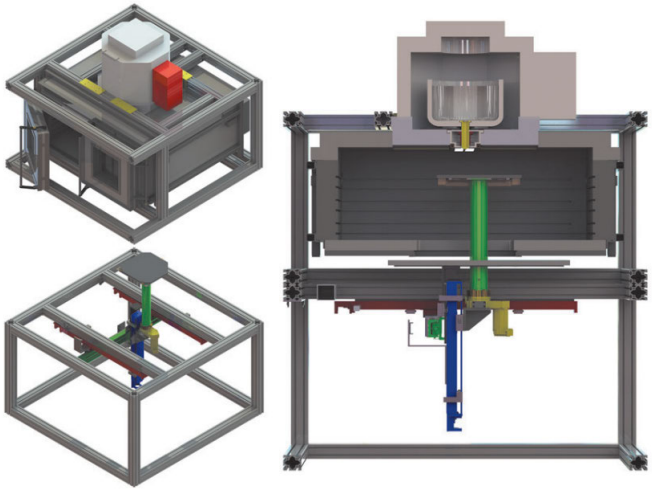

Figure 3.2: Left: exploded view of the upper thermal module and the lower motion control module. Right: a cross-section of the entire system that reveals the interior detail (Inamura et al., 2018)

Introduced in 2024, **G3DP3** is the latest advancement in this AM technology. Building upon its predecessor, G3DP3 incorporates several key improvements to enhance its capabilities for printing with recycled float and container glass (Stern et al., 2024). The system features infrared (IR) temperature monitoring for more precise temperature management during the printing process.

G3DP3 boasts an increased build volume of 325 x 325 x 380 mm, allowing for the production of larger glass objects. The printer's nozzle has been redesigned to accommodate higher temperature operations, with a maximum extrusion temperature of 1200°C, compared to G3DP2's 1100°C (Stern et al., 2024). This enhancement enables the printer to work with a broader range of glass formulations, including recycled float or container glass. The motion control system has been further refined, with improved tool pathing capabilities and prediction algorithms. This results in reduced variation among prints and enhanced overall print quality. Finally, G3DP3 offers a more flexible range of printing parameters, with bead heights ranging from 3.0 to 6.0 mm and widths from 9.0 to 16 mm, compared to the fixed dimensions of the G3DP2 (Stern et al., 2024).

Advantages

AM of glass offers excellent **recyclability**, which is a significant advantage in terms of sustainability. According to Oikonomopoulou, Ioannidis, et al. (2023), 3D-printed glass can be considered 100% recyclable. This is because unlike laminated or adhesively bonded glass components, which are difficult to recycle due to contamination from interlayers or adhesives, 3D-printed glass structures have an inherent connection achieved through melting and annealing. This means that it can easily be recycled by remelting the glass. A study by Stern et al. (2024) demonstrates the fact that AM of glass can use 100% recycled material even with various glass compositions. The researchers used recycled soda lime glass from two different waste streams: container

glass, referred to as Sapphire glass in the study and Optifloat float glass from Pilkington. Both types of recycled glass were successfully processed and printed by the G3DP3 printer. This study shows that the G3DP3 printer can be used to additively manufacture objects from various glass compositions, which possess a higher melting point and unique properties. It showcases the potential for upcycling post-consumer glass waste.

Through the use of **Topology Optimisation** (TO), glass components can be designed with maximum structural performance and minimal mass (Oikonomopoulou, Ioannidis, et al., 2023). This is done by utilising computational techniques to optimise material distribution in structures according to predefined objectives and constraints. The main aim is to improve structural performance while reducing material costs. TO is becoming increasingly important in construction, providing advanced methods for designing structures that are both strong and resource-efficient.

Lastly, AM offers significant **design flexibility**, particularly in creating components that support sustainability through Design for Disassembly (DfD). This flexibility allows for the production of complex geometries that can be easily dismantled and reused. According to Massimino et al. (2024), AM facilitates the creation of interlocking glass masonry units that eliminate the need for adhesives, which contaminate glass and hinder recyclability. The ability to customise each unit for specific structural loads without additional tooling costs further underscores the design flexibility of glass AM, making it a versatile solution for innovative architectural applications (Massimino et al., 2024).

Limitations

Standardisation of AM glass is hindered by **limited structural data** and understanding of its **anisotropic properties**. The layered structure results in different strengths along major and minor axes, according to Klein et al. (2015) strength differs by approximately 40% between these orientations. This is the level of anisotropy also monitored in plastic printed parts in other studies. This anisotropic behaviour in combination with poor layer adhesion can lead to delamination (Oikonomopoulou, Ioannidis, et al., 2023). Further experimental validation is required to obtain accurate engineering strength values and safety factors for AM glass components.

The current maximum printable area of the G3DP3 is limited to 325 x 325 x 380 mm with a flow rate of 5.2 kg/h and a maximum capacity of 30 kg of glass (Inamura et al., 2018). This **size constraint** is primarily due to the need for a controlled annealing chamber, which confines the glass object to the chamber's dimensions. Larger objects require segmentation and assembly, which can introduce additional challenges.
NPo or 00

Although AM glass itself is highly recyclable, the process may introduce **contamination** if adhesives are used to assemble larger structures. AM glass structures might require bonding of multiple printed segments, potentially compromising the recyclability of the final product if adhesives are used (Oikonomopoulou, Veer, Bristogianni, & Barou, 2019). This highlights the need for further research and development into a dry interlayer solution for AM glass.

Applications

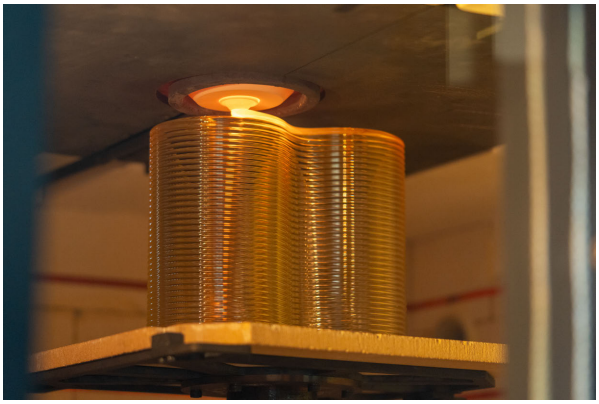

(a) AM of glass brick in G3DP3 printer

(b) AM glass structure by MIT

Figure 3.3: Interlocking AM glass masonry blocks by MIT (Massimino et al., 2024)

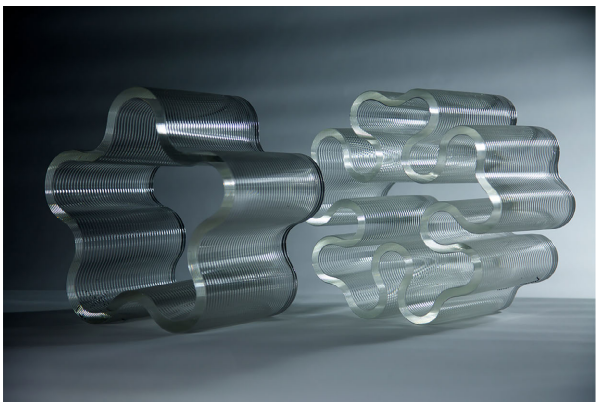

(a) AM glass column segment out of G3DP2 printer

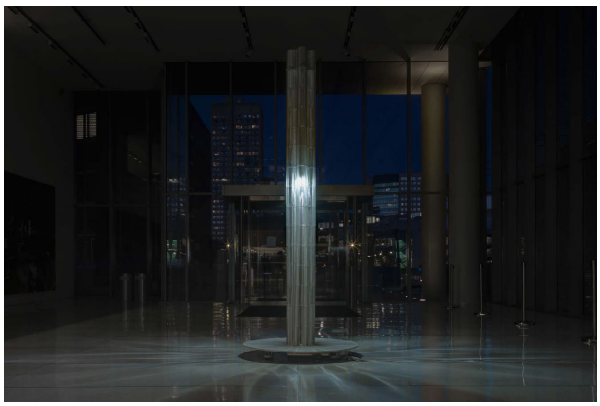

(b) AM glass column by MIT

Figure 3.4: AM glass column by MIT (Inamura et al., 2018)

Currently, AM of glass has not yet been applied in a lot of projects. This is because it is still in the research phase and is not yet commercially available. However, interesting research on this topic shows the potential of its application. The AM of the glass column by Inamura et al. (2018) is a solution which will be discussed in detail in Chapter 3.2.2. Another example of an additive-manufactured glass structure is the interlocking **glass masonry by Massimino et al. (2024)**, which is already briefly mentioned in the previous text. This research will be discussed in the following paragraphs.

The motivation of Massimino et al. (2024) to create interlocking masonry came from the brittleness of the material. Upon reaching the material's yield strength, fully glass structures can collapse without visual warning. Masonry however, provides a similar redundancy to this problem as laminating multiple panes; the failure of one component does not critically impact the whole structure. The remaining intact units will carry the loads from the failed unit. Glass masonry has already been implemented in projects where cast glass was used, for example in the Crystal Houses Facade (Oikonomopoulou, Bristogianni, Veer, & Nijsse, 2018). AM of interlocking glass masonry brings new advantages, like the ability to create various different geometries without extra and expensive tooling. Secondly, it could be used to create certain aesthetics only available with FDM and can be altered by varying printing parameters. Lastly, the G3DP3 has a build volume that is suited for the scale of a glass masonry unit.

Using the G3DP3, the researchers designed, manufactured, and tested AM interlocking glass masonry units based on the existing design of Oikonomopoulou, Bristogianni, Barou, Jacobs, et

al. (2018b), the type E: Figure Eight (see Figure 3.18). Massimino et al. (2024) developed three manufacturing methods: Fully Hollow (FH), Print-Cast (PC), and Fully Printed (FP) (see Figure 3.5a). Initial requirements of these masonry design were:

- Interlocking components allowing free rotation to support various assembly arrangements.
- Interlocking components suitable for casting or printing.
- Maximise surface area in hollow body walls to enhance load transfer and minimise stress.
- Minimise unsupported surface area in body walls to decrease bending and tensile stress.

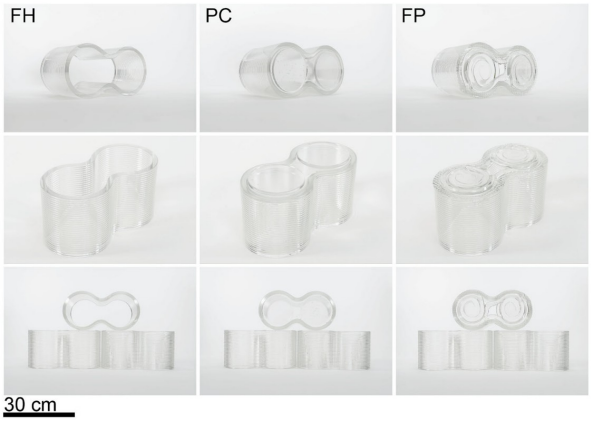

(a) Each manufacturing method shown from left to right: FH, PC, and FP (Massimino et al., 2024)

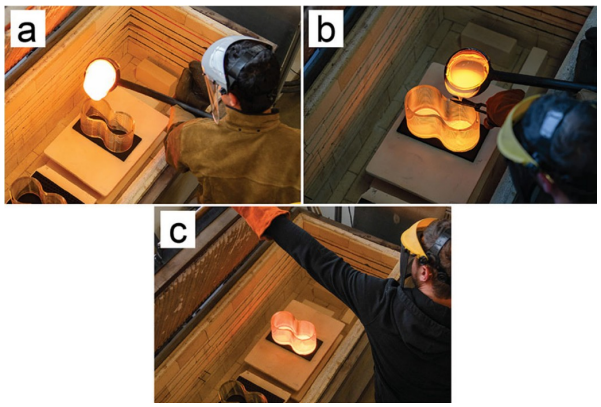

(b) PC casting process. A) FH unit is brought to 616 °C in a glass casting kiln. B) Molten glass is ladled into the interior of the masonry unit on top of a graphite mold. C) The bottom of the masonry unit is fully filled and casting kiln is closed (Massimino et al., 2024).

After designing, printing, and annealing, the components were machined. The grinding process was carried out to ensure precise height tolerance. To reduce stress concentrations from sawing and grinding, the edges were polished and beveled. Each proposed method was then quantified with the following methods: Geometric Analysis, Surface Roughness, and Mechanical Testing.

In the mechanical testing, the difference in the initial fracture strengths of the three methods was much larger than anticipated. Besides the measured properties, the most notable distinction between FH units and the others is the absence of a glass interlocking element in the FH units, resulting in no connection to the components' vertical wall. The high number of initial fractures in the tests were observed on the bottom surface for both PC and FP units, whereas for FH units, fractures appeared on both top and bottom surfaces. This indicates that fractures on the bottom surface could be due to surface interactions or stress concentrations and bending that exceeds the ultimate tensile strength. The stress flow was likely influenced by the interface between the interlocking features and the sidewall, which caused stress concentrations that led to failure. Other unexpected fracture patterns were also observed. During the tests, cracks halted at layer boundaries as the load intensified. This crack progression could suggest a certain degree of anisotropy in the printed layers (Massimino et al., 2024).

While each method showed promise, the FH units exhibited the highest load-bearing capacity, shortest production time, and most accurate and repeatable manufacturing process. However, this method would require a separate interlocking component to assemble the FH bricks. This would add time and untested variables. The PC and FP methods faced challenges such as lower strength and increased production complexity, but do have an inherent interlocking system. Future work would include investigating the anisotropy of the glass layers and for the FH elements another critical area for future research would be the development of a dry, interlocking interlayer system.

3.1.3 Casting Glass, Fabrication Method: Overview, Advantages, Limitations, and Applications

Overview

In recent years, much research and development has been done on cast glass in structural applications. Load-bearing facades existing of cast glass bricks have been applied in numeral examples already. For example, the Crystal Houses Facade in Amsterdam (Oikonomopoulou, Bristogianni, Veer, & Nijsse, 2018) and the Qaamat Pavilion in Greenland (Oikonomopoulou, Bristogianni, van der Velden, & Ikonomidis, 2022). Both examples demonstrate how cast glass could be implemented in future structures. Casting glass is a method of pouring molten glass into moulds to create solid, yet complex geometries. These massive components can form repetitive units for the construction of **self-supporting** glass facades and walls, eliminating the need for additional support structures Oikonomopoulou, Bristogianni, Barou, Jacobs, et al., 2018a. The large cross-sectional area and solid nature of cast glass components allow them to take full advantage of **glass's high compressive strength**, resulting in highly transparent structures that do not buckle due to the slender proportions (Oikonomopoulou, Bristogianni, Barou, Veer, & Nijsse, 2018a). However, the production of cast glass components is characterised by a precise and time-consuming **annealing process**. For example, the glass bricks used in the Crystal Houses Facade, with dimensions of 210mm x 210mm x 65mm and a weight of 7.2 kg, required 36-38 hours of annealing (Oikonomopoulou, Bristogianni, Veer, & Nijsse, 2018). This process is crucial to prevent the generation of residual stresses, but can significantly impact the commercial and financial viability of the components. Cast glass components can be designed with the help of topology optimisation to maximise strength while minimising mass, resulting in reduced annealing time and raw material requirements. Studies by Oikonomopoulou, Ioannidis, et al. (2023) have seen optimised nodes with a reduction in annealing time of 90% and 60% compared to the unoptimised geometries of Crystal Houses. This approach has been successfully applied to various architectural elements, including these structural nodes, slabs, and even pedestrian bridges (Oikonomopoulou, Ioannidis, et al., 2023).

Cast glass can be produced through two main methods: primary casting and secondary casting. **Primary casting** involves founding glass as a hot liquid from raw ingredients, typically using a hot-forming (melt-quenching) process. In this method, the raw materials are melted at high temperatures (usually above 1400 °C for soda-lime glass) in a furnace and then poured into moulds (Oikonomopoulou, Bristogianni, Barou, Veer, & Nijsse, 2018a). **Secondary casting**, on the other hand, uses pre-formed solid glass pieces that are re-heated until they can flow into the desired shape, employing a kiln-casting method (Oikonomopoulou, Bristogianni, Barou, Veer, & Nijsse, 2018a). This process generally requires operating temperatures lower than those of primary casting because the glass is already formed. This technique shows how cast glass offers excellent recyclability potential. In theory, it can be endlessly reused and recycled when kept free of contaminants (Bristogianni, Oikonomopoulou, de Lima, Veer, & Nijsse, 2018). The principal difference between the two methods, besides the initial state of glass, is the required infrastructure. Kiln-casting, used for secondary casting, employs a single kiln for both melting the pre-formed glass into the moulds and for the subsequent annealing process. In contrast, hot-forming or melt-quenching, used in primary casting, requires a furnace to melt the raw materials, followed by pouring the molten glass into a mould, which is then placed in a separate annealing oven (Oikonomopoulou, Bristogianni, Barou, Veer, & Nijsse, 2018a). The casting process for glass components can be achieved using two main types of moulds: permanent and disposable. **Permanent moulds** are typically used in combination with the melt-quenching technique and can be made of steel, stainless steel, or graphite. These moulds can be adjustable, fixed, or pressed, offering varying levels of accuracy and surface quality (Oikonomopoulou, Bristogianni, Barou, Veer, & Nijsse, 2018a). **Disposable moulds**, on the other hand, are used in kiln-casting and are made of materials such as silica plaster or alumina-silica fibre. These moulds offer more flexibility in terms of shape complexity, but generally result in lower accuracy and surface quality compared to permanent moulds (Bristogianni et al., 2018). The following sections will explore the advantages, limitations, and applications of cast glass in architectural and non-

architectural structures, offering a comprehensive overview of its potential and challenges in the built environment.

Advantages

Although traditional glass is often perceived as fragile, it possesses a high compressive strength. Studies done by Meredith and Swab (2020) found soda-lime silicate glass has a compressive strength value of around 1700 MPa (Meredith & Swab, 2020) and borosilicate 2000 MPa, which is higher than concrete and even steel (Oikonomopoulou, Bristogianni, Barou, Veer, & Nijsse, 2018b). Cast glass effectively uses this property, which enables massive cast glass elements to support significant loads in structures where **compression** is the primary force. Due to their large cross-sectional area, cast glass blocks are inherently **resistant to buckling**. Oikonomopoulou, Bristogianni, Veer, and Nijsse (2018) demonstrated that cast glass blocks with dimensions of 65 x 210 x 210 mm could withstand loads up to 6000 kN without buckling. This is in stark contrast to slender glass elements, which may buckle under much lower loads. This combination of high compressive strength and buckling resistance enables the creation of self-supporting structures made entirely of cast glass. By using an **interlocking geometry**, possible in cast glass, several advantages in terms of structural performance and circularity are possible (Oikonomopoulou, Bristogianni, Barou, Jacobs, et al., 2018a). The structural stability and stiffness arise from the combination of the construction's self-weight and the prevention of lateral movement through this interlocking geometry. The structure is held in place by its own weight. This self-interlocking system also provides the possibility of using a **dry interlayer** to prevent glass-on-glass contact and accommodate dimensional inconsistencies in the size of the cast units. More importantly, the dry-assembly design facilitates the circular use of glass components, enabling their undamaged recovery and reuse (Oikonomopoulou, Bristogianni, Barou, Jacobs, et al., 2018a). Cast glass presents excellent potential for **recyclability**. Theoretically, glass is 100% recyclable without loss of quality. Bristogianni et al. (2018) demonstrated that waste glass from various sources could be successfully recycled into cast glass components with comparable or even improved mechanical properties. If a dry interlayer is used in a cast glass structure, this 100% recycling rate can be achieved. In conclusion, transparency has emerged as a defining feature in modern architecture and design. Its inherent physical properties seek to connect spaces, people, and the environment. As modern architects and designers are seeking more open and transparent structures, cast glass could be a solution.

Limitations

Despite its potential, cast glass faces several challenges in architectural applications. First of all, the **annealing process**, a critical step in cast glass production, presents a major obstacle. This process can be extremely time-consuming, particularly for larger components, as the cooling period increases exponentially with size Oikonomopoulou, Ioannidis, et al., 2023. This limitation constrains the dimensions of individual cast glass elements, impacting their versatility in architectural designs. Also, it highly impacts the commercial and financial viability of the components due to its long process. The **production complexity** is another factor that impacts the potential of cast glass. The casting process demands specialized equipment and expertise to maintain both the structural integrity and aesthetic cohesion (Aloui & Bao, 2024), which leads to increased production costs. This complexity not only affects the economic viability of cast glass projects but also limits the number of manufacturers capable of producing high-quality cast glass components. Another significant concern in the use of cast glass structures is the issue of **adhesives** and recyclability. Traditional methods of assembling cast glass components often rely on adhesive bonding, which can present problems for future disassembly and recycling due to contamination (Bristogianni et al., 2018). The relatively recent development of cast glass as a structural material sees a **lack of standardisation** in the field. This complicates its use in architectural projects, as engineers and architects do not have established frameworks for incorporating cast glass into their designs. The brittle nature of glass and the potential for internal defects in cast components necessitate careful consideration of safety factors, redundancy in design, and the used bonding material to mitigate the risk of stress concentrations on the glass.

These factors add to the complexity of the use of cast glass in load-bearing applications. More research is being done in recent years, but a standardisation for cast glass is not available just yet.

Applications

Cast glass has a wide range of applications already. In architecture the transparent brick has been used in multiple projects in recent years, like the Crystal Houses facde, the Glass Vault and the Qaamat Pavillion. These projects will be discussed extensively in Chapter 3.2.1. Other applications can be seen in the creation of giant telescope mirrors, which are the largest monolithic pieces of cast glass these days. These mirrors, like the Hale telecope (see Figure 3.6d), typically employ a honeycomb structure to reduce weight. This telescope was the first mirror using such a structure. The 5m blank was casted in 1936 with a new glass blend with reduced expansion rate (Oikonomopoulou, Bristogianni, Barou, Veer, & Nijsse, 2018b). After casting the 15 tonnes mirror, it had to remain in an electrical heated annealer for 10 months to properly anneal. Cast glass is also used in glass sculptures, for example the ones by Roni Horn (see Figure 3.6f). One of perhaps the largest monolithic glass sculptures weighing at around 4,5 tonnes. The solid cube contains internal cracks, likely caused by inadequate annealing.

(a) Crystal Houses facade, *image credits: MVRDV*

(b) Glass Vault, *image credits: Maciej Grzeskowiak*

(c) Qaammat Pavilion, *image credits: Julien Lanoo*

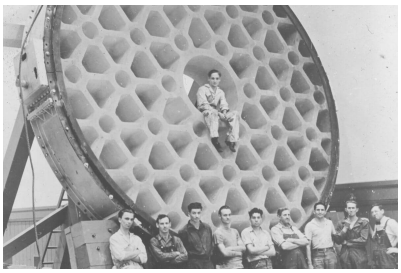

(d) Hale telescope, *image credits: Corning Museum of Glass*

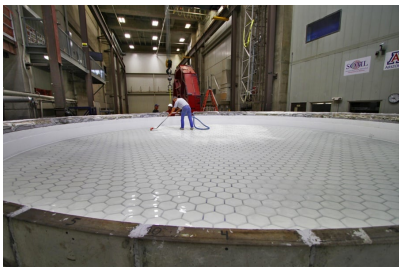

(e) Giant Magellan Telescope, *image credits: Harvard magazine*

(f) Glass sculptures, *image credits: Roni Horn*

Figure 3.6: Six applications of cast glass

3.1.4 (Sub)Conclusion

The exploration of Additive Manufacturing (AM) and cast glass techniques reveals their potential to create innovative modular structures in architecture. Both methods offer unique advantages and face certain limitations in their application to structural glass components.

Modularity and Circularity

Modular construction using AM and cast glass is essential for several reasons:

- *Customisation*: Both techniques allow for the creation of complex, customised components that can be assembled into larger structures.
- *Scalability*: Modular designs facilitate easier transportation and on-site assembly of large-

scale structures.

- *Circularity potential*: Modularity enables the disassembly and potential reuse or recycling of individual components, promoting sustainable building practices.

To fully realise the circular potential of these structures, a reversible assembly system is crucial. Such a system should ideally prevent contamination of the glass components, ensuring their recyclability and reusability. This approach aligns with the dry-assembly method mentioned for cast glass structures, which facilitates the undamaged recovery and reuse of components.

AM Glass Structures

While both AM and cast glass offer promising ways to architectural innovation, AM glass structures present particularly interesting possibilities:

- *Customisation*: AM allows for great freedom in designing complex geometries and customised connecting surfaces.
- *Material efficiency*: AM enables the creation of optimised structures that use material only where necessary, potentially reducing waste and improving structural performance.
- *Rapid prototyping*: The ability to rapidly produce and iterate designs can accelerate the development of novel structural solutions.

By focusing this thesis research on AM glass structures, the intersection of digital design, material science, and sustainable architecture will be explored, while pushing the boundaries of what is possible in structural glass applications.

3.2 Current Interlayer Systems in Structural Glass Applications

Interlocking glass structures exist of two essential elements: the glass component and an interlayer material in between the glass elements. Because glass is a brittle material, it is not able to deform plastically. When there is an unevenness in the contact surface of two hard materials like glass, local peak stresses are induced and this could result in local cracks, even when loaded in compression (Oikonomopoulou et al., 2019). Although glass has compressive strength properties of around 800-1000 MPa (Saint Gobain Sekurit, n.d.), tests done by Oikonomopoulou, Veer, Nijsse, and Baardolf (2015) present obvious cracks in the glass bricks in compression. This is due to excessive peak stresses generated due to microasperities on the surface of the rigid glass blocks and the even stiffer steel plates used in the compression test, as illustrated in Figure 3.7. To prevent this from happening, an interlayer is essential to distribute the stresses of the loading evenly and account for the surface micro asperities of the cast glass element (Dimas, Oikonomopoulou, & Bilow, 2022).

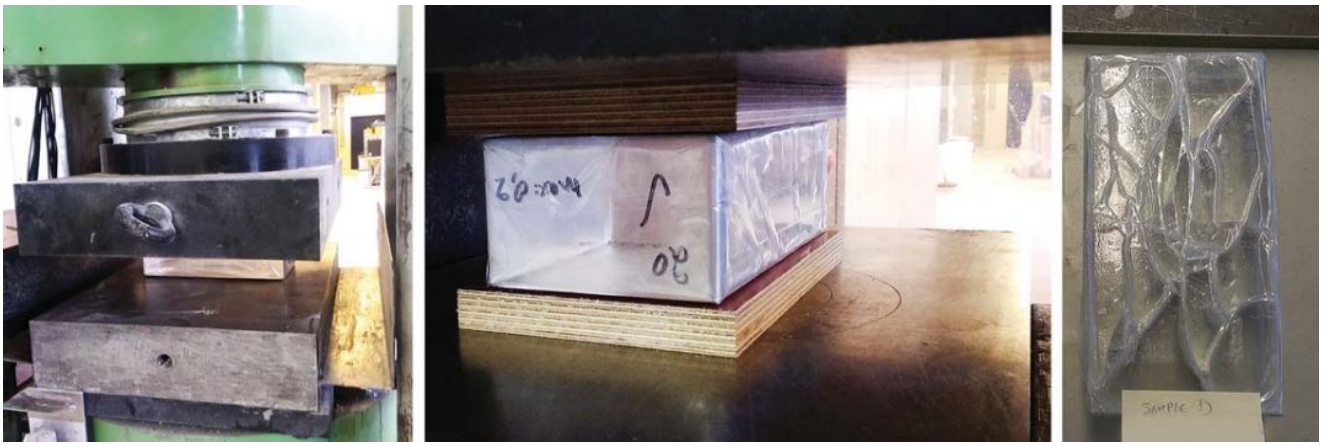

Figure 3.7: Compression tests of glass blocks. Left: Test set-up for the two first series of blocks. Middle: Test set-up for the last series of blocks. Right: Typical initial crack pattern in specimen. (Oikonomopoulou et al., 2015)

3.2.1 Permanent Interlayer Systems

The primary benefit of (permanent) adhesive connections is their ability to create a highly transparent and structurally integral joint (Oikonomopoulou, Bristogianni, Veer, & Nijsse, 2018). These connections can evenly distribute stresses across the bonded glass surface, reducing the risk of stress concentrations that could lead to premature failure in fragile materials such as glass. In addition, adhesive bonds can accommodate minor surface irregularities, enhancing the overall stability of the structure (Dimas et al., 2022). However, the use of permanent adhesives presents a major disadvantage in terms of sustainability and circularity. The irreversible nature of these connections makes it difficult to disassemble the structure without damaging the glass components. This hinders their potential for reuse or recycling (Oikonomopoulou, Bristogianni, Barou, Jacobs, et al., 2018a). Furthermore, the presence of adhesive contaminants on the glass surface also interferes with the recycling process. This could lead to unsuitability of the glass units for high-quality recycling streams. To illustrate the application and implications of permanent connections in glass structures, the next sub-chapters will examine five case studies, arranged in two categories: stiff and flexible adhesives. The stiff adhesives sub-chapter contains the Atocha Memorial (E, Glass Vault, and the Crystal Houses facade. The flexible adhesives appear in the Qwalala structure and Qaamat Pavilion. These different projects demonstrate different approaches to adhesive bonding in challenging environments and architectural contexts.

Stiff Adhesives

the Glass Vault

The Glass Vault project was a collaborative effort between SOM, Princeton University's c.r.e.A.te lab, and Form Finding Lab, with assistance from TU Delft Glass Group. This research demonstrates how automated robotic assembly can create a large-scale, double-curved glass brick vault without the use of scaffolding.

The structure, approximately 2 meters high and 2.6 meters wide, was assembled on-site by two robots during SOM's Anatomy of Structure 2020 exhibition in London. The vault follows a herringbone pattern and was designed as a compressive-only shape, using cast glass bricks as its primary building material (Oikonomopoulou & Bristogianni, 2022). The adhesive selection for this project was crucial, as it needed to stabilise the structure during assembly while accommodating the dimensional variations inherent in the casting process, but mostly the of geometry of the vault. After extensive testing and consideration of various factors, including budget constraints and assembly requirements, the team selected a fast-setting two-component epoxy putty (PIG™Multi-Purpose Epoxy Putty) as the bonding medium. This epoxy putty offered several advantages that made it suitable for the project's unique requirements. It provided a gap-filling capability of up to 20 mm, which was essential for managing the varying joint sizes resulting from the double-curved geometry. The putty's fast setting time of 3-5 minutes and full curing within 60 minutes facilitated rapid robotic assembly without the need for scaffolding (Oikonomopoulou & Bristogianni, 2022). Although not originally designed for structural applications, the epoxy putty chosen demonstrated satisfactory mechanical properties for this project. It exhibited a compressive strength of 55 MPa and a leap shear tensile strength of 6.2 MPa. These properties were deemed sufficient for the Glass Vault, as the adhesive primarily needed to withstand forces during assembly, the completed structure being self-supporting due to its compressive-only geometry (Oikonomopoulou & Bristogianni, 2022). Choosing this atypical adhesive for a structural glass application emphasises the importance of taking into account the unique requirements and limitations of a project when selecting materials.

Figure 3.8: Interlayer of the Glass vault, *image credits: Maciej Grzeskowiak*

Glass Vault	
Unit	Brick shaped cast glass
Material	Soda-lime silica glass
Interlayer	Stiff adhesive (PIG™Multi-Purpose Epoxy Putty)
Reason for interlayer	Gap-filling and fast-setting
Reversibility	No
Structure	Compressive-only
Transparency	Medium

Table 3.1: Joinery system Glass Vault

the Crystal Houses facade

The Crystal Houses façade in Amsterdam is an innovative architectural glass engineering design, see figure 3.9. This project, designed by MVRDV architects, aimed to recreate a traditional brick façade using solid glass bricks, preserving the city's historical aesthetic.

The facade's design presented unique challenges, especially in achieving a seamless, transparent structure without compromising structural integrity. To meet these demands, the project team opted for permanent adhesive bonding using a clear, stiff adhesive (Delo Photobond 4468)(Oikonomopoulou, Bristogianni, Veer, & Nijsse, 2018). This choice was made because of several factors. First of all, the adhesive's transparency allowed for maximum visual clarity, which was crucial for maintaining MVRDV's vision of an entirely glass façade. Its high bond strength provided the necessary structural integrity, allowing the facade to be self-supporting without relying on a metal substructure. The stiff nature of the adhesive ensured an even load distribution across the bonded surfaces, mitigating the risk of stress concentrations in the brittle glass material.

However, this approach was not without its challenges. The optimal performance of the adhesive required an extremely thin application layer (0.2-0.3 mm), demanding high precision in both the manufacturing of the glass bricks and the construction process. This required mechanical post-processing of each glass brick to achieve the required dimensional accuracy, significantly increasing production costs and complexity.

The construction process itself also became a piece of engineering precision. Each layer of the façade had to be precisely controlled to prevent accumulated deviations that could lead to improper bonding. This level of accuracy required a highly specialised construction team and innovative on-site quality control measures.

Although the permanent nature of the adhesive bonding system achieved the desired structural and aesthetic goals, it also presented long-term challenges. The irreversibility of the connections makes future disassembly or recycling of the façade components extremely difficult. This poses questions about the structure's end-of-life sustainability. Despite the challenges, the project ended up with a stunning facade that mimicked the original design, down to the layering of the bricks and the details of the window frames (MVRDV, 2016. With this design, MVRDV hopes to provide a solution to the loss of character in shopping areas around the world. Crystal Houses results in a flagship store that seamlessly blends historical aesthetics with cutting-edge materials science.

Figure 3.9: the Crystal Houses facade, (MVRDV (2016))

the Crystal Houses Facade	
Unit	Brick shaped cast glass
Material	Soda-lime silica glass
Interlayer	Stiff adhesive (Delo Photobond 4468)
Reason for interlayer	Stiff, high-strength and transparent
Reversibility	No
Structure	Compressive-only
Transparency	High

Table 3.2: Joinery system the Crystal House facade

Flexible Adhesive Connection

Flexible adhesives such as silicones, MS polymers, and polyurethanes provide strong tensile and shear capabilities (over 1 MPa) and accommodate the size and surface irregularities of the bonded bricks. Despite their sensitivity to creep, they perform effectively under dynamic conditions and accommodate joint movements, thanks to their flexibility. These adhesives are available in both transparent and opaque variants. The use of opaque adhesives can hinder the transparency of the assembly, depending on the joint size relative to the entire assembly (Aloui & Bao, 2024). Multiple examples of projects where flexible adhesives were used are available, the next sub-chapters will explain the use in the Qwalala Structure and the Qaamat Pavilion.

Qwalala Structure

The Qwalala structure is a sculpture originally commissioned for the Venice Art Biennale in 2017 and later relocated to the Claremont McKenna Campus in California. The structure consists of a curving glass wall extending over 78 m and consisting of 1500 glass bricks, see figure 3.10.

A permanent connection between the cast glass blocks is achieved using an opaque, flexible silicone. This adhesive was chosen for three main reasons (Aloui & Bao, 2024). Firstly, it provides the flexibility required to withstand significant seismic loads, which became a crucial consideration when the structure was moved to California. Secondly, silicone can absorb deformation movements, an essential property for a structure exposed to outdoor environmental conditions. Third, it demonstrates resistance to intensive UV light exposure, a critical factor given the structure's location. In contrast to this opaque adhesive, transparent flexible adhesives are typically susceptible to UV-exposure, therefore not considered in this project.

A two-part silicone product was selected over a one-part alternative due to the large bonding interface between the staggered bricks. One-part silicone requires sufficient relative humidity, a controlled temperature, and a longer curing time. Because of the deep geometry of the bricks, one-part adhesive would not be able to cure properly. Two-part silicone does not depend on atmospheric moisture for crosslinking; instead, it cures through the mixing of a catalyst, allowing it to set without a controlled environment (Aloui & Bao, 2024).

Figure 3.10: The Qwalala Sculpture, (Aloui and Bao (2024)
)

Modelling the mechanical behaviour of silicone bonds in cast glass applications is a challenging and computationally demanding task. As a result, existing methods often use simple and conservative models, which can lead to overuse of the adhesive. However, there are cases where reducing the silicone coverage is desired for aesthetic purposes. For this project, the client opted to minimise the silicone bonding area to maximise light transmission. By computational modelling, the researchers met this wish and decreased the silicone bonding area by 40% compared to the previous setup in Venice.

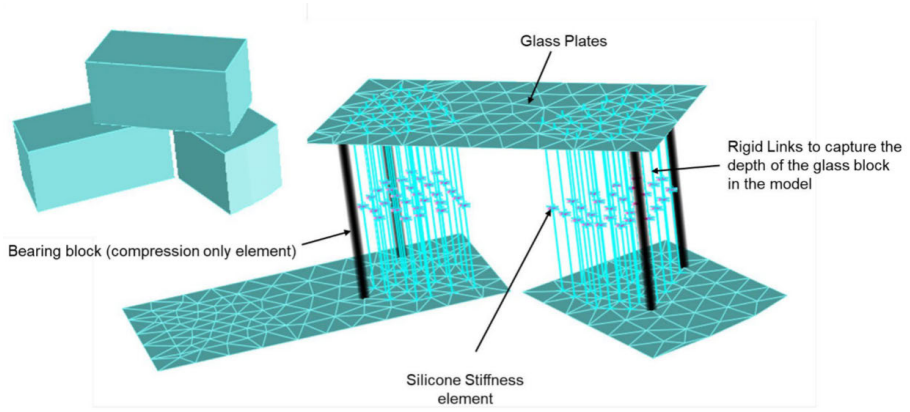

Figure 3.11: Finite element model of a glass block to glass block silicone connection (Aloui and Bao (2024))

By introducing a parametric design approach combining Grasshopper and Strand7 API, it was possible to capture the geometry in a Finite Element (FE) in Grasshopper, see figure 3.11. This model was used to recreate the effects of silicone bonds and to assess the performance of various silicone joint designs.

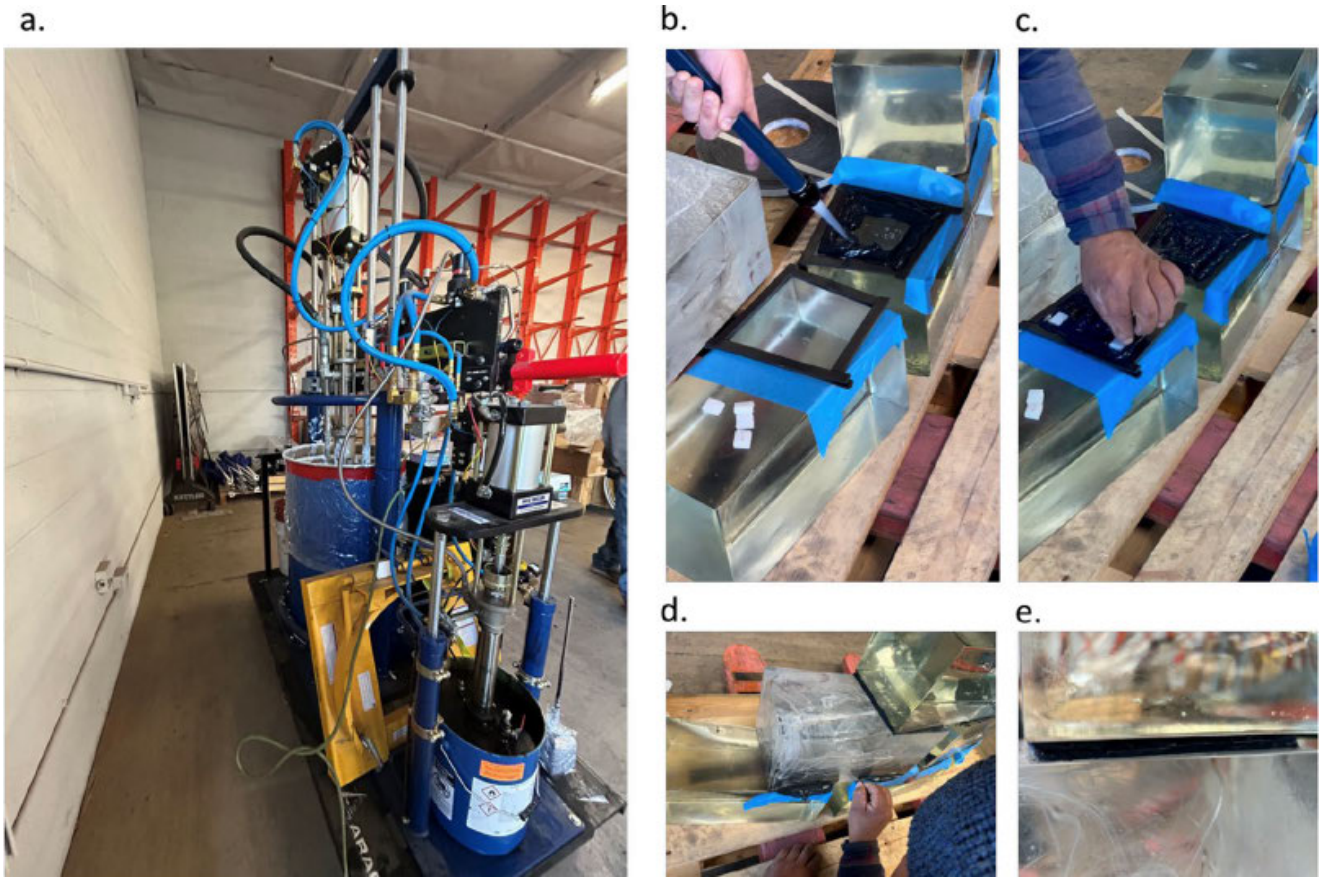

Figure 3.12: Silicone application procedure test: a) industrial grade pump used to control the flowof the silicone, b) Neoprene tape to accurately trace the bond area, c) Adding the setting blocks to the joint in order to transfer the weight of the glass and keep constant width of the joint, d) removing the neoprene tape after the silicone is cured, e) final resulting joint with clean edges (Aloui and Bao (2024))

To guarantee a precise application of silicone sealant in construction, extra measures were taken to reach the agreed recess values. Initially, neoprene tape was used to outline the bonding area, providing a clear application guide. The silicone was then applied within this outlined zone using

the pump shown in figure 3.12, ensuring uniform coverage and adherence to the boundaries. A preliminary mock-up test with black silicone was conducted to assess the technique and bond quality prior to the actual construction, reducing the risk of mistakes in the final setup.

Qwalala Structure	
Unit	Brick shaped cast glass
Material	-
Interlayer	Opaque, flexible silicone
Reason for interlayer	Flexible, two-part silicone and outdoor resistance
Reversibility	No
Structure	Compressive-only
Transparency	Medium

Table 3.3: Joinery system Qwalala Structure

Qaamat Pavilion

The Qaammat Pavilion in Greenland is a sculptural structure designed by Danish architect Konstantin Ikonomidis. The location of this remarkable pavilion was carefully chosen by the local community, the UNESCO site manager Paninnguaq Fleischer-Lyberth, and the architect. It currently serves as a landmark and gathering point within the UNESCO heritage of Aasivissuit - Nipisat in Greenland (Oikonomopoulou et al., 2022). The pavilion comprises two semicircular glass brick walls with dimensions of approximately 3.2 m in diameter and 2 m in height. This project presented unique engineering challenges compared to previous adhesively bonded glass brick structures.

The project's remote arctic location and limited budget necessitated a simple bonding system that could be implemented by local, unskilled workers. This requirement, combined with harsh environmental conditions, including temperatures as low as -35 ° C, required an innovative approach to adhesive selection and application (Oikonomopoulou et al., 2022).

To address these challenges, the research team selected two different adhesives: 3M™ Scotch-Weld™ Polyurethane Adhesive DP610 for the bottom rows, where a higher strength was required. A custom-developed DOWSIL Experimental Fast Curing Adhesive for the rest of the structure. The 3 mm gap filling capacity of the last adhesive was crucial in accommodating the $\pm$1.5 mm size deviations of the cast glass bricks and the potential accumulated construction tolerances (Oikonomopoulou et al., 2022).

To realise the architects vision within the logistic constraints, it was important to make early-stage decisions. Because of the lack of standardised guidelines for such structures, the research team experimentally validated the adhesive-bonds. Careful consideration had to be put into the specific restraints of the given project. This project highlighted the challenges of building in remote, extreme conditions. For example, difficulties in regulating temperature and humidity levels during adhesive application. It exemplifies that adhesive bonding enables innovative glass structures in these kinds of environments. However, careful selection of the adhesives and thorough testing are essential to balance the structural performance, constructability, and long-term durability requirements

Figure 3.13: The Qaamat Pavillion, (Lucia Brandoli (2021))

Qaamat Pavilion Structure	
Unit	Brick shaped cast glass
Material	Soda-lime glass
Interlayer high bricks	DOWSIL Experimental Fast Curing Adhesive
Reason for interlayer high bricks	Accomodate size deviations
Interlayer low bricks	3M™ Scotch-Weld™ Polyurethane Adhesive DP61
Reason for interlayer low bricks	Higher strength
Reversibility	No
Structure	Compressive-only
Transparency	High

Table 3.4: Joinery system Qaamat Pavilion

3.2.2 Reversible Joinery Systems in Glass Structures

These systems, contrary to permanent joinery systems, have connections between glass components that can be easily disassembled without damaging the glass. This allows for repair, replacement, or reconfiguration of the structure. Because these systems do not use adhesives, they achieve structural integrity in different ways, such as using an interlock or an external structure. In the next sub-chapters, some case studies will be reviewed and compared.

Metal Sub-Structure (Optical House, Japan)

The Optical House, designed by Hiroshi Nakamura & NAP Architects, features an 8.6 x 8.6 m facade constructed from 6000 solid glass blocks, see figure 3.14. This façade serves as

an example of how cast glass components can be used in self-supporting structures with a supportive substructure. The glass blocks used in this project are made of borosilicate glass, usually found in laboratory hardware or telescope mirrors (Oikonomopoulou, Bristogianni, Barou, Veer, & Nijsse, 2018b). Each block measures 235 x 50 x 50 mm and weighs 2.2 kg. The use of borosilicate glass allows for enhanced transparency while maintaining structural integrity.

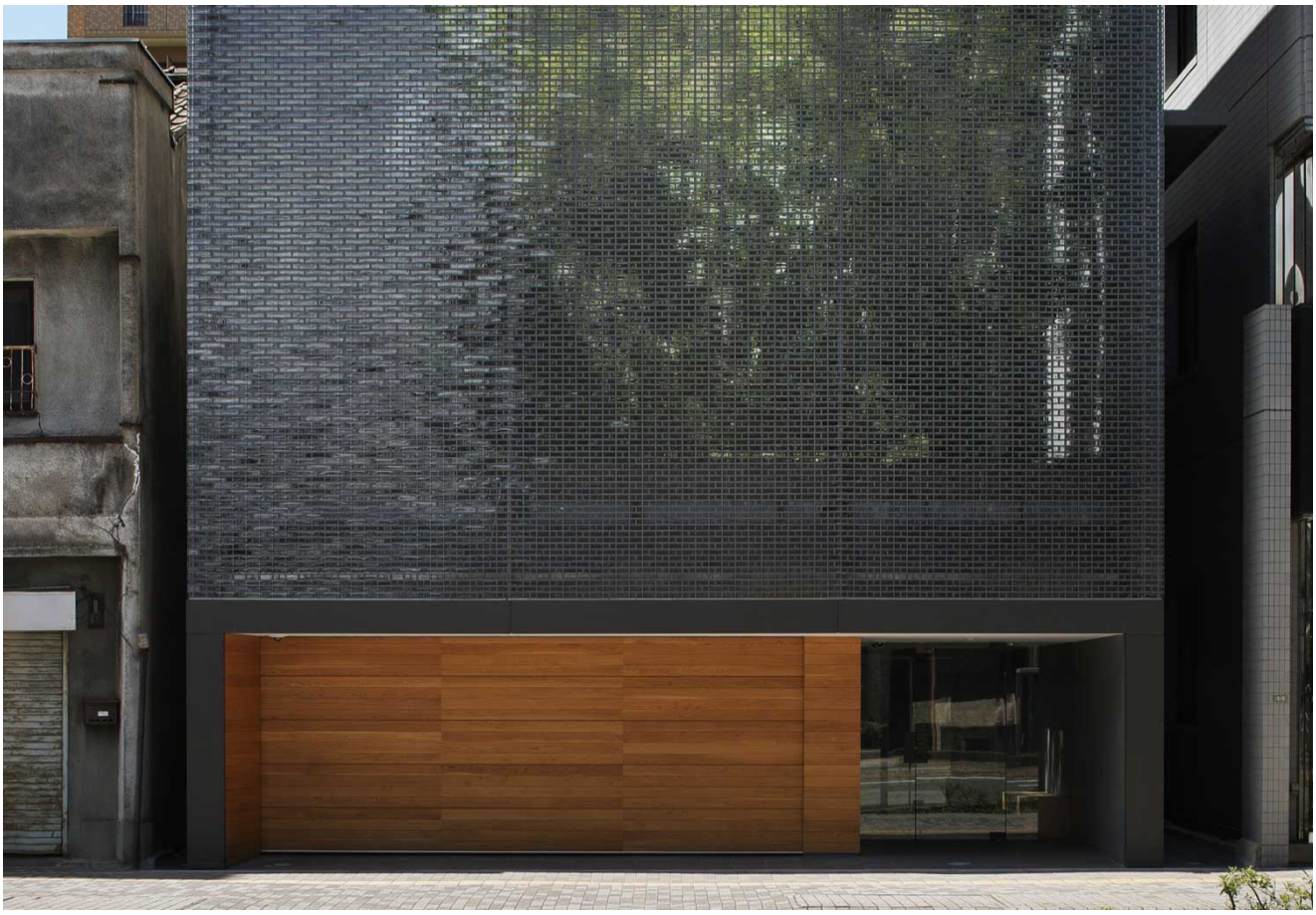

Figure 3.14: The Optical Glass House, Hiroshima, Japan, (*Image credits: Hiroshi Nakamura & NAP*)

The connection system employed in the Optical House is particularly noteworthy for its reversible nature. The glass blocks are cast with a puncture (see figure 3.15b and 3.15a) and are inserted from beneath into a tensioned vertical grid composed of 75 stainless steel rods (see figure 3.15d). The mesh is hung from a steel beam that is embedded in reinforced concrete. The innovative joinery system allows the glass wall to perform primarily under compression, while the steel substructure carries the tensile forces and ensures the desired stiffness and buckling resistance. To distribute lateral forces more evenly and reduce stresses on individual glass blocks, flat stainless steel bars (40 mm x 4 mm) are connected to the rods at 100 mm intervals. These bars are seated within the 50 mm thick glass blocks (see figure 3.15c). This arrangement creates an adhesion-free structure that can be disassembled if needed. The structural system addresses various forces acting on the façade. The glass blocks primarily resist compressive loads, utilizing the material's high compressive strength. Meanwhile, the steel mesh and additional vertical steel fins handle lateral forces, like wind loads. This division of structural roles allows for a façade of high slenderness while maintaining stability, transparency, and reusability.

(a) Casting of borosilicate brick)

(b) The brick geometry

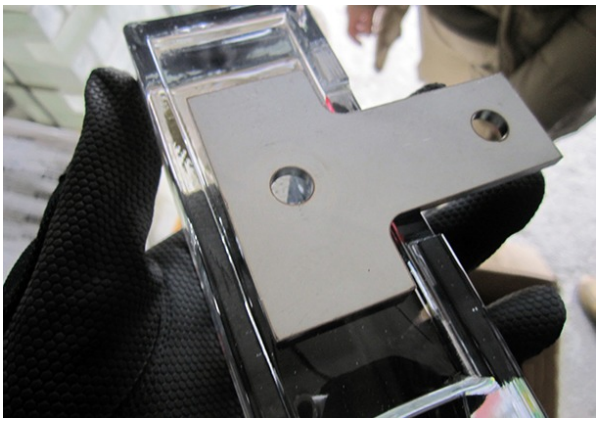

(c) Stainless steel flat bar integrated in the brick

(d) Assembly of the structure)

Figure 3.15: Optical Glass House, Hiroshima, Japan, (*Image credits: Hiroshi Nakamura & NAP*)

Optical House	
Unit	Brick shaped cast glass
Material	borosilicate
Interlayer	Stainless steel flat bar
Reason for interlayer	Distribute lateral forces
Reversibility	Yes
Structure	Compressive structure in glass blocks, steel grid for tensile forces
Transparency	Low-Medium

Table 3.5: Joinery system Optical House

Dry-Stacked Interlocking Glass Bricks using an Interlayer

This system uses cast glass components with interlocking geometries, assembled without adhesives, and employing a dry interlayer to mediate contact between elements Oikonomopoulou, Bristogianni, Barou, Jacobs, et al., 2018a. It uses the self-weight of the geometry and the interlocking connections to ensure stability, while the interlayer prevents direct glass-to-glass contact, reducing stress concentrations (Oikonomopoulou, Bristogianni, Barou, Jacobs, et al., 2018a). Various interlocking geometries have been explored in different projects, a few will be highlighted in the next paragraphs.

An advanced interlocking system was developed by Oikonomopoulou, Bristogianni, Barou, Jacobs, et al. (2018a), featuring osteomorphic blocks. These blocks feature non-planar concave-convex surfaces that interlock in both planar directions, providing lateral stability and preventing

relative movements between adjacent units (see figure 3.16). The smooth curves of these geometries minimise stress concentrations compared to conventional interlocking connectors or keys. Additionally, their symmetry allows for versatile configurations, including corners and columns, using a single block type (Oikonomopoulou, Bristogianni, Barou, Jacobs, et al., 2018a). Numerical modeling has shown that osteomorphic blocks exhibit a high shear capacity. The lower blocks are most susceptible to bending. This is different for the higher blocks, with failure typically occurring through shear lock, which is a numerical issue that can occur in finite element analysis (FEA), rather than bending (Oikonomopoulou, Bristogianni, Barou, Jacobs, et al., 2018a).

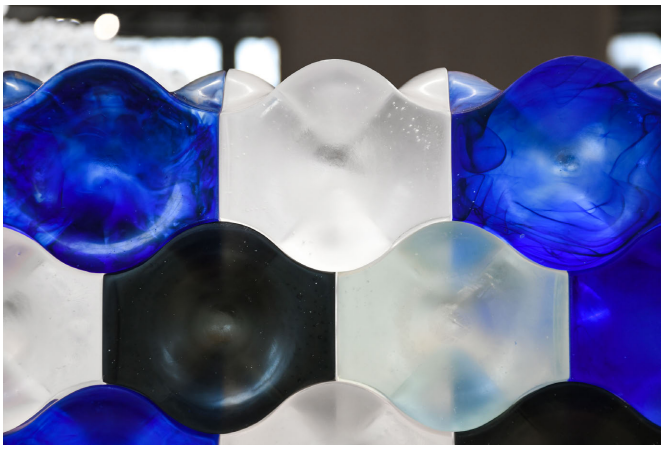

Figure 3.16: Osteomorphic interlocking blocks. (*Image credits: Faidra Oikonomopoulou*)

Another system explored is a two-component interlock; in this case bone-shaped bricks are used. They employ a male-female interlocking mechanism that provides additional freedom in design aesthetics and material combinations. For instance, one component can be made of glass while the other can be fabricated from metal or plastic (refer to Figure 3.17). This design ensures lateral stability but requires additional peripheral constraints for overall structural integrity. Furthermore, the asymmetry of these bricks limits their use in certain configurations, such as corners. Lastly, this system has challenges in achieving uniform stress distribution, due to the uneven annealing of the geometry (Oikonomopoulou, Bristogianni, Barou, Jacobs, et al., 2018a).

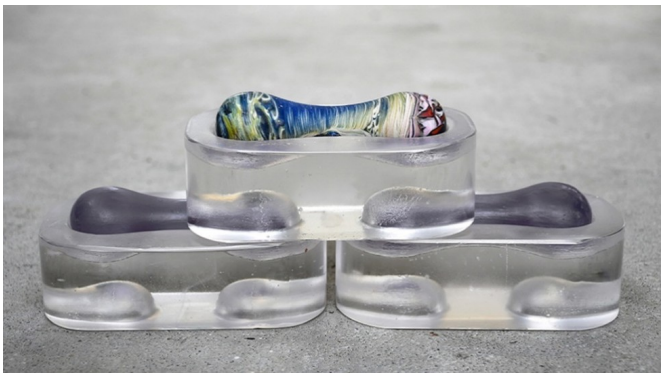

Figure 3.17: Type C Prototype. The bone-shaped components are made of recycled coloured glass. (*Image credits: Faidra Oikonomopoulou*

)

Rotational bricks feature semi-spherical keys that allows for assembly of both a planar and a cylindrical configuration. These geometries enhance flexibility in structural design while maintaining adequate shear capacity. However, the semi-spherical connections may lead to localised

shear stress concentrations under loading. Despite this limitation, rotational bricks offer unique opportunities for creating versatile architectural forms (Oikonomopoulou, Bristogianni, Barou, Jacobs, et al., 2018a).

Figure 3.18: Prototype using E1 and E2 glass blocks from clear glass and recycled mouth-blown coloured glass. (*Image credits: Faidra Oikonomopoulou*)

The most prominent feature of this system is its reversible ability. By avoiding adhesives and using dry interlayers, the structure can be disassembled, and components can be reused or recycled without contamination (Oikonomopoulou, DeBrincat, & Fuhrmann, 2023). Innovative geometries such as osteomorphic blocks and rotational designs achieve high structural performance while maintaining transparency and adaptability. More research is needed on designing and optimising the interlayer materials and manufacturing techniques to continue to expand the potential of this construction method.

Dry-stacked Interlocking Glass Bricks	
Unit	Interlocking cast glass
Material	Clear glass & recycled coloured glass
Interlayer	None
Reason for interlayer	-
Reversibility	Yes
Structure	Interlocking compressive structure
Transparency	High

Table 3.6: Joinery system Interlocking Glass

Dry-Stacked AM Glass Column

Inamura et al. (2018) developed a novel AM technique for transparent glass structures printed with the G3DP2 (Figure 3.1.2). This method was used to create a set of three-metre-tall structural glass columns for an architectural installation at Milan Design Week 2017. Inamura created an algorithm that takes three arguments as input values to define the cross-sectional profiles of the structures, seen in Figure 3.19. First, a point variable (R1) that notes the radius of the circle that defines the exterior boundary of the output geometry. Secondly, a point variable (R2) which defines the radii of the arcs and bitangent arcs that are around the exterior boundary circle. The last input is a point N that defines the number of arcs that are within the single closed curve (circle). In image 3.19 for example, both configurations have a radius (R1) of 150. On the other hand, the left configuration has the number of circles (N) of 1 and a radius of that circle (R2) of 150, which gives an output of a simple circle of 150. The right configuration sees 24 circles (N) around the exterior boundary circle with radii (R2) of 15, giving a flower-like output.

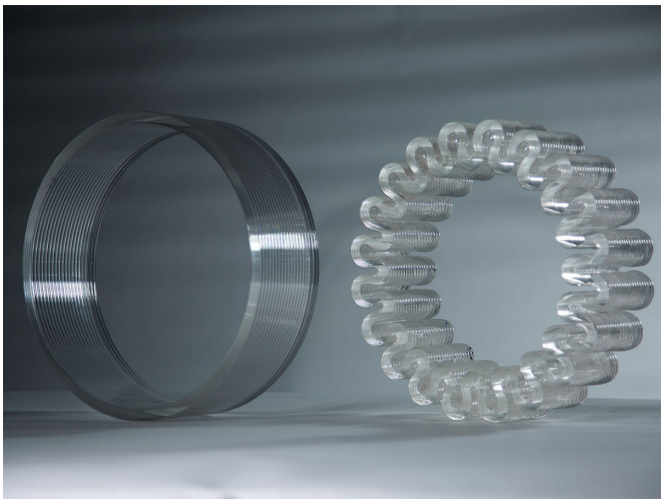

Figure 3.19: Left: 3D-printed glass object with R1 = 150, R2 = 150, N = 1. Right: 3D-printed glass object with R1 = 150, R2 = 15, N = 24. (*Image credits: CHIKARA INAMURA*)

Along the vertical axis, the radii (both R1 and R2) undergo incremental linear changes, resulting in a smooth transition of morphology in both lateral and longitudinal directions. This design strategy led to divergent structures in the lobe, which prevented stress concentrations at any local point across the columns (Inamura et al., 2018). This diverging structure (see Figure 3.20b) optimised the structural performance of the columns, due to the decreasing cross-sectional moment of inertia of the column. The greatest moment occurred at the point of maximum bending load, continuously decreasing towards the point of least load. This approach ensured optimal material distribution and structural efficiency. Each column was constructed from 15 unique 3D-printed glass components. These components were assembled vertically using a thin silicone film between the glass units, allowing for minor movements and preventing direct glass-to-glass contact that could lead to stress concentrations. A steel post-tensioning system further improved the stability of the column by applying a compressive force along the vertical axis, improving the resistance of the structure to lateral loads and bending moments (see Figure 3.20a).

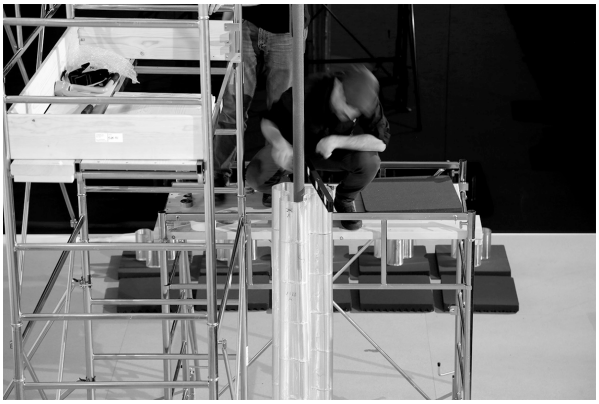

(a) Steel post-tensioning system, (Inamura et al., 2018)

(b) Diverging column, (Inamura et al., 2018)

Dry-Stacked AM Glass Column	
Unit	AM glass component
Material	-
Interlayer	Thin silicone film
Reason for interlayer	To prevent direct glass-to-glas
Reversibility	Yes
Structure	Steel post-tensioning system
Transparency	Medium

Table 3.7: Joinery system AM Glass Column

ReSolved Research

ReSolved is a project where an innovative joining technology can be seen (Hartwell et al., 2024). This method features a novel, high-strength, yet reversible bonding process using a 3D-printed, lead-free nano-alloyed solder. The joining technology showcased by ReSolved addresses the inefficiencies found in load-bearing multi-material components by enhancing fabrication simplicity, mechanical performance, and disassembly ease at the end of life. Its applications span multiple materials, but it is particularly advantageous for multi-material components with brittle homogeneous substances like engineered ceramics or glass. The product will be interesting for multiple industry sectors, thus unlocking practical opportunities for the ReSolved joining technology.

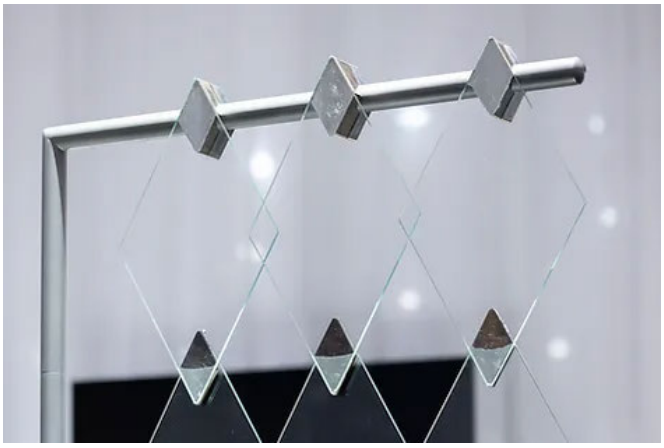

Figure 3.21: Stacked glass curtain with soldered connections, Glasstec 2024 (*Image credits: Andreas Wiese*)

ReSolved	
Unit	Float glass diamond-shape
Material	Float glass
Interlayer	Lead-free nano-alloyed solde
Reason for interlayer	To assemble
Reversibility	Yes
Structure	Stacked glass curtain with soldered connections
Transparency	High

Table 3.8: Joinery system ReSolved

3.2.3 Conclusion

The review of joinery systems in modular freeform glass structures reveals most current projects use adhesives to bond the glass structures. While stiff adhesive connections offer high strength and transparency, they pose challenges for disassembly, reuse, and recycling. In contrast, flexible adhesives provide better accommodation for thermal expansion and seismic loads but may compromise optical clarity. This approach could potentially be adapted for AM glass components. However, the pursuit of sustainability and circularity in architectural applications calls for a change to reversible solutions with appropriate interlayers between the glass elements. This analysis exposes the need for a deeper exploration of reversible joinery systems specifically tailored for AM glass structures. Such a system could potentially bridge the gap between the theoretical recyclability of glass and its practical implementation in architecture.

3.3 Reversible Joinery Systems in other modular structures

3.3.1 Interlocking bricks

Various forms

These bricks are manufactured by compressing a mixture of soil, sand, and cement, resulting in a self-locking design that eliminates the need for mortar (Civil Synergy, 2020). These types of brick offer several advantages, such as cost-effectiveness, durability, earthquake resistance, and easy labour. However, these interlocking bricks also have downsides. For example, the space between the interlocks of the bricks is large enough for insects to crawl into. In addition, rainwater that flows into cracks can rapidly alter the colour of bricks. Lastly, without additional support from columns, these bricks are limited to two-story buildings.

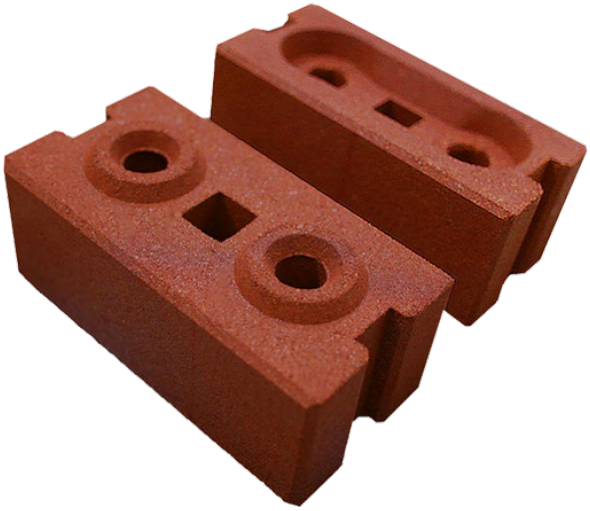

(a) Lego-like Interlock, (*image credits: Civil Synergy*)

(b) Central-axis Interlock, (*image credits: Civil Synergy*)

DryStack B.V.

DryStack B.V. employs engineered interlocking elements which eliminate the need for mortar to bond the stones. In this way, the system reduces CO2 emissions associated with traditional construction practices. The versatility of these components allows for the realisation of complex designs, including curved surfaces, wavy facades, and intricate patterns. With the construction industry seeking more environmentally friendly options, this mortarless system is a step towards circular building practices and reduced environmental footprint.

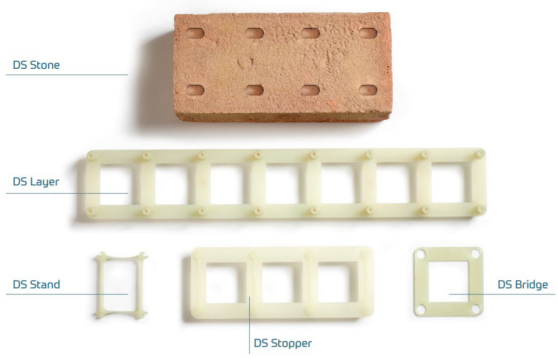

(a) DryStack elements, (*image credits: DryStack B.V.*)

(b) DryStack in practice, (*image credits: DryStack B.V.*)

The Coote 8

The Coote 8 Module interlocking block moulds are used in the production of individual precast concrete blocks, which can be employed in diverse applications without the need for mortar. These moulds are a solution for repurposing leftover ready-mix or waste concrete. The precast blocks are typically manufactured without reinforcement, although a two-stage casting process is feasible, wherein the mould is partially filled, reinforced, and then completed when additional concrete becomes available. A notable feature of this system is the availability of dividers in the mould, enabling the production of either a single half block or two half blocks within the same mould, thus increasing versatility.

Figure 3.24: Interlocking Block Moulds by Coote, (*image credits: Coote*)

3.3.2 Click-Systems in Products

Velcro®

Velcro® hook-and-loop fasteners are a widely used attachment system consisting of two components: a strip with tiny hooks and another with small loops. When pressed together, these components interlock, creating a secure but temporary bond that can be easily separated and reattached multiple times. This simple mechanism, inspired by nature, has found applications in a lot of industries, with the most common being Velcro® shoes. Velcro® is now getting a second life as makers are experimenting with a AM Velcro® (3Printr.com, 2023). These printed variants aim to replicate the functionality of traditional Velcro using various materials. According to 3Printr.com (2023), PETG was the optimal choice, providing an ideal mixture of flexibility and stiffness. During tensile strength tests, the hook-and-loop fastener endured an impressive 10 kg before joint failure.

(a) Velcro hook-and-loop, (*image credits: Fuugo*)

(b) AM part Velcro joint, (*image credits: 3D Jake*)

Snap-fit

Snap-fit joints are mechanical assemblies in which flexible components interlock (click) without additional fasteners, allowing easy assembly and disassembly. These joints are widely used in various products due to their convenience and durability.
Cantilever snap fits are the most common type (see Figree 3.26a), featuring a cantilever arm with an interlocking feature at its free end. During assembly, the arm deforms as it enters a cavity in the mating component, then snaps into place when the interlocking feature reaches its locking position. While durable, these joints can be susceptible to permanent deformation or breakage if hyper-extended (Wayken, 2023).

Annular snap fit joints consist of a circular hoop that expands when pushed onto a rigid, matching groove. The expansion generates stress in the hoop, creating frictional force to secure the joint. This design is suitable for high-stress applications due to uniform stress distribution, but may loosen over time with repeated use (Wayken, 2023).

(a) Buckle, cantilever snap-fit joint, (*image credits: Wayken*)

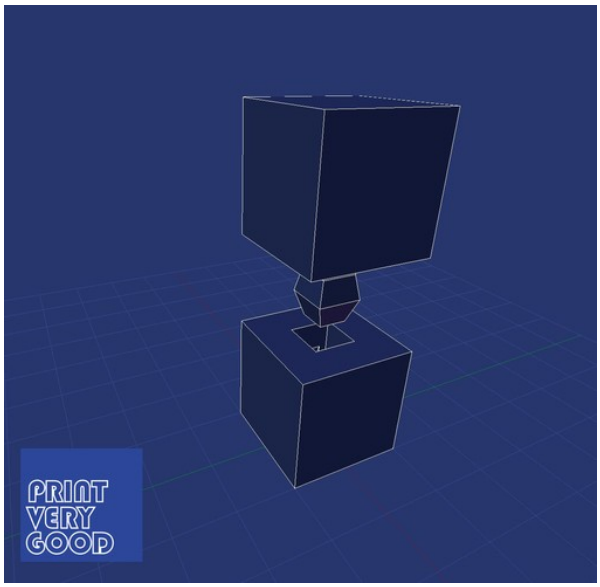

(b) AM part, annular snap-fit joint, (*image credits: Paul van Gaans*)

Figure 3.26: Snap-fit Designs

3.3.3 Interlocking Metasurfaces (ILM)

Interlocking Metasurfaces (ILM) are defined as configurations of features across a surface that transmit force and restrict motion between adjoining bodies in one or more directions (Bolmin, Young, Leathe, Noell, & Boyce, 2023. Unlike conventional joining technologies, ILMs act in an almost continuous manner across a surface, enabling the joining of complex shapes. The distributed load-bearing capability allows ILMs to carry high forces, with effective interface strengths that can be a large part of the base material strength.

One of the key advantages of ILMs is their versatility in design and application. They can be fabricated from the same material as the base components, which allows them to withstand similar thermal and chemical exposures. Unlike welds or adhesives, ILMs are non-permanent and support forces across a surface rather than at a joint. Furthermore, in contrast to bolts, they are integral to the bodies they attach and therefore do not require additional parts for assembly.

The design space for ILMs is extensive, covering a large spectrum of topologies. These can include sliding actions, vertical snapping, and even curved trajectories or rotational engagements, as can be seen in Figure 3.27. The specific design of an ILM can be tailored to meet various engineering objectives, like specific removal forces, tensile strength or constraints on relative movement between the joined surfaces (shear).

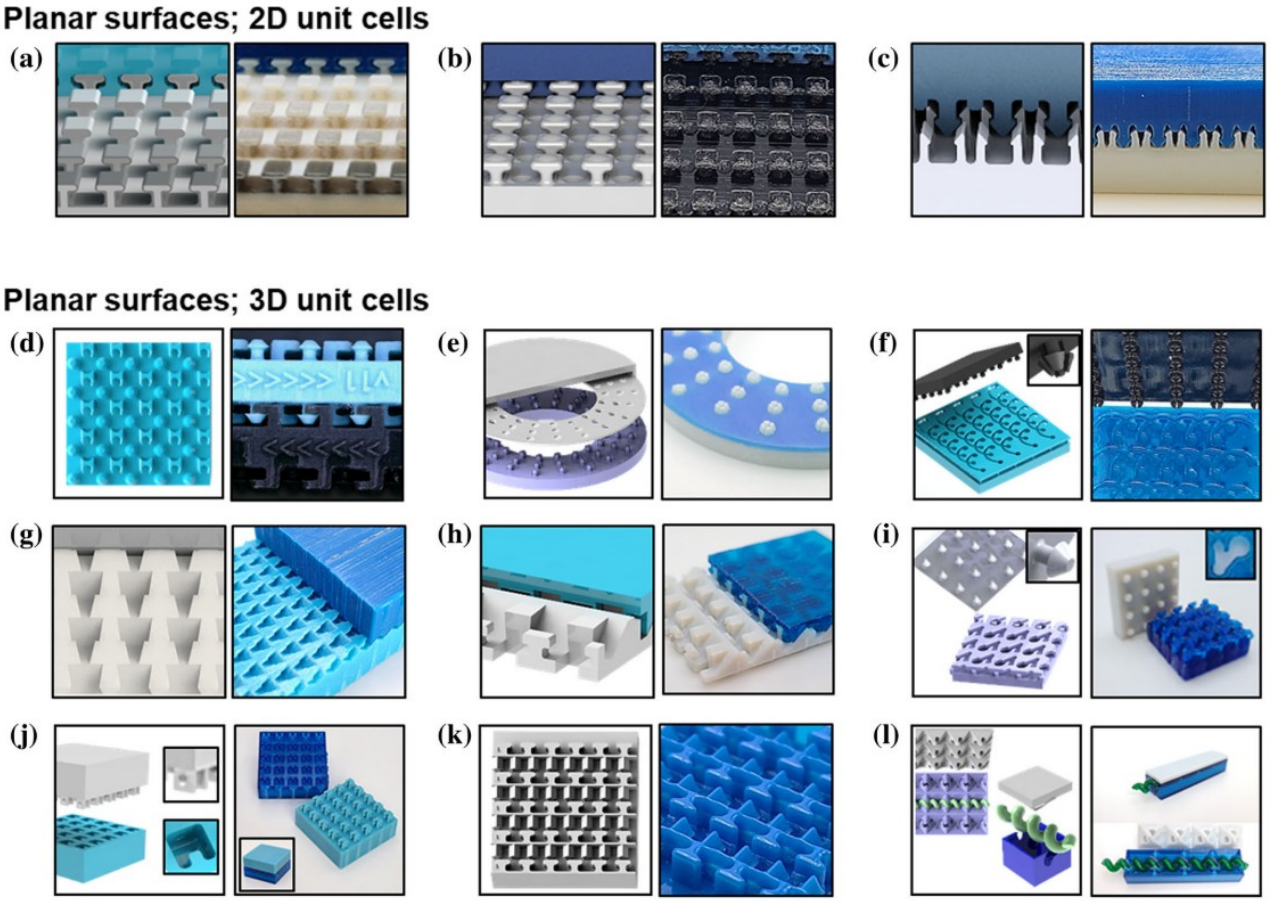

Figure 3.27: 12 variations on an interlocking metasurface illustrate the possibilities in the design space. CAD models (left images) are shown next to physical as-manufactured ILMs (right images) for each design. Every design possesses unique topological characteristics that set it apart from the others. (Bolmin et al., 2023)

Gloyer, Schek, Flöttmann, Wüst, and Völlmecke (2023) developed a novel interlocking metasurface (ILM) mechanism called ShroomLock, designed specifically for extrusion-based AM. This mechanism intends to create strong, reversible connections between planar surfaces using a snap-fit joint. The researchers focused on creating a manufacturing process that optimises mechanical properties, functionality, and printability. They utilised TPU filament for its flexibility, which is important for the proper functioning of the spring elements. The ShroomLock mechanism comprises pin and spring elements that lock together, as illustrated in Figure 3.28a. The pin elements securely snap into the spring elements, establishing a reversible connection between the two components. This design allows for the temporary fastening of two geometries to each other, with the snapping elements distributed over the contacting surfaces. This study demonstrates how AM-driven design can create innovative, functional, and reproducible interlocking mechanisms.

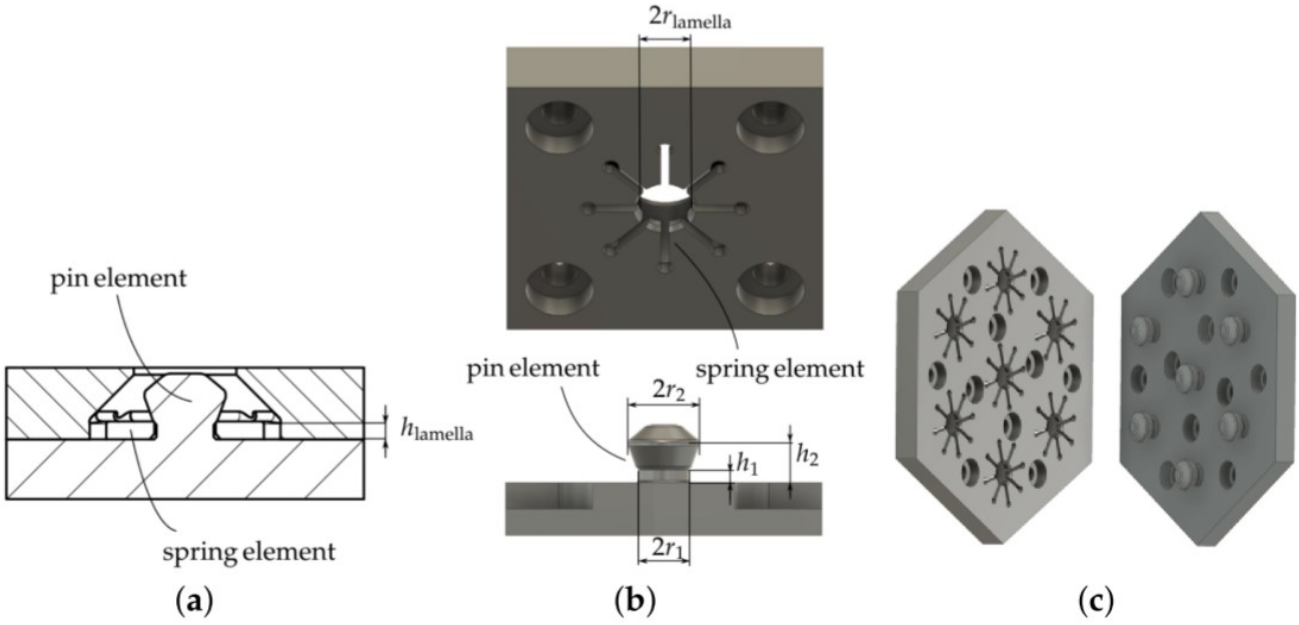

Figure 3.28: Design of the developed ILM: (a) sectional view of individual ILM cell in snapped state; (b) individual ILM mechanism cell in unsnapped state; (c) example of a hexagonal ILM in the unsnapped state. The locking mechanisms are distributed over the full contact surface area. (Gloyer et al., 2023)

3.3.4 Conclusion

Reversible joining systems for modular structures other than glass have also seen a lot of development in recent years. Some key insights can be taken from the other industries:

- **Material-Specific Design:** Systems such as DryStack and ShroomLock demonstrate the importance of tailoring the joining mechanism to the specific properties of the material. For glass structures, a similar approach considering its unique characteristics is essential.
- **AM Potential:** The ShroomLock mechanism shows how AM can be leveraged to create complex yet functional interlocking systems. Furthermore, it demonstrates how strong connections can be achieved while maintaining easy reversibility.
- **Integral Design:** ILMs could potentially be integrated into the glass components themselves, eliminating the need for additional fasteners and reducing potential contamination points.
- **Stress Distribution:** The principle of uniform stress distribution for annular snap-fit joints could be valuable for glass structures, where stress concentration is an important aspect.
- **Scalability and Versatility:** Systems such as DryStack illustrate how interlocking elements can be scaled to accommodate complex geometries, including curved surfaces and intricate patterns.

By adapting principles from these systems and considering the unique properties of glass, it may be possible to create innovative connectors in free-form glass structures. Key information is given in the research of Gloyer et al. (2023), where an ILM is achieved by AM of a TPU. This approach has similarities to the approach of this thesis.

3.4 Potential Materials for AM or injection moulding of an Interlayer in a Freeform Glass Structure

3.4.1 Specifications Needed for an Interlayer of a Freeform Glass Structure

In previous chapters extensively discussed already, an interlayer between glass elements is essential in a modular glass structure. This interlayer accounts for a homogeneous stress distribution and the surface micro asperities of the glass elements (Dimas et al., 2022). Ideally, this interlayer would, in combination with the geometry, also account for the lateral loads on the structure. To achieve circularity, this material should be dry without being permanently adhesive, enabling the system to be disassembled later.

Previous work of Aurik, Snijder, Noteboom, Nijsse, and Louter (2018) focused on the use of PU and PVC interlayers as candidates suitable for such an interlayer. However, their research focus was solely on the mechanical performance of the material. Work by Dimas et al. (2022) revised their design criteria and added to them. They examined the impact their material properties have on the application of an interlocking system. The research presents the process, from fabrication to construction of the assembly, as a chain reaction. The starting point is the choice of the interlayer. The following design and performance criteria for an interlayer material were considered in their research (Table 3.9):

Primary Criteria	**Secondary Criteria**
Ability to be shaped in desired geometry and shape with AM or injection moulding ($d \leq 3$ mm)	Interlocking/connecting ability
Slightly less stiff than glass ($E \leq 50$ GPa)	Optical quality (enhance transparency)
Compressive strength ≥ 2 MPa	Compatible thermal expansion coefficient to glass
Satisfactory creep resistance	Durability: Water, Fire & UV
Tear strength ≥ 34 N/mm	
Enable Circularity	

Table 3.9: Revised Primary and Secondary Criteria (original table from Dimas et al. (2022))

Dimas et al. (2022) categorises the materials considered for dry interlayers in "monomaterials" (polymer, elastomer, and metal) and "hybrid materials" such as metal / foam, laminated PU and soft-core aluminium, as seen in table 3.10. In the next paragraphs, these different materials will be explained and studies by Dimas et al. (2022) will be summarised.

Monomaterials			**Hybrid**		
Polymer	**Elastomer**	**Metal**			
PU, PVC, PETG (Vivak®)	Neoprene, Silicone, PTFE (Teflon)	Lead, Aluminium	Metal foam	Laminated PU	Soft-core aluminium

Table 3.10: Overview of considered materials for dry interlayer by Dimas et al. (2022)

Monomaterials

Polymers

Polymer interlayers are commonly used in laminated glass applications because of their shear strength and compressive capabilities. These materials, including polyvinyl butyral (PVB), ethylene-vinyl acetate (EVA), and ionomers, exhibit viscoelastic properties that allow them to adapt to applied forces. However, this characteristic also makes them susceptible to creep under static loads (Dimas et al., 2022). The research by Aurik et al. (2018) and Oikonomopoulou

et al. (2019) examined polyurethane (PU) and polyvinyl chloride (PVC) interlayers of varying thicknesses under high static loads (480kN and 40kN, respectively). Although PU70 and PU80 showed promise, their deformation did not stabilise during testing, indicating a potential long-term creep failure. It should be noted that the applied loads in these studies resulted in compressive stresses significantly higher than those typically experienced in glass-brick structures. Dimas et al. (2022) investigated PETG (polyethylene terephthalate glycol) sheets, marketed as Vivak®, which offer higher stiffness compared to PVC and PU. However, the results with respect to creep resistance were inconclusive. Comparisons made by Dimas et al. (2022), show that PVC exhibits high strength and shape factors depending on shore hardness, while PU and PETG score well on almost all criteria. It must be noted that PU is much less stiff than glass, and creep resistance is yet to be tested. Furthermore, these polymers offer transparency or translucency, making PU and PETG suitable for various architectural (glass) applications.

Elastomers

Elastomers such as neoprene, silicone, and PTFE (Teflon) are commonly used in architectural glass applications because of their performance under long-term compression. Although these materials have similar compressive strengths, PTFE exhibits the highest shape factor. Neoprene, a flexible and tear-resistant polychloroprene rubber, is preferred in long-term constructions due to its low maintenance requirements. It is often used in glass point fittings to protect glass from direct metal contact. Neoprene's compressive strength and flexibility make it suitable for interlocking geometries, but its creep behaviour in specific thicknesses and shapes requires further investigation, especially for non-perpendicular loading conditions (Oikonomopoulou et al., 2019). Silicone forms a strong bond with glass as a result of its similar composition, but this can lead to glass surface contamination upon removal, which conflictes with the goal of a demountable system. Furthermore, traditional silicone is also prone to creep under compression. However, Dow Silicones Belgium has developed a removable silicone spacer which could potentially solve these problems. Although it has not yet been tested on non-flat surfaces (Hayez, Gubbels, Dow, Belgium, & Bordet, 2019), this thesis research will look into the possibility with talks going on with Dow. PTFE, known for its durability and corrosion resistance, is commonly used in glass fixings. However, its low friction surface could pose challenges in interlocking applications.

Metals

Metals are advantageous as interlayer materials because of their creep resistance at room temperature. However, direct contact between glass and some metals can cause problems. Research indicates that glass directly in contact with steel or titanium may fail prematurely due to cracking. Oikonomopoulou et al. (2015) found that, in a compressive test, the glass blocks directly in contact with steel failed under 20-30 MPa, while the blocks with two 18 mm multiplex plate intermediaries handled loads exceeding 90 MPa, which was the maximum capacity of the hydraulic compression machine. This suggests a compressive strength that is higher than 90 MPa. Similarly, Akerboom (2016) reported early failure when a thin (1 mm) copper interlayer was used. However, not all metals exhibit this problem. In compressive glass experiments, thin sheets of lead and aluminium have been successfully used as intermediaries to distribute stress evenly. These metals have a Young's modulus similar to or lower than glass, allowing them to conform to surface micro-asperities while maintaining compressive strength. The key factor in selecting metals for direct glass contact is their stiffness relative to glass. Stainless steel, being much stiffer than glass, is unsuitable. Aluminium's stiffness is more comparable to that of glass, making it a promising candidate. Lead, while highly malleable and ductile, poses health risks due to its toxicity and is being phased out. Additionally, the thermal expansion coefficient of lead differs significantly from that of glass, potentially causing problems in construction.

Hybrid

Hybrid materials offer a solution to address the limitations of single-material interlayers in glass structures. These composites combine the beneficial properties of different materials to create an interlayer with enhanced performance characteristics. Two notable examples of hybrid

materials are soft-core aluminium and laminated polyurethane (PU). Soft-core aluminium, such as Alucobond®, consists of two aluminium sheets sandwiching a polyethylene core. This structure provides a balance of strength and flexibility, with the softer core improving the response of the interlayer to impact and vibrations. The aluminium outer layers offer durability and protection, while the polyethylene core allows for some deformation to accommodate stress. Mechanical tests done by Bendarma et al. (2025) clearly shows differences in deformation among the two materials during compression at different strain rates. The results highlight the distinctive behaviour of the Alucobond® composite, with each component playing a unique role in the overall mechanical performance. However, shaping this material for interlayer applications may require additional processing, such as bending or pre-forming individual components before assembly. Laminated PU incorporates metal plates within layers of elastomer or polymer. This configuration enhances the stiffness and creep resistance of the interlayer. The metal reinforcement restricts the creep in the elastomer layers, resulting in improved long-term performance under compression. Although this approach offers superior mechanical properties, it introduces additional complexity to the manufacturing process. Multiple layers must be shaped individually and then bonded together, typically using adhesives, to create a unified interlayer component. Both soft-core aluminium and laminated PU demonstrate how hybrid materials can potentially overcome the limitations of single-material interlayers, offering improved performance in composite structures. However, their increased complexity and cost of production must be balanced against this improvement.

Conclusion

These were the suitable materials coming from the research of Dimas et al. (2022): PETG sheet (Vivak), Neoprene, Polyurethane (PU), Laminated Polyurethane (PU), aluminium and Soft-core aluminium interlayer. Each of these materials can be used as an interlayer in glass structures. However, they all function in a different way and require different fabrication techniques, assembly sequences and use. For example, when creep risk is present (in materials PETG (Vivak®), Neoprene, and (Laminated) PU), on-site compression of the entire assembly is necessary to prevent facade settlement caused by the interlayer material. Compressing the glass block wall ensures consistent structural performance of the interlayers and uniform load transfer throughout the assembly. In addition, these interlayers are more prone to buckling, which limits the maximum height of the assembly. Without the risk of creep (in the materials aluminium and soft-core aluminium), the assembly can be taller, supporting a greater load. In conclusion, each of the material requires careful consideration of its unique properties.

To achieve circularity, the material should be dry without being permanently adhesive, enabling the system to be disassembled later. To investigate how these materials can be shaped to be used for AM or cast glass, the next chapter will go into the shaping of the materials with a focus on AM and injection moulding. This chapter will not only look into the materials from the research of Dimas et al. (2022), but will also add Surlyn, PLA and heat-cured silicon. Research by Yost et al. (2025) concludes that this transparent thermoplastic material (Surlyn) achieves a fracture strength that exceeds their glass fracture bearing stress target value of 36.6 MPa. Thus, fractures in glass columns are likely to precede interface issues, suggesting it as a potential interlayer between glass elements. Polylactic Acid (PLA) is a biodegradable thermoplastic derived from renewable resources. It's widely used in AM due to its ease of processing. According to Aloyaydi, Sivasankaran, and Mustafa (2020), printed PLA specimens can reach compression stress of around 66-72 MPa before fracture. Heat-cured silicone is added after talks with Dow Inc. deeming it a possible option.

With these three materials added, the fabrication methods of the following materials will be analysed in the next chapter:

1. PETG sheets (Vivak®)
2. Neoprene

3. Aluminium
4. Soft-core aluminium interlayer
5. Polyurethane (PU)
6. Laminated Polyurethane (PU)
7. Surlyn
8. PLA
9. Silicone

3.4.2 Fabrication Methods of Chosen Materials

1. PETG sheets

PETG (polyethylene terephthalate glycol) sheets, such as Vivak®, offer excellent thermoforming properties and are suitable for various shaping methods. Although laser cutting is possible, saws and routers are more commonly used to cut PETG (Akerboom, 2016). Vacuum forming is considered the most appropriate method for creating complex geometries in PETG sheets, surpassing free blown forming and line bending in terms of precision and versatility (Dimas et al., 2022). Studies done by Dimitescu, Babiş, Fica, Rugescu, and Enache (2023) have explored the potential of AM PETG. In addition to AM, PETG injection moulding has also been successfully implemented in various industries, offering high precision and more scalability. To enhance friction between the interlayer and glass components, sanding of the glossy PETG surface is recommended. Wet sanding techniques can be used to achieve the desired surface texture and maintain the transparent aesthetic (Akerboom, 2016).

2. Neoprene

Neoprene is a synthetic rubber which is known for its flexibility and durability. Typically, it is produced in sheets and shaped through industrial die-cutting or laser-cutting processes. For use as an interlayer in glass structures, neoprene sheets are cut to the desired dimensions and rely on compression to conform to complex geometries on-site (Dimas et al., 2022). The material's thickness plays a crucial role in its performance; sheets thicker than 3mm tend to be overly stiff, potentially compromising their ability to adapt to double-curved interlocking geometries and reducing the overall assembly stiffness. Although not as common as sheet production, injection moulding of neoprene is possible and can offer advantages in creating complex shapes with high precision. Neoprene is a form of synthetic rubber, which resists melting and instead burns when reheated. This makes it unsuitable for AM. Effective AM requires a material to fluidize controllably, a property that rubber does not possess. However, other rubber-like materials, like thermoplastic polyurethane (TPU), can be used for fused deposition modelling.

3. Aluminium

Mainly, aluminium can be shaped by press-forming and hydroforming. Press forming, specifically cold stamping, offers rapid production, but requires male and female moulds (Dimas et al., 2022). Hydroforming utilises fluid pressure to shape aluminium, resulting in fewer abrasions, superior surface finishes, and the need for only one mould. For aluminium interlayers, a minimum thickness of 2 mm is recommended to account for glass block microasperities while maintaining the inherent creep resistance of the material (Dimas et al., 2022). While press forming and hydroforming are established methods for shaping aluminium, advancements in AM have also made it possible to AM aluminium parts. Selective Laser Melting (SLM) and Direct Metal Laser Sintering (DMLS) can produce complex aluminium geometries with high precision. However, these methods are generally more expensive and time-consuming than traditional forming techniques for simple geometries such as interlayers. In the scope of this thesis research, aluminium cold forming appears to be the optimal method for this material.

4. Soft-core aluminium interlayer

Soft-core aluminium composites, such as Alucobond®, are a hybrid option. These typically consist of polymer panels bonded to aluminium sheets using adhesive films. While traditionally produced as flat sheets, press forming can achieve desired geometries. For a reversible alternative, mechanical fastening methods like flush rivets or ring snaps could be employed, though this approach requires more intensive labor (Dimas et al., 2022). The thickness of soft-core aluminium interlayers should be carefully considered to balance rigidity and creep resistance. A total thickness of 3mm, comprising two 0.5mm aluminium sheets and a 2mm soft core, is proposed as an optimal configuration.

5. Polyurethane (PU)

For research done by Oikonomopoulou et al. (2019) a dry interlayer made of PU was mechanically tested. To cast each polyurethane (PU) resin, a two-piece AM mould made from polylactic acid (PLA) was used. This ensured a uniform 3mm thick interlayer that conformed to the blocks' osteomorphic geometry used in their research. Each sample was manually poured into the mould and allowed to cure for 24 hours before being extracted. This is a tested way of manufacturing a PU, but AM of PU has since also become possible. Polyurethanes can be utilised as thermoplastics (TPUs) used in filament (FDM) and fine powder forms (SLS) Gantrade, n.d.. This way more design freedom is possible with PU's.

6. Laminated Polyurethane (PU)

Laminated PU interlayers consist of three layers: two PU sheets sandwiching an aluminium core. The manufacturing process involves shaping each layer separately, with PU typically formed through injection moulding (Dimas et al., 2022) or casting (Oikonomopoulou et al., 2019). To ensure proper adhesion, the aluminium surface requires careful preparation, including degreasing, abrasive blasting, and applying a chemical primer. However, the use of adhesives compromises the recyclability. An alternative, reversible bonding method involves casting PU into a mould containing a pre-shaped, perforated aluminium layer. This allows the PU to flow through the holes, encapsulating the aluminium without adhering to it, enabling future separation and recycling (Dimas et al., 2022). Based on previous research, a total thickness of 5mm is recommended, comprising two 2 mm PU layers and a 1 mm aluminium core.

7. Surlyn

Surlyn is a transparent thermoplastic material that has been used for many years in packaging, prosthetics, and sports equipment. It can be processed using extrusions or injection moulding to create various shapes or sheets. Yost et al. (2025) used Surlyn Grade 8940 sheets resized for mechanical testing, with a thickness of 3.175 mm and produced by DOW Corporation. For Surlyn Grade 8940, common material properties include a Shore D hardness of 65, a flexural modulus of 350 MPa at room temperature, a tensile strength of 15 MPa at yield, and 33 MPa at break, with a melting point of 94 °C. Peng, Zhao, Xia, Cakmak, and Vogt (2018) found co-extrusion in AM of a PolyCarbonate (PC) (45%) core and a Surlyn (55%) shell could reach a higher toughness and improved synergy between PC and Surlyn compared to pure PC and other blends, see figure 3.29.

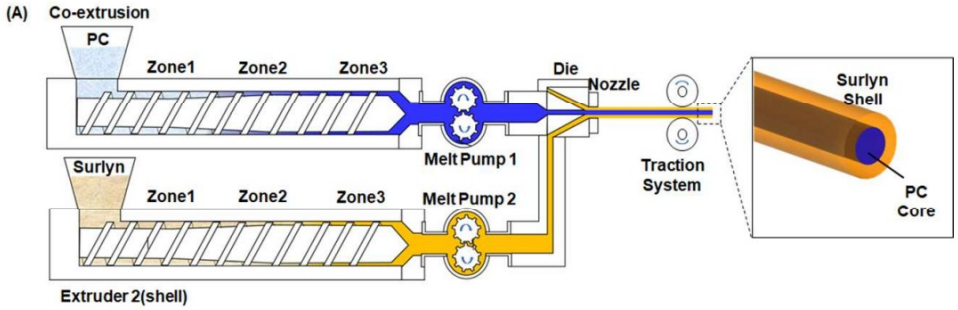

Figure 3.29: Schematic representation of coextrusion process to formulate core–shell structured PC/Surlyn filaments for AM, (Peng et al., 2018)

8. PLA

Polylactic Acid (PLA) is a biodegradable thermoplastic derived from renewable sources such as corn starch or sugarcane. It is widely used in additive manufacturing due to its ease of processing and favourable mechanical performance. PLA can be fabricated using both AM and injection moulding. Although AM PLA parts are known to exhibit anisotropy due to the raster pattern and layer bonding, printing parameters can be optimised to enhance mechanical strength. For instance, grid-patterned PLA produced via FDM has shown compressive strengths up to 72 MPa (Aloyaydi et al., 2020), demonstrating its potential for the load-bearing interlayer. Injection moulding of PLA, on the other hand, offers isotropic material behavior and higher surface quality, making it advantageous for serial production where geometric customisation is less critical.

9. Silicone

Silicone has a consistency very similar to that of glass (silicon dioxide), meaning when in contact with glass as it cures, a very strong bond can be formed. The removal of silicone typically results in contamination of the glass surface. Furthermore, silicones are susceptible to creeping under compression. However, Dow has introduced a novel, two-component condensation-cure technology that allows silicone materials to cure in bulk within several days at ambient temperature. This curing system can be designed without the addition of fillers, resulting in crystal-clear materials (see Figure 3.30; however, the lack of fillers leads to reduced material strength (Hayez et al., 2019). While injection moulding, compression moulding, or casting is currently the most common way to shape silicone. AM has also become possible with silicone 3D printers that can print with 100% pure silicone materials by SLA printing.

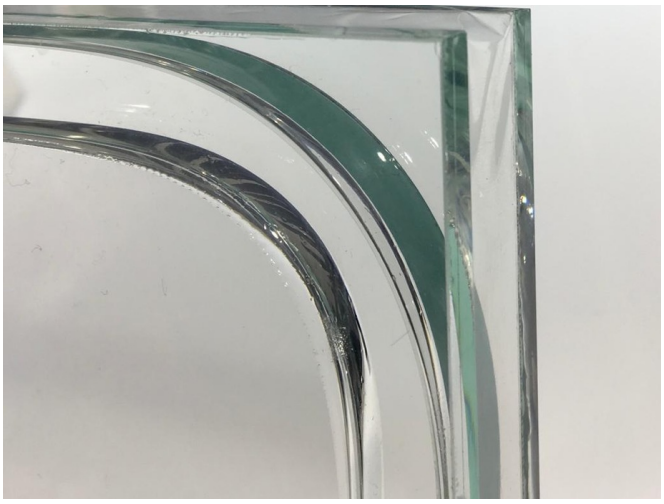

Figure 3.30: Flexible, transparent moulded silicone adhering on glass post cure, *credits: Matthias Rehberger*

Conclusion

Table 3.11 shows a summary of the materials discussed in previous paragraphs. The table combines the compatibility of the material with injection moulding and AM with the most important criteria the materials have to achieve. The interlayer must exhibit lower elastic deformation resistance than glass to accommodate surface irregularities; hence, a lower Young's Modulus is crucial. Insufficient hardness results in easy penetration, risking glass-on-glass contact and creep, whereas excessive hardness prevents the interlayer from conforming to the glass's microstructure, causing uneven load distribution and concentrated contact zones. Hardness is measured on a Shore hardness scale (see Figure 3.31), Shore A and Shore D are the most commonly used in the rubber and plastics industry. Shore A scale is used for softer materials, including soft rubbers, elastomers, and softer plastics. Shore D Scale is used for harder materials, such as rigid plastics and harder rubbers. The research by Oikonomopoulou, Bristogianni, Barou, Jacobs, et al. (2018b) categorises PU with Shore A70 hardness as the optimal material as an interlayer; therefore, this research will aim for a material with a shore hardness of A60-A95 and D10-D40.

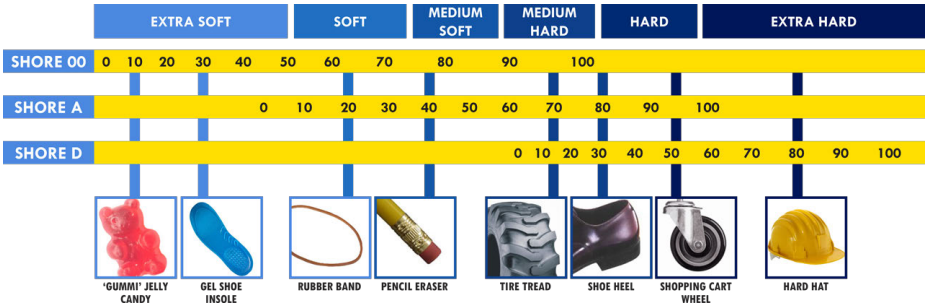

Figure 3.31: Table of Shore hardness (*image credits: Smooth-on*)

Three materials adhere to all four of the criteria, which are PETG, Surlyn and PLA. According to Yost et al. (2025), Surlyn is a proper interlayer material in between glass components. This, in combination with its AM and injection moulding compatability makes it one of the favoured materials. Next, PETG, is a more widely tested polymer and more familiar in the AM world. However, its creep resistance is still to be tested. PLA is a biodegradable material which has a very high process ability and good mechanical features. Due to its biodegradability, its long term abilities could form an issue in a structural application. Another material compatible with injection moulding and AM is Polyurethane (PU), however its stiffness is much less than that of

glass. The last material is Silicone, another material with a lower stiffness and low hardness. Nevertheless because of talks with Dow Inc. and their innovative ways of curing and treating silicone, this material will be taken into account in this thesis research. Because the other materials from the table are not compatible with the two manufacturing methods, they will be excluded from this research. Because of the research by Oikonomopoulou, Bristogianni, Barou, Jacobs, et al. (2018b), 3 mm PU70 will be used as a test material for PU. To reach this same shore hardness of the PU70, the research will use PETG with a 95 Shore A hardness. As used in the research of Yost et al. (2025), Surlyn Grade 8940 will be used, even though its shore hardness is Shore D 65, which is above the upper limit. Marketed silicone has a low shore hardness and is likely to be penetrated by the glass block. Some silicones on the market reach a Shore hardness of A60, which will be the researched silicone subject.

Material	Common Forming Method	Injection Mould Compatability	AM Compatibility	Correct hardness	Slightly Less Stiff than Glass ($E \leq 50$ GPa)
PETG sheets	Vacuum forming	+	+	+	+
Neoprene	Shaped by compressing sheets onto geometry	±	-	+	-
Aluminium	Press-forming and Hydroforming	-	±	+	+
Soft-core aluminium interlayer	Press-forming, Hydro-forming, bonding to Polymer panels	-	-	+	+
Polyurethane (PU)	Injection molding, Press forming / Hydroforming	+	+	±	-
Laminated Polyurethane (PU)	PU forming, aluminium forming, bonding	±	±	+	±
Surlyn	Sheet extrusion or injection moulding	+	+	±	+
PLA	FDM	+	+	+	+
Silicone	Injection moulding, compression moulding, or casting	+	+	-	-

Table 3.11: Comparison of Material Properties, Forming Methods, and Manufacturing Compatibilities

3.4.3 AM Techniques to Enhance Interlayer-Glass Interface

Printing on Thin Glass for Enhanced Strength

Pfarr and Louter (2022) discusses an approach to creating digitally manufactured thin glass composite façade panels, which could be relevant to optimising interlayer strength and polymer-glass connections. The researchers created a composite panel with thin glass sheets attached to a 3D-printed open-cell polymer core, optimising strength while keeping it rigid and lightweight.

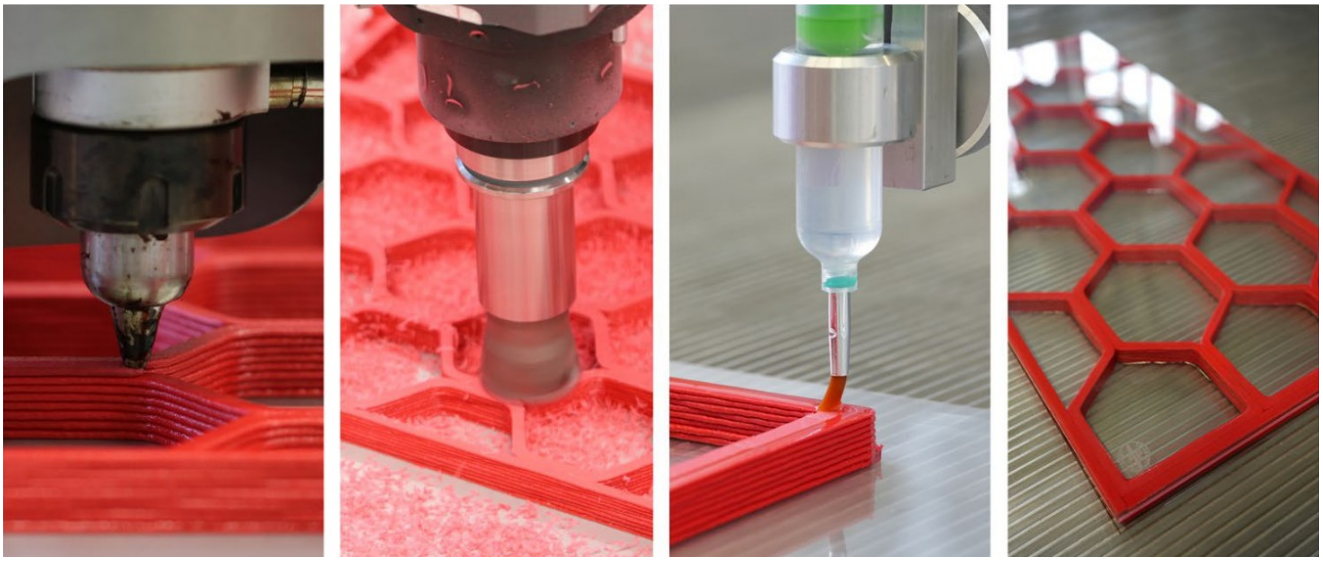

Figure 3.32: Substeps of the robotic manufacturing process of a thin glass composite panel from left to right: additive manufacturing, surface preparation, application of the adhesive and assembly with glass (Pfarr & Louter, 2022).

In choosing the polymer, numerous thermoplastic options are available for the extrusion process. Polycarbonate (PC) is attractive due to its heat and UV resistance and high rigidity. However, given the extra technical and financial demands of processing PC, glycol-modified polyethylene terephthalate (PETG) is being used for creating the initial prototypes.

For connecting the polymer to the glass, Pfarr and Louter (2022) employed a UV-curing acrylate adhesive (Loctite® AA 3345™). They found that mechanical surface preparation of the 3D-printed polymer core improved the adhesive bonding strength (Figure 3.32). Specifically, milling the core surface after printing resulted in higher tensile and shear strengths in the polymer-glass connections. The following techniques for creating an interlayer for free-form glass structures can be taken from this research:

1. The use of optimised cellular fill patterns, like a hexagonal, for 3D-printed interlayers could enhance structural performance.
2. Mechanical surface preparation of 3D-printed components can significantly improve adhesive bonding strength with glass.

Printing on Float Glass, Expanding AM Glass Surfaces for Enhanced Connectivity

AM of glass is a promising technique for using glass as a structural component. However, the surface area of the bottom and top of an AM glass component is limited to the width of the extrusion. This leads to difficulties in connecting components to be used in architectural applications. Stern et al. (2024) demonstrated an innovative way to increase this surface area to allow stronger connections. The researchers successfully AM glass directly onto float glass sheets with varying thicknesses (3.2, 6.4, and 9.5 mm) using the G3DP3 printer. The process involves preheating the float glass sheet on a ceramic build plate to just above its annealing temperature, ensuring stability during printing. The G3DP3's standard printing process is then executed with a vertical offset to account for the sheet thickness. This method enables the rapid

production of 2.5D structures, often referred to as "rib on plate" structures. These structures are relatively lightweight and stiff compared to solid slabs of the same material.

Stern et al. (2024) explored two design applications, the first one is a tapered hexagonal extrusion (Figure 3.33) which mainly served as a proof of concept and provided insights into the interaction between the printed material and the sheet glass. Apart from printing on Pilkington Optifloat, which was the same as used as feedstock, tests were conducted on other Pilkington products with varying high temperature coatings.

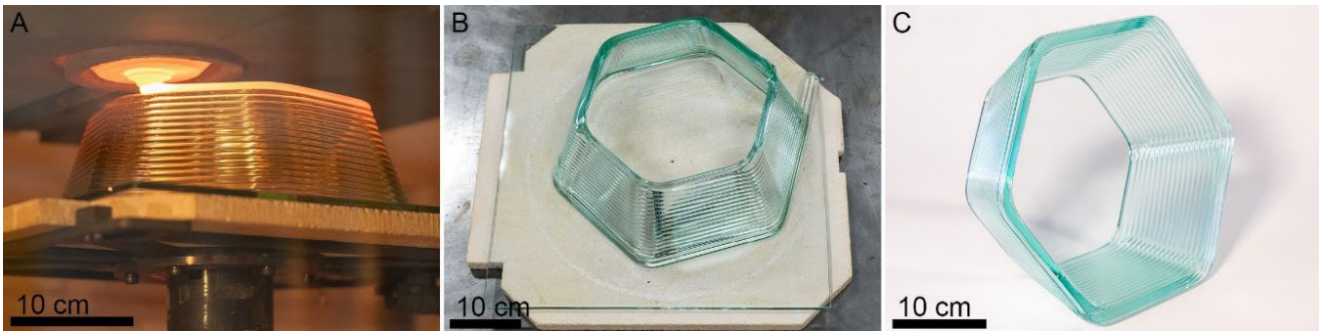

Figure 3.33: Hexagon form printed on Optifloat float glass A) Molten Printing B) After Anneal C) After cold processing. (Stern et al., 2024).

The second design explored was a cellular fill pattern optimised for glass printing (3.34). This structure was inspired by the glass-thermoplastic composite generated by Pfarr and Louter (2022) (Figure 3.32). The form featured gentle curvatures and was optimised to add stiffening to large glass panels. The success of both of these designs indicates that the remelted and printed glass maintains good thermal expansion compatibility with the base sheet glass.

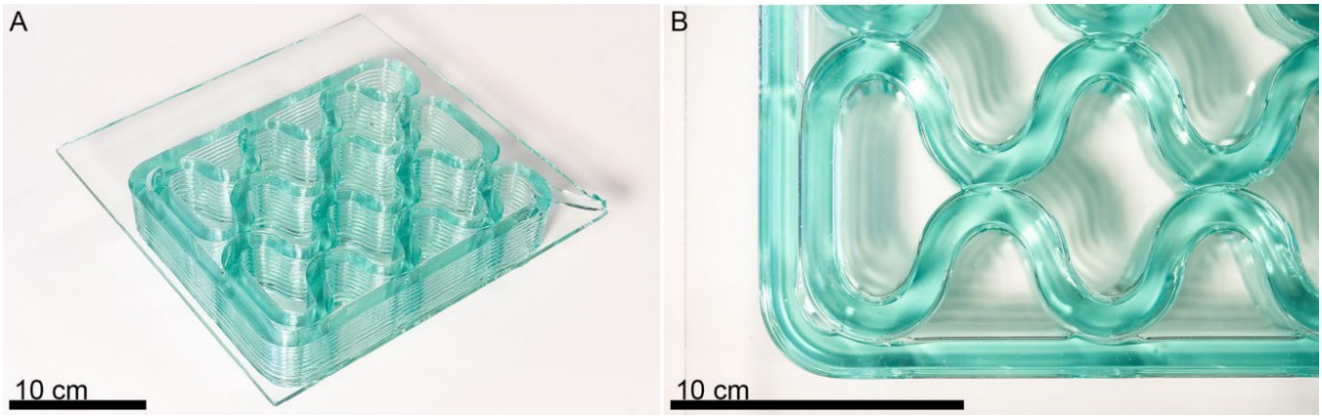

Figure 3.34: A) Cellular fill printed on 6.4 mm Optifloat float glass B) Detail view of extruded glass fusion between adjacent beads (Stern et al., 2024).

The ability to print directly onto float glass expands the design possibilities for modular, free-form glass structures. It allows for the creation of larger surface areas with integrated connection points, potentially simplifying assembly and improving load distribution between components. The successful printing on both uncoated and high-temperature coated float glass suggests broad applicability of this technique.

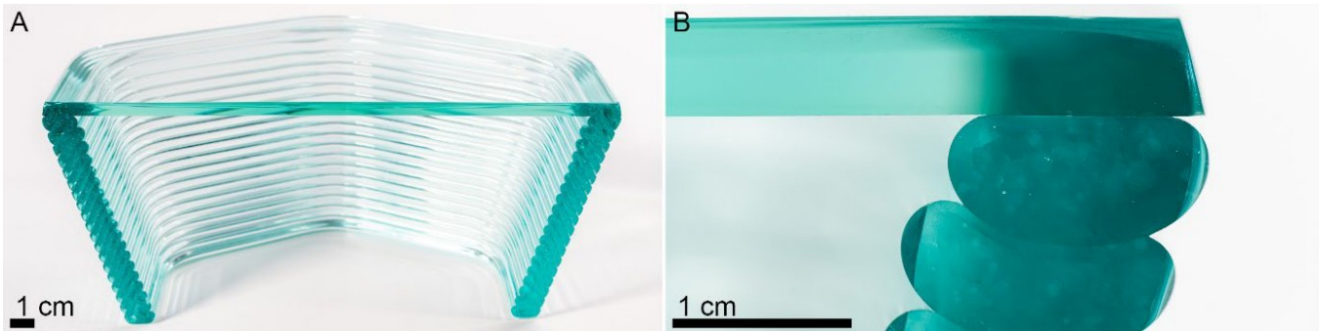

Figure 3.35: A) Cross section of printed float glass on 6.4mm Optifloat B) Detail view of fusion between float sheet glass and extruded glass as well as extruded glass and extruded glass. (Stern et al., 2024).

Further research is needed to fully characterise the strength of the bond between the printed glass and the sheet glass substrate. The cross-section seen in 3.35) reveals promising fusion between layers, but structural testing is required before implementing this technique at a larger scale.

3.5 Interface Optimisation

To ensure a structurally sound and reversible connection between glass components and the interlayer, the interface must be carefully designed and optimised. The following section addresses this through three key aspects: the geometric design of (glass) interlocks, surface treatment strategies to enhance adhesion, and emerging (de)bonding mechanisms.

3.5.1 Geometric Considerations for Interlocking Designs

Interlocking design systems already exist within other materials, like stone and plastics (see Chapter 3.3). Since systems like this have been designed with various other manufacturing and material characteristics in mind, it would not make sense to modify the same geometries for glass. Therefore, Oikonomopoulou, Bristogianni, Barou, Jacobs, et al. (2018a) created a set of design criteria specifically for cast glass components, considering the principles of current interlocking systems but adjusted to accommodate the unique features and properties of cast glass as a building material.

1. **Movement Confinement**: The interlocking mechanism should restrict movement in both longitudinal and transverse directions to enhance monolithic behavior and ensure structural stiffness against lateral forces.
2. **Smooth Convex Curvatures**: Interlocks with smooth convex shapes are preferred as they allow for more even distribution of shear forces at the interface area. This is particularly important because of the brittle nature of glass.
3. **Self-Alignment**: The geometry should promote self-alignment of the components during assembly.
4. **Optimised shear capacity**: The interlocking shape should be designed to optimise the shear capacity of the connection.
5. **Avoid Small Cross-Sectional Connectors**: Traditional connectors or keys with significantly smaller cross-sectional areas compared to the overall component should be avoided, as they can lead to stress concentrations and premature failure.
6. **Limited Number of Different Units**: Using repetitive geometry simplifies production and assembly, reducing manufacturing costs.

Interlock 1: Osteomorphic Shaped Glass Blocks

Osteomorphic-inspired geometries are characterised by non-planar concave-convex surfaces, offering several advantages for structural assemblies. The engineered shape facilitates full contact between adjacent elements; this promotes homogeneous load distribution while also restricting relative movements in both axial and transverse directions (Oikonomopoulou, Bristogianni, Barou, Jacobs, et al., 2018b). A key feature of this design is its symmetry in planar directions, allowing components to be placed either parallel or rotated 90 degrees relative to adjacent pieces. This flexibility simplifies corner construction using a single block unit.

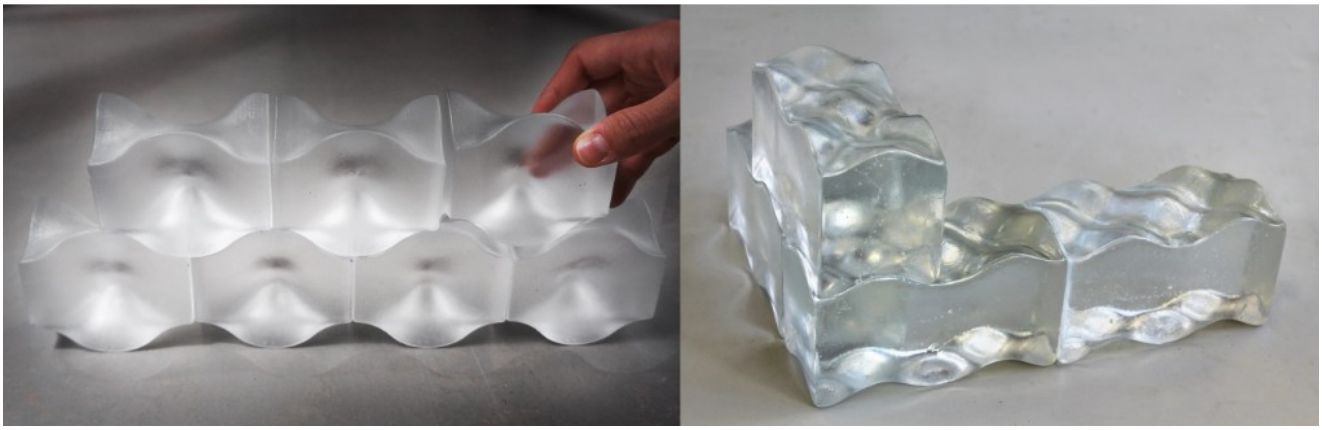

Figure 3.36: Symmetry in planar directions of osteomorphic shaped bricks (Oikonomopoulou, Bristogianni, Barou, Jacobs, et al., 2018b)

The smooth and curved surfaces of osteomorphic designs could address geometric considerations for glass structures addressed in the preceding paragraph. As seen in Figure 3.37b, Oikonomopoulou, Bristogianni, Barou, Jacobs, et al. (2018b) casted osteomorphic shaped glass units. Recent developments in AM of glass have seen the AM of these osteomorphic shaped components by Evenline (see Figure 3.37a). This confirms the possibility of this shape not only being cast, but also AM. However, the anisotropy of the printed unit has to be taken into account as no mechanical tests have yet been done on this particular axis. Mechanical test done by Massimino et al. (2024) for example, tested the AM unit on its y-axis. To use this AM osteomorphic brick in compression along its x- or z-axis, new tests have to be done.

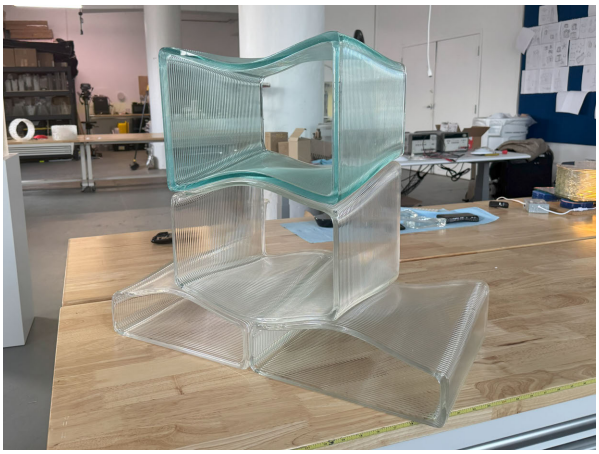

(a) AM, osteomorphic brick, *by Evenline*

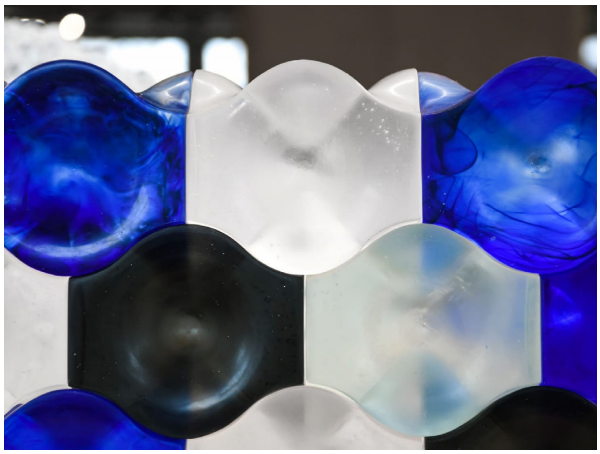

(b) Osteomorphic shaped cast glass structure, by TU Delft

Figure 3.37: Osteomorphic shaped glass structures

Interlock 2: Peanut Interlock by Daniel Massimo

The case study of Massimino et al. (2024) addresses the key criteria for interlocking designs. The design restricts movement in multiple directions, enhancing structural integrity. Furthermore, interlocking features facilitate self-alignment during assembly, while the overall geometry optimises shear capacity. By integrating the interlocking elements into the main body of the units, the design avoids small cross-sectional connectors that could lead to premature failure. Furthermore, the study demonstrates the feasibility of producing these complex geometries using glass AM, showing the potential to efficiently create a limited number of different unit types.

Figure 3.38: AM of interlocking glass masonry units, (Massimino et al., 2024)

Conclusion

In developing the the interlocking shape, several factors and criteria must be considered. Osteomorphic shaped glass components are very promising as they thick of all of the above mentioned criteria. Another example of a promising solution could be the interlocking glass masonry units by Massimino et al. (2024). Although they do not have a smooth convex surface, the repetitiveness and scalability of the AM components are encouraging.

3.5.2 Surface treatments for enhanced adhesion

Introduction

The selection of an appropriate adhesive is crucial when bonding materials with low surface energy, as these materials present significant adhesion challenges. Surface energy, defined as the excess energy on the surface of a material compared to its bulk, plays a pivotal role in determining the bondability of the material (Packham, 2003).

Adhesion Strength

Adhesive strength refers to the interfacial bond between an adhesive and a substrate. It is a critical factor in the creation of strong adhesive assemblies. However, even the strongest adhesive will fail if it is unable to properly bond to the substrate surface.

Cohesive Strength

Cohesive strength is the internal ability of an adhesive to resist stress and maintain its structure. This property, determined by the chemical composition of the adhesive, significantly impacts overall performance. Adhesives vary in cohesive strength, ranging from pressure-sensitive adhesives to structural epoxies and acrylics.

Substrate Surface Energy

Surface energy is a material property that defines how well an adhesive can spread and bond. It is measured with a dyne level, which is expressed in dynes per centimetre. It indicates how well liquids will wet or adhere to a surface. Increased dyne levels indicate improved wettability and adhesion, which are important for processes such as printing, coating, and bonding. In contrast, low-surface-energy materials resist wetting, leading to weaker adhesion (see Figure 3.39). Understanding the surface energy of all substrates in an assembly and ensuring adequate cleanliness are essential for optimal bonding. For example, glass has a Surface Energy of 200-300 Dynes/cm and Polyurethane that of 38 Dynes/cm (*Changing Surface Properties for Better Adhesion | 3M Science of Adhesion Educational Series*, n.d.).

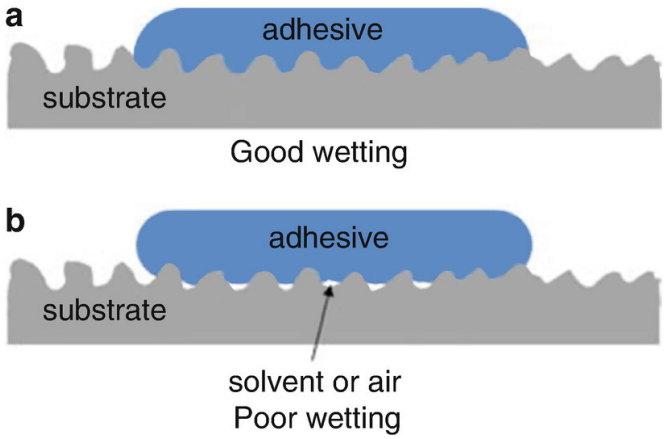

Figure 3.39: Better bonding with good wetting, (*image credits: adhesives.org*)

Changing Surface Properties for Better Adhesion

When bonding a material with low surface energy presents a challenge, choosing the right adhesive becomes crucial. Techniques to enhance the surface energy can significantly improve bonding capability. Fortunately, various methods are available to enhance surface energy, thus improving adhesion.

Priming

Primers enhance adhesion by applying a thin coating of functional molecules to the substrate surface. These molecules are designed to bond strongly to low-energy surfaces on one end and to adhesives on the other, improving compatibility and bond strength.

Plasma Treating

Plasma treatments expose the substrate to ionized gases, altering the surface's chemical reactivity. This method is versatile and widely used across industries to improve bonding on various materials.

Flame Treating

Flame treatment modifies the substrate's surface chemistry using the combustion process of a flame. Like plasma treatments, it enhances surface reactivity and is a common method for improving adhesion in industrial applications.

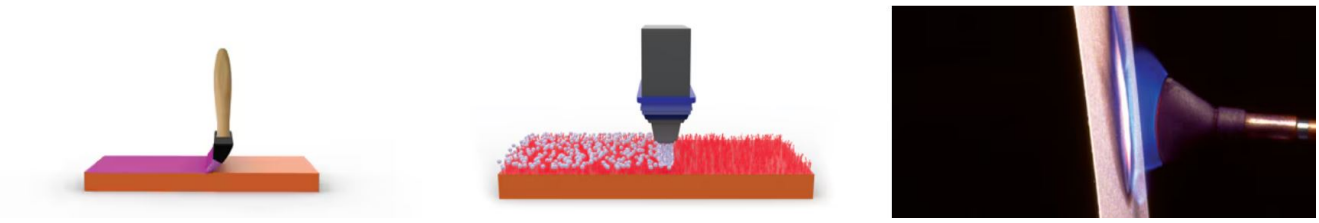

Figure 3.40: Chaning Surface Properties, from left to right: Priming, Plasma Treating, Flame Treating (*Changing Surface Properties for Better Adhesion | 3M Science of Adhesion Educational Series*, n.d.)

Surface Cleanliness

Surfaces to be bonded are often contaminated with substances like dust, oils, grease, or mold release agents (see Figure 3.41). These contaminants reduce adhesion by limiting contact, preventing wetting, and weakening the bond. Proper surface cleaning is vital to ensure reliable adhesion.

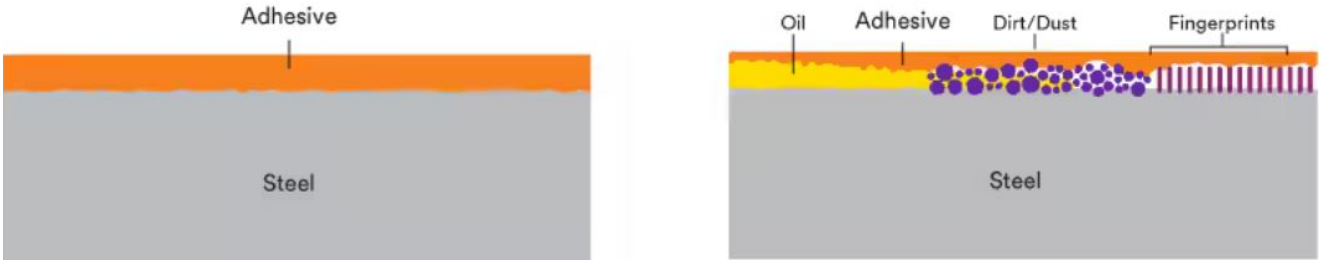

Figure 3.41: Cleanliness of the Surface, *Changing Surface Properties for Better Adhesion | 3M Science of Adhesion Educational Series*, n.d.

Abrasion

In cases where cleaning alone is not sufficient, abrasion may be required to remove contaminants such as mould release agents (after injection moulding), oxide layers, or industrial oils. Abrasion also improves bond strength by increasing surface roughness. The process typically involves the following:

1. **Initial Cleaning:** Removes loose debris to prevent smearing during abrasion.
2. **Abrasion:** Uses abrasive paper or pads to remove contaminants and create surface roughness.
3. **Final Cleaning:** Clears residual debris, leaving a clean surface for bonding.

By combining proper cleaning, surface modification, and abrasion techniques, stronger and more durable adhesive bonds can be achieved.

3.5.3 (de)Bonding Mechanisms (or adhesives)

Debondable adhesives have the characteristics to hold materials together but can be easily disconnected when needed. These, still in research, adhesives could potentially transform industries by creating reversible bonds. This could enhance product recyclability, facilitate repairs, and reclaim valuable materials at the end of a product's useful life. Under normal conditions, they maintain strong adhesion. However, when exposed to specific external triggers, they undergo a transformation, releasing their grip without damaging the bonded surfaces in typically 1 to 100 minutes (Mulcahy, Kilpatrick, Harper, Walton, & Abbott, 2022). This unique property stems from their engineered molecular structure, which responds to various stimuli (see Figure 3.42):

- **Magnetic Forces:** Interacts with embedded magnetic particles.

- **Ultrasonic Vibrations:** Disrupts intermolecular forces at the bond interface.
- **UV Light:** Prompts photochemical reactions, altering bond strength.
- **Chemical Agents:** Catalyzes specific debonding reactions.
- **Thermal Energy:** Initiates phase transitions or activates heat-sensitive components.
- **Electric Fields:** Excites conductive elements, weakening adhesion.
- **Microwave Radiation:** Causes localised heating, inducing separation.

The choice of trigger mechanism is tailored to the specific application, considering factors such as environmental conditions and desired debonding kinetics. This versatility makes debondable adhesives a powerful tool. Highly specific stimuli minimise the risk of exposure during the product's lifespan, which could otherwise cause debonding failures. Another example of minimising this risk is to use two different stimuli at once to evoke the debonding reaction. *DEBONDING ON DEMAND* (n.d.) created an adhesively bonded joint that detaches when heating the joint to 65 ° C while simultaneously applying a direct current of 48 V.

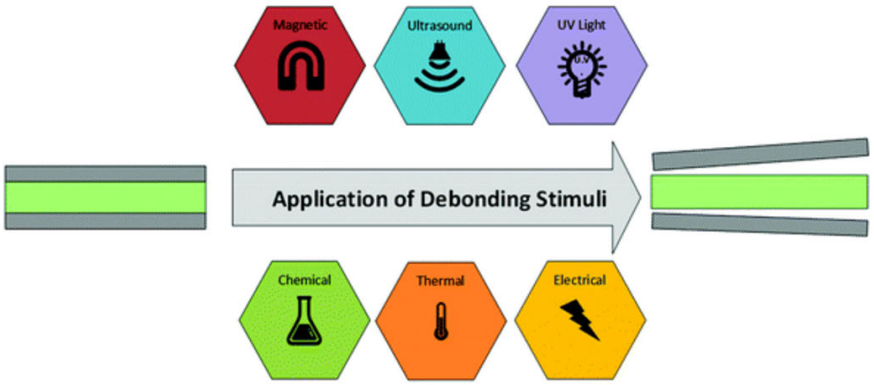

Figure 3.42: Adhesive Debonding, (Mulcahy et al., 2022)

3.6 Towards a 3D-printed dry assembly system for modular freeform glass structures

The literature review conducted for this thesis has provided valuable insights into the development of reversible connections between freeform glass components using Additive Manufactured (AM) or injection-moulded interlayers. This research is crucial for advancing sustainable and adaptable glass structures in architecture and engineering.

3.6.1 Most Promising Materials

Based on the reviewed literature and the criteria set up by Dimas et al. (2022), the most promising materials for AM or injection-moulded interlayers in glass structures are mentioned below. Because of the research by Pfarr and Louter (2022), where they opt for the use of Polycarbonate (PC) as an interlayer material between thin glass sheets, PC is considered. After checking the characteristics with 'Granta EduPack 2024R2', PC will be taken into account in this thesis research. Further testing should focus on these materials to determine their specific performance in reversible glass connections:

1. Polyethylene terephthalate glycol (PETG), 95 Shore A hardness, 3mm
2. Polyurethane (PU), 70 Shore A hardness, 3mm
3. Surlyn Grade 8940 (ionomer), 65 Shore D hardness, 3mm
4. Silicone, 60 Shore A hardness, 3mm
5. PLA, 80 Shore A hardness, 3mm
6. Polycarbonate (PC), 80 Shore D harness (high), 3mm

These materials have shown potential for creating reversible interlayer connections while maintaining structural integrity. Specifically, PU, PLA and PETG stand out due to their favourable mechanical properties and compatibility with glass. The hardness of these materials varies, with PU typically ranging from Shore A 70 to 95, PETG from Shore A 85 to 95, PC from D 70-80, PLA from D 60-90, Surlyn around Shore D 65 and silicon having a lower hardness in the range of Shore A 40 to 60. Because the Shore hardnesses of these materials differ quite a lot, more research and experimenting with these materials has to be done to get a better image of the materials that will be used in the final prototype.

3.6.2 Key Findings

The literature review has revealed several key findings that address the main problem statement and sub-questions:

Additive Manufacturing of Glass

The process creates 100% recyclable glass components due to the inherent connection achieved through melting and annealing. This method enables the creation of **interlocking glass masonry** units without the need for contaminating adhesives, which typically hinder recyclability. The use of masonry units in AM glass structures provides redundancy similar to laminated glass panes, where the failure of one component does not critically impact the entire structure. Currently, the **maximum print area** for AM glass (using the G3DP3 printer is limited to 325 × 325 × 380 mm, which is suitable for the scale of a glass masonry unit. A significant consideration in AM glass is its **anisotropy**. For example, strength can differ by approximately 40% between the major and minor axes. When designing and experimenting with different geometries, this has to be taken into account. Furthermore, during mechanical tests, cracks were observed to halt at layer boundaries as the load intensified, suggesting another degree of anisotropy in the printed layers.

Geometry Considerations

Innovative geometries have been explored to enhance the performance of glass structures. **Osteomorphic-shaped blocks**, featuring non-planar concave-convex surfaces, interlock in both planar directions. The smooth curves of these geometries minimise stress concentrations compared to conventional interlocking connectors. Numerical modeling has shown that osteomorphic-shaped blocks exhibit a high shear capacity and thus provide lateral stability and prevent relative movements between adjacent units. These characteristics show promise for this research on interlocking free-form glass structures. This geometry has not only been casted in glass but also has seen its AM variant recently. However, as can be seen in Figure 3.37a, these bricks carry the loads on their x-axis (contrary to the conventional y-axis), deeming mechanical tests necessary to proceed with this rotated AM shape. Another promising geometry is the **'peanut interlock'** by Massimino et al. (2024), a figure eight interlocking glass masonry unit. They explored three manufacturing methods for these units: Fully Hollow (FH), Print-Cast (PC), and Fully Printed (FP). Among these, the FH units demonstrated the highest load-bearing capacity, shortest production time, and most accurate and repeatable manufacturing process. However, FH units would require a separate interlocking component to assemble the bricks. An option to create an interlock and a larger surface area could be the printing directly on float glass, as done by Stern et al. (2024). This would create an extra inherent bond to the same material by bringing the float glass to annealing temperature and then directly AM on top of the float pane.

Interface Design

The interface between the glass component and the interlayer material is critical for structural integrity and ease of disassembly. Connecting glass to a polymer might be challenging, as most polymers have a low surface energy. **Surface treatments** such as priming, plasma activation, or flame treating can enhance surface energy and thus adhesion between glass and polymeric materials. Abrasion of the polymer can also remove contaminents and increase the bond strength by increasing the surface roughness. In addition, the use of **mechanical interlocking features** at the interface can improve load transfer and facilitate disassembly. Examples of this are snap-fit joints, interlocking elements and Interlocking Metasurfaces (ILMs). **ILMs** show particular promise as an effective interface design. ILMs act in an almost continuous manner across a surface, enabling the joining of complex shapes. They can be fabricated from the same material as the base components, allowing them to withstand similar thermal and chemical exposures. One of the key advantages of ILMs is their non-permanent nature and its way of supporting forces across a surface rather than at a joint. The design space for ILMs is extensive, covering a wide spectrum of topologies, including sliding actions, vertical snapping, and curved trajectories or rotational engagements. The 'ShroomLock' mechanism, an ILM designed for extrusion-based AM, 'shows how strong connections can be achieved while maintaining easy reversibility. Potentially, ILMs could be integrated into the glass components themselves, eliminating the need for additional fasteners and reducing potential contamination points. This approach could advance the development of structural and reversible connections in glass structures.

3.6.3 Research Directions

To fully address the research questions and develop a viable reversible connection system for free-form glass components, the following areas require further investigation:

1. Test if chosen materials are compatible with AM and/or injection moulding of an interlayer geometry.
2. Mechanical testing of the identified materials when either additive manufactured or injection-moulded to conclude on materials (compressive strength, creep resistance, UV resistance, thermal expansion).
3. Testing of adhesion between the interlayer and the glass component and optimise with various surface treatments.

4. Design multiple interlayer and glass component geometries to test and argue on which material/geometry should be AM or injection moulded.
5. Optimisation of the geometry of both the interlayer and glass components for maximum structural efficiency, ease of disassembly and accomodate dimensional production tolerances.
6. Production and mechanical testing of the optimised interlayer designs to determine their performance under different loading conditions.
7. Validation of the system using a case study.
8. Design of the prototype to showcase feasibility.
9. Final optimisation and validation testing of the prototype design.

3.6.4 Conclusion

The literature review presents several insights into the development of reversible connections between free-form glass components using Additive Manufactured (AM) or injection-moulded interlayers. The materials presented in 3.6.1 have demonstrated the potential to create reversible connections while maintaining structural integrity, with PU, PLA and PETG exhibiting the strongest potential due to their favourable mechanical properties and compatibility with glass. The key findings of the review highlight the importance of material selection, geometry optimisation, and interface design in the development of effective reversible connections. The anisotropic nature of AM glass, the potential of innovative geometries such as osteomorphic shapes, and the possibilities of Interlocking Metasurfaces (ILMs) for interface design are particularly noteworthy. To fully realise the potential of these materials and techniques, further research will be done in certain areas. These include mechanical testing of identified materials, optimisation of adhesion between interlayers and glass components, and design and testing of various interlayer-glass geometries. Shear and compression performance studies will draw a conclusion and ensure reliability of these innovative connection systems. Finally the prototype is designed, optimised, and validated to showcase the feasibility of the project.

4
Experimental Works

4.1 Polymer-Glass Compatibility

4.1.1 Experiment Objective and Set-up

To achieve a mechanical interlayer between AM glass units, the chosen polymer must be compatible with glass, not only mechanically, but also in terms of adhesion. Ideally, the polymer would stick to the glass without the use of an adhesive. Experimental works have been done to test the adhesion of multiple different AM polymers to waterjet cut glass samples (100 mm x 100 mm). In the experiments conducted, several key factors influencing adhesion between 3D-printed materials and glass were examined:

1. **Glass Cleanliness**
   To ensure optimal adhesion, all glass surfaces were thoroughly cleaned using isopropyl alcohol, followed by drying with high-quality kitchen paper. This method removed contaminants while minimising residues. Caution was taken to prevent fingerprints, which could compromise adhesion.
2. **Glass Roughness**
   Surface roughness was explored as a means of enhancing adhesion. Fine sandpaper (100 and 120 grit) was used to create a scratched texture in two different directions, ensuring grooves for improved mechanical interlocking.
3. **Bed Levelling and Flatness**
   Precise bed levelling and surface flatness were maintained throughout the experiments. A dial indicator gauge was used where needed to achieve an accurate and uniform print surface, ensuring consistent first-layer adhesion.
4. **Filament**
   Various filament types and brands were tested, considering that different additives influence adhesion strength.
5. **Printer Settings**
   Optimal print parameters were determined through iterative testing. Difference in printing speeds, active cooling, and under-/over-extrusion are some of settings tested.
6. **Temperature Effects**
   The impact of print bed temperature on adhesion was evaluated. Because each material has different inherent properties, in the experiments several different bed and nozzle temperatures were tested to optimise the polymer-glass adhesion. A problem faced in the experiments was warping, which caused the interlayer to pull of the glass bed. Warping in thermoplastics is primarily caused by thermal contraction during cooling (FacFox, 2023). When the filament is extruded at high temperatures, it begins to cool and solidify immediately upon deposition. As it cools, the material undergoes shrinkage. The first layer, however, is mechanically constrained by its adhesion to the build surface. This prevents it from contracting freely. The mismatch in dimensional change induces internal stresses within the print. As more and more layers continue to cool and contract, these stresses accumulate and result in upward bending forces at the base and corners of the print (see Figure 4.1).

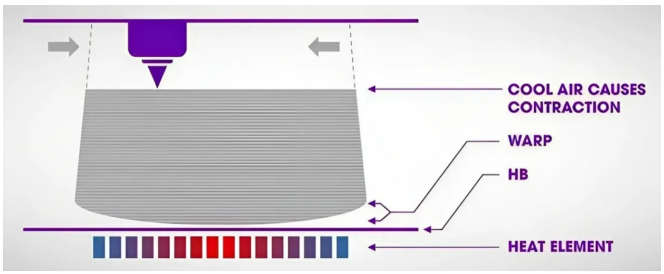

Figure 4.1: Warping explained, (*FacFox, 2023*)

The glass used is Pilkington float-glass with a thickness of 8mm. The glass samples were waterjet cut into squares of 100 mm by 100 mm. These squares were used as the print bed on the Anycubic 3D printer (nozzle size 1.0 mm). This means that the initial nozzle height was raised to 8.25 mm to cope with the sample height and the double sided tape was used to keep the sample in place on the print bed of the 3D printer (See image 4.2 for the experiment set-up). A hexaganol design was made and tested with five different materials to obtain insight in the working of the different materials in regard to the glass. The result of the adhesion of the material to glass will be ranked in 5 levels (–, -, +-, +, ++), going from no adhesion at all to very high adhesion. In the next sub-chapters, the different materials and insights into their working are discussed and an initial material selection for the interlayer is made. Because of availability of certain materials and specific printers at the LAMA lab at the TU Delft, choices had to be made to change some of the initial materials to make sure sample testing with AM was possible. Silicone needs a highly specific 3D printer not available at the TU Delft, this material will therefore not be tested in this research. Furthermore, Surlyn is not available to order as a filament and will therefore not be possible to test. Next, a combination of PolyCarbonate and ABS will be used to test the possibility of PC as an interlayer material. Finally, flexPlolyester, a highly elastic filament, will be looked into due to its availability and correct properties as an interlayer.

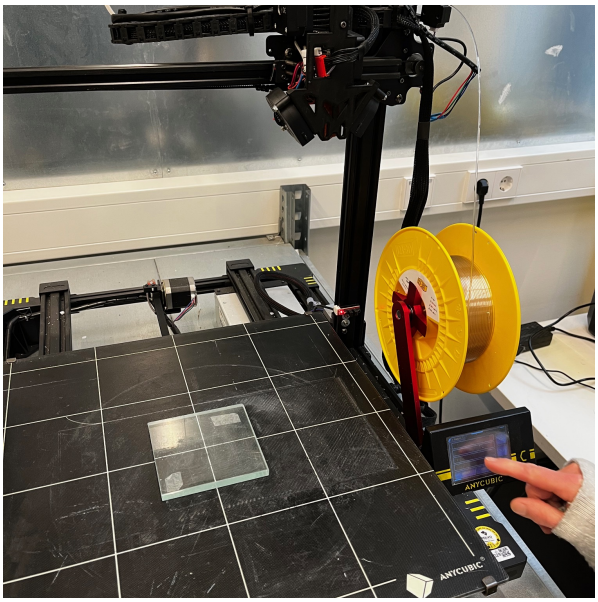

(a) Test Set-up, float glass sample attached to print bed of the Anycubic 3D printer

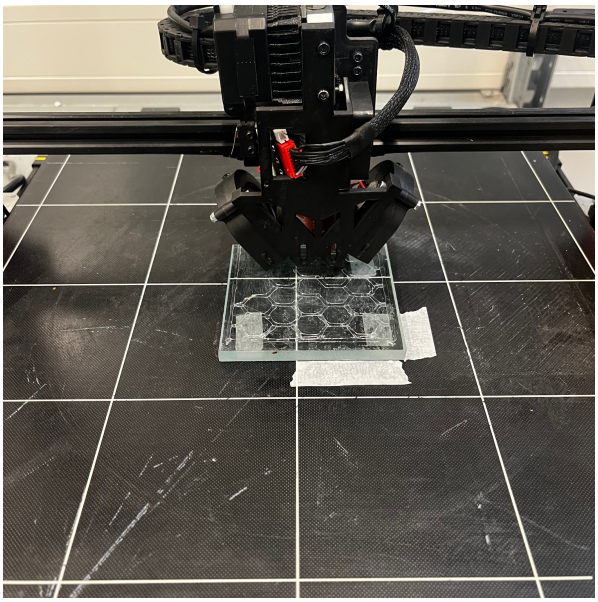

(b) Test Set-up, printing directly on top of the sample

Figure 4.2: Test Set-up

4.1.2 PETG (transparent, Jupiter series 123-3D)

PETG (Polyethylene Terephthalate Glycol) is a popular AM filament known for its strength, chemical resistance, and transparency. It has better layer adhesion than PLA and is less brittle, while still being easier to print than ABS. PETG has a relatively high shrinkage rate when cooling down due to its high thermal expansion coefficient. This can create significant internal stresses. These stresses can lead to cracks in the glass if the bond is tight and the shrinkage is not evenly released.

Key Findings

Strong Adhesion & Glass Damage

Samples 4 and 9 showed very strong adhesion (++), to the point of ripping off glass flakes (see Figure 4.3a). These prints used high bed (90°C) and nozzle temperatures (240°C), slow print speed (60 mm/s), and reduced fan cooling (40% after layer 2). Sample 9 showed the best adhesion with Wood Glue. When the PETG cooled and shrank, the resulting stress tore off pieces of glass, indicating strong adhesion to the glass.

Moderate Adhesion

Samples 2 to 3 had increasing adhesion as the bed temperature increased from 80°C → 90°C, showing that a hotter bed helps PETG stick better to glass — likely due to better wetting of the surface and reduced initial shrinkage.

Poor or No Adhesion

Samples 1, 5, 6, 7, and 8 all showed weak to no adhesion (– or - -). Samples 5 and 6, with Bison high-temp kit, did not adhere, possibly because the adhesive acted as a barrier instead of a adhesive. Samples 7 used glue stick as adhesion but actually reduced the bonding — again, these may have formed a film preventing PETG from 'grabbing' the glass (see Figure]4.3c).

Conclusion

Warping and shrinkage of PETG actively contributed to less bonding by pulling the surface of the glass during cooldown. High bed and nozzle temperatures + reduced cooling = optimal adhesion, but at the risk of damaging the glass due to the stress transfer from shrinkage.

Sample	Bed Temp. (°C)	Nozzle Temp. (°C)	Print Speed (mm/s)	Fan Cooling %	Additive	Result
1	50	220	100	100	None	–
2	80	220	100	100	None	+-
3	90	220	100	100	None	+
4	90	240	60	40 after layer 2	None	++
5	90	230	100	100	Bison high temp. kit	–
6	60	230	100	100	Bison high temp. kit	–
7	60	220	100	100	Pritt Glue	-
8	0	220	100	100	Wood Glue	-
9	90	240	60	40 after layer 2	Wood Glue	++

Table 4.1: Experiments with PETG adhesion to float glass

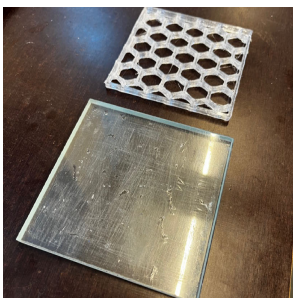

(a) PETG sample 4, strong adhesion, even breaks glass after ripping it off.

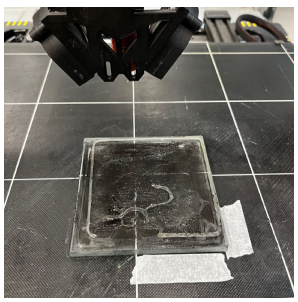

(b) PETG sample 5, no adhesion with Bison high temp. kit applied on print bed.

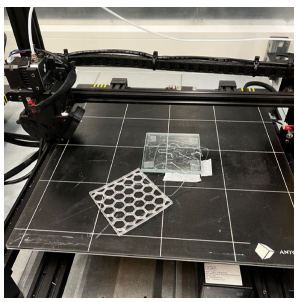

(c) PETG sample 7, no adhesion with Pritt glue applied on print bed.

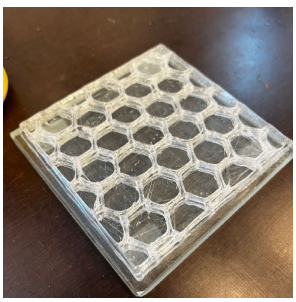

(d) PETG sample 9, very strong adhesion with Wood glue applied on print bed.

Figure 4.3: Experimental PETG samples tested.

4.1.3 TPU (Thermoplastic Polyurethane)

Flexible filaments like TPU (Thermoplastic Polyurethane) are known for their elasticity and impact resistance. However, TPU is highly hygroscopic; this means it absorbs moisture from the air. Absorbed moisture can cause various print issues such as stringing, holes, and popping sounds during extrusion. All of these issues can compromise both print quality and adhesion. To mitigate part of these issues, the TPU filament used in the experiments was stored in an airtight filament dryer and dried at 55°C before printing (see Figure 4.4d). This ensured more stable extrusion and minimised moisture-related defects.

Key Findings

Warping & Poor Adhesion

Across most samples (1, 2, 3, 7, 8, 9), TPU showed significant warping in initial print layers, which prevented effective adhesion to the glass surface. Even at higher bed temperatures (up to 90°C), the flexible nature of TPU caused it to peel away from the glass in the corners before the bond could form (see Figures 4.4a and 4.4c).

Limited Improvement at Higher Bed Temperatures

Samples 4, 5, and 6 showed slightly improved results (+-) when printed at bed temperatures between 60°C and 70°C with slower speeds (20–30 mm/s) and no fan cooling. While these settings reduced immediate warping slightly, the bond remained weak overall.

Conclusion

Warping was the dominant factor influencing TPU's poor adhesion to glass. Even with pre-dried filament and controlled settings, TPU tended to lift off the surface due to its flexibility and shrinkage upon cooling. Slight improvements were seen with slower speeds, higher bed temperatures and no cooling, but actual bonding remained absent. Adhesive aids generally did not improve results and in some cases worsened adhesion.

Sample	Bed Temp. (°C)	Nozzle Temp. (°C)	Print Speed (mm/s)	Fan Cooling %	Additive	Adhesion result
1	0	230	30	0	None	–
2	30	230	41,6	100	None	-
3	60	230	41,6	100	None	-
4	60	220	30	0	None	+-
5	60	230	20	0	Wood glue	+-
6	70	220	30	0	None	+-
7	70	220	30	0	Pritt glue stick	-
8	70	220	30	0	Hair spray	-
9	90	220	30	0, after layer 2: 30	None	-

Table 4.2: Experiments with TPU adhesion to float glass

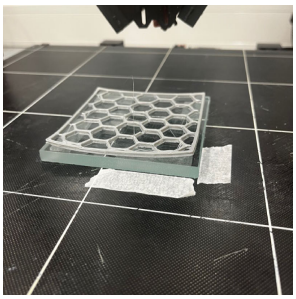

(a) TPU sample 3, low adhesion due to warping in the corners

(b) TPU sample 5, average adhesion; corners still warp

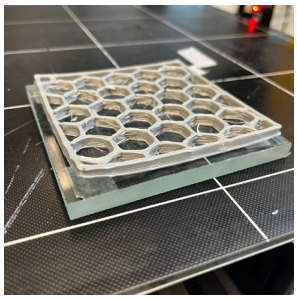

(c) TPU sample 7, low adhesion and warping

(d) Fixdry filmanet dryer

Figure 4.4: Experimental TPU samples tested

4.1.4 FlexPolyester 40D Shore (Plastic2Print)

FlexPolyester 40D from Plastic2Print is a semi-flexible filament with a Shore hardness of 40D. A characteristic in between rigid and soft flexible filaments like TPU. It offers good chemical resistance and toughness, while still maintaining some degree of flexibility. However, the material is more challenging to print than standard filaments due to its tendency to warp and ooze.

Key Findings

Warping in Corners

One of the main challenges observed with FlexPolyester was warping in the corners of prints (see Figure 4.5b). Despite using a high bed temperature of 90°C and no cooling for the first layers, the material still lifted at the corners during printing. While FlexPolyester bonds moderately well to heated glass, internal stress from cooling continues to pull the print surface away, especially at corners.

High Oozing and Stringing

Sample 5, which was printed at a high speed (66 mm/s) with gradual fan cooling, showed relatively good adhesion (+), but suffered from excessive oozing and stringing. This behaviour is characteristic of flexible polyesters, especially when printing too hot or too fast. The material tends to extrude inconsistently, leaving fine threads between travel moves and excess material in some areas. Slower printing and careful retraction settings are likely required to improve print cleanliness.

Conclusion

FlexPolyester 40D demonstrated moderate adhesion capabilities on glass but struggled with warping in corners and extensive stringing. Good adhesion was generally achieved at 90°C bed and 220°C nozzle temperatures, with limited cooling. However, print problems like oozing and warping remained.

Sample	Bed Temp. (°C)	Nozzle Temp. (°C)	Print Speed (mm/s)	Fan Cooling %	Additive	Result
1	0	220	30	0, 0, 30	None	–
2	90	200	30	0, 0, 25	None	+-
3	90	220	30	0, 0, 30	None	+-
4	90	200	40	0, 30, 60	None	-
5	90	200	66	0, 50	None	+
6	90	220	30	0, 0, 30	Wood Glue	+
7	100	220	30	15, 15, 30	None	-

Table 4.3: Experiments with FlexPolyester adhesion to float glass

(a) FlexPolyester sample 5, pretty good adhesion but can be taken off

(b) FlexPolyester sample 2, medium adhesion, warping in the corners

Figure 4.5: Experimental FlexPolyester samples tested

4.1.5 PC-ABS (Polycarbonate/Acrylonitrile Butadiene Styrene) – Dimension3D

PC-ABS is a blend of polycarbonate (PC) and ABS. This filmanet combines the strength and heat resistance of PC with the flexibility and ease of printing of ABS. This material is commonly used in automotive and industrial applications due to its toughness and durability. However, PC-ABS is known for its high tendency to warp during AM, especially on non-enclosed printers.

Key Findings

Severe Warping

Both tested samples (1 and 2) showed significant warping and detachment from the glass surface, particularly at the corners. Despite using a high bed temperature of 105°C and a nozzle temperature of 260°C, the prints failed to adhere. The warping was so severe that the prints curled upwards during printing (see Figure 4.6a), making it impossible to finish the print. The primary cause of excessive warping in this material, is its high thermal expansion coefficient and low flexibility once cooled. Without an enclosed and uniformly heated building environment, the temperature difference between layers and surrounding air heighten the stress difference. This stress causes the edges of the print to lift or detach entirely from the print bed.

Conclusion

PC-ABS is a challenging material to print due to its high tendency to warp. To mitigate this warping, it be would essential to maintain a consistent and high ambient temperature around the print, achieved by using an enclosure. This is not possible when printing with a robot arm in a big space and this makes this material unsuitable.

Sample	Bed Temp. (°C)	Nozzle Temp. (°C)	Print Speed (mm/s)	Fan Cooling %	Additive	Result
1	105	260	66	100	None	–
2	105	260	66	100	None	–

Table 4.4: Experiments with PC-ABS adhesion to float glass

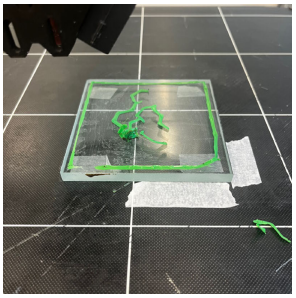

(a) PC-ABS sample 1, initial sample failed due to no adhesion

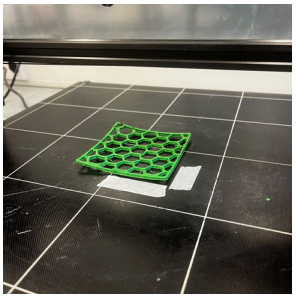

(b) PC-ABS sample 2, printed but warped off the bed immediately

Figure 4.6: Experimental PC-ABS samples tested

4.1.6 PLA (Polylactic Acid)

PLA is a widely used biodegradable thermoplastic polymer derived from renewable resources such as corn starch or sugarcane. It is known for its ease of printability, high stiffness, and low thermal shrinkage compared to other AM filaments. Because of its biodegradability and low processing temperature, PLA is a material used in numerous prototyping applications.

Key Findings

Adhesion Improves with Bed Temperature

Three PLA samples were tested with increasing bed temperatures: 0°C, 40°C, and 60°C. The results clearly showed a correlation between bed temperature and adhesion strength. At 0°C (Sample 1), adhesion was poor (-), with the print detaching from the glass early in the process (see Figure 4.7a). At 40°C (Sample 2), adhesion improved to a good level (+), and at 60°C (Sample 3), excellent adhesion was observed (++)(see Figure 4.7b). Higher temperatures allow the PLA to soften and flow better into the micro-textures of the glass surface, leading to enhanced mechanical interlocking and wetting.

Low Warping and Stable Printing Behaviour

Compared to other materials tested (e.g., PC-ABS and TPU), PLA exhibited low warping. This is consistent with Farah, Anderson, and Langer (2016) describing PLA as having a relatively low thermal expansion coefficient (60µm/(m*°C))(Simplify3D, n.d.) and high stiffness, which helps to preserve dimensional accuracy during cooling.

Conclusion

PLA demonstrated progressively better adhesion to the float glass samples with increased bed temperatures. Optimal results were obtained at 60°C bed- and 210°C nozzle temperature. Given its low warping and ease of processing, PLA is a reliable candidate for AM on glass surfaces, provided the print bed is sufficiently heated.

Sample	Bed Temp. (°C)	Nozzle Temp. (°C)	Print Speed (mm/s)	Fan Cooling %	Additive	Result
1	0	210	60	0, 0, 30	None	-
2	40	210	60	0, 0, 30	None	+
3	60	210	60	0, 0, 30	None	++

Table 4.5: Experiments with PLA adhesion to float glass

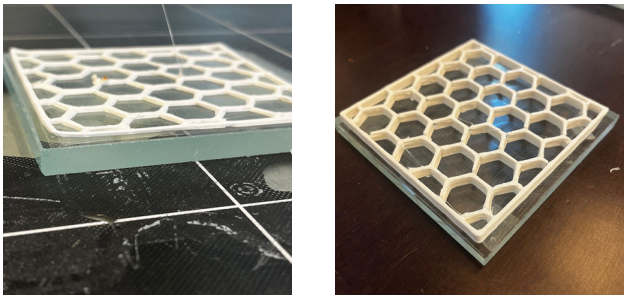

(a) PLA sample 1, corners warp a bit, adhesion is good

(b) PLA sample 3, adhesion is very good, no warping

Figure 4.7: Experimental PLA samples tested

4.1.7 Sub-Conclusion & Material Selection

Based on the adhesion tests and observed material behaviour, PLA and PETG were selected for further development as potential interlayer materials between modular glass units.

PLA demonstrated excellent adhesion to glass at moderate bed temperatures (60°C), with minimal warping and high dimensional accuracy. Its low thermal shrinkage and ease of processing make it reliable for creating stable and precise prints directly on glass surfaces. However, its vulnerability to weathering and lower mechanical strength compared to other polymers may limit its long-term structural use. If used outdoor, this has to be taken into account.

PETG, on the other hand, showed superior strength and chemical resistance. It showed very high adhesion to glass under specific conditions, particularly at higher bed (90°C) and nozzle (240°C) temperature in combination with low cooling. Despite its tendency to warp due to thermal contraction, the strong bond even led to partial delamination of the glass surface. This indicates the potential for a strong mechanical interlock, provided that warping can be mitigated through careful process control.

Answering sub-question 1 of this thesis "Which materials are suitable for additive manufactured or injection-moulded interlayers in glass structures?": PLA was chosen for its dimensional reliability and excellent adhesion, while PETG was selected for its mechanical robustness and bonding performance. These materials present specific strengths and will be further investigated in the context of developing the actual interlayer designs.

5 Geometry Design

5.1 Conceptual Design

The objective of this study is to explore two different geometric approaches for creating a reversible connection system between Additively Manufactured glass units. The aim is to develop an assembly method that allows glass bricks to interlock securely while maintaining the possibility of disassembly and reuse. Both concepts are based on osteomorphic-shaped AM glass units developed by Evenline Inc. (3.37a), providing a structured form that facilitates mechanical interlocking. The following sub-chapter will answer sub-question 2 of this thesis *"How can the geometry of the interlayer and glass units be optimised for both strength and disassembly?"*.

5.1.1 Option 1 - the Dry Click-System

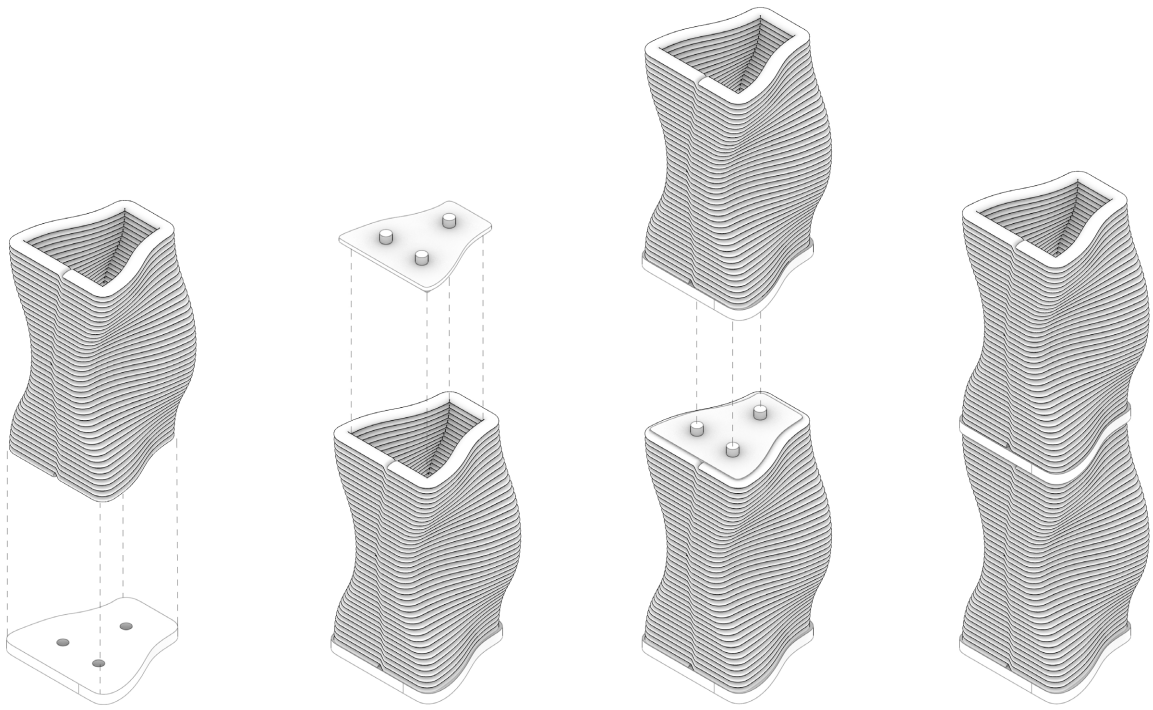

Figure 5.1: Option 1; From left to right: Additive Manufacturing of the glass unit directly on top of the waterjet float glass, the dry-click insert of the PETG interlayer, clicking another AM glass brick on top of the interlayer, the conceptual result

In the first concept, the focus is on a fully reversible connection between AM glass units. Both of the options 1 and 2 start with the osteomorphic shaped AM unit created by Evenline inc. (see Figure 3.37a). In option 1 the osteomorphic glass shape is directly printed on top of a waterjet float glass plate which already has connection holes incorporated (technique also explained in 3.4.3). This creates a glass unit with a closed bottom surface, expanding the surface area to connect with. The next step is the attachment of the injection moulded interlayer on the top of the glass unit. This creates an opportunity for the next glass unit to interlock on the top surface. The shape of the glass unit makes interlocking on the top, bottom and side surface possible. However, in this concept, the sides of the glass units are exposed glass-on-glass.

Initial Tests

The idea behind Option 1, the dry click-system, is to create a reversible connection between glass units using an interlayer that can easily be clicked in and out of the float glass base. The later objective is to scale this system up by using injection moulding, which would allow for high-volume production and consistent quality. However, before reaching this stage, 3D printing was used to test and prototype different interlayer forms.

AM Geometry

To achieve this, four different iterations of the AM interlayer were designed (see Figure 5.2). AMenabled rapid prototyping, allowing quick experimentation with different designs and refining the functionality between layers in a fast and cost-effective way. However, as the interlayers were printed layer by layer, this method introduced some limitations. Due to the anisotropic behavior of AM (3.1.2), the interlayer could potentially snap off under stress, particularly along the layer lines.

To mitigate this issue and improve strength, a diagonal printing approach was tested (see Figures 5.2a and 5.2b). By changing the orientation of the print layers, the aim was to increase the interlayer's structural integrity and ensure a more reliable connection.

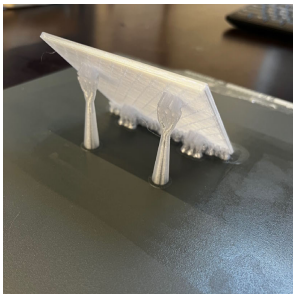

(a) Sample 1, diagonally printed with tree support

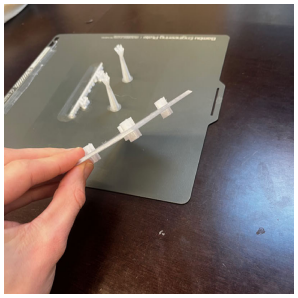

(b) Sample 1, diagonally printed with 4 snap joints on both sides

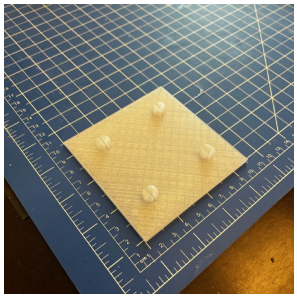

(c) Sample 2, horizontally printed with 4 snap-fit joints on one side

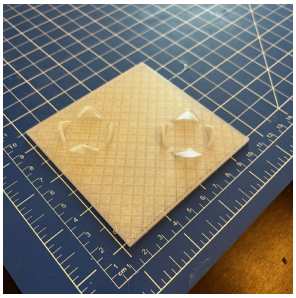

(d) Sample 3, horizontally printed with 2 bigger snap-fit joints on one side

Figure 5.2: AM PETG interlayer test samples

Waterjet-Cut Float Glass

The waterjet-cut float glass samples were designed to correspond with the snap-fit joints of the AM interlayers. Some samples featured one, two, or four holes to test different configurations. However, while AM introduces slight shrinkage due to temperature variations, the waterjet-cutting process presented its own precision challenges. Small deviations in cutting accuracy meant that the snap-fit joints did not always align perfectly with the glass holes, affecting working of the connection. The interlock is over-constraint in a way that a lot of post-processing is needed in order to finetune the different connections.

A second issue observed in the glass samples was breakage. This could be attributed to stress concentrations around the cut holes, particularly if micro-cracks formed during the cutting process. Variations in edge quality or residual stresses in the float glass may also have contributed

to fracture during the cutting.

The next phase for concept 1 will involve analysing the performance of the AM click system with waterjet-cut float glass samples. These evaluations will determine if the system can provide the required strength for a secure, reversible connection and guide further optimisation of the design.

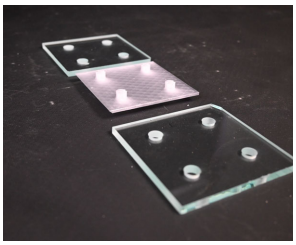

(a) Sample 1 with the 6 mm float glass samples

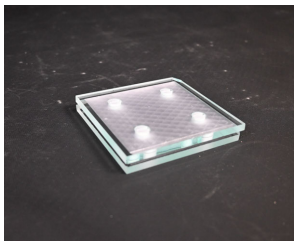

(b) Sample 1 sandwiched between two 6 mm float glass samples

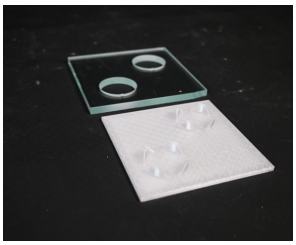

(c) Sample 2 next to the waterjetcut glass sample

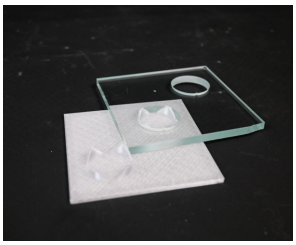

(d) Sample 2 clicked into the glass sample, the other joint does not align perfectly

Figure 5.3: AM PETG samples inserted in waterjet cut float glass samples

5.1.2 Option 2 - The Direct Print

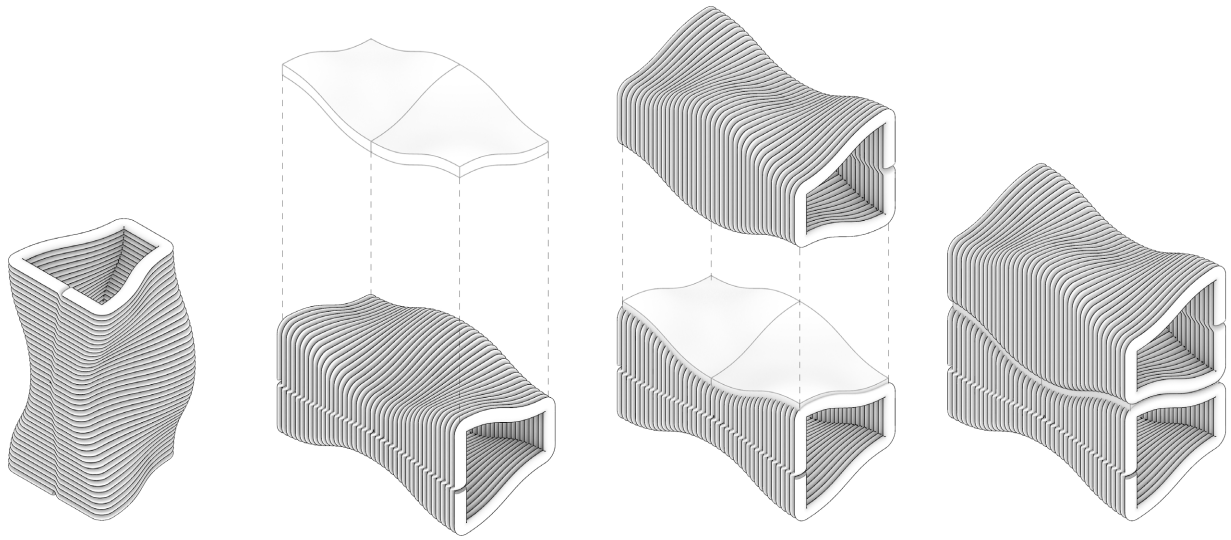

Figure 5.4: Option 2; From left to right: Additive Manufacturing of the glass unit, rotating and printing an interlayer directly on top of the (heated) top surface with a robot arm, interlocking another AM glass unit with its interlayer printed on the bottom side, the conceptual result

In the second concept, a manufacturing method is proposed where the glass bricks are interconnected using a 3D-printed interlayer directly attached to each brick. This interlayer is designed to provide a reversible assembly system, enabling the easy disassembly and reuse of the glass bricks. The process starts with the AM of the (osteomorphic shaped) glass brick. The interlayer is then printed on the top surface of the glass brick using a robotic additive manufacturing process. A six-axis robot is used because the top surface of the brick is non-planar, this means that a traditional cartesian 3D printer is not able to print on this surface as it it would collide with the brick when printing. A six-axis robot, in this case the UR5, is able to move in every direction to avoid collision and print the interlayer on the non-planar surface. This printed interlayer features extrusions that are designed to interlock with corresponding features on the next brick. The interlayer is printed on both the top and bottom surfaces of the brick. This allows the system to function as a simple, but effective, connection mechanism for the glass units.

Elastic Averaging

Elastic averaging is a method used to address the dimensional inaccuracies common in rapid fabrication processes, such as additive manufacturing. In traditional manufacturing, high precision is usually achieved through post-processing. However, AM often results in parts with rough surfaces and limited dimensional accuracy. These inaccuracies can make it difficult to use 3D-printed parts in precision applications (Teo & Slocum, 2017).

Elastic averaging uses the flexibility and compliance of materials to "average out" small misalignments between the parts. This ensures that the overall assembly works even when individual components deviate slightly from the desired dimensions. The principle has been applied in fields like MEMS devices and microfluidics, where precision alignment is essential despite manufacturing limitations (Teo & Slocum, 2017).

For the glass brick interlock, Lego-type extrusions are designed to use elastic averaging. These extrusions are printed on the top surfaces of the bricks, allowing them to interlock. When the bricks are assembled, the elastic features of the interlocking extrusions help align the parts. This makes the connection stable, even if there are minor misalignments in the printing process. As a result, this approach reduces the need for precise manufacturing or post-processing, enabling easier scaling of the system and use of a robotic arm.

Velcro type interlock

The Velcro-type interlock is inspired by the interlocking nature of Velcro. However, instead of using traditional hook-and-loop fasteners, the system relies on 3D-printed extrusions. These extrusions are printed on the top and bottom surfaces of the bricks. When the bricks are stacked, the extrusions interlock with each other, creating a secure connection.

The design is flexible; the extrusions can "snap" into place, providing a stable connection. This flexibility enables the system to accommodate minor variations in part dimensions or alignment. The connection remains strong and stable, without losing ease of assembly and disassembly. This feature makes the system ideal for creating modular glass brick assemblies.

5.1.3 Sub-conclusion

Option 1 relies on a dry click-system with an injection-moulded interlayer. While this method offers the reversibility required, it also presents challenges. Waterjet cutting of the glass introduced (micro-)cracks, which can propagate under load and could lead to failure. Furthermore, the over-constraint design requires a very high precision and makes it difficult to rapidly manufacture with AM as it would require a lot of post-processing to achieve the desired snap-fit. This precise fit with few extrusions would mean stress concentrations around the waterjet-cut holes and extrusions will arise. Under high-loading this stress could propagate early failure of the glass or interlayer.

Option 2, however, integrates a 3D-printed interlock directly onto the glass bricks. The elastic

averaging mechanism compensates for the printing tolerances of a 1.0 mm nozzle, reducing reliance on post-processing. The Velcro-type interlock creates a secure yet flexible connection, allowing for easy assembly and disassembly. Unlike option 1, this method does not rely on precisely machined holes. This eliminates the stress concentrations and risk of cracks around these holes.

To answer the sub-question 2 *"How can the geometry of the interlayer and glass units be optimised for both strength and disassembly?"* the 2 options are compared and one is concluded. Comparing the pros and cons of both options, option 2 is the preferred solution. It offers a scalable and reversible approach. It creates an easy and steady interlock with an elastic averaging mechanism which does not rely on precisely machined holes in the glass. This method will be further prototyped and developed to refine the interlock performance and evaluate its application in modular glass assemblies.

5.2 Developing Option 2 - The Direct Print

5.2.1 Interlocking Interlayer

Interlayer Design Iterations

The interlayer design process began by focusing on the geometry of the interlock without considering the glass substrate. PLA and PETG were both tested using 50 × 50 mm prints to prototype small-scale interlocks. This allowed for calibration between the digital 3D model and real 3D prints, accounting for material shrinkage, printer tolerances, and the limitations of the 1.0 mm nozzle. To compensate for printing deviations, the principles of elastic averaging were used in the design, allowing interlocks to self-align. This led to the initial design mimicking a 3D pritned Velcro type of interlayer (Sample 1 in Figure 5.6a). A simple Grasshopper script was developed to adjust the diameter and angle of extrusions quickly. As shown in Figure 5.6a, the first samples showed issues with oozing and stringing. Designs with too fine extrusions proved too fragile to print cleanly. After several iterations, Sample 7 was selected for further testing due to its proper fit and clean print quality (see Figure 5.7a).

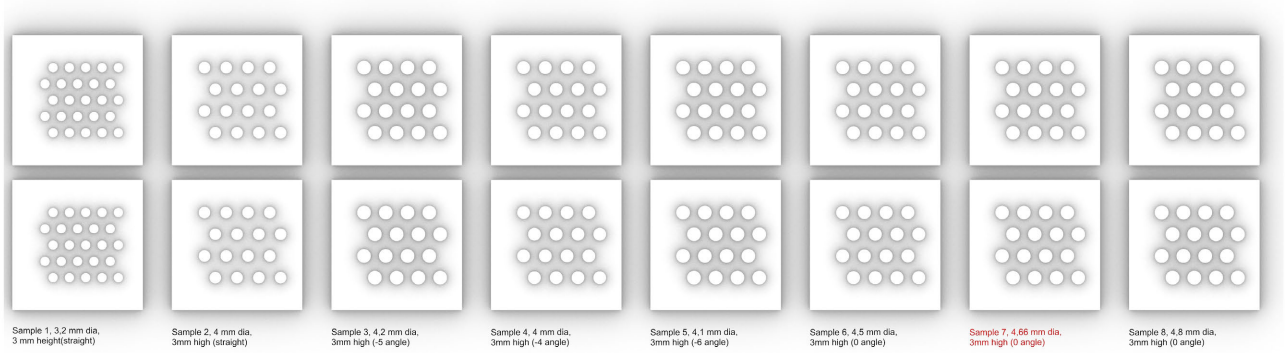

Figure 5.5: Overview of the small samples printed

Material Considerations

PETG exhibited strong adhesion to glass but showed significant warping due to thermal contraction during cooling. The mismatch in thermal expansion between PETG and glass caused stress that cracked the glass (see Figure 5.6b). Attempts to reduce this effect by printing isolated circles to reduce thermal stress buildups (Figure 5.6c) or reducing the overall surface area of the prints to decrease adhesion stresses (Figure 5.6d) were unsuccessful and the parts still detached and/or damaged the substrate.

PLA performed better. Its lower printing temperature and reduced shrinkage resulted in more stable prints. Warping was mostly limited to sharp corners, where printhead acceleration and deceleration create uneven heat distribution. To avoid this, prints with fewer corners were tested. Circular shapes showed good results, and a square interlayer with 15 mm fillets on all corners proved to be the most reliable in minimizing warping.

Overall, PLA offered better print consistency on glass, while PETG's high shrinkage limited its suitability for this application.

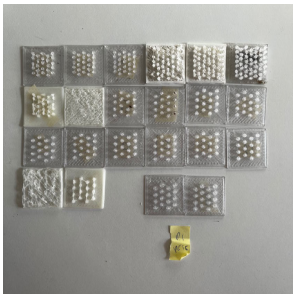

(a) 50mm x 50mm samples of different materials

(b) PETG snapping and breaking the float glass

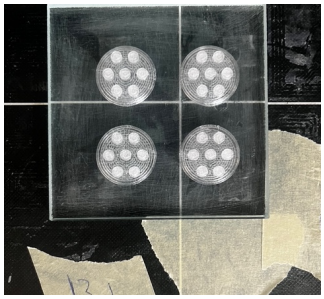

(c) Small prints of PETG to lower the thermal expansion

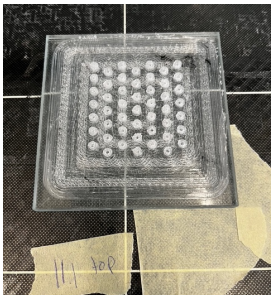

(d) Lowering the print surface to prevent warping

Figure 5.6: Optimising interlayer geometry for specific material properties *Own images*

Sub-conclusion

To summarise and answer question 3 of this thesis *"What interface strategies between glass and interlayer ensure performance and reversibility?"*, the development of the Velcro-type interlayer focused on tuning the geometry for both mechanical interlocking and print reliability on float glass. Among the tested variants, sample 7, printed in PLA, demonstrated optimal interlock performance and minimal stringing or oozing (see Figure 5.7a). However, when this geometry was printed directly onto glass, PETG was found unsuitable due to excessive warping and high thermal contraction, which led to breakage of the glass substrate. PLA showed significantly better adhesion and stability due to its lower printing temperature and reduced shrinkage. Warping was still observed at sharp corners, a result of uneven thermal loads during printhead acceleration and deceleration. To address this, the selected geometry was modified by adding 15 mm edge fillets to all four corners, resulting in a smoother toolpath and more even material cooling. This, in combination with a concentric infill resulted in a perfectly straight print. A blessing in disguise is the low glass temperature of PLA (60 °C), this has the downfall of losing stifness in a structure when high temperatures are reached. On the other hand it means if a glass brick is heated up till above this temperature, the PLA can be peeled of of the glass to be reused. In the Figures 5.8, the interlocking system is heated up from 0 to ß0 °C, at this moment the PLA reaches its glass transition temperature and can be transformed to be peeled off of to reclaim the glass and polymer cleanly. The final PLA sample (see Figure 5.7c and 5.7d) will serve as the base geometry for the interlayer which will be printed on top of the osteomorphic shaped glass bricks. This final sample will also be mechanically tested in shear to validate the concept and its properties in Chapter 6. In Table 5.1 the print settings of this sample are shown, which will be used for further prints.

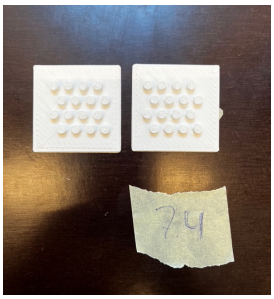

(a) The chosen PLA 50mm x 50mm, sample 7

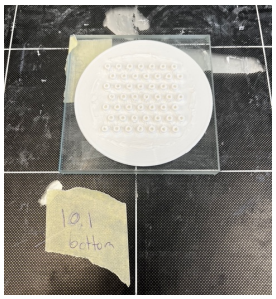

(b) Circle print to prevent warping

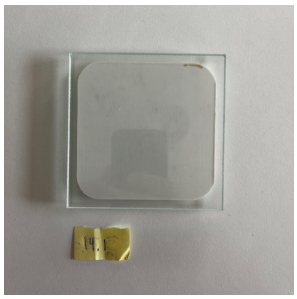

(c) Backside of chosen PLA on float glass plate, sample 14.1

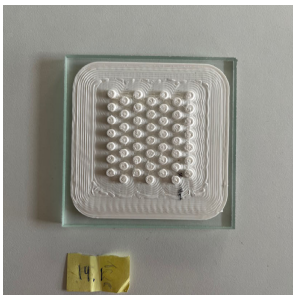

(d) Frontside of chosen PLA on float glass plate, sample 14.1

Figure 5.7: Iterations of velcro type interlayer

Chosen sample	
Material	PLA
Layer Height	0.3 mm
Nozzle diameter	1.0 mm
Extrusion Multiplier	0.9
Nozzle temperature	210 °C
Bed temperature	60 °C
Print Speed	30 mm/s (first layer 50%)
Skirt/Brim	1 layer, no offset
Fan Speed	layer 1-5: 0%, layer > 5: 50%
Retract Speed	15 mm/s
Retract Distance	2.0 mm
XY Travel Speed	111 mm/s
Solid Layer Infill	Concentric

Table 5.1: Print Settings Final Sample

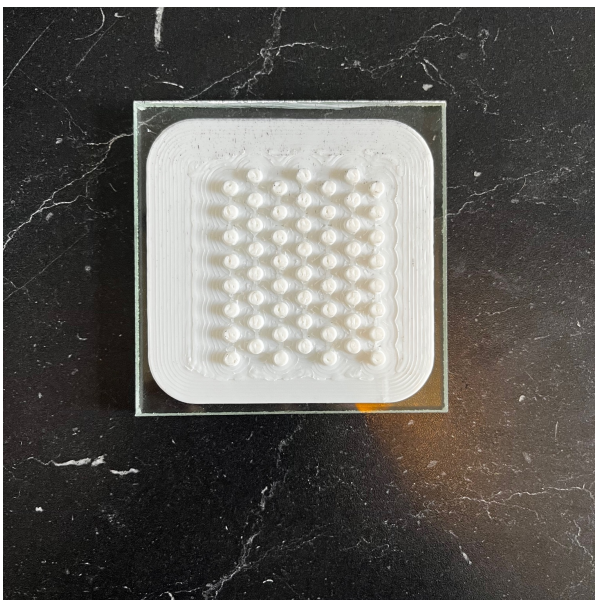

(a) PLA sample 7, room temperature: good adhesion

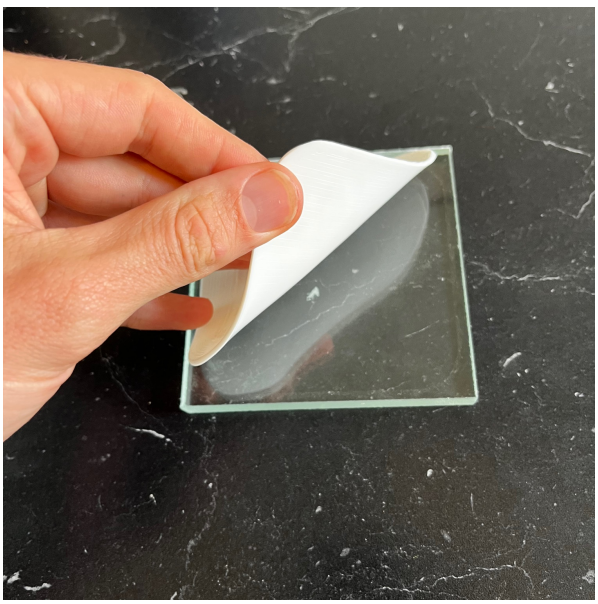

(b) PLA sample 7, ~80 °C: glass transition and can be peeled off

Figure 5.8: By heating up to ~80 °C, the polymer can be reclaimed cleanly from the glass surface

6 Mechanical Validation

6.1 Glass-Interlayer-Glass, shear tests

6.1.1 Specimen Testing Objectives

To assess the shear capacity and failure mechanisms of the velcro-type interlayer (see Chapter 5.2.1), ten identical specimens were produced by 3D-printing the interlayer geometry directly onto 100 mm × 100 mm float-glass plates (8 mm thickness). Two of these served as test samples, while the remaining eight were tested in shear at the Stevin 2 laboratory (see Chapter 6.1.2).

Each assembly comprised two interlocked plates clamped at top and bottom. A horizontal actuator imposed a lateral displacement on the upper plate, pushing it out of the interlayer while the lower plate remained fixed (see concept in Figure 6.1). By recording the peak horizontal force required to push the top plate out of its interlock under a known normal preload, the shear strength of the interlayer was directly measured. This peak force, divided by the applied normal load, gives the 'friction coefficient' μ for the interlocking geometry. For context, Eurocode friction coefficients for common structures are: μ = 0.40 for timber-timber, μ = 0.40 for steel-steel and μ = 0.60 for steel-concrete (Europeenne & Norm, 2006 & *NEN-EN 1995-1-1:2023 Ontw. en*, 2023).

Throughout each test, Digital Image Correlation (DIC) was used. This is an optical technique that tracks high contrast speckle pattern on the specimen surface to measure displacements and strains. The combination of force curves and DIC imaging distinguishes between brittle debonding of the polymer, rupture of the interlock geometry or fracture of the glass itself. These results will guide future optimisation of interlayer geometry and material.

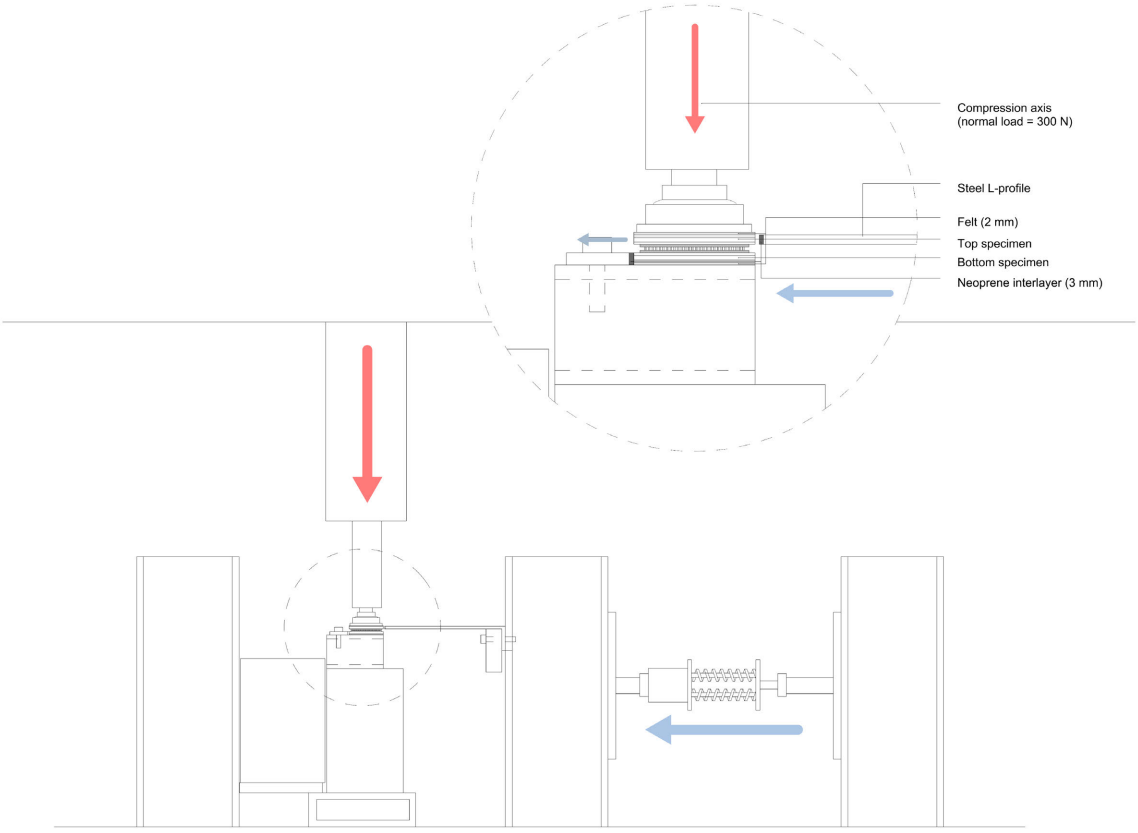

Figure 6.1: Principle test set-up at Stevin 2 lab, CitG,

6.1.2 Test Set-up

Before setting up the test space, each specimen was painted and sprayed with a random speckle pattern in order to perform DIC in the tests. This pattern provides identifiable features across the surface, which the DIC software tracks frame-by-frame. This enables accurate correlation of local displacements and strains (Figure 6.2a).

For each test, one glass plate with its 3D-printed interlayer was placed on a rigid steel base plate and secured against a bolted backplate to prevent any movement of the bottom specimen during loading. A second glass plate was then interlocked on top and clamped with a 300 N normal force to ensure full engagement of the interlocking surfaces and to simulate the Glass Vault structure's self-weight (see Figure 6.2d). This normal force correlates, on an interlayer surface of 8100 mm^2, with a normal stress of σ = 0.037 Mpa. Initial trials with the test specimens showed side crushing where the glass contacted metal (see Figure 6.2b); to eliminate this, a thin felt layer was inserted between metal and glass on the top and bottom faces and neoprene strips were added along the sides. A steel plate between the actuator and felt further improved force distribution.

Shear loading was applied by an L-shaped steel adapter mounted to the horizontal actuator, which pushed the top plate laterally out of its interlock while the lower plate remained fixed. The DIC camera and synchronized flash were calibrated to monitor the speckled side surfaces throughout loading. Load and displacement were recorded continuously; the detailed results

for each specimen can be seen in Chapter 6.1.3.

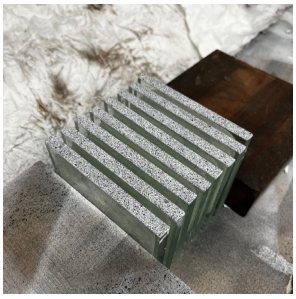

(a) Spray painted specimens, in order to perform dic analysis

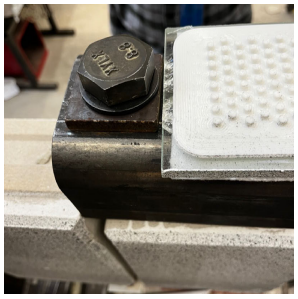

(b) Failure of test specimen due to glass on metal contact

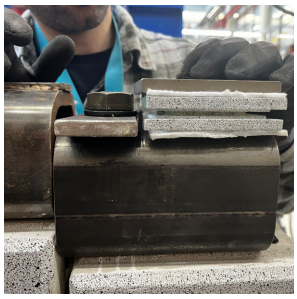

(c) Specimens are interlocked and placed on top of the steel base

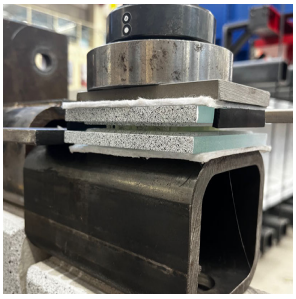

(d) Normal force is applied on teh specimen by a compression machine

Figure 6.2: Set-up steps of the experiment

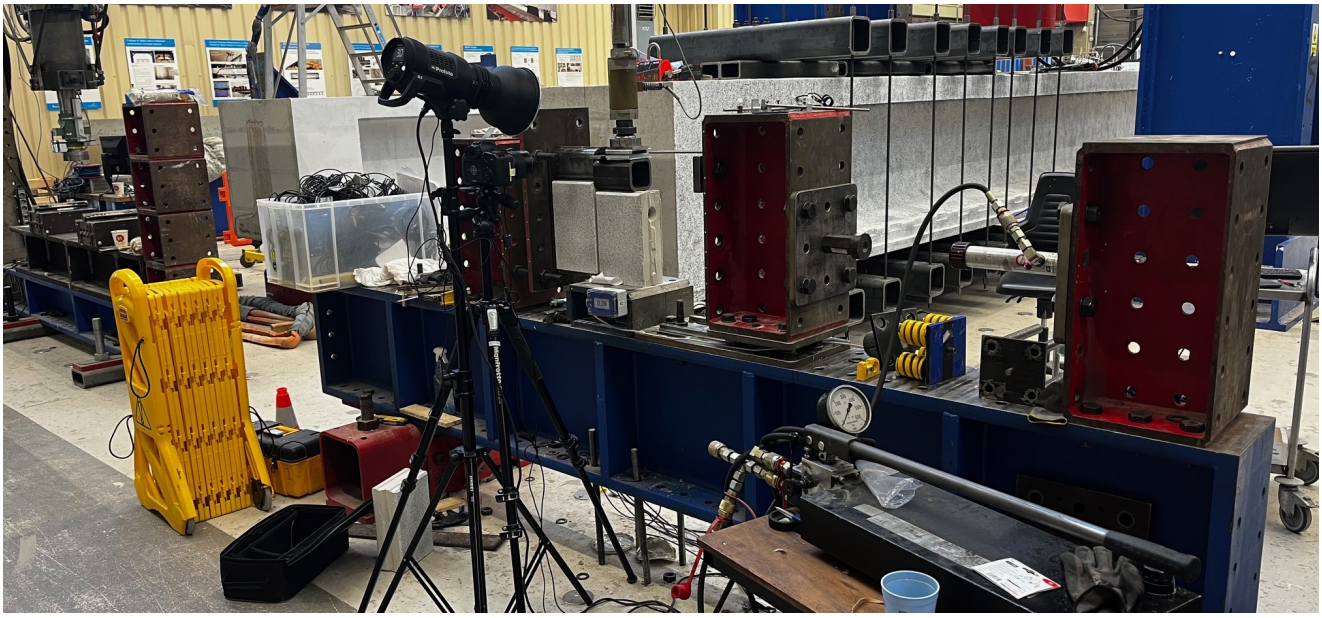

Figure 6.3: Overview of set-up at Stevin 2 lab, CitG,

6.1.3 Results

The mechanical response of the interlock is captured through two complementary loading channels: horizontal (shear) force curves and vertical (normal) compression curves. The horizontal force reflects the resistance to sliding of one specimen's face over the other, while the vertical force records the compressive load applied to the interlock. Together, these curves reveal how the interlocking features transmit shear under a given normal load and where a brittle failure or slip occurs.

Displacement measurements are provided with digital image correlation (DIC) analyses (expressed here as Dy and Dx). This data produces spatial maps of surface displacement across the interlock interface, showing local deformation patterns, displacement and bending.

Friction (μ_i) in this context is defined at each instant as the ratio of the measured lateral shear force to the applied normal force:

$$\mu_i = \frac{|F_{\text{vertical},i}|}{|F_{\text{horizontal},i}|} \tag{6.1}$$

It quantifies the interlock's resistance to sliding under compression: values above zero indicate effective shear transfer, while any sudden drop in friction corresponds to interlock disengagement or material failure. By correlating the friction coefficient, load–displacement curves, and DIC images, the tests provide an understanding of the behaviour of each sample under combined loading.

Specimen	Thickness (mm)	Pre-load (kN)	$F_{\text{shear,max}}$ (kN)	F_{normal} (kN)	μ	Failure Mode
G2	8	0.50	2.53	2.86	0.818	Polymer debond Top
G3	8	0.30	6.13	3.90	1.448	Polymer debond Bottom
G4	8	0.30	1.77	1.31	0.983	Polymer debond Bottom
G5	8	0.30	2.58	2.03	0.990	Polymer debond Top

Table 6.1: Peak shear force, concurrent normal load, average friction ratio, and failure mode for specimens G2–G5.

The shear tests on specimens G2–G5 (Table 6.1 and more detailed in A) revealed the following overall trends:

- **Failure Mode**
  All four specimens failed by abrupt delamination of the PLA interlayer, with two failures occurring on the top interface (G2, G5) and two on the bottom (G3, G4).
- **Shear Capacity**
  Peak shear forces ranged from 1.77 kN (G4) to 6.13 kN (G3), under preloads of 0.30–0.50 kN, yielding apparent friction ratios (μ) between 0.818 and 1.448.
- **Load Tilting**
  In every test the glass plates rotated about the axis perpendicular to loading (see Figure 6.4), lifting one side and locally altering the normal pressure under shear. This tilting inflates the calculated μ and introduces bending stresses in both glass and polymer, indicating that the assumed uniform pre-load is not perfectly maintained.

6.1.4 Sub-conclusion

Across all tests, the lateral force produced a noticeable rotation of the glass plates about the axis perpendicular to loading, lifting the right side of the plate upwards. For example in the G3 DIC in Figure 6.4, point 5 rotates upwards from dY -0.27 to dY +1.87 mm. This tilting is unfavourable in the testing because as shear increases, the top plate is pressed unevenly against the actuator, which locally elevates resistance. In other words, it affects the normal load across the interlayer, invalidating the assumption of uniform compression and thus making the friction ratio misleading. Furthermore, it introduces bending stresses in the glass and polymer, which can localise stress concentrations and trigger premature debonding.

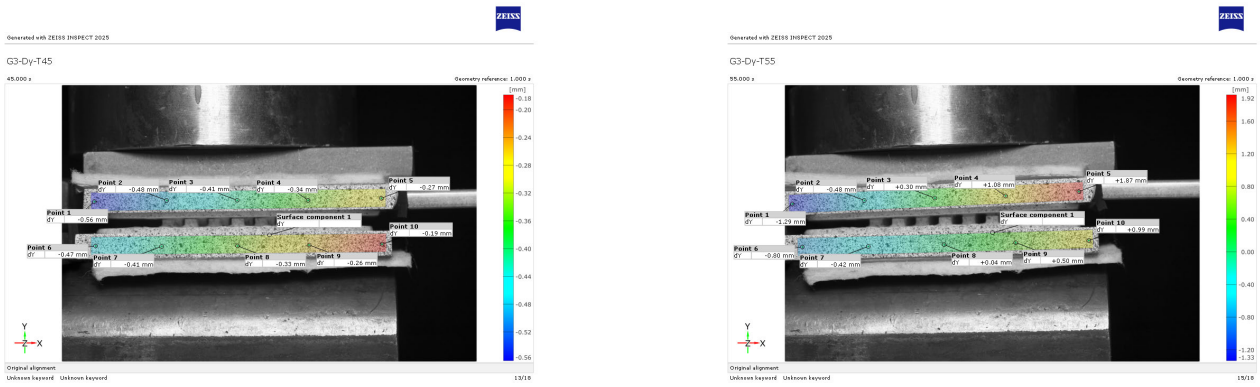

(a) DIC analysis of specimen G3: Dy displacement under 300N normal force

(b) DIC analysis of specimen G3: Dy displacement at moment of delamination

Figure 6.4: DIC analysis of specimen G3: Dy displacements

Despite these errors in the setup, the interlayer itself demonstrates impressive shear resistance. However, the abrupt and clean failures show that the adhesive bond to the glass remains the weak link. Improving surface treatment, adding adhesive or interlayer formulation to delay or soften the delamination event will be important for achieving more ductile behaviour.

6.2 Glass-Interlayer-Glass, compressive tests

Prior work by Oikonomopoulou, Bristogianni, Barou, Jacobs, et al. (2018b) performed axial compressive tests on the osteomorphic shaped cast-glass bricks in direct contact, observing brittle failure at an average compressive stress of 20–30 MPa. To mitigate stress concentrations, a 3 mm-thick PU70 interlayer was introduced in this assembly. Experimental characterisation of PU70 showed a stable compressive response under static loads. This indicates that the interlayer would redistribute contact stresses and delay the cracking compared to direct glass–glass interfaces.

In this thesis research, polylactic acid (PLA) was selected as an alternative interlayer material owing to its compatibility with additive manufacturing, compressive strength in the range of 60–100 MPa, and a Young's modulus of approximately 3 GPa. Although PLA is stiffer than PU70, its ability to be printed in conformal 2 mm-thick layers ensures precise alignment with the osteomorphic block geometry. PLA also exhibits minimal creep at room temperature, making it suitable for static compressive loading.

Due to time and material constraints, a full compression test on the osteomorphic block assemblies could not be performed. Instead, failure modes documented by Oikonomopoulou, Bristogianni, Barou, Jacobs, et al. (2018b) give insides into why the assemblies with PU interlayers fail under load:

6.2.1 Insufficient Contact due to Manufacturing Tolerances

Specimens fitted with PU70A and the firmer PU80A interlayers all fractured in a Y-shaped pattern, with cracks originating at the apex of the concave (shorter) section. This was driven by insufficient interlayer contact in that region, due to the kiln-cast bricks' dimensional tolerances, which created localised tensile peaks. As the interlayer deformed under load, in-plane shear stresses concentrated around the least contact zones, weakening the interface and promoting crack propagation in a characteristic "Y" pattern, see Figure 6.5a.

6.2.2 Tearing of the Interlayer Leading to Direct Glass–Glass Contact

Assemblies using PU75A and PU60A interlayers failed when the polymer tore at the sharp interlock edges, allowing direct glass-to-glass contact (see Figure 6.5b).

In contrast, a conformal interlayer fabricated by robotic additive manufacturing, whether made from PLA or TPU, can be produced directly from the brick's CAD geometry, ensuring exact surface compatibility and eliminating zones of mismatch. Consequently, such an interlayer achieves complete surface contact by conforming to every micro-asperity. In this way, the printed layer prevents the formation of isolated tensile peaks. In addition, uniform thickness and smoothly contoured interlayer geometry distribute shear strain more evenly, mitigating edge-initiated perforation. So, although compressive tests have not been performed on the additive manufactured PLA interlayer, the paper by Oikonomopoulou, Bristogianni, Barou, Jacobs, et al. (2018b) provides a basis for anticipating that both PU70 and PLA interlayers will enhance load distribution.

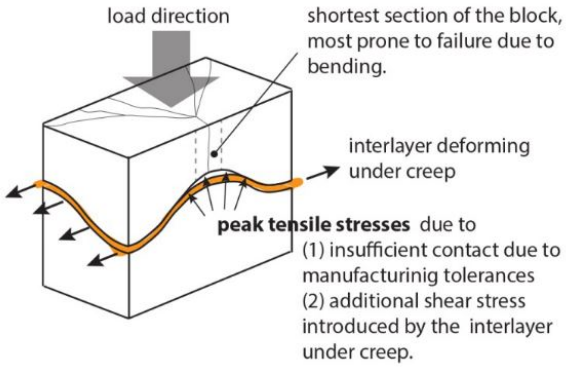

(a) Possible explanation of the cause of failure of the specimens interleaved with PMC770 (70A) and Task16 (80A)

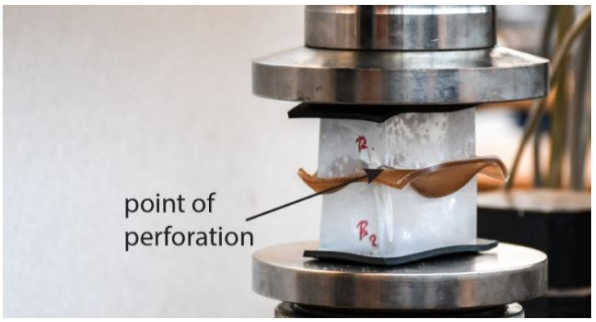

(b) Typical failure at the edge of the assembly caused by the perforation/tearing of the interlayer (specimen 60A1)

Figure 6.5: Failure modes in Compression tests done by Oikonomopoulou et al. (2019)

6.3 Conclusion

6.3.1 Test Results

The mechanical validation demonstrated that the interlocking interlayer is capable of transmitting very high shear loads under modest normal preload. In every test the polymer layer delaminated from the glass at the load peak, producing a sudden force collapse. This adhesive failure shows that, while geometric interlock and polymer deformation effectively carry shear, the bond between glass and polymer is the limiting factor of the system. The specimens reached peak forces between $F_{\text{shear,max}}$ = 1.77 kN and 6.13 kN with average friction ratios averaging μ = 1.060, seen in Figure 6.6. This means theoretically, if a normal force of 100N is applied, the interlock resists a shear force of 106 N. This substantially exceeds the typical friction coefficient values of timber-timber μ = 0.40 (*NEN-EN 1995-1-1:2023 Ontw. en*, 2023), steel-steel μ = 0.40 and steel-concrete μ = 0.60 (Europeenne & Norm, 2006).

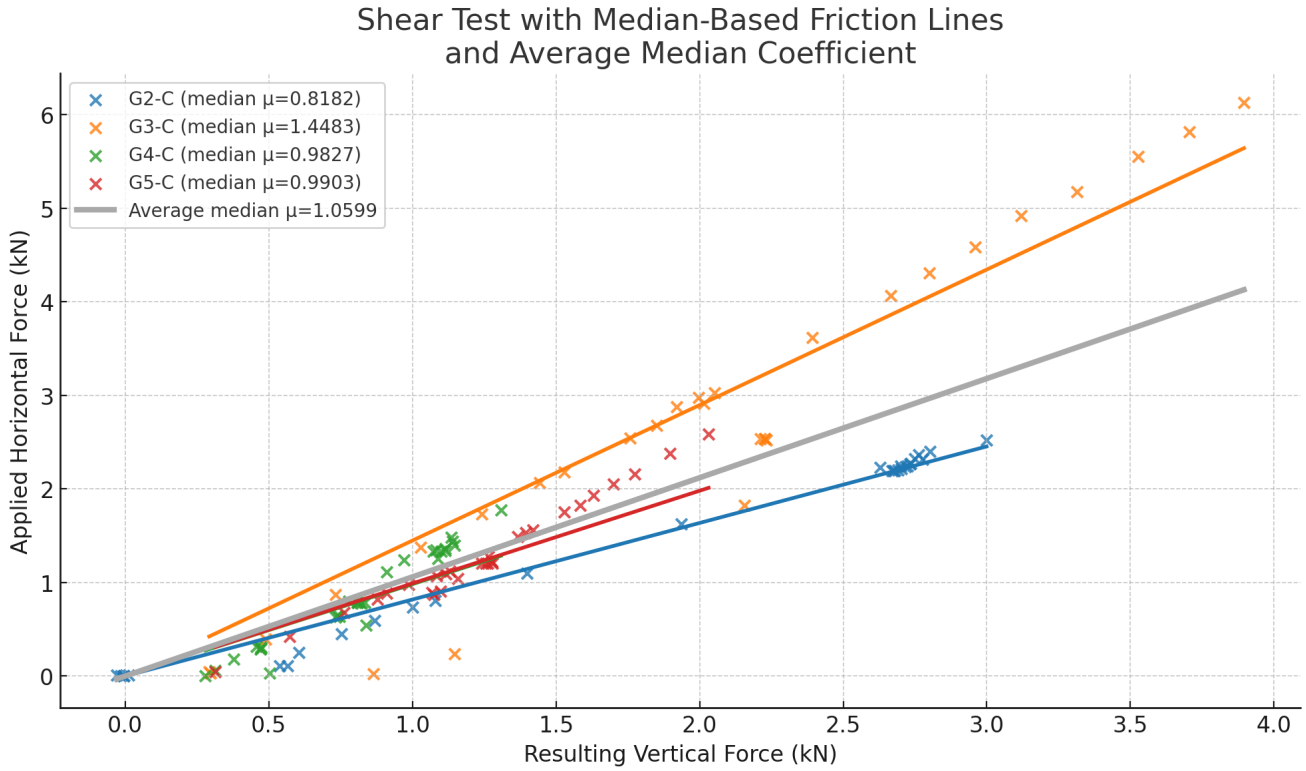

Figure 6.6: Results of shear testing of four specimens, friction coefficient as slope

Shear tests into masonry shear done by Vermeltfoort and Martens (2016), sees similar coefficient trends, although of a higher force application (see Figure 6.7).

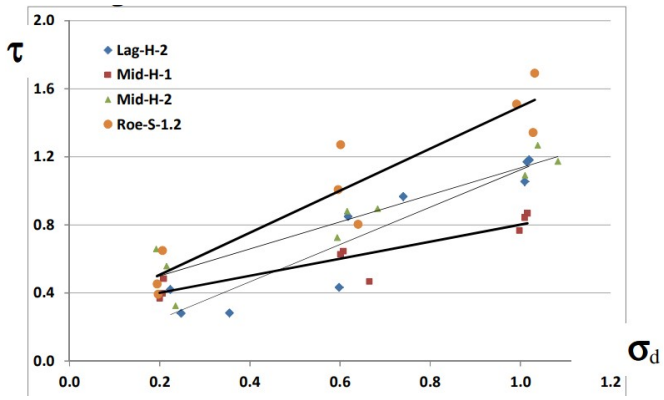

Figure 6.7: Example of four series of shear tests with extreme results. (Vermeltfoort and Martens (2016))

Looking at the results, sub-question 3 "How does the proposed system compare to existing methods in terms of mechanical behaviour?" has been answered. The interlocking system can reach friction coefficients of well above Eurocode unities and these values are comparable to a studies done by Vermeltfoort and Martens (2016) into masonry structures. Important to note is the sudden failure mode of the interlock. This implciates that further research has to be done into enhancing surface bonding to reach a state of ductile failing instead of brittle.

6.3.2 Relating to Case Study

In the Glass Vault case study from Chapter 7, the lowest interlayer carries roughly σ = 0.063 MPa of compressive stress. In the shear tests, the peak normal force of specimen G3 hit 3.90 kN, which on the samples correlates to σ = 0.481 MPa. Both are well below polymer compressive strengths (PLA: 60–100 MPa), so in service the interlayer can safely carry vault self-weight. The shear tests then acted out lateral loads, which is essential for understanding how wind or accidental impacts might disengage the vault. Assuming a straight wall of 2.5 m high, basic wind velocity of v_b = 27.00 m/s, terrain category II; z_0 = 0.050 m and $z_{\min}$ = 2.0 and ρ_{air} = 1.25 kg/m^3, according to EurocodeApplied.com (n.d.), wind can reach a peak velocity pressure of:

$$k_r = 0.19\left(\frac{z_0}{z_{0,II}}\right)^{0.07} = 0.19\left(\frac{0.050\,\mathrm{m}}{0.050\,\mathrm{m}}\right)^{0.07} = 0.1900 \qquad \text{(Terrain Factor)}$$

$$c_r(z_e) = k_r\,\ln\!\left(\frac{\max\{z_e, z_{\min}\}}{z_0}\right) = 0.1900\,\ln\!\left(\frac{\max\{2.500\,\mathrm{m}, 2.0\,\mathrm{m}\}}{0.050\,\mathrm{m}}\right) = 0.7433 \qquad \text{(Roughness Factor)}$$

$$v_m(z_e) = c_r(z_e)\,c_0(z_e)\,v_b = 0.7433 \cdot 1.000 \cdot 27.00\,\mathrm{m/s} = 20.07\,\mathrm{m/s} \qquad \text{(Mean Wind Velocity)}$$

$$I_v(z_e) = \frac{k_I}{c_0(z_e)\,\ln\!\left(\frac{\max\{z_e, z_{\min}\}}{z_0}\right)} = \frac{1.000}{1.000 \cdot \ln\!\left(\frac{\max\{2.500\,\mathrm{m}, 2.0\,\mathrm{m}\}}{0.050\,\mathrm{m}}\right)} = 0.2556 \qquad \text{(Wind–Turbulence)}$$

$$q_b = \tfrac{1}{2}\,\rho\,v_b^2 = \tfrac{1}{2}\,(1.25\,\mathrm{kg/m^3})\,(27.00\,\mathrm{m/s})^2 = 456\,\mathrm{N/m^2} = 0.456\,\mathrm{kN/m^2} \qquad \text{(Basic Velocity Pressure)}$$

$$q_p(z_e) = \big(1 + 7\,I_v(z_e)\big)\,\tfrac{1}{2}\,\rho\,v_m(z_e)^2 = \big(1 + 7 \cdot 0.2556\big)\,\tfrac{1}{2}\,(1.25\,\mathrm{kg/m^3})\,(20.07\,\mathrm{m/s})^2 = 702\,\mathrm{N/m^2} \qquad \text{(Peak Velocity Pressure)}$$

1 glass brick has an average side surface area of A = 25600 mm^2. This means with a velocity pressure of 702 N/m^2 = 0.000702 N/mm^2, 1 single brick has to take up a wind load of: 0.000702 * 25600 = 18 N. In the tests, the specimens took a lateral load of F_{normal} > 1.31 kN before failure. This suggests the interlock can safely handle wind loads.

6.3.3 Set-up Refinement

Throughout the tests, a slight upward rotation of the free edge of the glass plates was observed as shear increased. This tilting was a consequence of the fixturing — imperfect alignment and support surfaces in the set-up — and not an inherent flaw in the interlock concept itself. To obtain definitive insights into the true strength and post-peak behaviour of the interlayer, the experimental set-up must be refined: stiffer side supports, improved plate alignment and more uniform clamping. This will eliminate unintended bending and ensure that shear is resisted purely by the interlock under uniform compression.

In short, the interlocking geometry paired with a 3D-printed polymer layer can achieve shear coefficients well above typical structural contacts (μ>0.4), but its ultimate performance is limited by debonding at the glass–polymer interface and by unintended plate tilt in our fixture. To realise a vault capable of reliably resisting service loads without sudden failure, future work must focus on strengthening that adhesive bond and refining the test conditions to ensure pure-compression engagement.

7

Case Study and Validation, the Glass Vault 2.0

After validating the interface of the interlayer connection with mechanical tests. This chapter will look into how this principle can come to life in an architectural application. The case study that will be look at is the transformation of the Glass Vault by SOM, Princeton University and TU Delft (see Chapter 3.2.1). Their research demonstrates how automated robotic assembly can create a large-scale, double-curved glass brick vault without the use of scaffolding. To achieve stability during construction and accommodate the inherent dimensional variations, a fast-setting two-component epoxy putty was used. In the following chapter, the Glass Vault will be reimagined using the osteomorphic shaped bricks created by TU Delft (see Figure 3.37b) in combination with the AM interlocking interlayer, Instead of a herringbone pattern, the bricks will be stacked with a stretcher bond, facilitating easy assembly of the bricks. The goal is to achieve the same vault, but with a fully reversible character.

7.1 Fabrication and Assembly Method

To create the Glass Vault 2.0, the next sub-chapters will delve into the fabrication and assembly methods. Starting off with how the osteomorphic bricks can be shaped by either casting or AM of the glass. After that the interlayers are printed on top of the bricks to form the interlock and at that moment the Vault can be assembled.

7.1.1 Creation of Osteomorphic Bricks

Cast-Glass Bricks

The cast-glass option begins by CNC-machining or 3D-printing a gypsum mould for the osteomorphic block geometry. Recycled soda–lime glass is melted in a kiln at approximately 1100 °C and poured into the moulds. Once cooled, the glass is annealed in a controlled furnace at 480–520 °C for around 36 hours to relieve internal stresses. After annealing, each brick is removed from its mould, and the two opposing faces are ground and polished to a flatness tolerance of ± 0.1 mm.

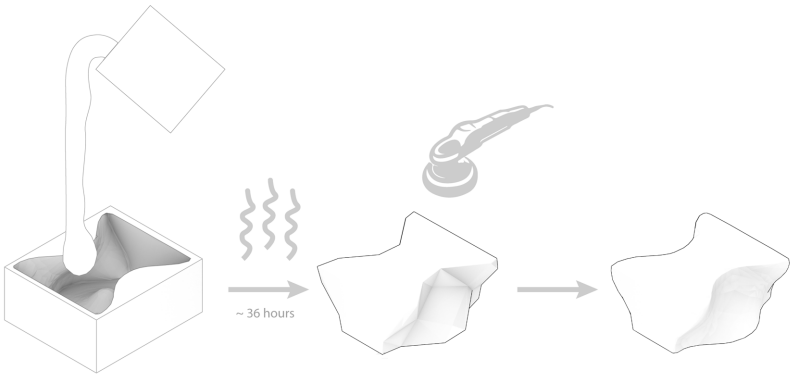

Figure 7.1: Creation of Cast Glass Blocks

3D-Printed-Glass Bricks

In the additive-manufacturing approach, each osteomorphic brick is printed layer-by-layer from recycled float-glass using the G3DP3 system. The printer deposits molten glass in paths that create the block's unique interlock geometry. Upon completing the print, the brick is transferred to an annealing chamber at 480–520 °C for 12–24 hours, scaled to the part's thickness.

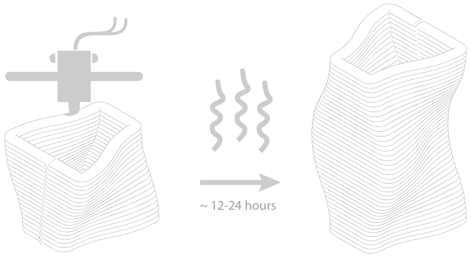

Figure 7.2: Creation of AM glass blocks

7.1.2 Heating and Printing of Polymer Interlayers

Cast-glass bricks casted in disposable moulds undergo individual grinding and polishing, surface variations occur between units; to accommodate these differences, each cast brick is scanned in using a Go!SCAN 3D (GeoScan) system (see Chapter 8.1.1). The resulting mesh is imported into 3D model software, where the interlayer is generated to match that brick's unique topography. By contrast, cast glass bricks from industrial grade metal moulds and 3D-printed-glass bricks are produced from the same digital model that guided their fabrication, delivering uniform dimensions and surface geometry to create a uniform interlayer. To AM the interlayer, each finished brick is placed in a heated environment that raises its contact faces to the desired temperature (60°C) for polymer adhesion. A six-axis robotic arm, also in this heated chamber, carries a direct-drive extruder loaded with PLA. A human operator secures the brick in a fixture and orientates it for the first interlayer print on the top face. This triggers the robot to deposit the 3 mm interlayer with interlocking features across the 'top'-surface. Once the first side is complete, the operator rotates the brick by hand in the same fixture, flips it, and locks it in place. Then, the robotic arm prints the other interlocking interlayer across the 'bottom'-surface.

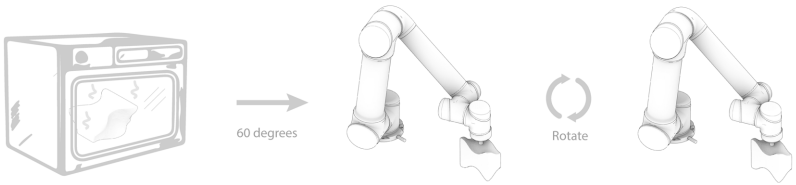

Figure 7.3: Heating and Printing the Polymer Interlayer

7.1.3 Vault Assembly with Dual-Arm Robotics

On site, a crew installs ground-anchored steel casings (with matching neoprene protections) at each footing to place the vault's base bricks. Then, they create a temporary scaffolding that defines the catenary arch geometry. Two robotic arms, each confined to its own linear rail on opposite sides of the formwork, collaborate to build the vault. On the one side, one robotic arm retrieves a brick from its casing, aligns its extrusions to the interlayer of the previous brick and inserts it into place. Simultaneously, the second arm does the same for the other side. As each brick is engaged, the interlocking interlayers ensure the load path remains in pure compression. Once both halves of the arch meet at the top, workers can remove the framework, leaving a self-supporting glass vault with reversible joints.

(a) Ground anchored steel casings.

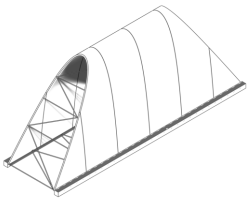

(b) Temporary scaffolding is placed.

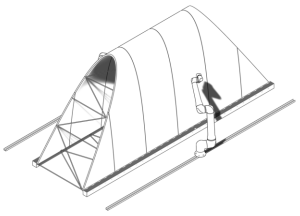

(c) Two robotic arms are placed on linear rails.

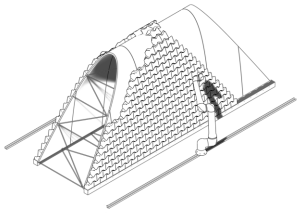

(d) Bricks are interlocked with the AM interlayer.

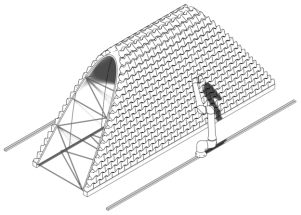

(e) Arch geometry and self-supporting structure is achieved.

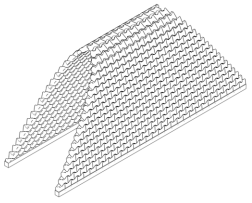

(f) Temporary scaffolding is removed.

Figure 7.4: Assembly sequence of the Glass Vault 2.0

7.1.4 Repurposing and Recycling the Structure

At the end of life of the current configuration of the Glass Vault 2.0, the glass bricks can be disassembled by the same robotic workflow as the assembly. This way, a new Glass Vault 3.0 can be assembled with the same bricks in a different location of configuration. When the glass brick or polymer has reached its end of life, this can happen due to different circumstances like damage or losing strength, the glass and polymer have to be deattached from each other. This happens by heating each of the bricks to a temperature of > 80 °C, a bit above the glass

transition temperature of PLA (60 °C). This way, the PLA becomes more elastic and can be peeled off from the glass cleanly. Using this workflow, the glass brick as well as the polymer can be recycled and used again.

7.1.5 Cast-Glass vs. 3D-Printed Glass in Fabrication and Assembly

The osteomorphic shaped cast-glass bricks used in this thesis research (see Figure 3.37b) were produced with the use of disposable moulds and the lost-wax technique. This type of cast glass production demands extensive post-processing. After kiln-casting and annealing, each block often contains residual bubbles, micro-cracks, or surface imperfections that must be removed through precision grinding and polishing to achieve the flatness tolerance of $\pm$0.1 mm. This adds significant labour time and cost per unit, as operators carefully inspect and correct each face before interlayer printing. On the other hand, when using industrial scale casting with the use of metal moulds, high accuracy can be obtained and post-processing can be evaded. 3D-printing glass bricks typically produces parts with few defects from its CAD-file, mostly owing to controlled extrusion and real-time infrared monitoring. Although these printed bricks still undergo an annealing cycle, their surfaces usually require only minimal polishing, reducing manual labour and turnaround time.

In the interlayer print stage, both brick types follow the same wokrflow - heating, printing on top, manual rotation, and printing on the bottom - to produce an interlayer with interlocking features. However, the smoother initial finish of AM bricks enhances dimensional consistency, whereas cast bricks sometimes need additional adjustment to account for slight grinding variations. This consistency eliminates the need for individual scans: in AM glass, the original CAD file is used to generate both the top and bottom interlayers, streamlining the workflow and reducing setup time before printing.

During vault assembly with robotic arms, the post-processed uniformity of cast glass bricks allows placements with little calibration per unit. However, the initial finishing effort can slow down production. On the other hand, AM bricks require only minor surface finishing and come with accurate digital records, so the robots can be programmed and deployed quickly. This makes AM especially well suited for projects that require fast adjustments or unique and custom shapes.

7.2 Drawings

7.2.1 Overview and technical drawings

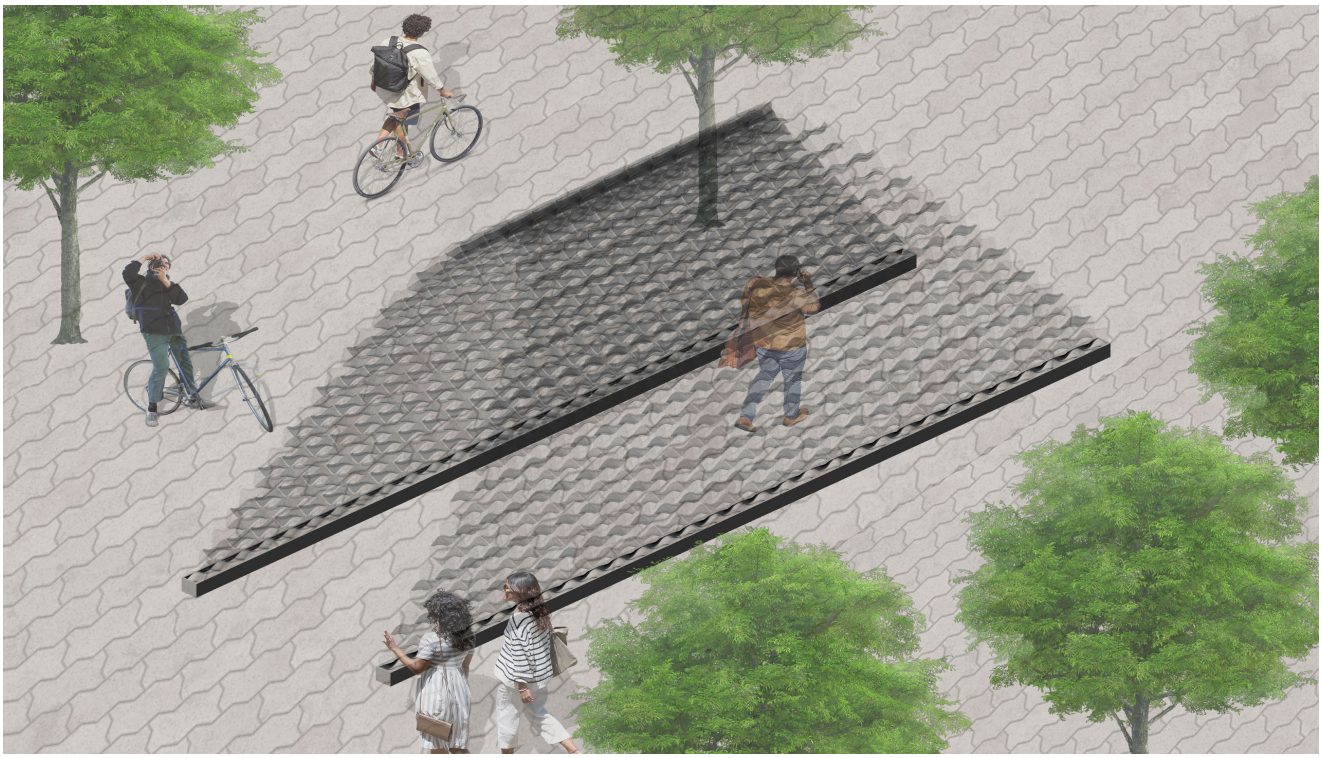

Figure 7.5: Impression of the Glass Vault 2.0

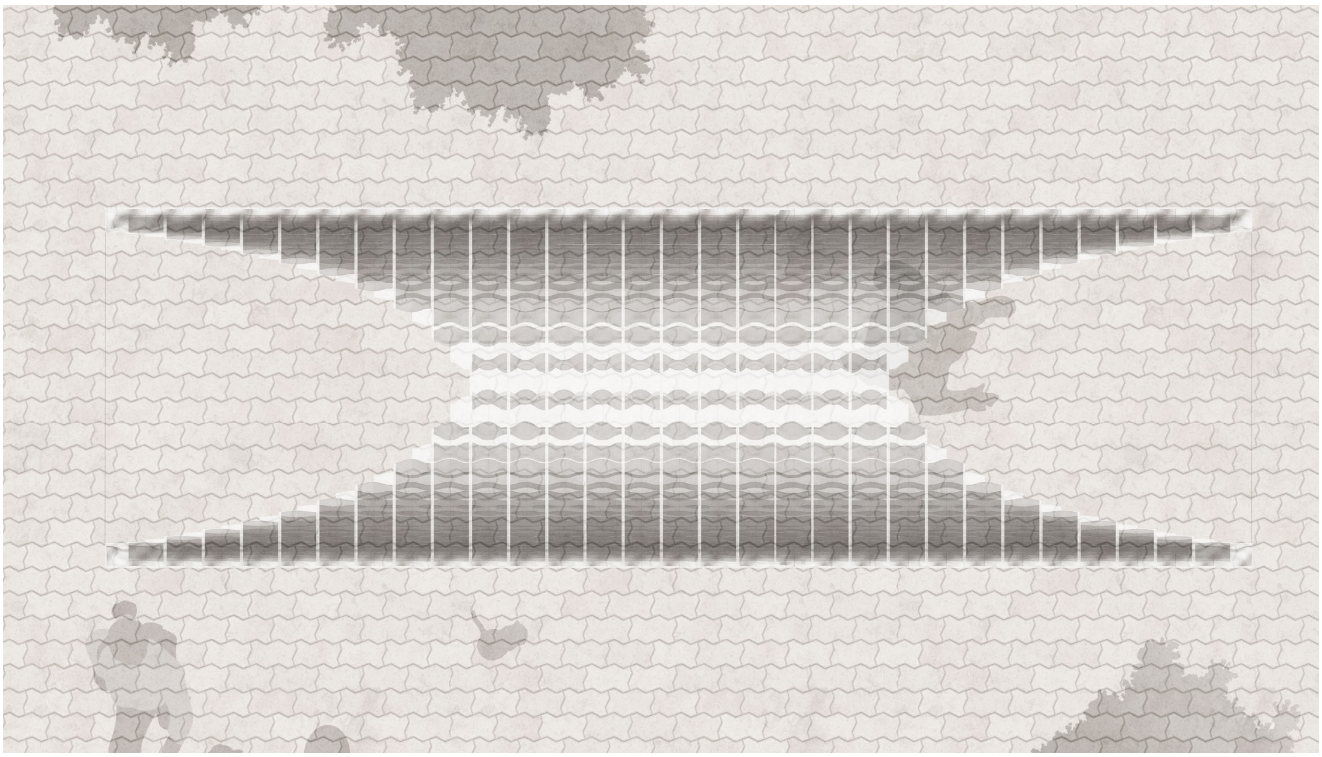

Figure 7.6: Top view of the Glass Vault 2.0

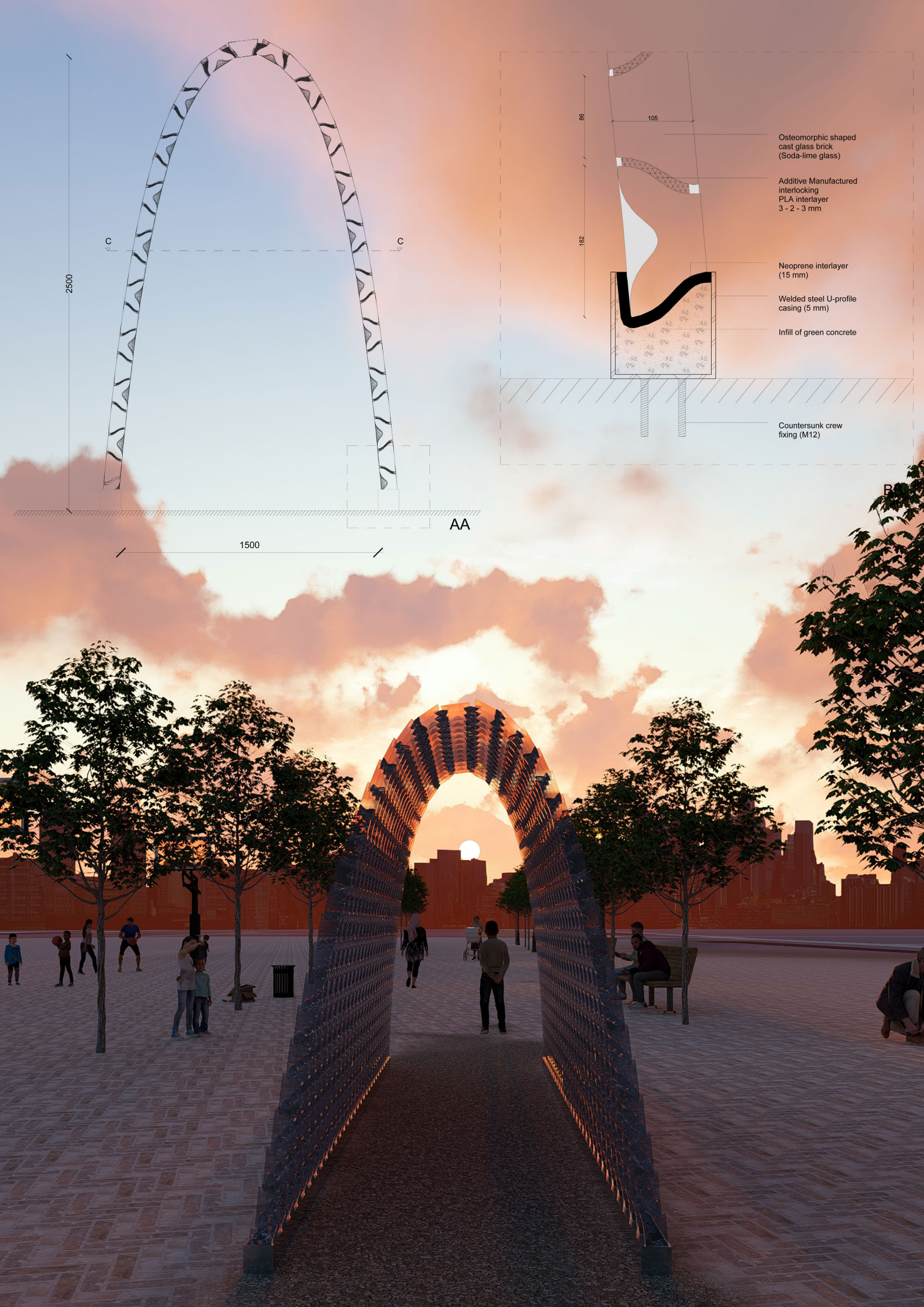
C
C
2500
AA
1500
86
105
182
Osteomorphic shaped
cast glass brick
(Soda-lime glass)
Additive Manufactured
interlocking
PLA interlayer
3 - 2 - 3 mm
Neoprene interlayer
(15 mm)
Welded steel U-profile
casing (5 mm)
Infill of green concrete
Countersunk crew
fixing (M12)

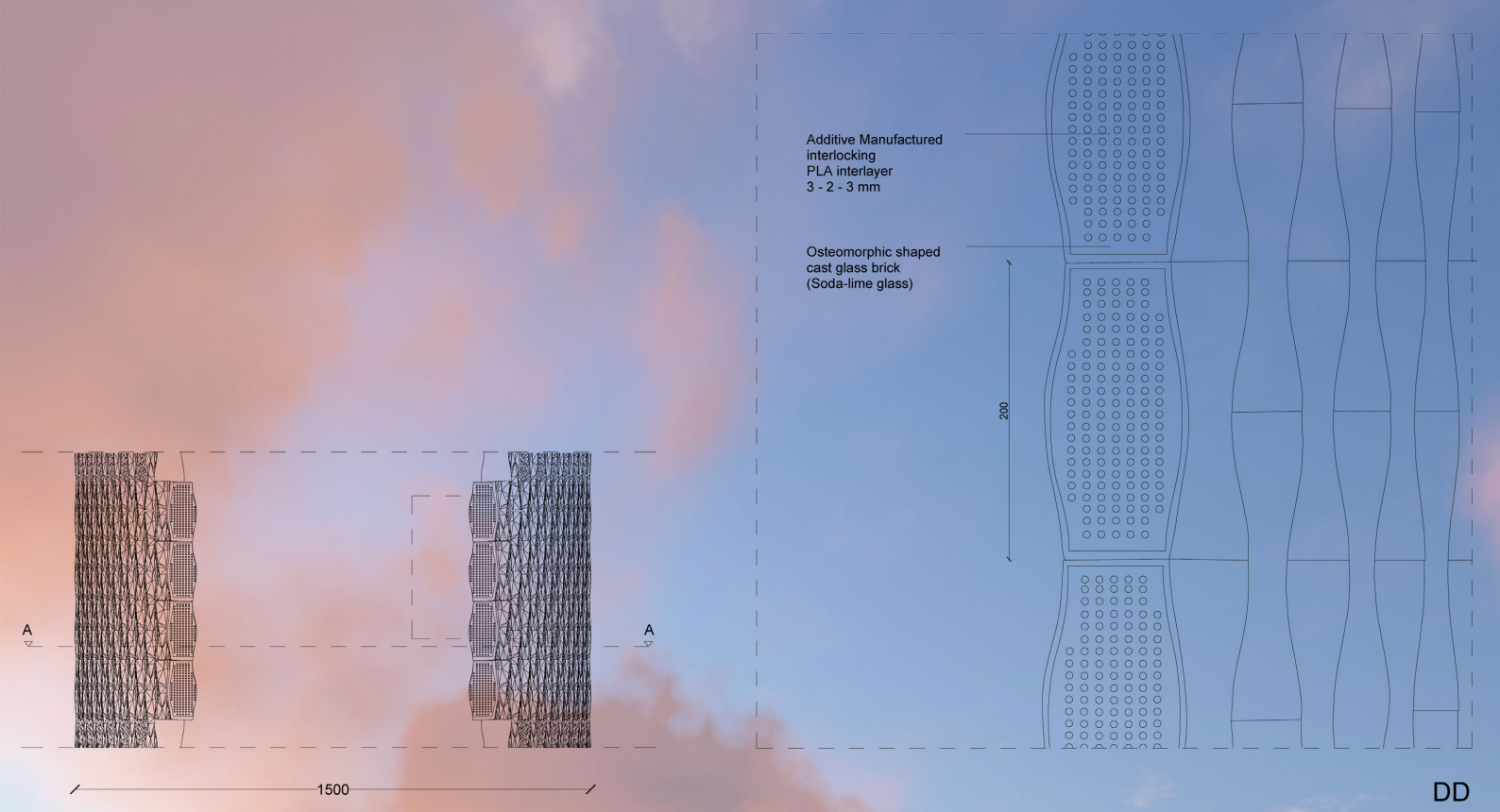
A
A
1500

CC

Additive Manufactured
interlocking
PLA interlayer
3 - 2 - 3 mm
Osteomorphic shaped
cast glass brick
(Soda-lime glass)
200

DD

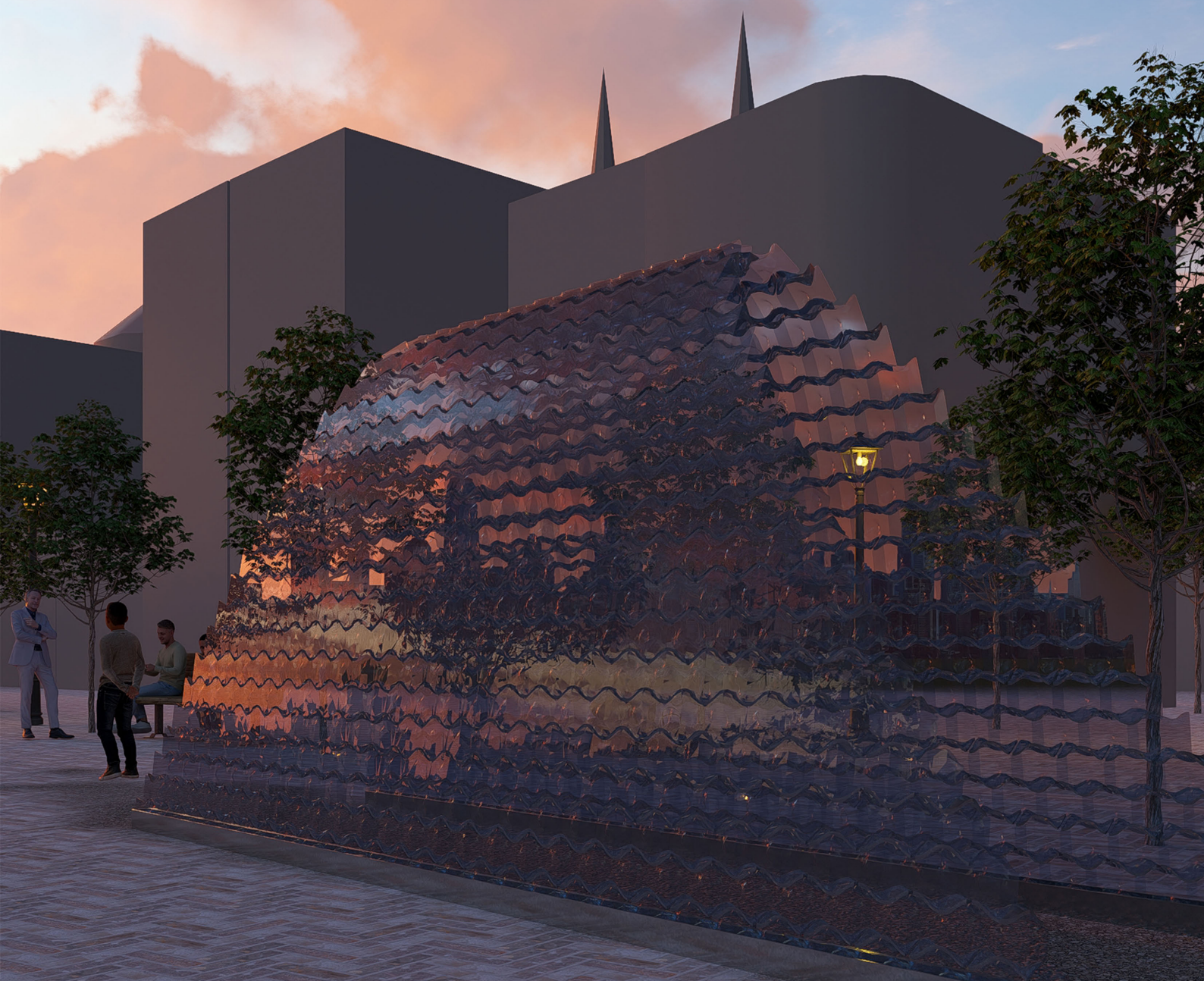

7.3 Validation (hand calculations)

7.3.1 Overview

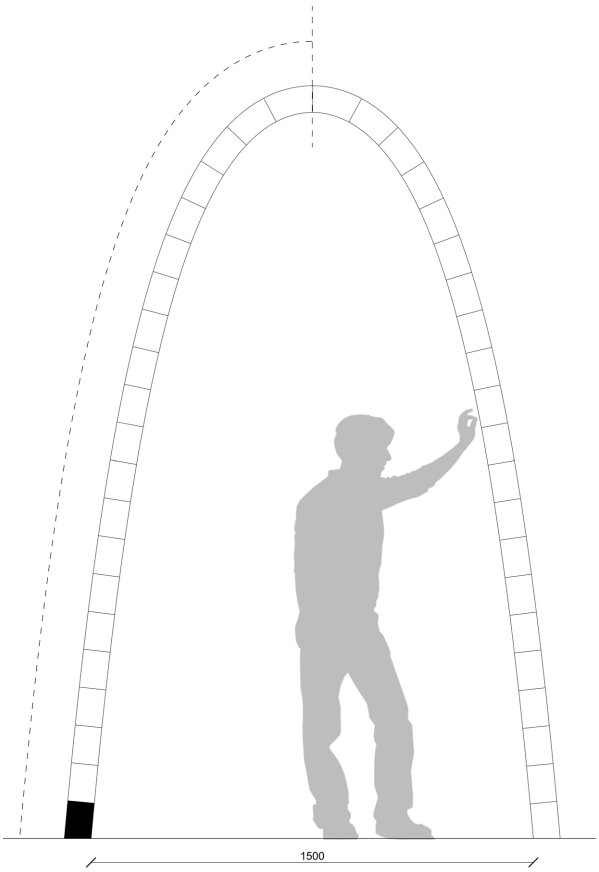

(a) Compressive-only catenary arch, simplification

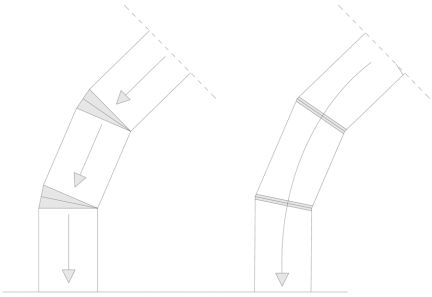

(b) Left: cast glass blocks with bespoke interlayer, right: bespoke glass blocks with universal interlayer

Figure 7.7: Simplification of the compressive-only catenary arch

Figure 7.7a shows a simplified two-dimensional representation of the glass catenary arch, used for concept validation and hand-calculation purposes. The catenary arch comprises 42 identical glass blocks, spanning 1.5 m horizontally and rising 2.5 m vertically. Considering one half of the arch (Figure 7.7a), the combined weight of 21 blocks is carried by the lower-left unit. Each fully solid cast glass block weighs 5.46 kg, the resulting normal force on the block–interlayer assembly is:

$$F_{N_{castblock}} = 21 \times 6.46\,\text{kg} \times 9.81\,\text{m/s}^2 \approx 1124,1\,\text{N}. \tag{7.1}$$

The additive manufactured glass blocks are not fully solid blocks and are therefore a lot lighter (see Figure 7.8b). They each have a volume of 698.25 cm^3. Assuming a glass density for soda lime silicate glass of 2.49 g/cm^3 (İlerisoy & Çolak, 2018), the weight per unit is: 698.25 * 2.49 = 1738.64 g, which correlates to 1.74 kg. The resulting normal force on the lowest additive manufactured glass blocks is therefore:

$$F_{N_{AMblock}} = 21 \times 1.74\,\text{kg} \times 9.81\,\text{m/s}^2 \approx 358.18\,\text{N}. \tag{7.2}$$

With a contact area of A = 17791.2 mm^2, the compressive stress on the top surface of the glass blocks (and its interlayer) are:

$$\sigma_{castblock} = \frac{1124.1 \text{ N}}{17791.2 \text{ mm}^2} \approx 0.063 \text{ N/mm}^2. \tag{7.3}$$

,

$$\sigma_{AMblock} = \frac{358.18 \text{ N}}{17791.2 \text{ mm}^2} \approx 0.020 \text{ N/mm}^2. \tag{7.4}$$

,

both values are well below the 2 MPa design criterion (Table 3.9).

(a) Osteomorphic shaped cast glass brick

(b) Osteomorphic shaped Additive Manufactured glass brick

Figure 7.8: Comparison between a cast and additive manufactured glass brick

7.3.2 Force Difference in Cast Glass vs. 3D-Printed Glass Arch

To achieve the exact catenary curvature with cast-glass blocks, each pair of blocks requires a unique interlayer to fill the angular gap between their faces. The slight misalignment between the surface normals and the load vector introduces off-axis forces that can accumulate and risk buckling (see Figure 7.7b). By contrast, 3D-printed glass blocks can incorporate the angular correction into the block geometry itself, allowing the use of a uniform interlayer and ensuring an on-axis load path throughout the structure, simplifying assembly and improving structural reliability. On the other hand, this means a more intensive designing phase of the printed glass blocks.

7.4 Conclusion

For the cast-glass Glass Vaults the compressive stress on the lowest block's interlayer is at about σ = 0.063 N/mm², while for the and 3D-printed Glass Vault it is σ = 0.020 N/mm², both well below the 2 MPa minimum design compressive strength set in previous chapters and the max compressive stress of PLA (60-72 MPa). This means the polymer interlayer comfortably carries the compressive load. The cast-glass workflow relies on mature techniques, but the primary bottleneck lies in the labour-intensive finish work on the current osteomorphic shaped bricks: each block must be ground, polished, scanned, and matched with a custom interlayer. This intensive post-processing stage can be evaded by using industrial-scale metal moulds which reach a very high accuracy. Furthermore, the same geometry for every brick introduces slight off-axis normal forces. By contrast, 3D-printed bricks focuses on printing angular corrections into their geometry allowing a compression-only build and the use of a uniform interlayer. Also, the interlayer can be printed with info derived from the CAD file and does not need scanning. The trade-off is that AM shifts complexity into an intensive upfront design phase and depends on specialised AM hardware, like the G3DP3, whereas cast glass prioritises simpler material workflows at the expense of extra post-processing labour and assembly setup.

The potential to additive manufacture polymer interlayers directly onto any shaped glass surfaces means that, as long as the 3D model anticipates to the curves of the glass brick, the same robotic workflow can adapt to all different kind of structures. In this case it is a Vault, but it could also be used in domes or free-form facades for example. Another significant advantage of the direct additive manufacturing on the brick without adhesives is the possibility to reclaim the polymer from the glass without leaving traces. This means both the glass and the polymer can be recycled completely.

7.4.1 Cast Glass Bricks

In the cast-glass scenario, a single (osteomorphic) brick geometry can serve for any vault or free-form structure when paired with bespoke, 3D-printed interlayers. By parametrically generating each interlayer to compensate for local angular tolerances, the same cast block can be used to match this thesis' catenary vault without altering the mould design. Because the polymer interlayer is AM robotically, even highly double-curved vault geometries become feasible. For example, even flat (left in Figure 7.9) or slightly slanted (right in Figure 7.9) cast glass bricks could benefit from a precise interlocking reversible interlayer that would not only account for the angular correction needed to create an arch but also carry the lateral loads and account for micro-asperities of the glass.

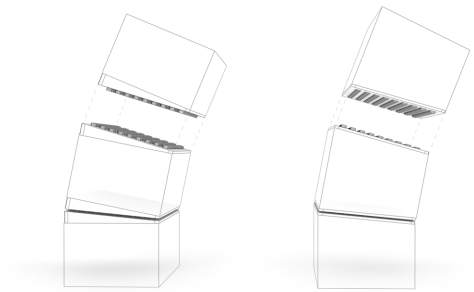

Figure 7.9: Concept: a precisely printed AM interlocking reversible interlayer that carries lateral loads as well creates angular correction to form an arch for example

In this research, osteomorphic shaped cast glass bricks were produced with disposable moulds and a lost-wax technique. Their dimensional variability necessitates individual 3D scanning and custom interlayer fabrication, which adds significant labour to the workflow. For large-scale deployment of this system, replacing these moulds with precision-machined metal moulds would achieve high accuracy directly out of the kiln, eliminating the grinding, polishing, and scanning steps. Then, each cast brick could receive its interlayer from a single CAD routine, streamlining the production workflow. So, by using a custom 3D-printed interlayer, a single cast-glass mould can realise limitless form variations, only constrained by the robot's reach.
However, even with precision metal moulds, small dimensional deviations in the glass and interlayer ($\pm$0.1–0.2 mm) will accumulate across many bricks. The current PLA interlayer's rigidity limits its ability to absorb these misalignments, though the "Lego-like" interlock offers some self-adjustment. To improve compliance, a thicker interlayer printed from a softer thermoplastic elastomer (e.g. TPU) could be employed. Its lower stiffness would accommodate the offsets without compromising compression-only behaviour. However, printing TPU at this scale demands a specialised nozzle and tuned extrusion parameters to ensure reliable layer adhesion and dimensional accuracy (see Chapter 4.1.3).

7.4.2 Additive Manufactured Glass Bricks

With additively manufactured glass, angular corrections are integrated directly into the block geometry during printing. Each brick is produced from a CAD model that embeds the exact form-twist or taper needed for its position in the vault. This removes the need for individualised scanning and angular compensation in the interlayer design. As a result, the interlayer can be swapped from a custom AM to a high-volume injection-moulded thermoplastic interlayer with standardised interlock features. Injection moulding can reach tight tolerances of up to 0.050 mm (Melito, 2022) at production rates of hundreds per hour, driving down per-unit cost. To create a proper and reversible adhesion between the injection-moulded interlayer and the glass brick, a snap-fit joint has to be designed. For example, a universal interlayer clips into each AM brick, which then seals the the brick and creates an interlocking interlayer for the next brick to clip on (see Figure 7.10). Here, the design complexity shifts into the digital modelling phase of the bricks and its interlayer adhesion, while physical assembly of the structure becomes more streamlined. Using a high-volume moulding for the interlayer saves up a lot of labour and time in specialised robotic extrusion.
While AM bricks reproduce their CAD form closely, process variability (e.g. layer adhesion, thermal shrinkage) can still introduce tiny mismatches. Relying on a rigid, injection-moulded thermoplastic interlayer risks poor fit if deviations exceed the tolerance. A more compliant silicone

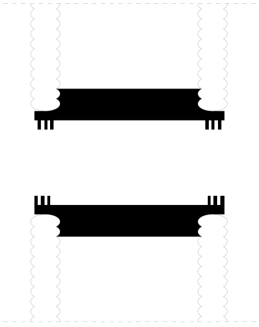

Figure 7.10: Concept: section, An AM snap-fit joint (black hatch) snaps into the AM glass bricks, sealing the brick by utilising its beads. On the other side of the snap-fit, an interlock is additive manufactured which can interlock with the next brick.

interlayer would offer lower stiffness and greater damping of angular or lateral offsets, ensuring reliable engagement under manufacturing tolerances. This softer material layer preserves reversibility while significantly increasing the system's tolerance to dimensional variation.

Looking forward, both of the workflows can be used for different purposes. Cast-glass bricks paired with bespoke, robotically 3D-printed interlayers offer limitless form variations from a single mould, ideal for creating structures where the bricks can later be reused in a different variation with other interlayers. AM glass embeds angular corrections directly into each brick's CAD-driven geometry, enabling the use of standardised, injection-moulded interlayers. This type of design can be used for more specialised and bespoke structures. In summary, cast glass excels in adaptive reuse of a single block design, while AM glass streamlines production through upfront digital complexity of the brick and mass-manufactured interlayers. Analysing critically which workflow to use best for a specific project, a structure like the Glass Vault 2.0 can evolve into a manufacturable and reversible system for any shaped glass structure.

8
Prototyping ‘the Direct Print’

8.1 Preparing the Glass Brick

8.1.1 Scanning of the Prototype Glass Brick

For this research both cast and AM osteomorphic glass bricks will be looked at. However, because the G3DP3 is located at Evenline inc. in Rochester, New York, only the 1:2 cast glass brick variant by TU Delft is tested on, see Figure 3.16. As discussed in 5.1.2, the osteomorphic shaped brick has a non-planar top surface. So,to create a printable interlayer on this surface, a 3D model of the brick is needed. However, the 3D models used to create the mould for the casting are not exactly the outcome of the bricks. This is due to the heavy post-processing of the bricks after casting. For example, after annealing, the bricks are ground and polished with a Dremel rotary tool with diamond pads to eliminate imperfections (Oikonomopoulou, Bristogianni, Barou, Jacobs, et al., 2018a). The UR5 robot needs an exact top surface of the bricks in order to print the interlayer with high accuracy. That is why the three bricks used in this thesis were scanned in with a CreaForm Go!SCAN 3D at the NewMedia Centre at the TU Delft, see Figure 8.1. Because the blocks are made out of glass, the 3D scanner has difficulty scanning as it scans trough the block. That is why an AESUB vanishing scanning spray is applied to the brick. This leaves a white, dry to handle coating that evaporates automatically after scanning, as seen in Figure 8.1b. The brick is lifted in order to be able to scan the hard-to-reach sides of the brick. The scan is then sent to the software in real-time making it easy to handle and see where more scanning is required. After the scanning is complete, the model is exported as a .stl model and the spray evaporates leaving no residuals. This was done for all of the three bricks because they all have small differences.

(a) Scanning spray

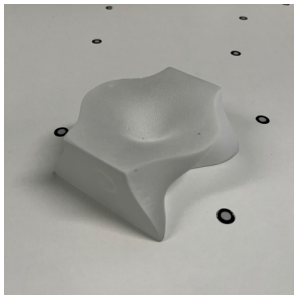

(b) Glass brick sprayed white

(c) The scanning of the brick

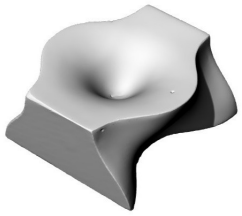

(d) The scanned 3D model

Figure 8.1: Scanning of the osteomorphic shaped cast glass bricks with a CreaForm Go!SCAN 3D

8.1.2 Geometry of the non-planar interlayer

The final flat interlayer sample, designed and optimised in Chapter 5.2.1, needs to be altered to fit onto the top surface of the scanned osteomorphic shaped bricks. In this example scan number 3 is used because the top surface and scan were chosen to be the best out of the three scans. For this interlayer a Grasshopper script is written and as a basic geometry input in Rhino, scan 3 is used. The first step is the projection of a rectangle onto the top surface of the brick. This creates the outline of the interlayer. This outline is then patched together to create a surface.

The surface is then extruded 3.5 mm to create an interlayer with a well divided thickness. The top surface of this interlayer is then divided into points and the vector directions of these points are taken. These vectors are used as base planes for the Lego type extrusions. 2 types are made: a top interlayer and a bottom interlayer. The bottom interlayer has shifted extrusions so when clicked together they align well in the open spaces of the top interlayer. The last step is the fillet of the edge to create a smooth toolpath for the 3D printer.

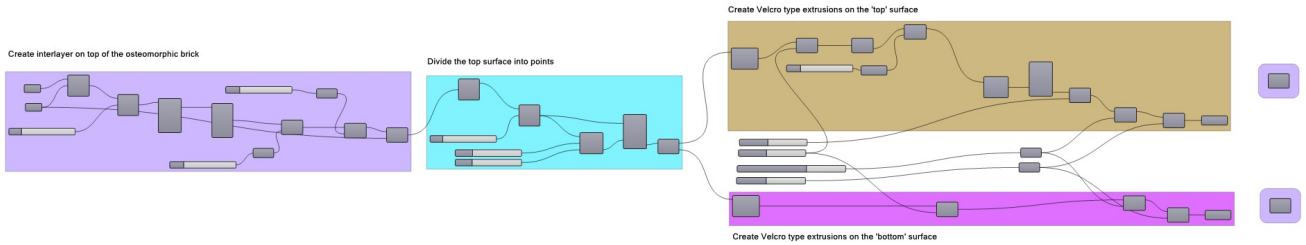

Figure 8.2: Grasshopper script used to create the interlayer on top of the brick

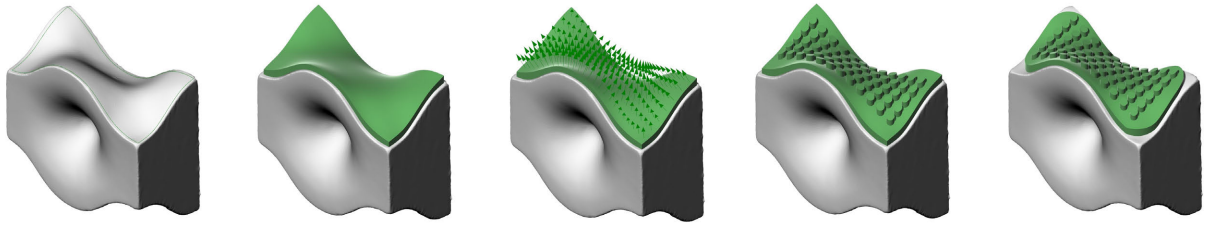

Figure 8.3: Interlayer 3D model design steps, from left to right: a rectangle is projected onto the scanned osteomoprhic shaped brick, this projection is patched and extruded, the top surface is divided into direction vectors, these vectors are used to create Velcro type extrusions on the surface, the corners are fillet to create a smooth print path (Own image)

8.2 AM with a UR5 robot

The curvature of the osteomorphic glass brick makes conventional Cartesian 3D printers, in which the nozzle moves strictly along orthogonal X, Y and Z axes, incapable of following its non-planar surfaces without collision. In contrast, a six-axis robot such as the UR5, with six revolute joints, can maintain the extruder normal to the curved surface and avoid collision during deposition. Consequently, this thesis employs a UR5 robotic arm fitted with a custom filament extruder to prototype the interlayer directly onto the non-planar brick, necessitating a bespoke multi-axis fabrication workflow described in the following sections.

8.2.1 Background, Multi-axis vs. Cartesian Printing

Cartesian printers (3-axis)

A Cartesian 3D printer is the conventional style of FDM printer with three linear axes (X, Y, and Z). The print head and/or build platform move linearly along orthogonal X, Y, and Z axes to position the nozzle in three-dimensional space top3dshop, 2019. For example, the nozzle might move in the X–Y plane while the bed moves in Z, or vice versa. These 3-axis printers constrain the printhead to motions in a Cartesian grid, building objects layer-by-layer in horizontal planes.

Six-axis robots

A 6-axis robot is an articulated robotic arm with six degrees of freedom, typically realised by six revolute joints Standard Bots, 2025. These joints (often labeled base, shoulder, elbow, and wrist joints 1–3, see Figure 8.4), allow the robot to position and orient its end-effector in 3D space. The six axes of motion (all rotational in a UR5) are as follows:

1. Axis 1 – Base: A revolute joint at the base that rotates the arm left-right around a vertical axis (robot yaw).
2. Axis 2 – Shoulder: A revolute joint that lifts or lowers the arm in a vertical plane (shoulder pitch) by rotating around a horizontal axis.
3. Axis 3 – Elbow: A revolute joint that bends or extends the arm (elbow pitch), moving the forearm in/out relative to the upper arm.
4. Axis 4 – Wrist 1: A revolute "wrist" joint that twists the forearm (rotates around the arm's length axis).
5. Axis 5 – Wrist 2: A revolute wrist joint that tilts the wrist up or down (pitch, typically around an axis parallel to the shoulder joint).
6. Axis 6 – Wrist 3: A revolute wrist joint at the end-effector flange that rotates the tool around its central axis (tool roll/yaw).

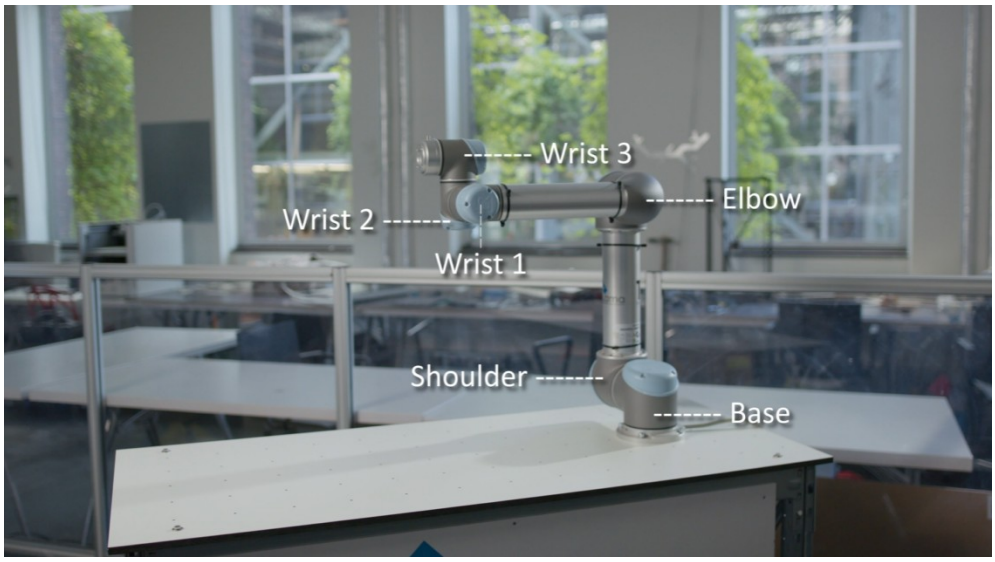

Figure 8.4: 6 axis of the UR5 robot at the LAMA lab

Five-axis slicing

Although the UR5 is a 6-axis robot, slicing software from 5'DOTX system controls' is described as 5-axis. This is because the software plans toolpaths using five degrees of freedom (typically 3 positional axes + 2 orientational axes), the sixth axis seems to be redundant. In practice, five axes are sufficient to control a nozzle's position and orientation for printing; the final 6th degree of freedom (rotation about the nozzle's own axis) does not change the deposition orientation and is thus not needed in path planning. In other words, a 5-axis slicer can orient the printhead normal to the surface and move along the part, so the robot's extra joint is not explicitly utilised by the slicer algorithm.

8.2.2 Hardware

The non-planar 3D-printing system centers on a Universal Robots UR5 six-axis arm fitted with a bespoke glass-brick fixture and a direct-drive extrusion module. All elements are configured to enable the nozzle to maintain the correct orientation and distance from the curved osteomorphic surface while controlling filament flow and temperature. This setup integrates closely with the software workflow, described in the next chapter, to synchronise robot movement with slicing and extrusion commands. This collaboration ensuresinterlayer deposition on non-planar geometries.

1. UR5, a Six-Axis Robotic Arm

As described, the core of this workflow is a UR5 robotic arm mounted on a rigid workstation at TU Delft's LAMA lab. Its six axes create full positional and orientational freedom, allowing the extruder to approach any surface normal or desired angle without collision. Prior to operation, the combined robot-extruder assembly is calibrated in RoboDK: the Tool Centre Point (TCP), total mass, and center of gravity are defined via the teach pendant and simulation environment to guarantee kinematic accuracy and dynamic stability during multi-axis printing.

2. Extruder & Gripper

A direct-drive extruder is fixed to the UR5 flange via a custom-made bracket (see Figure 8.5). A dedicated heatsink and cooling fan are attached to maintain nozzle temperature. All cables – heater, thermistor, fan power, stepdriver and PTFE filament tube - are routed along the arm in a flexible sleeve to prevent snagging during multi-axis motions. For extra safety a tie wrap is placed around the extruder in case of failure of the bracket.

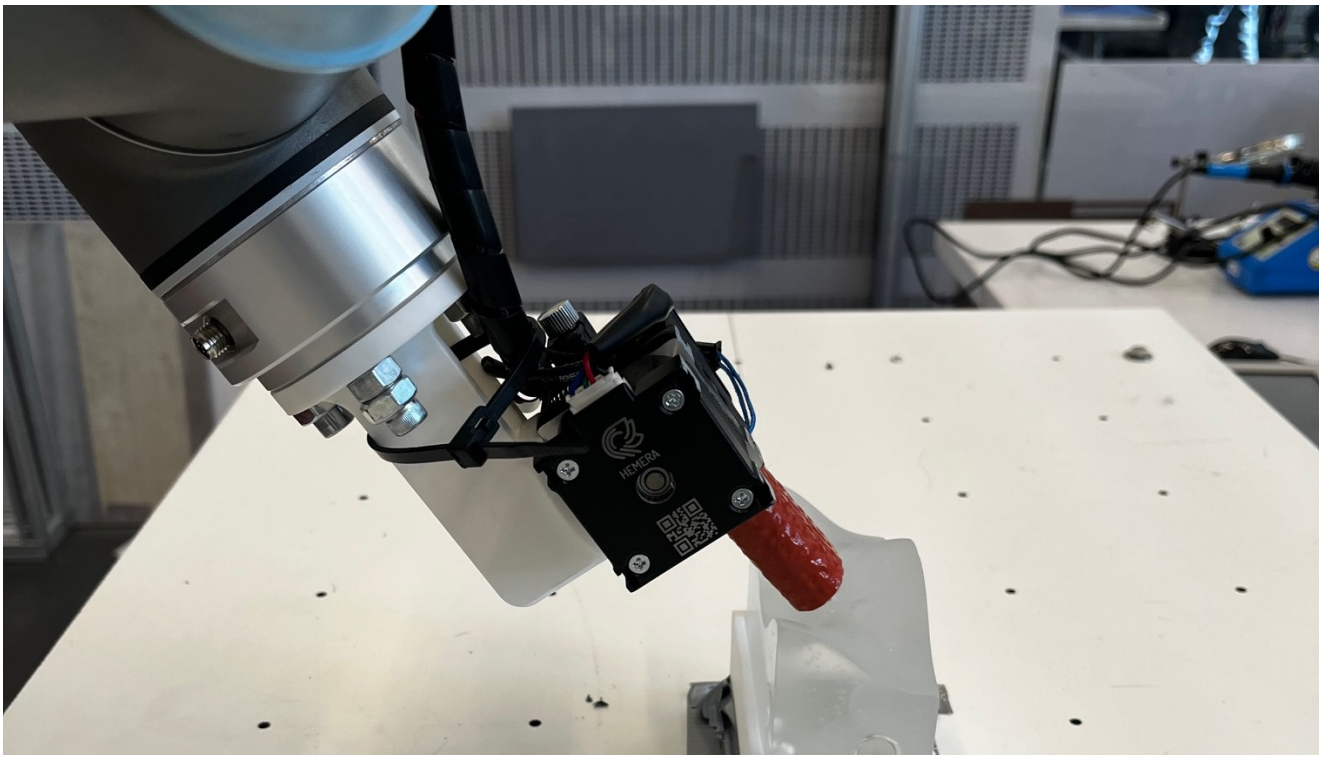

Figure 8.5: Custom bracket connecting the extruder to the UR5-head

3. Osteomorphic brick & Casing

The osteomorphic glass block is seated in a 3D-printed PLA casing that conforms exactly to its scanned geometry. The casing inserts with pins into the workstation base, locking the brick in place relative to the UR5 and exposing the top surface for printing.

4. Arduino MEGA 2560 microcontroller

a. Drive the Stepmotor

An Arduino MEGA 2560 is used for two purposes, firs of all to convert the UR5's analog extrusion signal (0–5 V) via its A0 pin to step/dir pulses for the extruder motor driver. Ground is shared between the robot and Arduino, with twisted-pair wiring to minimise noise.

b. Temperature Measurement

Accurate temperature measurement of the 3D printer's heat block relies on a voltage-divider circuit. An NTC thermistor, whose resistance decreases with increasing temperature, is paired with a reference resistor. Both are connected in series between the Arduino's 5 V supply and ground. The midpoint voltage, which varies as the thermistor's resistance changes, is sampled by the Arduino's 10-bit analog-to-digital converter (ADC). In this configuration, the output voltage at this point is described by the divider equation:

$$V_{\text{out}} = V_{cc} * \frac{R_{\text{ref}}}{R_{\text{ref}} + R_{th}(T)}$$

where V_{cc} = 5V, R_{ref} is a fixed 100 kΩ resistor selected to match the thermistor's nominal resistance at room temperature, and $R_{th}(T)$ is the temperature-dependent thermistor resistance. By choosing R_{ref} close to the thermistor's resistance at the target operating temperature, the circuit achieves maximal sensitivity, as the rate of change dV_{out}/dR_{th} is then greatest in the desired measurement region.

The Arduino's ADC converts V_{out} to a digital count N between 0 and 1023. This relationship is

given by:

$$N = \text{analogRead}(A0), \quad V_{\text{out}} = \frac{N}{1023} V_{cc}$$

Rearranging the divider formula to solve for the thermistor resistance gives the following:

$$R_{th}(T) = R_{\text{ref}}\Big(\frac{V_{cc}}{V_{\text{out}}} - 1\Big) = R_{\text{ref}}\Big(\frac{1023}{N} - 1\Big)$$

c. 5V Relay
This computation transforms the raw ADC reading into an accurate resistance value, which serves as the basis for the temperature calculation (see Chapter 8.2.3). When the measured temperature exceeds the threshold of 210 °C, the Arduino sends a digital output to a 5 V relay. This relay is wired in series with the power of the heater cartridge (12V). When activated, its contacts open, interrupting the power supply from the PSU and immediately halting heat generation. When the temperature goes below the 210 degree threshold, the contacts close again, creating a power supply to the heater, which heats up the heat block. Together, this hardware setup delivers a high-precision resistance measurement that creates reliable temperature control of the heat block. More details will be discussed in Chapter 8.2.3.

5. Stepper driver & motor
A stepper driver, powered at 12 V, drives the extruder motor at 1/32 microstep resolution. The driver's STEP/DIR pins connect to the Arduino's digital outputs.

6. Filament
1.75 mm PLA filament is fed through a PTFE tube from a spool holder mounted behind the workstation. The tube terminates at the extruder's inlet, ensuring smooth feeding during multi-axis printing.

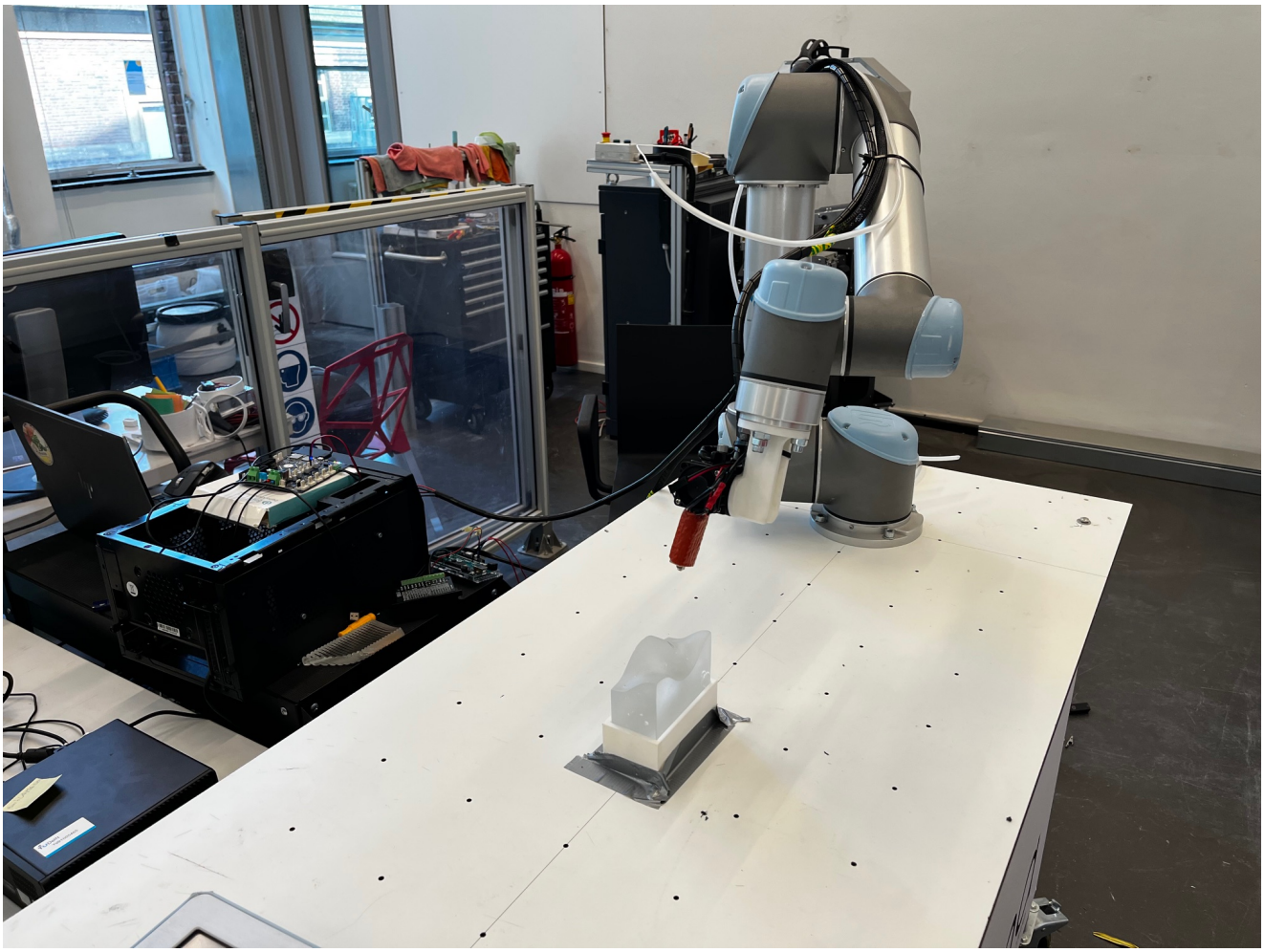

Figure 8.6: UR5 robotic arm set-up

Connection overview

- UR5 AOUT1 (0–5 V) → Arduino ANALOG IN A0
- Arduino digital pins 2 and 3 → stepdriver STEP-/DIR-
- Arduino digital pin 10 → IN relais
- Arduino 5V → thermistor in
- Thermistor out → Arduino ANALOG IN A4
- PSU (12V) → Arduino controlled relay
- Arduino controlled relay → Heatblock

A simplified block diagram of these connections is shown in Figure 8.7.

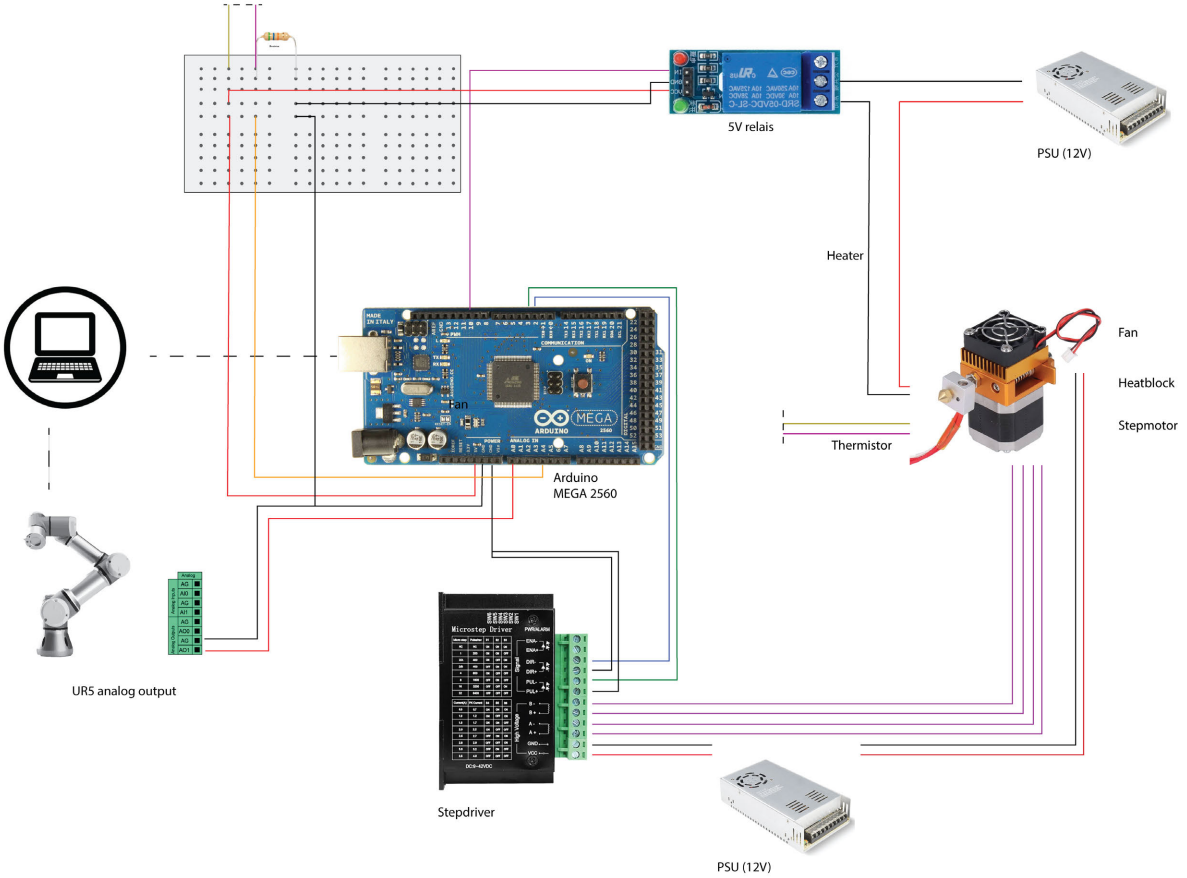

Figure 8.7: Hardware wire connection overview: robot & electronics

8.2.3 Software

1. Model (.stl) to print instructions (.gcode)

One of the biggest challenges is the creation of the print toolpath for a non-planar surface. Conventional AM relies on a layer-by-layer slicing method, where the model is divided into horizontal layers that a 3D printer builds up from the bottom of a planar print bed. The printer is then instructed by a .gcode, which tells the printer the prints' specifications, like the toolpath, nozzle temperature and bed temperature. In this concept, however, the print bed is the top surface of an osteomorphic-shaped glass brick, which is non-planar. As a result, the printer cannot simply start from the bottom and build upwards in a conventional manner. Instead, the slicing process must be adapted to allow a robotic arm with an extruder attachment to follow the non-planar surface and print directly onto this curved surface.

To achieve this, the slicing software must generate a specialised and dynamic .gcode that instructs the printer on how to follow the non-planar geometry. This customised approach ensures that non-planar printing is possible and can be adapted for various shapes. For this step, the 5-axis slicer by DOTX system control is used (see Chapter 8.2.1). A slicing software specialised in non-planar and conformal slicing. The latter is mostly used to to easily apply coatings to existing products (see Figure 8.8).

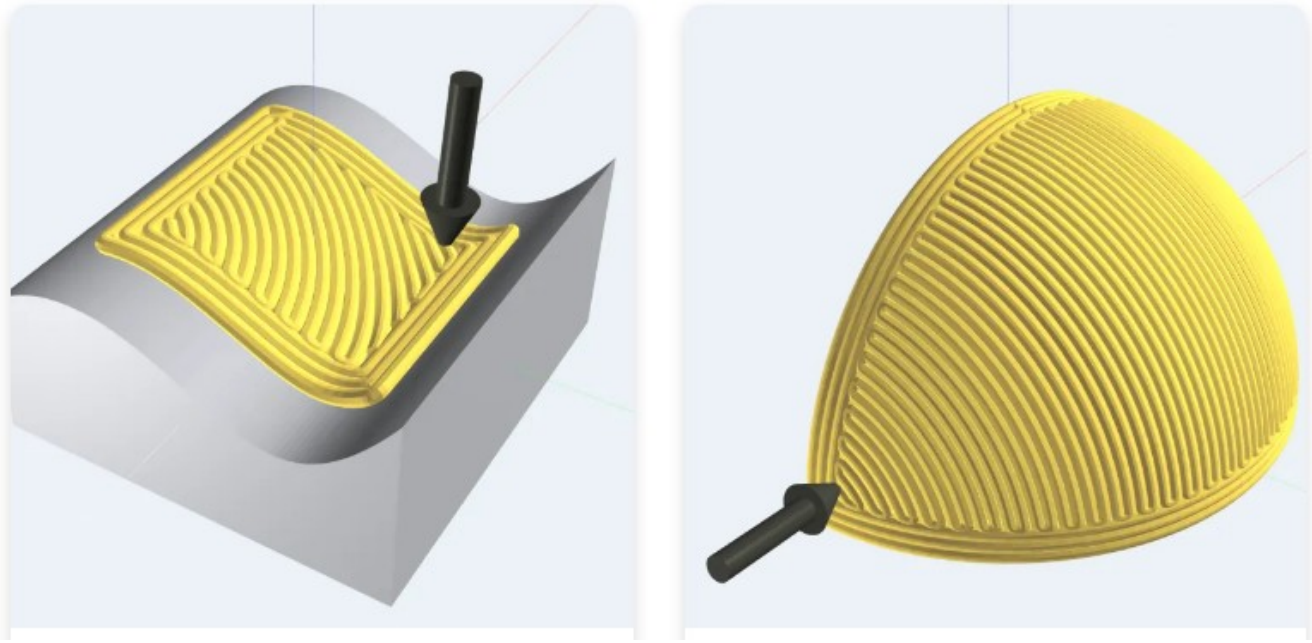

Figure 8.8: 5-axis slicer by DOTX; left: non-planar slicing, right: conformal slicing, DOTX control solutions (n.d.)

This slicer converts the .stl 3D model of the interlayer with interlock to a non-planar toolpath (.gcode). This toolpath is able to instruct the robot arm to follow the print path and to extrude filament at the right moments. In image 8.9 the steps can be seen from creating the conformal interlayer on top of the non-planar target geometry, to the toolpath generation in order to execute the print. The 5-axis slicer slices the geometry into a toolpath with normal vectors that follow the shape of the target geometry precisely. In Figure8.9.c, the vectors along the surface can be seen. Between each of these vectors is a small part of the toolpath, the distance of this toolpath correlates to an amount of extrusion depending on the layer height and print speed. So, between the movement from one vector to another, a certain amount of PLA is extruded by the print head. This concept will be further discussed in the following sub-chapters.

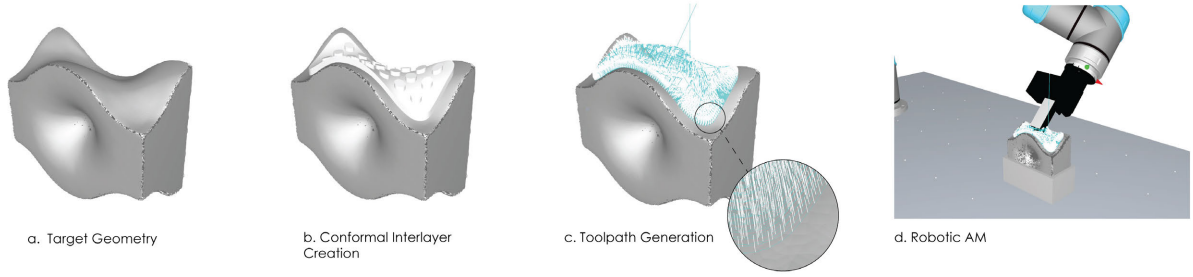

Figure 8.9: Non-planar, conformal, robotic AM workflow

2. RoboDK environment

To simulate and set up the robot, offline programming in RoboDK is used. Using this software, an accurate model of the robotarm can be created. The robot arm, workbench, glass block and the casing of the glass block are modelled in Rhino3D and imported into RoboDK as .stl files. The extruder tool used is also modelled, imported and attached to the robot arm in RoboDK. Important here is the Tool Centre Point (TCP), which tells the robot arm what the central point is of the tool it uses, in this case the extruder.

Next, the .gcode created with the 5-axis slicer is loaded into RoboDK and the toolpath is placed in the correct location relative to the glass block's shape. Settings and the complete RoboDK workflow will be discussed in Appendix C.

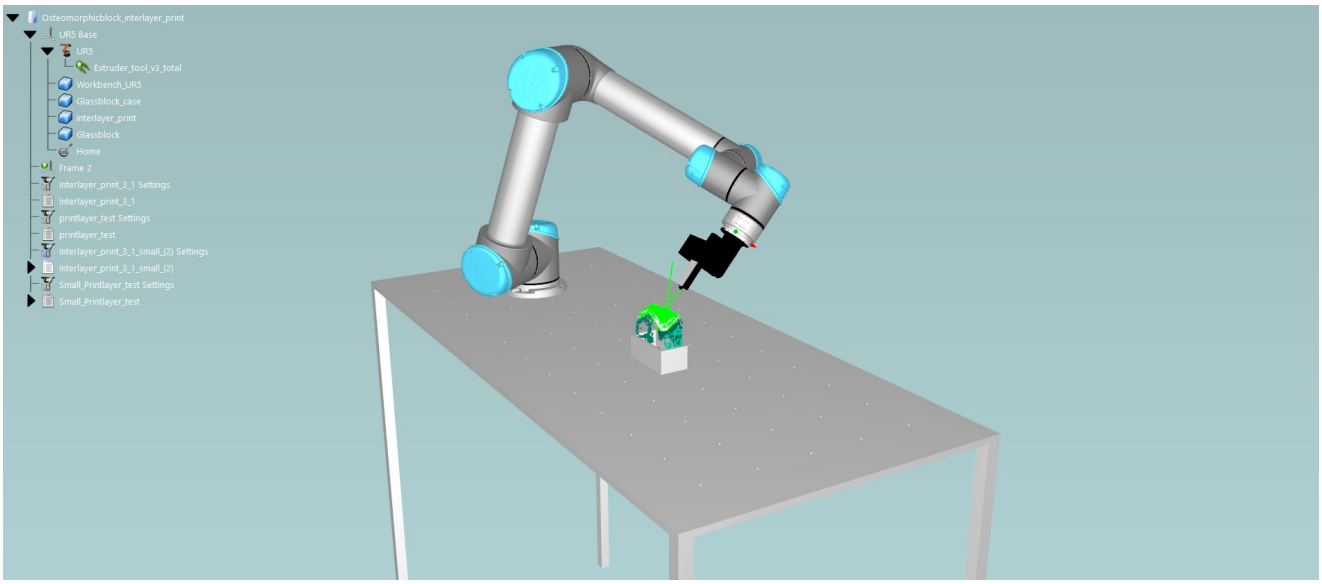

Figure 8.10: Offline programming in RoboDK

3. Post-processing

RoboDK exports its program as a .script, created by a post-processor, that instructs a variety of robot arms. In this case, the UR5 robot arm is used as well as the Universal_Robots.py post-processor. However, a robot arm is not directly able to process a .gcode as a print instruction because an external extruder is mounted on the robot arm. The robot program gets instructed with the Extruder() command from the .gcode but cannot directly instruct an external extruder to extrude. To get as close to the gcode script as possible, a small script is added to the post processor (see Figure A). These lines tell the post-processor to take the number of extrusion (Extruder(...)) and set this as an analog output. It also tells it to delete the actual Extruder() command and only leave the number because the Extruder() is not a tool the robot knows. This

means that every time the Extruder(...) command is given, the post-processor takes this number and outputs this as a number between 0-0.5, which correlates to a voltage level between 0 and 5 V. This voltage level is later converted to steps within the stepmotor in an Arduino sketch.

```
def RunCode(self, code, is_function_call=False):
    """Intercept Extruder(x) calls to generate a 0–5 V analog output, then skip the call."""
    if is_function_call:
        code = get_safe_name(code)
        lc = code.lower()

        # --- EXTRUDER INTERCEPT ---
        if lc.startswith("extruder("):
            # extract the numeric inside the parens
            try:
                val = float(code[len("Extruder("):-1])
            except ValueError:
                val = 0.0

            # map 0–5 → 0–0.5 (i.e. divide by 10), then clamp again just in case
            mapped = val / 10.0
            mapped = max(0.0, min(mapped, 0.5))


            # emit full 0–5 V analog output
            self.addline(f"set_standard_analog_out(1, {mapped:.3f})")
            return
```

Figure 8.11: Addition of extruder call interception to RoboDK Post-Processor

Because the points in the toolpath sometimes are closer than 1 mm, the post processor sets its blend radius (corner smoothing) value to 0.000. This is because it checks that the blend radius covers 50% of the move (at most), with a move smaller than 1 mm it does not cover this 50%. This means no corner smoothing, and so the robot will accelerate and deaccelerate at each point, causing a vibrating movement. To prevent this from happening, a small code is added to the Post-Processor to have the lowest blend radius at a minimum of 1 mm. This enables a smooth operation even at the closest points:

```
def blend_radius_check(self, pose_abs, ratio_check=0.5):
# check that the blend radius covers 50% of the move (at most)
    blend_radius = 'blend_radius_m'
    current_pos = pose_abs.Pos()

    if self.LAST_POS_ABS is None:
        blend_radius = '0'
    else:
        distance = norm(subs3(self.LAST_POS_ABS, current_pos))  # in mm
        # compute raw blend: capped at 50% of segment or global max
        if ratio_check * distance < self.BLEND_RADIUS_M * 1000:
            raw = round(ratio_check * distance * 0.001, 3)
        else:
            raw = self.BLEND_RADIUS_M
        # enforce a minimum of 1 mm (0.001 m)
        raw = max(raw, 0.001)
        blend_radius = '%.3f' % raw

    # update LAST_POS_ABS so next call uses this as the "previous" point
    self.LAST_POS_ABS = current_pos

    return blend_radius
```

Figure 8.12: Addition of blend radius minimum to RoboDK Post-Processor

4. Arduino Software Architecture

This section describes the sketch running on the Arduino Mega 2560, which integrates two primary functions into one sketch:

I. Commanding the stepper motor based on the UR5's analog extrusion signal, and **II. Commanding and reading the heat-block** temperature loop using a thermistor and a relay.

The sketch uses the AccelStepper library to generate step/direction pulses for the extruder motor and implements a custom Steinhart–Hart formula for thermistor-based temperature control. In the following sub-chapters these two sketches will be disucced consequently, the full combined sketch can be seen in Appendix B.

I. Commanding the Stepper Motor

The stepper-motor control continuously maps an incoming analog voltage (0–5 V) from the UR5 robot into a target feed rate (in steps per second) and output the corresponding STEP/DIR pulses. A safety cap on maximum speed prevents over-extrusion.

1. Initialisation

In `setup()`, the analog input pin is configured and the AccelStepper object is initialised:

```
const int dirPin = 2;
const int stepPin = 3;
const int analogInPin = A4;
const int maxSpeedValue = 6125;

#define motorInterfaceType 1
AccelStepper myStepper(motorInterfaceType, stepPin, dirPin);

void setup() {
  // Configure analog-to-digital input
  pinMode(analogInPin, INPUT);
  // Set the maximum allowed speed for safety
  myStepper.setMaxSpeed(maxSpeedValue);
  // (Serial port and heat-block setup omitted here)
}
```

- `analogInPin = A4` reads the UR5's extrusion command (0–5 V).
- `AccelStepper myStepper(motorInterfaceType, stepPin, dirPin)` creates a stepper driver instance using the designated STEP and DIR pins.
- `myStepper.setMaxSpeed(maxSpeedValue)` clamps the highest permitted steps/second to 6125. In this case, 6125 was chosen after testing and deeming it the right extrusion speed for printing with a print speed of 10 mm/s.

2. Reading and Mapping the Analog Command

Within the `loop()`, the Arduino sketch executes:

```
// Read raw ADC (0–1023) from A4
sensorValue = analogRead(analogInPin);
sensorValue = constrain(sensorValue, 0, 1023);

// Map to steps/sec with a safety maximum
outputValue = map(sensorValue, 0, 1023, 0, maxSpeedValue);
```

- `analogRead(analogInPin)` returns an integer N [0.1023] proportional to the input voltage.
- `constrain(...)` ensures the reading cannot exceed the 10-bit ADC range if noise spikes appear.
- `map(sensorValue, 0, 1023, 0, maxSpeedValue)` linearly scales
- N into a stepper speed S [0,6125]. When N=0 (zero volts), S=0; when N = 1023 (5 V), S = 6125 steps/s.

3. Generating STEP/DIR Pulses
Once S is computed, the code sets the stepper speed and runs it at a constant:

```
myStepper.setSpeed(-outputValue);  // Negative to match mechanical orientation
myStepper.runSpeed();
```

- `setSpeed(...)` establishes the step rate in steps per second. A negative sign may be used to reverse motor direction if the filament feed direction is inverted.
- `runSpeed()` issues the required STEP pulses and toggles the DIR pin only when necessary.

4. Motor Idle Behaviour
If the analog voltage is zero (N=0), then `outputValue=0`, and thus `setSpeed(0)`. In this case, `runSpeed()` issues no STEP pulses and the motor remains stationary. Consequently, extrusion is coupled: zero UR5 extrusion command → zero stepper motion. This is used in case when a print move is made where no extrusion is needed, like a Zhop.

Example
At a certain movement of the nozzle, the UR5 sends a 2V signal. When the UR5 outputs a 2V analog signal to the Arduino Mega, it is read as approximately 409 by the analog-to-digital converter (0–1023 scale). This value is linearly mapped to a stepper motor speed using map(409, 0, 1023, 0, 6125), resulting in a feed rate of about 2450 steps per second. Since the stepper driver is set to 1/32 microstepping and the motor has 200 full steps per revolution (6400 microsteps per revolution), this corresponds to roughly 0.383 revolutions per second (23 RPM). The Arduino sends 2450 STEP pulses per second to the stepper driver, while the DIR pin determines the rotation direction. Each STEP pulse prompts the driver to move the motor one microstep, ensuring smooth and controlled extrusion synchronised with the UR5's signal.

II. Commanding and Reading the Heat Block

The following paragraphs explain how the Arduino sketch samples the thermistor voltage via the ADC, converts it to temperature with a Steinhart–Hart formula, applies a simple digital on and off control, and toggles a 5 V relay to switch the heater on or off at a 210 °C threshold.

1. Thermistor Sampling and Averaging
A single raw ADC read may be noisy or produce glitches; to mitigate this, the sketch implements an N = 8 sample average:

```
const int thermistorPin = A2;
const int numSamples = 8;
int samples[numSamples];
int sampleIndex = 0;
bool   samplesFilled = false;

unsigned long lastTempRead = 0;
const unsigned long tempInterval = 500;  // ms

void setup() {
  // Pre-fill sample buffer to avoid startup spikes
  for (int i = 0; i < numSamples; i++) {
    samples[i] = analogRead(thermistorPin);
  }
  filteredTemp = readTemperature(analogRead(thermistorPin));  // initial filter state
}

void loop() {
  unsigned long now = millis();
  if (now - lastTempRead >= tempInterval) {
    lastTempRead = now;
    // Insert new reading into circular buffer
    samples[sampleIndex] = analogRead(thermistorPin);
    sampleIndex = (sampleIndex + 1) % numSamples;
    if (sampleIndex == 0) samplesFilled = true;

    // Compute average of valid samples
    int total = 0;
    int count = samplesFilled ? numSamples : sampleIndex;
    for (int i = 0; i < count; i++) {
      total += samples[i];
    }
    int avgRaw = total / count;

    double newTemp = readTemperature(avgRaw);
    // (Validation and control logic follow…)
  }

  // (Stepper control code runs continuously below…)
}
```

- Every $T_{interval}$ = 500 ms, the code reads `thermistorPin = A2`, storing it in `samples[]`.
- Once all 8 samples have been read in, `samplesFilled=true`, and the average is always over these 8 values;

- This rolling-sum approach reduces noise and transient spikes, creating a more stable raw-ADC value $Nraw$ [0,1023].

2. Converting ADC to Temperature (Steinhart–Hart)
The function `readTemperature(int rawADC)` implements the single-point Steinhart–Hart approximation. The Steinhart–Hart "Beta" approximation is essentially a way to convert the resistance you measure from the NTC thermistor into an actual temperature:

```
double readTemperature(int rawADC) {
  float resistance = seriesResistor * ((1023.0 / rawADC) - 1);
  // Rth = Rref * (1023 / N - 1)

  float steinhart = resistance / nominalResistance;     // Rth / R0
  steinhart = log(steinhart);                           // ln(Rth / R0)
  steinhart /= BETA;                                    // (1/β)·ln(Rth / R0)
  steinhart += 1.0 / (nominalTemp + 273.15);            // + 1 / (T0 + 273.15)
  steinhart = 1.0 / steinhart;                          // → T (K)
  steinhart -= 273.15;                                  // → T (°C)
  return steinhart;
}
```

- `seriesResistor` = 100.000 Ω (R_{ref}), `nominalResistance` = 100.000 Ω (R_0), `nominalTemp` = 25 °C (T_0)
- BETA 3950 K is the thermistor β-coefficient (β)
- N = rawADC
- First,

$$R_{th}(T) = R_{\text{ref}}\left(\frac{1023}{N} - 1\right)$$

(8.2.2)

- Then, applying

$$\frac{1}{T} = \frac{1}{T_0} + \frac{1}{\beta}\ln\left(\frac{R_{th}}{R_0}\right),$$

solves for the temperature T in kelvins, which is converted to °C

3. Low-Pass Filtering and Validation
To avoid "false" spikes (e.g., when the thermistor is disconnected), the code:

- Checks that 0 < `newTemp` < 350 °C
- If out of range, the reading is discarded, any ongoing heating is shut off, and an error message is logged over `Serial`.
- If valid, an exponential-moving average (EMA) filter is applied:

$$T_{\text{filtered}} = \frac{3\,T_{\text{filtered(old)}} + T_{\text{new}}}{4}$$

This 75 % carry-over filter smooths random jitter while still responding within a few seconds to temperature changes.

4. Hysteresis Control of the Relay

A digital output (`relayPin = 10`) drives a 5 V relay coil. The code maintains a boolean flag `heating` and implements a hysteresis (a threshold) around the 250 °C setpoint (5°C). The initial temperature of 210 °C is increased to 250 °C after testing and deeming it the ideal temperature. This change in temperature can be explained by faults in thermistor readings or a mistake in the Steinhart formula. This does not mean the heat block actually prints at 250 °C, rather at 210 °C but retruns a 250 °C value.

```
const float targetTemp  = 250.0;  // °C
const float hysteresis  =   5.0;  // °C
bool heating = false;

// Inside the valid-reading branch:
double temp = filteredTemp;
if (!heating && temp < (targetTemp - hysteresis)) {
  digitalWrite(relayPin, LOW);   // Energize relay ⇒ HEATER ON
  heating = true;
}
else if (heating && temp > (targetTemp + hysteresis)) {
  digitalWrite(relayPin, HIGH);  // De-energize relay ⇒ HEATER OFF
  heating = false;
}
```

- When `filteredTemp` < 245 °C and heating = false, the relay is pulled LOW (active-LOW), closing the heater's 12 V circuit turning the heater on.
- Once `filteredTemp` > 255 °C and heating = true, the relay is driven HIGH, opening the 12V circuit cutting off the heater.
- This prevents rapid on/off cycling around the setpoint, ensuring a stable control loop.

5. Checking Values through Log

Every T = 2000ms, if the reading is valid, the code transmits over `Serial`:

```
Temp: <filteredTemp> °C | Heating: <ON/OFF> | Speed: <outputValue>
```

This continuous log allows the user to verify that temperature, heater state, and stepper speed track expected values. If an invalid temperature appears, the log prints an error message (e.g., "Ongeldige temperatuurmeting genegeerd.") and flags that the heater was disabled.

Example

The Arduino Mega reads the thermistor signal from analog pin A2 every 500 ms, taking 8 consecutive samples to compute a stable average. This averaged ADC value (0–1023) is then

converted into temperature using the Steinhart–Hart Beta approximation, based on the 100kΩ NTC thermistor with a β value of 3950 K used. The formula computes the thermistor resistance and transforms it into a temperature in °C. If the calculated temperature falls within the set valid range (0–350 °C), it is passed on. Then, a hysteresis-based (threshold) control loop then toggles a 5 V relay on pin 10 to control the 12 V heat-block: heating is activated when the filtered temperature drops below 245 °C and turned off when it exceeds 255 °C, preventing rapid switching. While the true physical temperature is approximately 210 °C, the system maps this to 250 °C due to an offset likely caused by thermistor inaccuracies or a miscalibration in the Steinhart–Hart parameters. Every 2 seconds, valid temperature readings and heater states are logged via Serial for monitoring.

Working Together

In this sketch, the stepper logic and the temperature routine work together at the same time: the stepper-motor routine calls runSpeed() on every pass through loop(), allowing AccelStepper's to generate STEP pulses as fast as possible. The temperature routine checks and updates the thermistor reading only once every 500 ms. Because neither section uses large delays, the stepper logic continues uninterrupted even while the temperature code waits for its next interval. In practice, this means the Arduino is simultaneously generating high-frequency STEP/DIR pulses to match the UR5's extrusion command and, every 500 ms, averaging thermistor samples and toggling the heater relay. This way, extrusion speed and heat-block control run in parallel without one stopping the other.

8.2.4 Robotic Non-Planar Printing Results

Calibration

Accurate replication of the RoboDK simulation in the physical setup requires a calibration procedure to align the UR5's Tool Centre Point (TCP) and print parameters with the osteomorphic brick's geometry. Calibration is performed iteratively: an initial test print on the glass brick reveals positional and material-flow misalignments, which are then corrected by adjusting key parameters. These include (1) the TCP offset to ensure the virtual and real nozzle positions align, (2) the interlayer placement to match the intended offset to the surface, (3) print speed to balance PLA deposition continuity against robot movements, and (4) print temperature to optimise melt temperature and adhesion to glass. Through trials and fine-tuning of these parameters in small prints, the physical print outcome aligns with the offline RoboDK toolpath, ensuring accurate interlayer AM on the non-planar glass brick. In Figure 8.13 the different small prints that were used can be seen. The first test prints mostly consisted of the first moves of the total interlayer as can be seen in Figure 8.13a and 8.13b, later calibrations were made with the outer toolpath of the first print layer, as seen in Figure 8.13c.

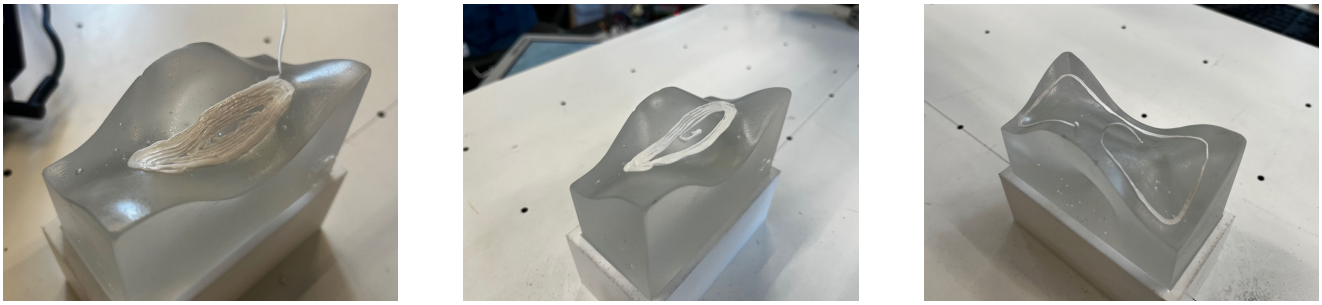

(a) Calibration block 3, A (b) Calibration block 3, B (c) Calibration block 3, C

Figure 8.13: Offline - Real life placement calibration

Iterations

Once the offline-real-life calibration was correct, several print iterations were done to eventually create the desired outcome. The first iterations were done with a .gcode with a layer height of 0.3 mm (Figure 8.14a and 8.14b). These iterations showed over-extrusion creating a sloppy first layer. Because of this, the interlayer started sagging and sliding on the glass in the concave zone. This created small bumps during printing which the print head collided with creating an even more chaotic print and an eventual bending and breakage of the heatbreak. To improve the extrusion more specific to the interlayer, the post-processor was altered creating a more precise extrusion. In combination with a .gcode with a 0.6 mm layer height, collision of the print head and over-extrusion were avoided. Figure 8.14c shows the print (32%) of the second iteration. This iteration showed more accurate extrusion but in the corners of the concave zone some under-extrusion in combination with an off calibration is noticed. This created a layer height of > 0.6 mm which creates a collision with the next layer deposition. The print was stopped due to collision and bending of the heatbreak at 32%.

(a) Iteration block 3, A (b) Iteration block 3, B (c) Iteration block 3, C

Figure 8.14: Robotic printing iterations of the interlayer on the osteomorphic shaped cast glass bricks

Problems Faced

Despite achieving close similarity between the simulated toolpath and real-world setup, the non-planar printing process remained sensitive to multiple factors. Variations in material flow, slight misalignments in TCP calibration, and the complex curvature of the substrate frequently resulted in extrusion irregularities and nozzle-bead collisions. These interactions not only compromised print quality but also placed stress on the heat-break assembly and other critical components, demanding careful tuning of both hardware and slicer parameters. The following problems were faced in the print iterations:

- **Over-extrusion:** Excessive filament deposition in early iterations caused sagging in downward-curved (concave) areas, creating bumps that the nozzle subsequently struck.
- **Under-extrusion in convex regions:** Insufficient material flow at sharp curvatures produced gaps larger than the target layer height, causing the nozzle to collide with the previously deposited bead.
- **Heat-break damage:** The heat break serves as the transition point between the hot heat block and the cold extruder. Because this heat-break is a delicate part, it is the weakest point of the set-up. Repeated collisions and thermal cycling weakened the stainless-steel and titanium heat-break, resulting in bending or fracture.
- **Calibration sensitivity:** Even minor misalignment of the TCP offset or interlayer placement produced prints that either scraped the glass or failed to adhere, emphasising the need for precise, iterative calibration before actually printing.
- **Collisions due to messy toolpaths:** Deviations in filament placement accumulated over multiple layers, leading to unplanned nozzle impacts that further degraded print quality and risked hardware damage.
- **Cooling of the target glass:** The cast glass brick is heated up to 60 degrees to ensure good adhesion. However, because the brick is not in a heated enclosure, the brick starts to cool down once tis it removed from the oven. This means that the print has to start right away to take advantage of the heated bed.
- **Stepmotor heating up:** Due to the many pulses the stepmotor receives, the stepmotor heats up until the point of expanding and even melting the PLA before reaching the heat break. This creates a print stop and necessitates a cooldown of the stepmotor once in a while.

Results

Block 1 (76% printed)

After printing 76%, the nozzle collided with the interlayer causing the heatbreak to bend. Bending the heatbreak back broke it and stopped the print. The several problems discussed in the previous sub-chapter cause the print to have certain defects. Overall, the print adheres very well to the glass and serves as an interlayer. The interlocking features of the interlayer are not

printed in this iteration due to the print stop at 76%.

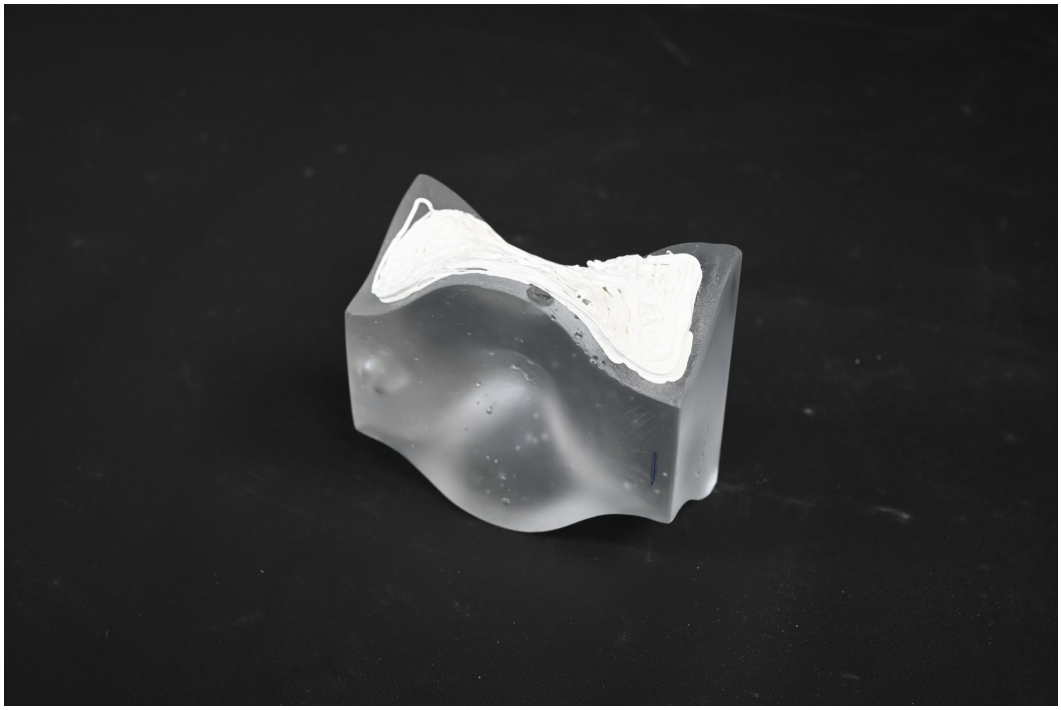

Figure 8.15: Block 1 final print

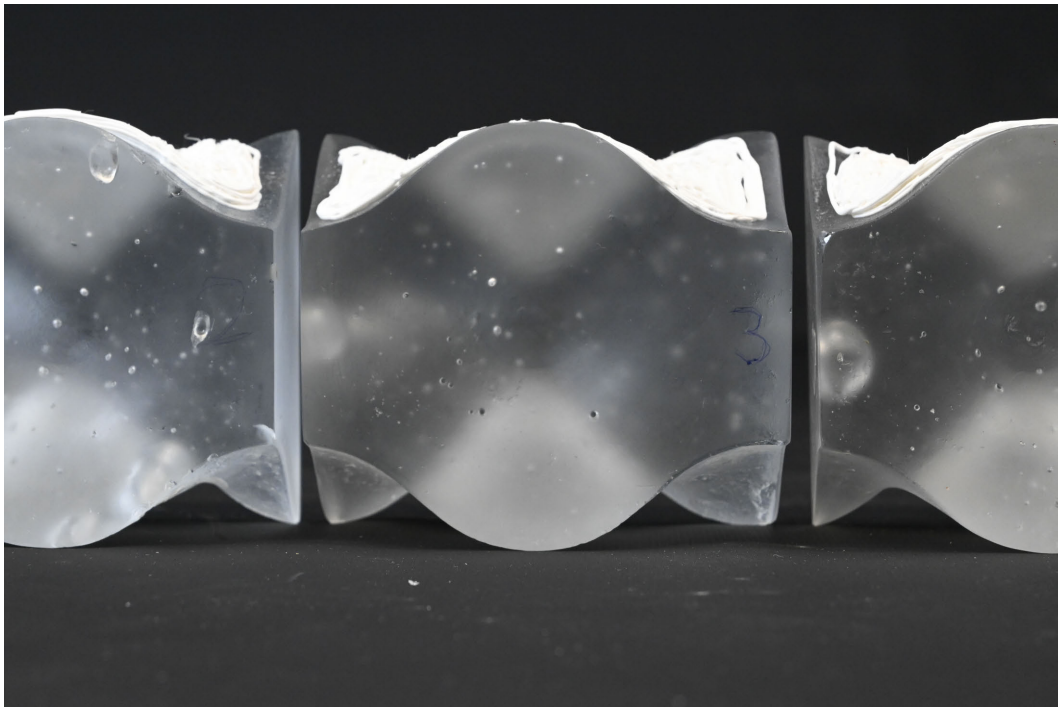

Figure 8.16: Osteomorphic shaped cast glass bricks with conformal AM interlayers

Block 2 (100% printed)
Block 2 is fully printed. The results show an interlayer print where the interlocking features can be seen but are not printed as designed. The robotic additive manufacturing and slicer software turns out to have lot of small deviations causing the end result to differ from the design. The concept works and the interlayer is completely printed on the osteomorphic shaped cast glass brick. Optimisation has to be done to go from this proof of concept to an accurate representation of the initial design.

Figure 8.17: Block 2 final print

Block 3 (56% printed)
Block 3 was the first brick printed on and the most widely tested. After multiple iterations on this brick (Figure 8.14), eventually a print was done up untill 56%. At this moment, the beatbreak got stuck in the stiff interlayer itself and bent because it kept on printing. The print was stopped and the result is 56% of the print done. This means no interlocking features can be seen on this print.

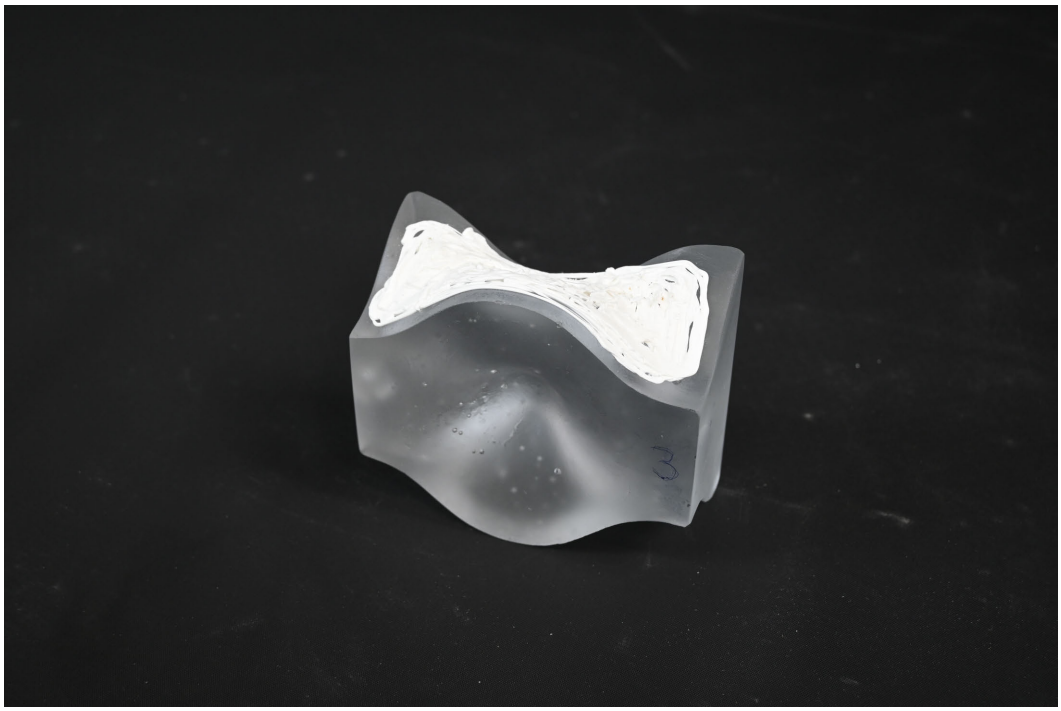

Figure 8.18: Block 3 final print

Figure 8.19: Osteomorphic shaped cast glass stacked with AM interlocking interlayer

8.2.5 Conclusion

Chapter 8 has validated that the proposed non-planar 3D-printing workflow, which combines DOTX's 5-axis slicer with a UR5 robotic arm, can indeed additively manufacture conformal PLA interlayers onto osteomorphic glass bricks. Calibration tests aligned the offline RoboDK simulation with the physical setup by iteratively tuning the TCP offset, interlayer placement, print speed, and temperature. Subsequent print iterations, shifting from 0.3 mm to 0.6 mm layer heights and refining the post-processor, avoided over-extrusion but still faced localised under-extrusion in concave zones and unintended nozzle collisions that bent and even broke the heat-break.

While these experiments confirm the feasibility of the concept, the results remain too irregular for reliable production. First, the brittle PLA interlayer and the delicate heat-break struggled with the small bumps caused by extrusion deviations, leading to hardware damage and print abortion. Second, the entire process hinges on ultra-precise, manual calibration; even tenths of a millimetre misalignment between the simulated and real-world TCP generate collisions or adhesion failures. Third, the current workflow lacks any in situ compensation; once the printhead deviates, errors compound over each layer, further degrading accuracy.

To develop this proof-of-concept into a robust fabrication method, three critical improvements are needed:

1. **Hardware Reinforcement:** Adopt a collision-tolerant end-effector, mainly a stiffer heat-break, to withstand minor impacts without hardware failure.
2. **Adaptive Control:** Integrate real-time feedback (e.g., scanning or extrusion-flow monitoring) to correct for incorrect calibration in TCP or (a lack of) material flow reducing dependency on static calibration and furthermore, operate in a heated chamber to avoid cooling of the target geometry.
3. **Workflow Refinement:** Create a smoother toolpath in the .gcode without 180 degrees turns and compensation in the post-processor to minimise corner-sharpness and test more compliant interlayer materials (e.g., TPU) to absorb misalignments.

In conclusion, Chapter 8 demonstrates that robotic non-planar printing can produce custom interlayers on free-form glass, but also shows that achieving high repeatability demands a more resilient setup, adaptive controls, and design strategies tolerant of small geometric variances.

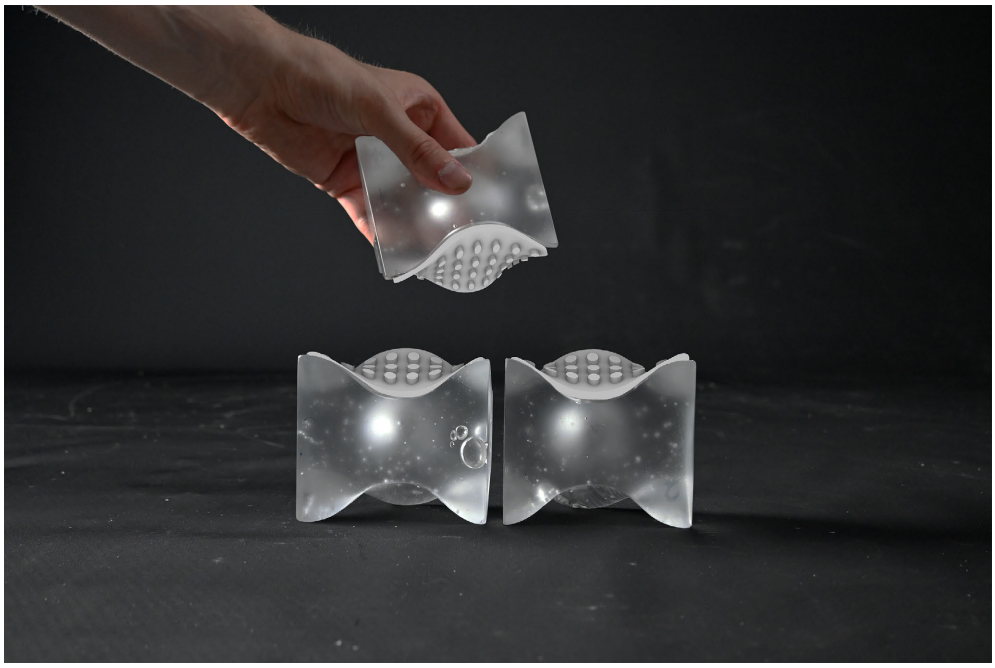

Figure 8.20: Osteomorphic shaped cast glass stacked with the intended AM interlocking interlayer

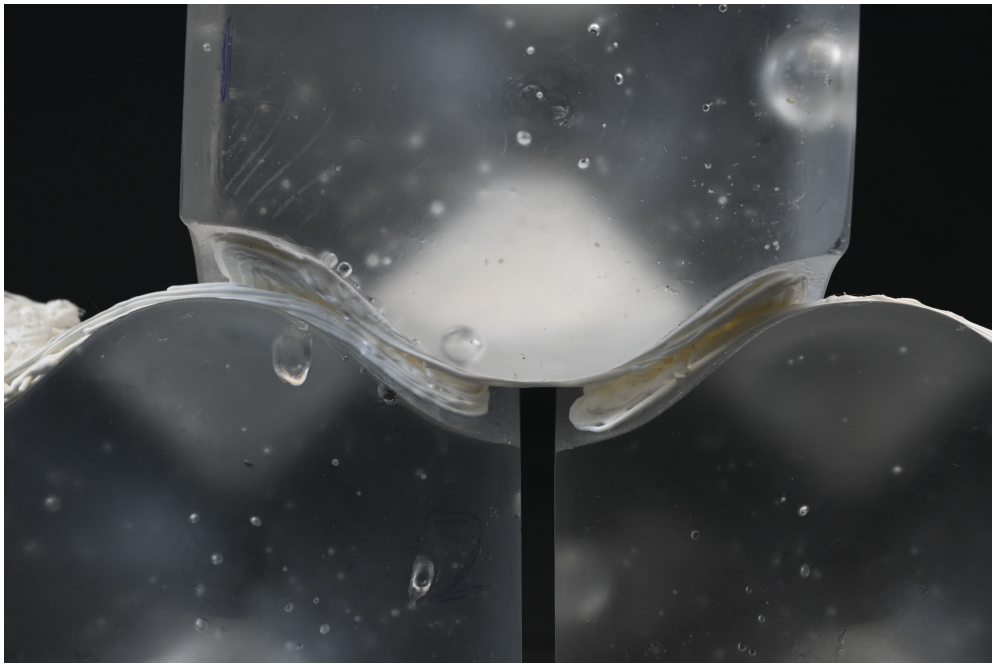

Figure 8.21: Osteomorphic shaped cast glass stacked with AM interlocking interlayer, close-up

9 Discussion

9.1 Results

The primary goal of this research was to develop and validate a reversible glass–polymer interlocking system for structural applications, focusing on disassembly and reuse. Through material exploration, geometry optimisation and mechanical testing and a case study with a custom robotic AM process, a novel connection method was proposed. This discussion interprets the results and reflects on limitations and trade-offs. As the findings demonstrate the promise of the system, they also highlight important challenges that must be addressed for future implementation.

9.1.1 Material–Interface Performance

The material exploration revealed that not all common AM polymers bond effectively to glass. For example, PETG filament initially adhered strongly to the glass surface, but its significant shrinkage upon cooling led to warping-induced stresses that even chipped of glass after cooling. PC/ABS, an engineering blend expected to offer high strength, similarly suffered severe warping without a heated enclosure, making it impractical with the available equipment. Flexible thermoplastics like TPU (Thermoplastic Polyurethane) and other elastomeric polyesters with material properties were also tested; these showed some warping but mostly lacked the stiffness to maintain the interlock geometry, resulting in poor print quality or sagging connections. In contrast, standard PLA emerged as a practical compromise. PLA exhibited reliable printing behaviour on glass (with minimal warping and good first layer adhesion) and sufficient stiffness to form the interlocking geometry. However, PLA has a low glass transition temperature, which could create problems in the long-term. These findings emphasise that material choice and surface interaction are as critical as the interlock design itself.

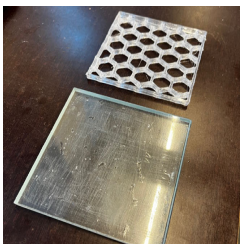

(a) PETG-glass adhesion failed: shrinkage caused PETG to chirp of glass pieces

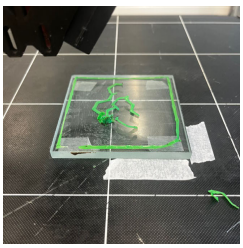

(b) PC/ABS-glass adhesion failed: extensive warping caused print to fail

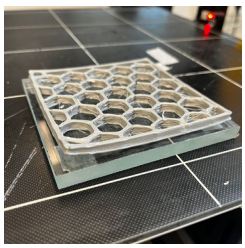

(c) TPU-glass adhesion failed: warping caused lack of adhesion

(d) FlexPolyester-glass interlock failed: low stifness caused lack of print quality

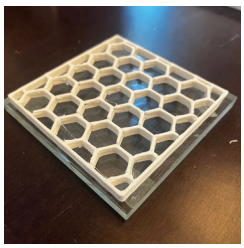

(e) PLA-glass adhesion: reliable and clean print with good adhesion

Figure 9.1: Additive Manufactured material experimentation on glass adhesion

The good result with PLA does not imply it is an ideal structural material, but rather that the processing constraints of AM forced a trade-off in material selection. The polymer–glass interface proved to be a potential weak link: in shear tests, failure occurred by adhesive failure at the interface (the printed polymer sliding off the glass surface) rather than through the polymer or glass. This indicates that without additional surface treatment or mechanical interlocking

features, the bond between a smooth glass substrate and printed polymer can limit performance. In practice, current glass joinery systems often rely on permanent adhesives, which complicates disassembly and contaminates the glass, hindering recycling and reuse. The use of PLA with a low glass transition temperature enables its removal upon heating above this temperature (>60°C), opening up possibilites for recycling and reusing of the glass brick and (biodegradable) polymer. While this thesis's strategy of avoiding permanent adhesives aligns with circular design principles, it trades off some mechanical strength. Future work could explore surface primers or use of polymers that chemically bond to glass yet remain reversible (heat-softenable glues or reversible adhesives). In the end, the material experiments reveal a broader insight: the "best" material on paper may fail if it cannot be reliably processed or if it introduces new problems like stresses on the glass. Thus, material-interface compatibility is a key design criterion for any reversible glass-polymer interlock system.

9.1.2 Geometry Choices, Optimisation and Mechanical Behaviour

This thesis explored two different geometric approaches for creating a reversible connection system between free-form glass unit.

Option 1; the Dry-Click

The first one, called 'the Dry-Click', focused on a fully reversible connection. In this option the AM glass unit is printed directly on top of a heated float glass pane to create an inherent connection and enlarge surface area. Prior to printing, holes are waterjet into the float pane to form connection holes. The next step is the interlock of the snap-fit injection moulded interlayer on the top of the glass unit. This creates an opportunity for the next glass unit to interlock on the top surface in the same way. While this method offers the reversibility required, it also presents challenges. The over-constraint design requires a very high precision and creates high stressed around the connectors. Additionally, waterjet cutting of the glass introduced (micro-)cracks, which can propagate under load and could lead to failure.

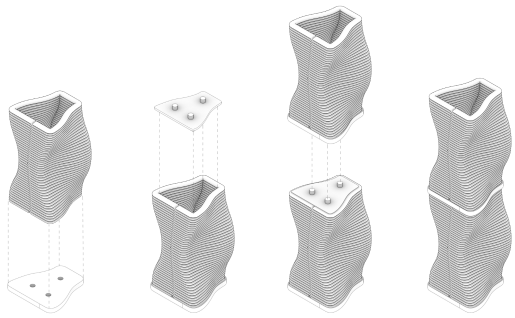

(a) Option 1: the Dry-Click

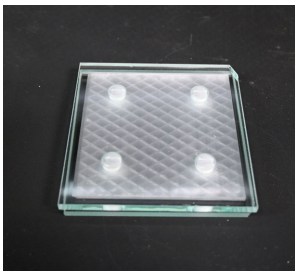

(b) Option 1, sample 1 - sandwiched between two 6 mm float glass samples

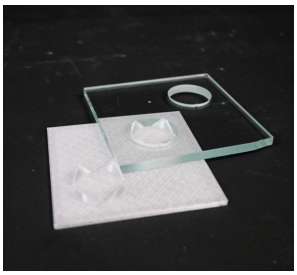

(c) Option 1, sample 2 - clicked on one of the snap-fit joints

Figure 9.2: Option 1: AM PETG samples inserted in waterjet cut float glass samples

Option 2; the Direct Print

In the second concept, glass bricks are joined by an interlayer that is directly AM onto each brick's top and bottom surfaces. A six-axis robot is used because the surfaces of the brick are non-planar, this means that a traditional Cartesian 3D printer is not able to print on these surfaces as it would collide with the brick when printing. However, a six-axis robot is able to move in every direction to avoid collision and print the interlayer on the non-planar surface. The interlayer features extrusions that interlock with corresponding geometries on adjacent bricks. The elastic averaging mechanism compensates for the printing tolerances of a 1.0 mm nozzle, reducing reliance on post-processing and high stress concentrations. By printing the interlayer onto both

the top and bottom faces, this method establishes a simple yet robust connection mechanism.

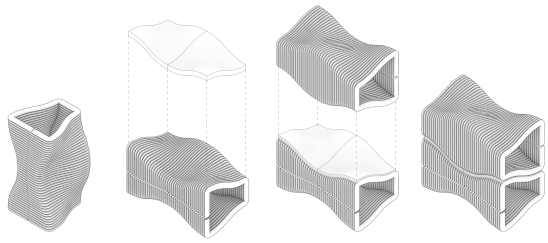

(a) Option 2: the Direct Print

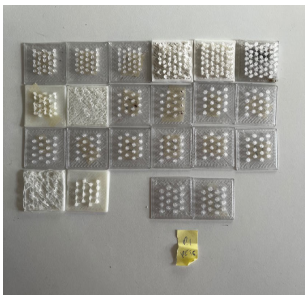

(b) Option 2, 50mm x 50mm samples of different materials

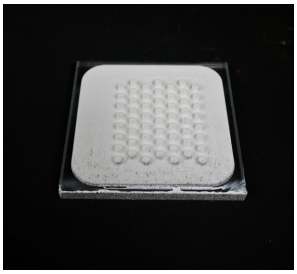

(c) Option 2, frontside of chosen PLA on float glass plate, sample 14.1

Figure 9.3: Option 2, iterations and chosen interlayer geometry *Own images*

Unlike the first option, which requires precisely machined holes and can introduce stress concentrations and cracking, the Direct Print approach eliminates high-stress regions and facilitates secure, repeatable assembly and disassembly. Therefore, this thesis advanced the Direct Print using a robotic AM workflow as the preferred method for connecting the free-form glass units.

Finetuning the Interlock

The geometry of the interlayer was a critical factor in creating a reversible connection. Instead of relying on permanent adhesives, the connection strength derives from a mechanical interlock engineered into the shape of the interlayer. A LEGO-like design was developed to accommodate minor manufacturing tolerances. This means that any small deviations from the AM process are averaged out by the shape, allowing the components to fit together smoothly. This geometric design not only optimises load transfer and structural performance, but also eases assembly and disassembly of the modules. Iterative design refinements of the interlock geometry led to significantly enhanced mechanical engagement. Through iterative printing and designing (e.g. adding fillets to corners, adjusting connector dimensions, and tuning infill patterns), the interlayers were improved to better distribute stress and enhance print reliability. Among the around fifty printed specimens, a filleted profile with concentric infill (Sample 14.1, see Figure 9.3) achieved the smoothest print quality and the most reliable interlock engagement. The addition of 15 mm corner fillets and a concentric infill (where the filament is deposited following the shape's contours) ensured a continuous print path; the printer does not have to slow down and speed up like it has to in 90 degree angle corners. This ensures that the filament is deposited equally which improved mechanical engagement between the polymer and glass and therefore likely contributed to more consistent load transfer.

Mechanically Validating the Concept

Mechanical validation through quasi-static shear tests produced peak shear forces between 1.77 kN and 6.13 kN under starting preloads of 0.30–0.50 kN. The effective friction coefficients correspond to ($\mu = F_{\text{shear}}/F_{\text{normal}}$) of 0.82–1.45 (see Figure 9.4), markedly above typical Eurocode values of 0.4 for timber-timber or steel-steel contacts. While these high μ values confirm that interlock geometry and polymer deformation deliver exceptional shear resistance, every specimen failed by clean delamination of the polymer from the glass. This consistent failure mode points out the glass–polymer interface, rather than the interlock shape, as the performance limiter of the system. This brittle failure mode means when ultimate stress is reached, the interlayer will fail without warning. Future research may look into improving the interlayer bonding so a more ductile failure behaviour is reached, which provides a margin of safety. For example, polymer yielding could be visually or instrumentally detected during inspections.

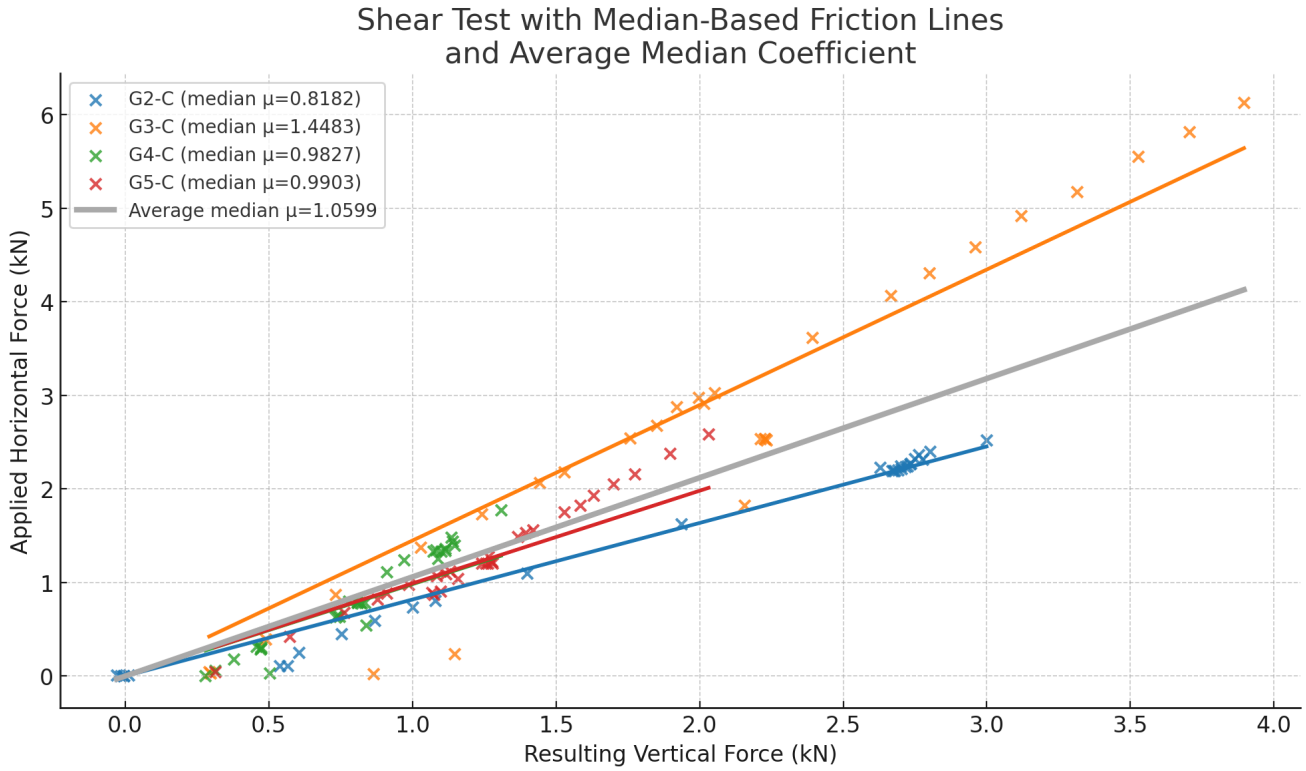

Figure 9.4: Results of shear testing of four specimens, friction coefficient as slope

DIC strain maps provided insight into local deformation and uncovered a recurrent upward rotation of the free edge of the glass plates under shear (see Figure 9.5). This plate tilt was due to eccentricity of the normal force actuator compared to the axis of the interlocking system (see Figure 9.5a). In Figure 9.5b, Dy displacement at point 5 of +1.87 mm can be seen. This displacement is resulting from the rotation, causing alteration of the local normal stress distribution and introduced bending moments in the system that likely led to accelerated delamination. This error also caused the plate to guide the shear force more into the normal actuator, creating a higher normal loading. This fault needs to be addressed through a more clamped fixture of the plates to isolate the real shear behaviour of the interlayer. Nonetheless, the qualitative findings (failure patterns, order of magnitude) are valid and informative. They confirm that with proper design, a dry-assembled polymer interlayer can act as a structural shear key between glass elements, an essential proof-of-concept for the reversible system.

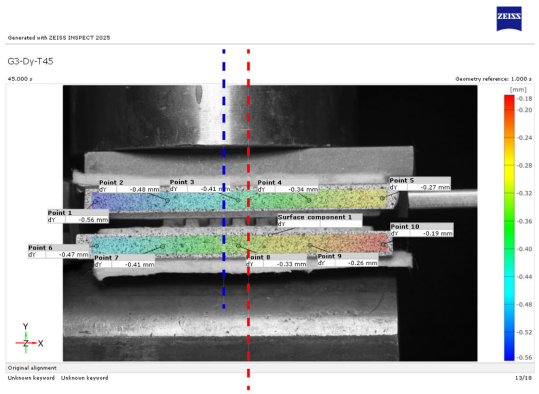

(a) DIC analysis of specimen G3, blue: axis of normal actuator, red: axis of interlock system

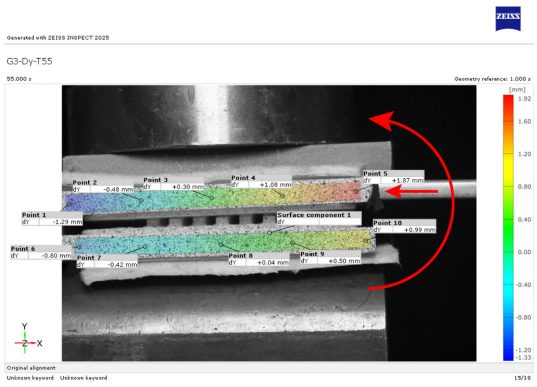

(b) DIC analysis of specimen G3: rotation of the plate due to eccentricty of the normal actuator

Figure 9.5: DIC analysis of specimen G3: Dy displacement and rotation

9.1.3 Case Study: Reversible Glass Vault Assembly

To explore the system-scale performance, a glass vault structure was designed using the glass–polymer interlocks. This case study demonstrated how the developed connection performs in an architectural structure where the glass blocks were joined into a self-supporting, compressive-only arch. Validation calculations of the vault case study show that the polymer interlock has to carry compressive stresses on the order of 0.063 MPa without failure of the connection. Shear test results point out a normal force ranging between 1.31 to 3.90 kN at failure of the shear connection. This correlates, on a surface of 90 mm x 90 mm to a stress level of: $\sigma = F_{normal}/A_{surface} = 1.3 - 3.90/8100 = 0.16 - 0.48 N/mm^2$. This result does not mean it cannot withstand more compressive force, but it is the compressive force at the moment the lateral load made the interlock fail in this thesis' shear tests. Compressive strength of AM PLA ranges typically from 62 MPa- 72 MPa. Wind calculations made in sub-chapter 6.3 show a service lateral loading of 18 N on one brick. Results from the shear test show the interlayer system has an average friction value of μ = 1.06. With a normal compressive loading on the lowest brick of $F_{N_{castblock}}$ = 1124.1 N and $F_{N_{AMblock}}$ = 358.18 N. These values correlate to the ability of the system to withstand lateral loading of 1.06 * $F_{N_{castblock}}$ = 1191.5 N > 18 N and 1.06 * $F_{N_{AMblock}}$ = 379.7 N > 18 N.

The ability to dismantle the vault afterward confirms the reversibility: all glass components can remain undamaged and could be reused. The polymer interlayers can be removed from the glass by heat, and be reprinted or replaced as needed. This outcome shows a broader design implication: by leveraging form (e.g. arch geometry) to put materials in their optimal roles one can achieve stability without permanent adhesion.

Prototyping these geometries on 1:2 sized glass bricks required a robotic fabrication workflow. By scanning each brick's surface with a Go!SCAN 3D system and importing the mesh into Grasshopper, a tailored interlayer was created with the interlocking features from the optimised geometry. This .stl file formed the base to create the non-planar G-code with help from 'DOTX system controls'. RoboDK post-processing and a UR5 robot arm set-up proved capable of AM conformal, 3 mm-thick interlayers without manual alignment. This workflow demonstrated that non-planar slicing and robotics can bridge complex glass topographies and polymer printing constraints. However, it also has to be noted that tight construction tolerance are required for such a printed interlock. Small misalignment or differences in the glass blocks could prevent the interlayer from adhering or failure of the hardware and termination of the print. This highlights a practical challenge for larger-scale use: either precision in fabrication and assembly will be critical or a more robust design strategy is needed. Overall, the vault case study provided a validation of the interlocking concept in an architectural context. This case it is a vault using

osteomorphic shaped cast glass bricks, but the beauty of this system is that it can adapt to any form of bricks if it has a surface to print on. However, optimising and standardising could prove to be useful for the concept.

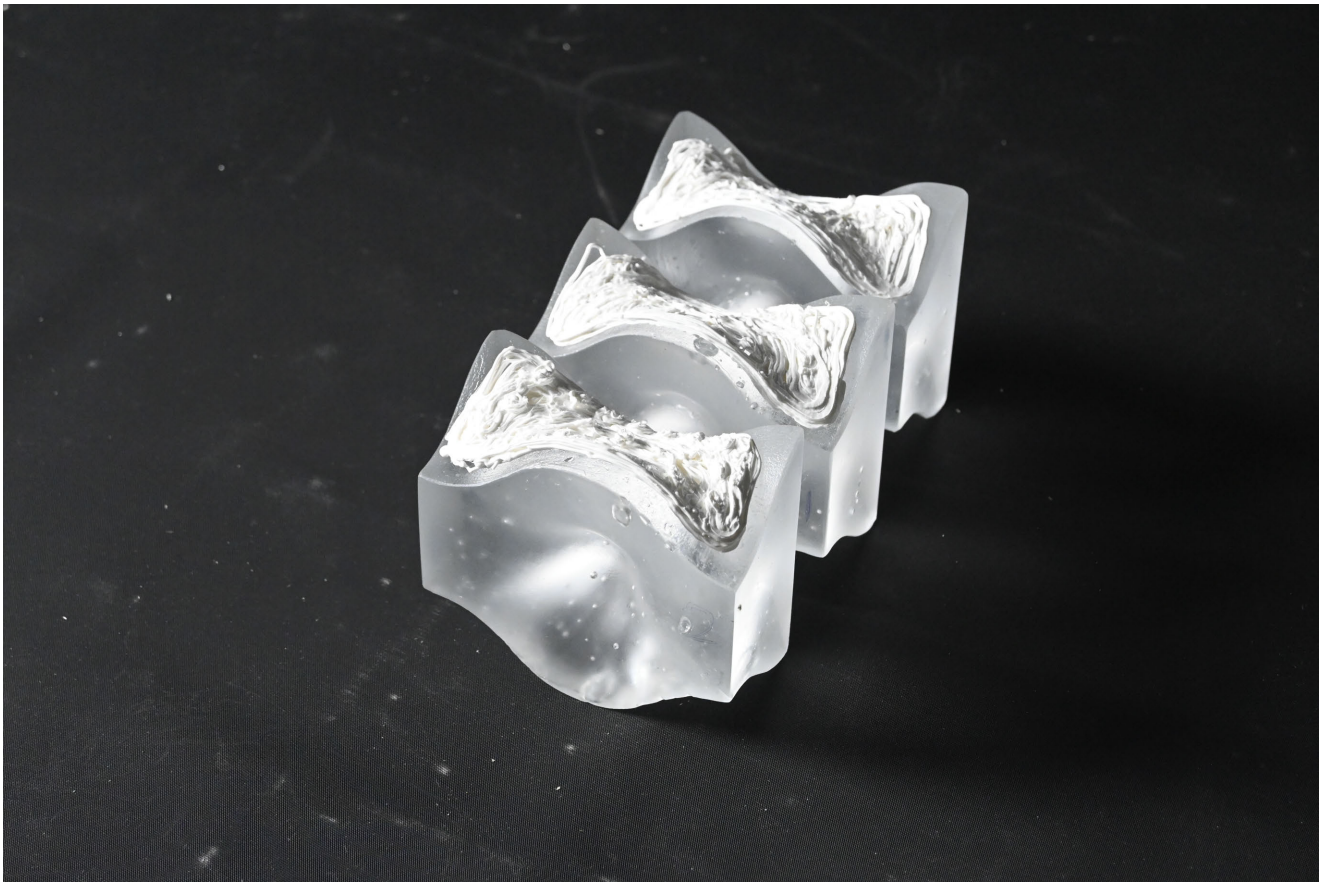

Figure 9.6: The osteomoprhic shaped cast glass brick with corresponding interlayers

9.2 Limitations and Challenges

Despite the promising results, the research also revealed several limitations in the current system that must be addressed in future developments.

9.2.1 Polymer Durability

The long-term performance of the chosen polymer, PLA, is questionable for structural applications. PLA can degrade or embrittle over time, especially under UV exposure and varying temperatures. Furthermore, its low glass transition temperature of around õ60°C means it softens at relatively low temperatures. In a façade or roof application, solar heating could approach or exceed this threshold, risking a loss of stiffness in the connector. Other polymers with higher temperature resistance exist, but as noted, they introduce manufacturing difficulties in the current system. These durability aspects were beyond the scope of these short-term tests and remain an open question.

9.2.2 Interface Reliability

As discussed, the glass–polymer interface can be the weak link. Without a permanent bond, the connection mostly relies on friction and the mechanical features provided by the interlock

geometry. Any irregularity or contamination on the glass surface (dust, oil) can further reduce the adhesion. In the shear tests, it was observed that the polymer layer debonded cleanly from the glass at lower loading than anticipated for some of the specimen. This points to the need for either improved surface preparation, such as plasma treatment, or designing physical interlocks that make the polymer interlayer 'capture' the glass geometry, so it cannot detach without deliberate unlocking. The challenge is to do so without resorting to permanent alterations of the glass. Achieving a reliable yet reversible interface is a delicate balance.

9.2.3 Fabrication Constraints

The use of robotic non-planar AM proved feasible but adds complexity to the fabrication process. Printing such a delicate design directly onto a vertical or curved glass surface requires precise calibration, strong hardware and close attention to prevent collisions. The UR5 robotic setup, while flexible, demanded an intensive upfront digital workflow – from 3D scanning the glass components to generating custom toolpaths for non-planar AM. This means that the barrier to adoption is relatively high: specialised equipment and expertise are needed, unlike traditional glass construction which might use off-the-shelf adhesives. The trade-off for eliminating adhesives is a more complex manufacturing phase. For widespread application, it may be necessary to simplify this process. For instance, pre-fabricated polymer interlocks (perhaps produced via injection moulding once an optimal shape is known) that can be easily inserted between glass elements on-site, rather than printed for each assembly. Additionally, controlling the thermal environment (to prevent warping) is a challenge in non-planar printing. The setup at the LAMA lab also had this limitation; no heated chamber for the robot, which constrained material choice as described. Scaling up production will require addressing these process stability issues, possibly through improved hardware or alternative fabrication methods.

9.2.4 Structural Performance Trade-offs

Achieving reversibility inevitably comes with trade-offs in ultimate strength and stiffness of the connection. There is also the question of load cases beyond what was tested. While high shear and in-plane compression were successfully resisted, a realistic structure might see out-of-plane forces, vibrations, or even dynamic loads (wind, earthquakes). The performance of the interlocks under such conditions is yet unknown. Furthermore, fire safety cannot be overlooked: polymers are vulnerable to high heat. In a fire scenario, the interlocks could soften or burn, potentially causing a partial or total collapse of the assembly. Traditional solutions like adhesives have known fire performance (often poor as well, but solutions like intumescent coatings exist); similar considerations would be needed to make polymer interlocks viable in regulated building environments. Acknowledging these limitations is important, however the current system is best suited for temporary or moderate-scale structures, experimental pavilions, or internal installations where conditions are controlled.

In summary, these challenges frame the boundary conditions for its application. Understanding where the system is likely to succeed (and thus where it is likely to fail) is crucial for guiding future research and for any potential real-world implementation.

10 Conclusion

10.1 Towards Reversible Structural Glass: Conclusions on a Reversible Interlock System

The central question guiding this research was:
"How can an Additive Manufactured (AM) or injection-moulded interlayer be designed to create reversible connections between free-form glass components while maintaining structural integrity?",
Through the course of this thesis, each facet of this question was explored. The most important considerations included selecting an appropriate interlayer material, optimising the geometry of the interlock, developing a manufacturing process, evaluating its structural performance, and ensuring full reversibility. In this concluding chapter, each of these aspects is discussed in turn, showing how they collectively answer the research question.

10.1.1 Interlayer Material

An important aspect of the interlayer behaviour was the choice of polymer. Initial trials with several thermoplastics revealed large differences in compatibility with the glass substrate. For example, PETG filament initially adhered strongly to the glass surface, but its significant shrinkage upon cooling led to warping-induced stresses that even cracked the glass during printing. PC/ABS, an engineering blend expected to offer high strength, similarly suffered severe warping without a heated enclosure, making it impractical with the available equipment. Flexible thermoplastics such as thermoplastic polyurethane (TPU) and other elastomeric polyesters were also tested; these showed minimal warping but lacked the stiffness to maintain the interlock geometry, resulting in poor print quality or sagging connections. In contrast, standard PLA emerged as a practical compromise. PLA exhibited reliable AM behaviour on glass (with minimal warping and good layer adhesion) and sufficient initial stiffness to form the interlocking geometry. Its thermal plasticity allows it to be shaped via additive manufacturing into the desired form and later melted down and reused. However, PLA has a low glass transition temperature (60°C), meaning that in service conditions approaching this temperature the polymer could soften and lose its load-bearing capacity. Likewise, PLA is a biodegradable thermoplastic; prolonged exposure to humidity or UV light can embrittle or degrade it over time. These characteristics raise concerns about the performance of the interlock over the lifespan of a structure. In summary, the selection of PLA was a pragmatic choice balancing printability and current performance, but its inherent material properties mean that future iterations of the system should explore more durable polymers or protective measures.

10.1.2 Geometry Optimisation

The geometry of the interlayer was another critical factor in creating a reversible connection. Instead of relying on permanent adhesives, the connection strength derives from a mechanical interlock engineered into the shape of the interlayer. A LEGO-like design was developed to accommodate minor manufacturing tolerances. This means that any small deviations from the AMing process are averaged out by the shape, allowing the components to fit together smoothly. This geometric design not only optimises load transfer and structural performance, but

also eases assembly and disassembly of the modules. Through iterative printing and designing (e.g. adding fillets to corners, adjusting connector dimensions, and tuning infill patterns), the interlayers were improved to better distribute stress and enhance print reliability. A 15 mm fillet on the corners of the interlayer ensured a continuous print load path through the polymer and thereby reduced stress concentrations inside the polymer, leading to less warping and higher adhesion. Similarly, using a concentric infill pattern (where the filament is deposited following the shape's contours) increased the uniformity of the internal structure. Altering the dimension and angle of extrusions on the interlayer improved printing reliability with a 1 mm extruder nozzle used in the robotic workflow.

10.1.3 Robotic Non-Planar Fabrication

Potential

Designing an effective interlayer is only useful if it can be fabricated directly onto free-form glass surfaces. To tackle this, this thesis pioneered a robotic non-planar AM workflow to fabricate custom interlayers on complex glass geometries, such as osteomorphic shaped glass bricks. By 3D scanning each cast or AM brick and generating a matching interlock profile, a non-planar printing toolpath could be created and executed by a 6-axis robot (UR5), validating that free-form polymer interlocks can be produced on non-flat glass components. The printed interlayers match their glass counterparts, demonstrating that this digital fabrication technique can potentially produce consistent interlocks on a wide variety of free-form glass structures.

Limitations

While this demonstrates the viability of fabricating custom interlocks on free-form glass, the current implementation remains insufficiently robust for consistent application. Several limitations were encountered during prototyping. First, the brittleness of the PLA interlayer and the fragile heatbreak made the system highly sensitive to minor extrusion irregularities, often resulting in mechanical failure or print termination. Second, the process depends heavily on precise manual calibration; even sub-millimetre discrepancies between the simulated toolpath and the robot's actual TCP caused collisions or poor adhesion. Third, the workflow lacks real-time error correction, meaning that once deviations begin, they propagate layer by layer, compounding positional errors and degrading overall fidelity. To evolve this proof-of-concept into a scalable and production-ready method, three key developments are required: mechanical reinforcement of the extruder hardware to tolerate uneven paths and higher friction; integration of adaptive control strategies, such as closed-loop feedback or surface tracking; and refinement of the digital workflow to reduce reliance on manual alignment and improve tolerance to geometric variance.

Applications

In the end, this thesis only prototyped the interlayer via additive manufacturing. For widespread application, it may be needed to simplify this process or look more into injection moulding of a standardised interlayer.
Looking forward, both workflows, cast-glass with bespoke 3D-printed interlayers and AM-glass with mass-manufactured interlayers, unlock different advantages. Cast-glass bricks paired with robotically printed interlayers offer limitless form variations from a single mould, ideal for structures in which bricks may later be reused in a new configuration with different interlayers. On the other hand, AM glass embeds angular corrections directly into each brick's CAD geometry, enabling the use of standardised, injection-moulded interlayers for more bespoke architecture. In summary, cast glass excels in adaptive reuse of a single block design, while AM glass streamlines production through upfront digital complexity of the brick and mass-manufactured interlayers. Critically assessing which workflow best suits a given project, such as a future Glass Vault 2.0, can create a fully manufacturable, reversible system for any shaped glass structure.

10.1.4 Structural Performance

To validate the the strength of the polymer-glass interlock, a shear test set-up was created to apply lateral loads onto the top plate of the system. This was done while applying a normal load on the top surface simulating a real-life scenario. These quasi-static shear tests produced peak shear forces between 1.77 kN and 6.13 kN under starting preloads of 0.30–0.50 kN. The effective friction coefficients in these tests correspond to ($\mu = F_{\text{shear}}/F_{\text{normal}}$) of 0.985–1.803, markedly above typical Eurocode values of 0.4 for timber-timber or steel-steel contacts. While these high μ-values confirm that interlock geometry and polymer deformation deliver high shear resistance, every specimen failed by clean delamination of the polymer from the glass. This means that the ultimate capacity is governed by adhesive failure at the glass–polymer interface, underscoring that enhancing interfacial bonding is critical to unlocking more ductile, post-peak behaviour. Therefore, future efforts should prioritise optimised surface treatments or adhesive formulations and a refined fixture design to ensure uniform compression and to fully realise the structural potential of the interlock.

10.1.5 Concluding

Embracing reversibility requires accepting certain trade-offs. The complexity shifts to the design and fabrication phase, and may demand more careful engineering. However, the payoff is a system that enables easy disassembly, reuse of high-value components (glass), and adaptability of structures. Designers must therefore consider the broader system integration. For example, creating structures that take advantage of the materials' strengths, like pairing these glass-polymer interlocks with structural forms that naturally stabilise, like compressive-only vaults. The decision to use such a system should be informed by a holistic view of sustainability and performance. The trade-off between structural performance and circular economy benefits lies at the heart of the design philosophy for reversible structures. However, this research tries to lower the loss in structural performance as full circularity is achieved step by step.
The reality is that each prototype requires careful tuning, and the conditions of a controlled lab are different from a construction site. Also, the innovative nature of the system means there is little regulatory guidance – building codes do not yet have provisions for 3D-printed removable joints, so proving equivalence or safety will require additional research and likely some conservatism. On the other hand, the very same novelty is what makes the system exciting. It demonstrates a new direction for structural joints that could inspire further research and development. The promise of the system lies in its potential impact on sustainability: if such connections were perfected, one could build large glass structures (facades, vaults, even entire walls or enclosures) and confidently disassemble them at end of life or when needs change. This adaptability could reduce demolition waste and preserve the value of high-quality materials like structural glass. The promise of the glass–polymer interlock is a future where structural ingenuity, aesthetics and environmental responsibility go hand in hand, even if there are still challenges to solve before that future is fully realised.

11 Impact

11.1 Broader Impact on the Built Environment

The interlocking system proposed in this thesis offers broader implications for sustainable construction beyond the scope of the individual case study. By enabling reversible assembly, material separation, and component reuse, the system challenges linear building practices and introduces a scalable model for circular construction. The integration of digital fabrication, modularity, and disassembly contributes to a more adaptable built environment. As buildings face increasing demands for flexibility, repairability, and material accountability, systems like this one can play a critical role in extending structural lifespans while reducing waste and embodied energy.

11.1.1 Sustainability

Reversibility

The key benefit of the glass–polymer–glass interlock is its full reversibility: each brick assembly, including its 3D-printed polymer interlayers, can be disassembled and redeployed without any permanent alteration to the glass units themselves. In practice, entire bricks fitted with interlayers can be decoupled from a structure and installed into a new configuration. This "plug and play" characteristic minimises material waste at the assembly level and enables straightforward reconfiguration of load-bearing systems. Following reuse of the glass bricks, the polymer interlayers can then be thermally separated from the glass by heating above the polymer's glass-transition temperature (> 60°C). At elevated temperatures, the interlayer softens sufficiently to allow clean removal from the glass surface. Once detached, the thermoplastic material can be collected, re-granulated, and re-extruded into new interlayers without loss of mechanical performance. This two-stage recovery process, first reusing brick and interlayer units, then recycling the polymer at end of life, supports a truly circular workflow in which both glass and polymer components circulate through construction and recycling streams. By combining modular disassembly of whole bricks with recyclability of the polymer interlayers, this interlocking system offers a sustainable pathway toward adaptive, low-waste building practice and extends the service life of structural elements.
This thesis investigated free-form glass bricks with a polymer interlayer. The same workflow could be adopted to work for different material combinations, for example:

1. (AM) ceramic bricks with an epoxy interlayer
2. Interlocking stone bricks (granite/limestone) with a TPU interlayer
3. AM concrete bricks with a cementitious interlayer

These options need to be researched, but the workflow has the potential to reach far wider than just the printing of a PLA interlayer on a non-planar glass geometry. With this workflow, a (non-planar) interlayer can be printed onto a standard (flat) brick, and the interlayer creates a reversible interlock with the adjacent brick. This interlayer could account for the angles needed to create an arch for example. The tests performed in Chapter 6 confirm the interlayer's ability to take up the lateral and compressive loads required. A robotic arm is necessary for non-planar surfaces but could also achieve a more efficient process on planar surface where a lot of

interlayers are required. Using this workflow on flat bricks creates a more precise interlayer. The interlayer itself creates the form of the structure by being able to print in different angles. This way, the glass brick can be the same and can be reused with different iterations of interlayers to form new structures (see Figure 11.1).

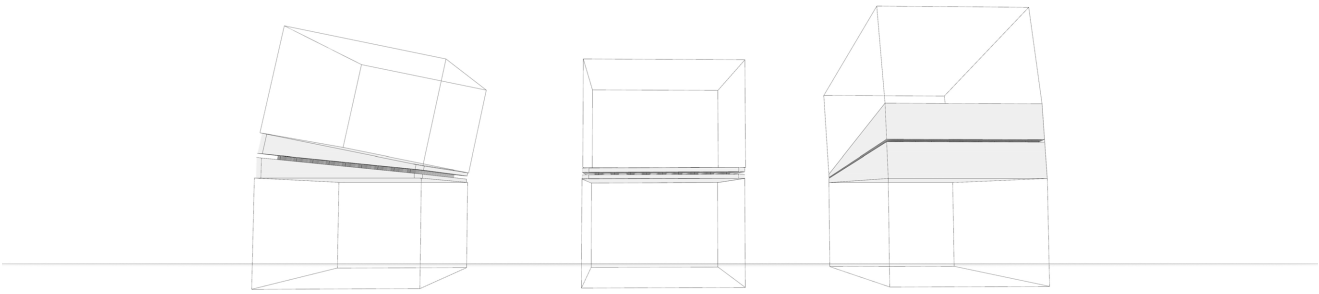

Figure 11.1: Three different structures with the same cast glass brick but a different interlayer design

Recyclability

The system proposed in this thesis directly facilitates the clean separation, reuse, and recycling of glass. Unlike conventional laminated or adhesively bonded assemblies, this reversible joinery avoids contamination and preserves the monolithic quality of the cast units, enabling true circularity. This makes it possible to repurpose post-consumer or discarded glass into structural elements with a future-proof design intent (Bristogianni et al., 2018).
Because both the polymer interlayer and the cast glass bricks remain mechanically coupled but separable, full material recovery is possible. The polymer can be removed through mild heat treatment, leaving the glass uncontaminated and ready for direct reuse or remelting. This is a significant advance, considering that current post-consumer architectural glass recycling rates are almost negligible, most of what gets recycled does not even leave the factory (offcuts and rejects during production and processing) (Oikonomopoulou, DeBrincat, & Fuhrmann, 2023).
Recycled glass cullet requires ~40% less energy to remelt than virgin glass (Kamau et al., 2021). As such, the proposed dry interlayer strategy is not only structurally effective and demountable but also a potential solution for a closed-loop glass design.

11.1.2 Other Applications of the Workflow

Apart from the application researched in this thesis, the robotic workflow and additive manufacturing on non-planar surfaces can be used in other applications in the built environment. The following sub-chapters will show some potential examples which would require further research.

On-Site Repair and Retrofitting

For example, cracked concrete beams, sculptures and columns can be scanned in situ, and a 5-axis path can be generated to extrude repair mortar onto/into the original surface repairing the object. For a stone facade, a 6-axis arm can follow the uneven geometry of aged brick or stone façades to deposit matching mortar or other repair mixtures directly into cracks and voids.

Figure 11.2: Printing of concrete directly into cracks, *Image generated with image generator pro by ChatGPT*

On-site Printing of Foundations on Sloped Terrain

Mounting a six-axis robotic arm with an extrusion nozzle onto a vehicle, allows the user to lay concrete directly onto uneven terrain, such as hillsides or terraced sites. This way it is possible to accurately trace the existing site without the need for formwork. This "printing-while-moving" enables fabrication over terrain larger than the robot's static reach.

Figure 11.3: Printing on a Sloped Terrain, *Image generated with image generator pro by ChatGPT*

Integrating Acoustic Baffles on Free-form Ceilings/Walls

Acoustic foam can be printed onto free-form ceilings/facades, whether concrete, wood, or plaster, to provide sound absorption in concert halls or offices without cutting bespoke panels or discard an architectural design.

Figure 11.4: Printing of acoustic foam on free-form wooden ceiling, *Image generated with image generator pro by ChatGPT*

Non-Planar Concrete AM

AM columns non-planarly, optimised for strength and material per situation.

Figure 11.5: Robotic AM of non-planar concrete columns, *Image generated with image generator pro by ChatGPT*

12 Recommendations

12.1 Implications for Future Research

The creation of the glass–polymer–glass interlock in this research, even within its limits, has several important implications for the future of reversible structural design, with focus in glass structures:

12.1.1 Hybrid Material Systems

The interlock leverages the strengths of two very different materials, brittle but strong glass and ductile but weaker polymer, to create a composite action. This suggests that hybrid systems can overcome the limitations of individual materials. The key is that the joint carries mechanical load while remaining separable by reversing the assembly process (or by targeted heating in this case if a polymer needs softening to remove). Test results showed sudden failure in the glass-polymer connection in all of the specimens. Strengthening the bond between the interlayer and the glass while remaining separable is one of the biggest challenges in this research. If this can be achieved and a more ductile failure mode can be reached, the interlock could be used in practice. As noted in Chapter 7.4.1, using a softer thermoplastic elastomer (e.g., TPU) instead of PLA could accommodate the $\pm 0.1 - 0.2$ mm deviations that still occur, even with metal moulds and high accuracy robot printing. Future work should characterise elastomers' compressive strength, creep resistance, and long-term durability, specifically when printed in thin ($\tilde{3}$ mm) layers. Investigating how different shore hardness grades of TPU affect both shear performance and tolerance accommodation will clarify the trade-off between compliance (to absorb these misalignments) and stiffness (to ensure compression-only structural behaviour). This thesis' findings provide a foundation for hybrid material approaches in glass, but emphasise the need for proper material selection and their cooperation in future research.

12.1.2 Development of Interlocks

While AM was used as the fabrication method in this thesis (due to its flexibility in prototyping), future development could refine the connector design for other production methods. Injection moulding or casting of the polymer interlocks in a more robust plastic or even a composite could be viable for mass production. This would retain the reversible, dry-join benefits while potentially offering better material properties, tighter tolerances and consistency than printed PLA. The current "Lego-like" interlock uses elastic averaging to reduce the impact of small printer and casting tolerances, further geometry refinements may improve cumulative alignment. Parametric studies (varying interlock protrusion angles, fillet radii, and engagement depths) could identify designs that maximise self-alignment over a wider range of offsets. Additionally, exploring new polymer formulations specifically for this purpose is a promising avenue. For instance, there may be more thermoplastic elastomers that adhere well to glass or thermoset polymers that can be reversibly cured. Importantly, any such development should keep reversibility in focus, e.g., using a polymer that can be softened or dissolved on command to release the glass if needed, or a connector shape that can be unlocked rather than destroyed to disassemble.

12.1.3 Developing the Non-Planar Robotic Workflow

While the non-planar robotic workflow presented in this thesis research works like it is supposed to, it is far from perfect. If this system were to be scaled, the workflow needs to be adjusted accordingly. The main problem with this workflow is the delicacy of the setup; with the combination of a 0.8-1.0 mm nozzle and a rigid material like PLA, every deviation or mistake in the print will be seen because the error margins are so small and mistakes will develop in the print; this led to many failures in the hardware. A suggestion could be to print with a thicker nozzle and a more robust extruder with a more compliant material. This would also mean changing the design from a LEGO-like interlock to a more robust design which the robotic arm can print.

12.1.4 Structural Applications and Scaling:

The demonstration on a vault is just one scenario. For future structures, one could envision using similar interlocks in glass façade systems, floor panels, or even space frames made of glass elements. Each application would bring its own requirements. The concept is versatile but would need adaptation, perhaps combining multiple interlock units for larger interfaces, or mixing rigid and flexible connectors to allow controlled movements. One implication of these results is that reversible systems might perform best when integrated into the overall structural design from the start. Rather than retrofitting a reversible joint into a conventional design, the whole structure could be conceived to work with the more flexible and modular nature of these connections. This could lead to new architectural forms optimised for demountability. However, extensive further testing (including long-term and environmental tests) and refinement will be necessary before such systems can meet building codes and safety factors. This thesis research work serves as a proof-of-concept, and it encourages taking the next steps in structural applications: testing larger prototypes, subjecting them to realistic loads and cycles, and developing the necessary design calculations or simulation tools to predict their behaviour.

12.1.5 Design for Disassembly in Architecture

This work provides a concrete example of designing a structural connection specifically for disassembly. It reinforces the idea that with creativity, it is possible to move beyond traditional permanent joints. In an era where sustainability and circular construction are paramount, structures that can be taken apart and reassembled or recycled are and will be increasingly important. The developed system shows one way to achieve this for glass structures, pointing toward a future where buildings might be conceived as temporary assemblies of permanent components. The glass components, often energy-intensive to produce but infinitely recyclable, can be reclaimed at end of life without damage, fulfilling a key principle of circular design. Future work should take circularity into account as one of the pilalrs of the research.

12.2 Reflection

12.2.1 Graduation Process

How is your graduation topic positioned in the studio?

This thesis research fits within the Building Technology's focus on material innovation, circular construction, and digital fabrication. It builds on the existing research in 3D-printed and cast glass structures but takes a new approach by exploring reversible interlayers. This makes it relevant to both architectural design and sustainable construction.

How did the research approach work out (and why or why not)?

The methodology combined literature review, material experimentation, iterative design, mechanical testing, and a case study with robotic prototyping. The research began with an extensive literature study, comparing existing glass structures. Next, the interlocking interlayer was designed, 3D-printed and shear tests were performed on these systems. Positive shear-test results validated the key concepts and guided further iterations. A small-scale arch case study, in combination with the prototyped glass brick with interlayer, demonstrated feasibility. Overall this integrated approach worked well: each phase informed the next, though time and resource constraints meant some ambitions (like a bigger scale, different shapes and long-term effects) remain future work. Throughout the research several parties or people were needed to get to the next stage in the thesis. For example, a software was needed to slice a .stl file into a non-planar print toolpath where there was no budget; the waterjet-cutter needed broke down; a professional RoboDK license was needed to export the big .script I had and at some important stages in the research people were unavailable due to different circumstance causing delays in the process. Because of the dependency on these different parties, when something falls away, it causes unforeseen delays. This approach, although in this case inevitable, is something to take into account for the future. My planning should be a bit larger to take into account unforeseen events.

Did the research lead to the results you aimed for? (SWOT of the method)

- Strengths: A mix of literature review, computational modelling, and physical testing has given a solid foundation for developing a reversible interlayer.
- Weaknesses: Novelty of the topic meant a lot of experimental research which takes up a long time, leaving less time to validate and design the final result. Therefore, some uncertainties remain, especially around (long-term) material performance and scalability.
- Opportunities: This research could be a beginning for future studies on (robotic) 3D-printed interlayers and modular glass structures, potentially influencing future structural applications.
- Threats: Technical uncertainties with glass AM. Furthermore, bringing this concept to full-scale use is still a challenge, as there are open questions about material behaviour and assembly in practice. The research approach started of a bit too broad, that's why it took longer to narrow it down to actually get good results.

How are research and design related?

The research directly influenced the design decisions. Literature on joinery systems and material testing has shaped the interlayer design. Experimental work has further pushed me to alter/refine the geometry and connections. Then, mechanical validation of the interlayer created new design ideas yet to be implemented. In this thesis, every physical print became a form of experiment: the performance of a printed interlayer became evidence that shaped the next design step. This synergy ensured that design decisions were evidence-driven rather than speculative.

Moral and ethical considerations

I was motivated by the ideal of a circular economy: glass is infinitely recyclable if uncontaminated, yet current building practices largely ignore this potential. So, the biggest ethical question

has been balancing sustainability with strength and practicality. Removing adhesives makes glass structures more recyclable, but it also introduces structural challenges. Another question is whether this system can realistically be scaled up or if it will remain a niche concept. These are things future research could point out.

12.2.2 Societal Impact

How applicable are the results?

The results of the thesis are promising but bounded by practical constraints. All prototypes were small scale and printed on a robotic arm in the LAMA lab – a proper setup, but one that imposed limitations. For instance, printing precision and nozzle control were challenging; complex geometries require careful calibration of flow rates and cooling times. The dry-interlock system shows potential, but it's still in the testing phase. It could work for modular facades or temporary structures, but more work is needed to prove its durability and ease of use in real projects.

To what extent has the projected innovation been achieved?

To a significant extent, the thesis achieved its innovation goal. A new way to create dry-assembled glass structures using 3D-printed interlayers was designed and mechanically tested and a novel non-planar robitic workflow was introduced. The positive shear test results of the interlayer connection were validating: the tests found load capacities above the order of expectations, confirming that the interlayer geometry could transfer forces effectively. Importantly, it allows disassembly without damaging the glass. That said, the full vision of a large, free-form glass arch using these connections was only partially realised. A small-scale prototype was formed as a proof-of-concept, but time and scale constraints meant a bigger prototype remained unbuild at the moment. Nonetheless, within the thesis scope, the central objective was met: confirming that additive-manufactured interlayers enable a demountable glass assembly.

Does the project contribute to sustainable development?

Yes, it moves toward circular design by allowing glass to be reused without contamination. However, a lot of work is still to be done in order to actually tell if this is a sustainable solution.

This project advances sustainable development in construction. By avoiding permanent adhesives, it aligns with circular economy principles (reuse, recycling, minimal waste). As pointed out earlier, glass can be recycled indefinitely if kept pure, which is a major advantage that this design preserves. In practical terms, a structure made with these interlocks would avoid the waste of glues and because components can be reused, the embodied energy in the glass is leveraged multiple times instead of being downcycled or landfilled.

Impact on people, planet, and economy

- *People*
  Raises awareness about new ways to use glass in construction. It offers educational value and suggests a future workflow in digital fabrication and demountable construction. By emphasising reuse, it also promotes carbon awareness in materials.
- *Planet*
  Reduces waste by making glass structures reusable. The impact of the interlayer materials still needs research but can also be reused or reycled.
- *Economy*
  While AM and free-form glass creation have upfront costs, the long-term savings could be substantial. Modular glass units allow for faster on-site assembly and disassembly, reducing construction costs. The avoidance of adhesives and the ability to re-use expensive glass components can lower material expenses over its lifetime.

How does the project affects architecture / the built environment?

Throughout this project, reversibility was the central design goal, and pursuing it required navigating several trade-offs. It means that this research created an example that structures can be both stable and intentionally impermanent. This is somewhat against the grain of traditional structural engineering, which often prioritises maximum strength and durability without regard for disassembly. The broader meaning of the results is that it is feasible to prioritise future reuse over initial performance. In this case, that meant accepting a lower bond strength in exchange for a clean separation of parts. The implication for future structures is profound: if architects and engineers begin to value the end-of-life stage as much as the in-use stage, design criteria will expand to include questions of recover ability and adaptability. This interlocking system directly engages with that paradigm, suggesting that even critical structural connections can be designed to come apart. This could facilitate not only recycling, but also repair and reconfiguration of structures. If successful, this system could change how we design and build glass structures by making them more flexible and reusable. Finally, the use of robotic arms and the proposed digital fabrication method could become a wider used concept for construction in other applications than the one proposed in this thesis. It has high precision and can be fully programmed off-site, reducing time on site and errors.

Glass Unlocked

Designing an Additively Manufactured
Reversible Interlayer Connection
for Structural Use of Free-Form Glass Units

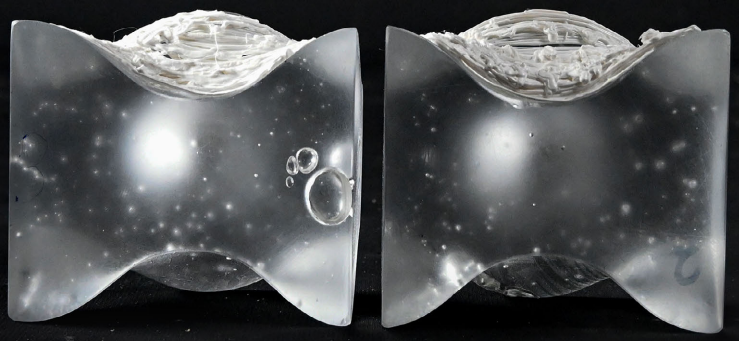

TU Delft

References

3Printr.com. (2023, 9). *Maker presents completely 3D printed Velcro fastener.* Retrieved from https://www.3printr.com/maker-presents-completely-3d-printed-velcro-fastener-0664616/

Akerboom, R. (2016). *Glass Columns, exploring the potential of free-standing glass columns assembled from stacked cast* (Tech. Rep.). Delft: Delft University of Technology.

Aloui, O., & Bao, M. (2024). Structural design optimization of cast glass artwork via a digital design solution. *Glass Structures and Engineering*. doi: doi:10.1007/s40940-024-00278-9

Aloyaydi, B., Sivasankaran, S., & Mustafa, A. (2020, 7). Investigation of infill-patterns on mechanical response of 3D printed poly-lactic-acid. *Polymer Testing*, *87*. doi: doi:10.1016/j.polymertesting.2020.106557

Aurik, M., Snijder, A., Noteboom, C., Nijsse, R., & Louter, C. (2018, 5). Experimental analysis on the glass-interlayer system in glass masonry arches. *Glass Structures and Engineering*, *3*(2), 335–353. doi: doi:10.1007/s40940-018-0068-7

Bellapart. (2007). *Monumento 11M .* Retrieved from https://www.bellapart.com/project/monumento-11m/

Bendarma, A., Rusinek, A., Czarnota, C., Jankowiak, T., Bernier, R., & Lodygowski, T. (2025, 1). Experimental characterization of aluminum/polymer/aluminum sandwich structures under various loading rates and temperatures: Establishing a constitutive relationship for LDPE. *Composite Structures*, *351*, 118616. doi: doi:10.1016/j.compstruct.2024.118616

Bolmin, O., Young, B., Leathe, N., Noell, P. J., & Boyce, B. L. (2023, 1). Interlocking metasurfaces. *Journal of Materials Science*, *58*(1), 411–419. doi: doi:10.1007/s10853-022-08015-9

Bristogianni, T., Oikonomopoulou, F., de Lima, C. J., Veer, F. A., & Nijsse, R. (2018). Cast glass components out of recycled glass: Potential and limitations of upgrading waste to load-bearing structures. In *Challenging glass 6: Conference on architectural and structural applications of glass, cgc 2018 - proceedings* (pp. 151–174). TU Delft Open. doi: doi:10.7480/cgc.6.2130

Canestrari, F., Ferrotti, G., Partl, M., & Santagata, E. (2005, 1). Advanced Testing and Characterization of Interlayer Shear Resistance. *Transportation Research Record: Journal of the Transportation Research Board*, *1929*, 69–78. doi: doi:10.3141/1929-09

Changing Surface Properties for Better Adhesion | 3M Science of Adhesion Educational Series. (n.d.). Retrieved from https://www.3m.com/3M/en_US/bonding-and-assembly-us/resources/science-of-adhesion/changing-surface-properties/

Civil Synergy. (2020, 7). *INTERLOCKING BRICKS.* Retrieved from https://civilsynergy.wordpress.com/2020/07/20/interlocking-bricks/

close the glass loop. (2021, 11). Close the Glass Loop, Press Release. Retrieved from https://www.closetheglassloop.eu

DEBONDING ON DEMAND (Tech. Rep.). (n.d.). Frauenhofer IFAM. Retrieved from www.ifam.fraunhofer.de

Dimas, M., Oikonomopoulou, F., & Bilow, M. (2022). IN BETWEEN: An Interlayer Material Study for Interlocking Cast Glass Blocks. *Challenging Glass Conference Proceedings*, *8*. doi: doi:10.47982/cgc.8.416

Dimitescu, A., Babiş, C., Fica, S. A., Rugescu, A. M., & Enache, I. C. (2023, 11). 3D printing by Fused Deposition Modeling - FDM technology - with PETG type filament in horizontal position A. *Journal of Research and Innovation for Sustainable Society*, *5*(2), 120–125. doi:

doi:10.33727/JRISS.2023.2.15:120-125

DOTX control solutions. (n.d.). *5 Axis Slicer.* Retrieved from https://5-axis-slicer.com/

EurocodeApplied.com. (n.d.). *Calculation of wind peak velocity pressure - Eurocode 1.* Retrieved from https://eurocodeapplied.com/design/en1991/wind-peak-velocity-pressure

Europeenne, N., & Norm, E. (2006). EUROPEAN STANDARD Eurocode 3-Design of steel structures-Part 2: Steel Bridges.

FacFox. (2023, 12). *ABS Print Warping: How to Stop It.* Retrieved from https://facfox.com/docs/kb/abs-print-warping-how-to-stop-it

Farah, S., Anderson, D. G., & Langer, R. (2016, 12). Physical and mechanical properties of PLA, and their functions in widespread applications — A comprehensive review. *Advanced Drug Delivery Reviews*, *107*, 367–392. doi: doi:10.1016/j.addr.2016.06.012

Gantrade. (n.d.). *Polyurethanes in 3D Printing.* Retrieved from https://www.gantrade.com/blog/polyurethanes-in-3d-printing#:~:text=The%20versatility%2C%20toughness%2C%20heat%20resistance,%2C%20engineering%2Dgrade%203D%20materials.

Gloyer, P., Schek, L. N., Flöttmann, H. L., Wüst, P., & Völlmecke, C. (2023, 12). Extrusion-Based Additive Manufacturing-Driven Design and Testing of the Snapping Interlocking Metasurface Mechanism ShroomLock. *Inventions*, *8*(6). doi: doi:10.3390/inventions8060137

Göppert, K., Paech, C., Arbós, F., & Teixidor, C. (2004). *Glass Monument in Remembrance of the Terrorist Attacks in Madrid of* (Tech. Rep.).

GPI. (n.d.). *Facts About Glass Recycling.* Retrieved from https://www.gpi.org/facts-about-glass-recycling

Hartwell, R., Overend, M., Veer, F., Bristogianni, T., O'Callaghan, J., & Oikonomopoulou, F. (2024). *Resolved.* Retrieved from https://www.restructgroup-tudelft.nl/resolved

Hayez, V., Gubbels, F., Dow, G. C., Belgium, S., & Bordet, J. (2019). *Maximizing façade transparency with crystal clear silicone spacers* (Tech. Rep.).

Inamura, C., Stern, M., Lizardo, D., Houk, P., & Oxman, N. (2018, 12). Additive Manufacturing of Transparent Glass Structures. *3D Printing and Additive Manufacturing*, *5*(4), 269–283. doi: doi:10.1089/3dp.2018.0157

Kamau, P., Stec, M., Tu, L., & Schlorke, S. (2021, 7). *Strengthening Sustainability in the Glass Industry* (Tech. Rep.). IFC Manufacturing, Agribusiness & Services (MAS). Retrieved from https://documents1.worldbank.org/curated/en/469111646904407368/pdf/Strengthening-Sustainability-in-the-Glass-Industry.pdf

Klein, J., Stern, M., Franchin, G., Kayser, M., Inamura, C., Dave, S., ... Oxman, N. (2015, 9). Additive Manufacturing of Optically Transparent Glass. *3D Printing and Additive Manufacturing*, *2*(3), 92–105. doi: doi:10.1089/3dp.2015.0021

Lucia Brandoli. (2021, 10). *Qaammat, the glass pavilion celebrating the Inuit and their land.* Retrieved from https://www.domusweb.it/en/news/gallery/2021/10/27/qaammat-the-greenlands-pavilion-celebrating-land-and-people.html

Madhumitha Jaganmohan. (2024, 5). *Emissions from glass production worldwide and in Europe in 2022.* Retrieved from https://www.statista.com/statistics/1071205/carbon-dioxide-emissions-from-glass-production-worldwide/#statisticContainer

Massimino, D., Townsend, E., Folinus, C., Stern, M., & Becker, K. (2024, 9). Additive manufacturing of interlocking glass masonry units. *Glass Structures & Engineering*. Retrieved from https://link.springer.com/10.1007/s40940-024-00279-8 doi: doi:10.1007/s40940-024-00279-8

Melito, S. (2022, 12). *Injection Molding Tolerances | The Ultimate Guide.* Retrieved from https://www.fictiv.com/articles/injection-molding-tolerances-an-in-depth-look

Meredith, C. S., & Swab, J. J. (2020, 12). *Compression Strength of Borosilicate and Soda-Lime Silicate Glasses Using a Dumbbell-Shaped Specimen* (Tech. Rep.). Devcom. Retrieved from https://www.researchgate.net/publication/346574845

Mulcahy, K. R., Kilpatrick, A. F., Harper, G. D., Walton, A., & Abbott, A. P. (2022, 1). *Debondable adhesives and their use in recycling* (Vol. 24) (No. 1). Royal Society of Chemistry. doi: doi:10.1039/d1gc03306a

MVRDV. (2016). *Crystal Houses.* Retrieved from https://www.mvrdv.com/projects/240/crystal-houses

NEN-EN 1995-1-1:2023 Ontw. en. (2023, 9). Retrieved from https://www.nen.nl/nen-en-1995-1-1-2023-ontw-en-315434

Oikonomopoulou, F., & Bristogianni, T. (2022). Adhesive solutions for cast glass assemblies: ground rules emerging from built case studies on adhesive selection and experimental validation. In *Challenging glass 8: Conference on architectural and structural applications of glass, cgc 2022* (pp. 293–317). Challenging Glass Conference (CGC). doi: doi:10.1007/s40940-022-00178-w

Oikonomopoulou, F., Bristogianni, T., Barou, L., Jacobs, E., Frigo, G., Veer, F. A., & Nijsse, R. (2018a). *Interlocking cast glass components, Exploring a demountable dry-assembly structural glass system* (Vol. 63; Tech. Rep. No. 1). Delft University of Technology, Politecnico di Milano.

Oikonomopoulou, F., Bristogianni, T., Barou, L., Jacobs, E., Frigo, G., Veer, F. A., & Nijsse, R. (2018b). A novel, demountable structural glass system out of dry-assembly, interlocking cast glass components. In *Challenging glass 6: Conference on architectural and structural applications of glass, cgc 2018 - proceedings* (pp. 11–26). TU Delft Open. doi: doi:10.7480/cgc.6.2118

Oikonomopoulou, F., Bristogianni, T., Barou, L., Veer, F. A., & Nijsse, R. (2018a, 11). *The potential of cast glass in structural applications. Lessons learned from large-scale castings and state-of-the art load-bearing cast glass in architecture* (Vol. 20). Elsevier Ltd. doi: doi:10.1016/j.jobe.2018.07.014

Oikonomopoulou, F., Bristogianni, T., Barou, L., Veer, F. A., & Nijsse, R. (2018b, 11). *The potential of cast glass in structural applications. Lessons learned from large-scale castings and state-of-the art load-bearing cast glass in architecture* (Vol. 20). Elsevier Ltd. doi: doi:10.1016/j.jobe.2018.07.014

Oikonomopoulou, F., Bristogianni, T., van der Velden, M., & Ikonomidis, K. (2022, 5). The adhesively-bonded glass brick system of the Qaammat Pavilion in Greenland: From research to realization. *Architecture, Structures and Construction*, *2*(1), 39–62. doi: doi:10.1007/s44150-022-00031-2

Oikonomopoulou, F., Bristogianni, T., Veer, F. A., & Nijsse, R. (2018, 3). The construction of the Crystal Houses façade: challenges and innovations. *Glass Structures and Engineering*, *3*(1), 87–108. doi: doi:10.1007/s40940-017-0039-4

Oikonomopoulou, F., DeBrincat, G., & Fuhrmann, S. (2023, 9). *Glass and circularity* (Vol. 8) (No. 2). Springer Science and Business Media Deutschland GmbH. doi: doi:10.1007/s40940-023-00230-3

Oikonomopoulou, F., Ioannidis, M., Koniari, A. M., & Bristogianni, T. (2023). *Fabrication methods for topology-optimized massive glass structures* (Tech. Rep.). Retrieved from https://www.researchgate.net/publication/381655297

Oikonomopoulou, F., Veer, F., Bristogianni, T., & Barou, L. (2019, 8). Dry interlayers out of cast polyurethane rubber for interlocking cast glass structures: Experimental exploration and

validation. In *Advances in engineering materials, structures and systems: Innovations, mechanics and applications* (pp. 1709–1714). CRC Press. doi: doi:10.1201/9780429426506-295

Oikonomopoulou, F., Veer, F., Nijsse, R., & Baardolf, K. (2015, 5). A completely transparent, adhesively bonded soda-lime glass block masonry system. *Journal of Facade Design and Engineering*, *2*(3-4), 201–221. doi: doi:10.3233/fde-150021

Packham, D. E. (2003). Surface energy, surface topography and adhesion. *International Journal of Adhesion and Adhesives*, *23*(6), 437–448. doi: doi:10.1016/S0143-7496(03)00068-X

Peng, F., Zhao, Z., Xia, X., Cakmak, M., & Vogt, B. D. (2018, 5). Enhanced Impact Resistance of Three-Dimensional-Printed Parts with Structured Filaments. *ACS Applied Materials & Interfaces*, *10*(18), 16087–16094. doi: doi:10.1021/acsami.8b00866

Pfarr, D., & Louter, C. (2022). Prototyping of digitally manufactured thin glass composite façade panels. In *Challenging glass 8: Conference on architectural and structural applications of glass, cgc 2022* (pp. 263–273). Challenging Glass Conference (CGC). doi: doi:10.1007/s44150-022-00080-7

Saint Gobain Sekurit. (n.d.). *Glossary | Sekurit.* Retrieved from https://www.saint-gobain-sekurit.com/global-excellence/our-production-processes/glossary

Simplify3D. (n.d.). *Filament Properties Table.* Retrieved from https://www.simplify3d.com/resources/materials-guide/properties-table/

Standard Bots. (2025, 4). *What is a 6-axis robot? A simple guid.* Retrieved from https://standardbots.com/blog/six-axis-robot?srsltid=AfmBOop30mcEGw0MbXZG8Is3fezs3aATlK3Gg0dvmX00WuvYf3vMLCqE

Stern, M., Townsend, E., Massimino, D., & Becker, K. (2024). Advancing Sustainable 3D Printing: The Feasibility of Recycled Glass as a Building Material With Additive Manufacturing. doi: doi:10.47982/cgc.9.583

Teo, T. J., & Slocum, A. H. (2017, 7). Principle of elastic averaging for rapid precision design. *Precision Engineering*, *49*, 146–159. doi: doi:10.1016/J.PRECISIONENG.2017.02.003

top3dshop. (2019, 10). *3D Printer kinematic types.* Retrieved from https://top3dshop.com/blog/3d-printer-kinematics-explained

Vermeltfoort, A. T., & Martens, D. (2016, 6). *Compression and shear properties of masonry cut from walls, three to ninety-five years old, compared with laboratory made masonry* (Tech. Rep.). Eindhoven University of Technology, Eindhoven. doi: doi:http://dx.doi.org/10.1201/b21889-259

Wayken. (2023, 3). *Snap Fit Joints: Types, Benefits, and Best Practices.* Retrieved from https://waykenrm.com/blogs/snap-fit-joints/

Yost, J., Cregan, M., Bolhassani, D., Chhadeh, P., Schneider, J., Lu, Y., & Akbarzadeh, M. (2025, 11). Experimental investigation of the bearing capacity between short hollow glass columns and a transparent thermoplastic interface material. *Engineering Structures*.

İlerisoy, Z. Y., & Çolak, B. B. (2018). *DISCOVERY OF INNOVATIVE MATERIALS IN STRUCTURAL SYSTEM DESIGN: GLASS STRUCTURES* (Tech. Rep.). Retrieved from https://www.researchgate.net/publication/328007176

Appendices

A Appendix A

A.1 Mechanical Test Results

Specimen G2

The first specimen got pre-loaded with a normal force of 0.5 kN. When this number was attained, the horizontal laoding got applied. This started at roughly second 300 and the interlock failed at around second 380 (the highest peak), when the top interlayer delaminated off the glass. Specimen G2 reached a peak lateral force of $F_{\text{shear,max}}$ = 2,53 kN, which occurred at the same time as the normal (vertical) load of F_{normal} = 2,86 kN. The average friction coefficient from the moment loading was applied is μ = 0.818.

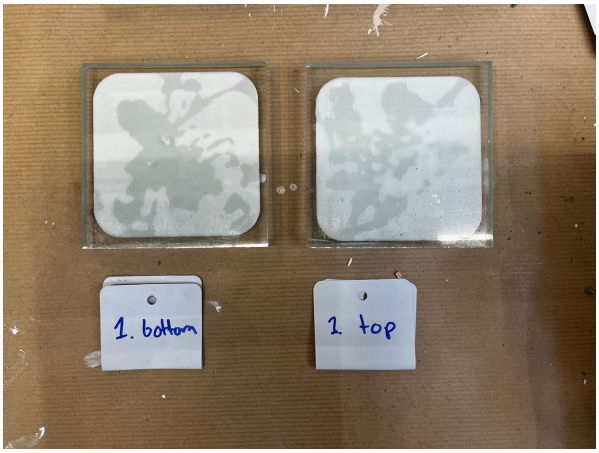

(a) Adhesion pattern on the backside of specimen G2, prior to testing

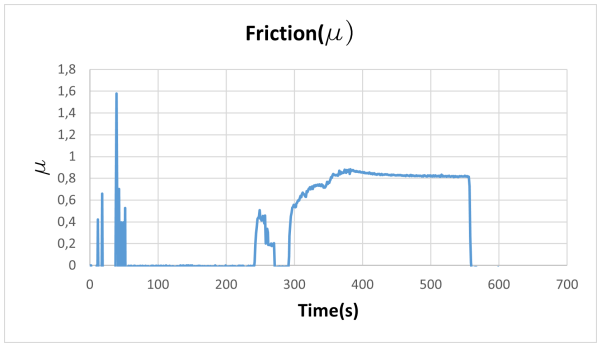

(b) Friction graph of specimen G2

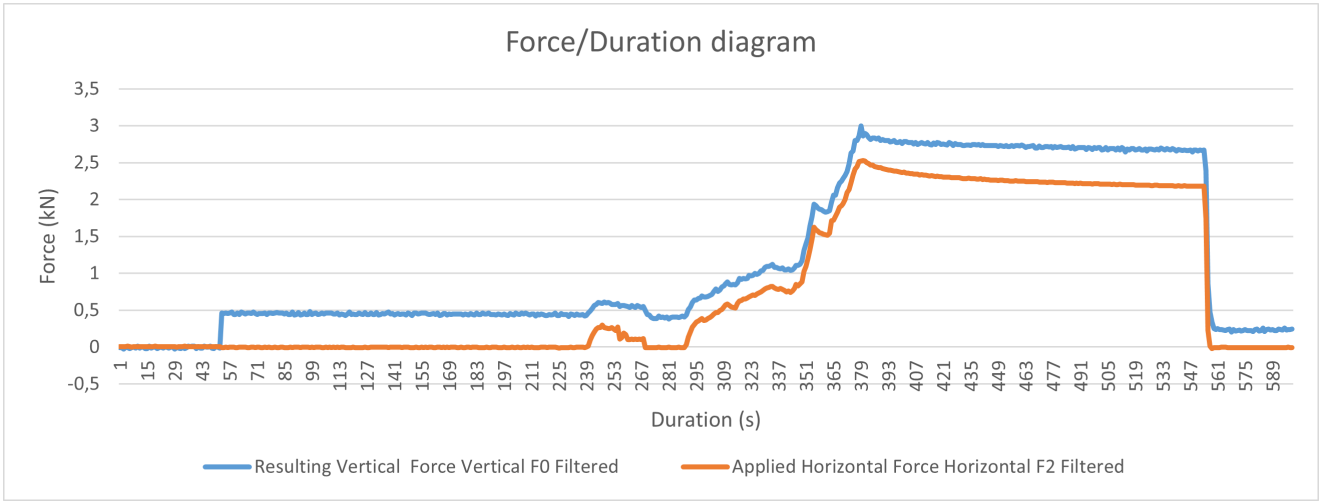

(c) Force/Time graph of specimen G2

Figure A.1: Force diagrams of testing of specimen G2

The load-curves showed a sharp drop immediately after peak shear load, indicating an immedi-

ate failure rather than ductile yielding. In the DIC images one can see the spcimens behaviour under normal loading and horizontal loading just before failure on the left image (see Figure A.2a). In this image can be seen that already some displacement took place in the whole configuration. But also a minor displacement (0.54 mm) between the top (Point 5: -3.22 mm) and bottom (Point 10: -2.68 mm) plates. The moment of full delamination at 2.53 kN can be seen in the right image (see Figure A.2b). At this moment, the total difference in displacement is 4.60 mm and it can be seen that the top plate has delaminated from the interlayer leading to failure of the interlock

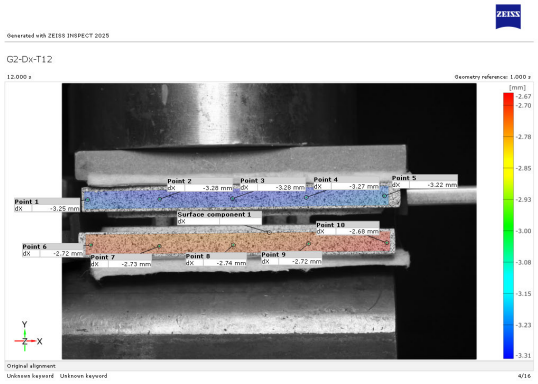

(a) DIC analysis: Dx displacement of specimen G2 under 500N normal force only

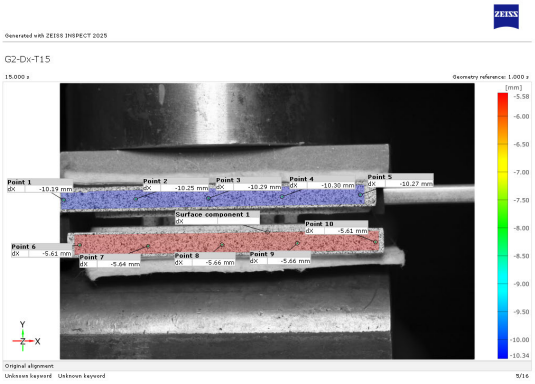

(b) DIC analysis of specimen G2: Dx displacement at moment of delamination

Figure A.2: DIC analysis of specimen G2: Dx displacements

Specimen G3

Specimen G3 again failed by clean delamination of the polymer interlayer from the glass. G3 was initially clamped under a normal force of about 0.30 kN. As soon as lateral loading began the interlocking features engaged. The interlock resisted sliding up to $F_{\text{shear,max}}$ = 6.13 kN of shear force, occurring simultaneously with a normal load of F_{normal} = 3.90 kN. This peak is more than twice G2's capacity, underscoring the strength of the interlock geometry under moderate preload. Between the moment sliding started and the peak, the ratio of shear to normal force averaged μ = 1.448, indicating that mechanical interlock and polymer deformation engaged more in the load transfer.

The shear force fell almost immediately to near zero as the interlayer was cleanly peeled from the glass. This abrupt drop marks the failure threshold of the adhesive bond and is characteristic of brittle delamination in all specimens. 6.13 kN shear peak under only 3.90 kN of preload shows that the interlocking features can deliver very high resistance. The post-peak collapse highlights interlayer adhesion as the limiting factor.

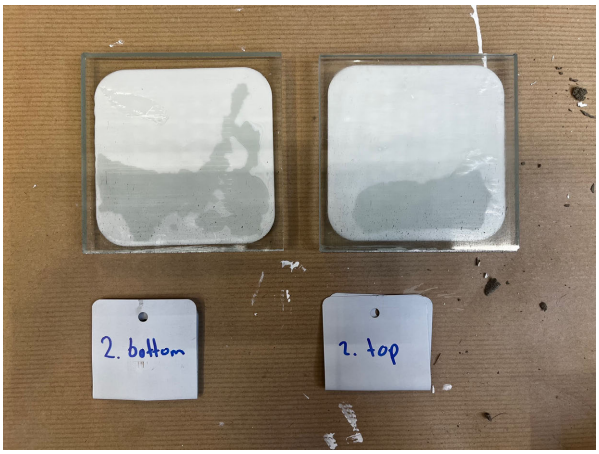

(a) Adhesion pattern on the backside of specimen G3, prior to testing

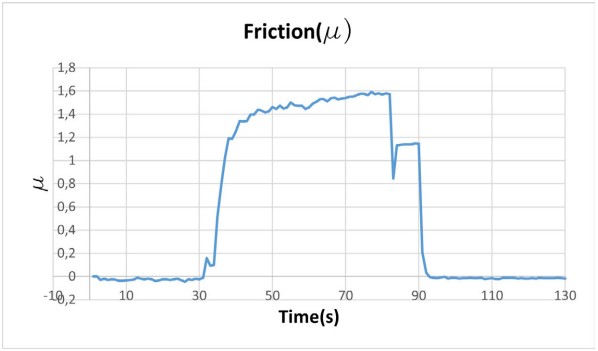

(b) Friction graph of specimen G3

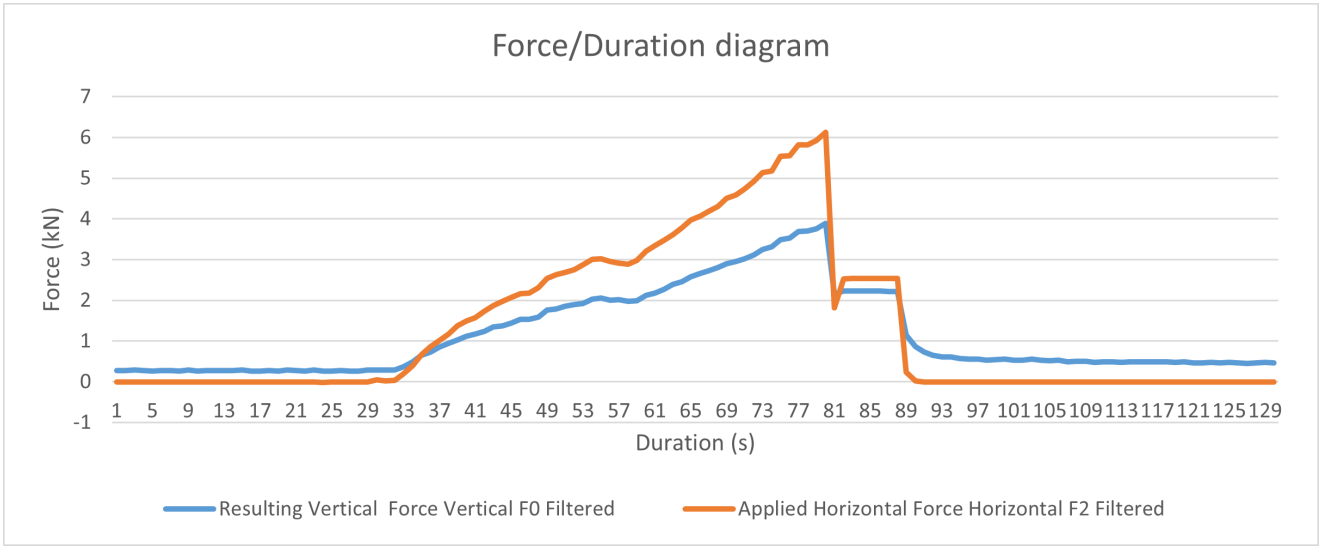

(c) Force/Time graph of specimen G3

Figure A.3: Force diagrams of testing of specimen G3

In Figure A.4 one can see the displacement and the delamination of the bottom interlayer. Between the two image, a rotation into the y-direction can be seen. This could mean that the top plate got pushed against the actuator and therefore had more friction at the top.

(a) DIC analysis of specimen G3: Dx displacement under 300N normal force

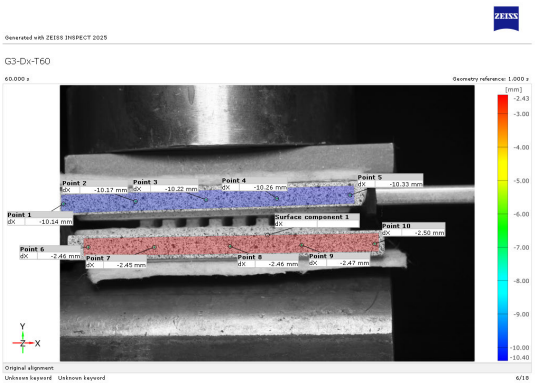

(b) DIC analysis of specimen G3: Dx displacement at moment of delamination

Figure A.4: DIC analysis of specimen G3: Dx displacements

Specimen G4

The interlock was compressed under approximately 0.30 kN of normal load, ensuring full engagement of its interlocking features before any lateral force was applied. When applying lateral loading, the interlock resisted loads up to a peak shear force of $F_{\text{shear,max}}$ = 1.77 kN, which coincided with a normal load of F_{normal} = 1.31 kN. Over the interval from start to peak loading, the ratio of shear to normal force averaged μ = 0.983 This indicates that mechanical interlocking and polymer deformation mostly governed the load transfer, rather than surface friction only. Immediately following the peak, the shear force collapsed almost to near zero as the interlayer debonded from the glass.
Compared with specimens G2 and G3, G4's maximum shear capacity was noticeably lower, suggesting either a weaker polymer–glass bond or inconsistencies during interlayer deposition. Nevertheless, its high friction coefficient demonstrates that the interlocking features still engaged effectively. Canestrari, Ferrotti, Partl, and Santagata (2005)

(a) Adhesion pattern on the backside of specimen G4, prior to testing

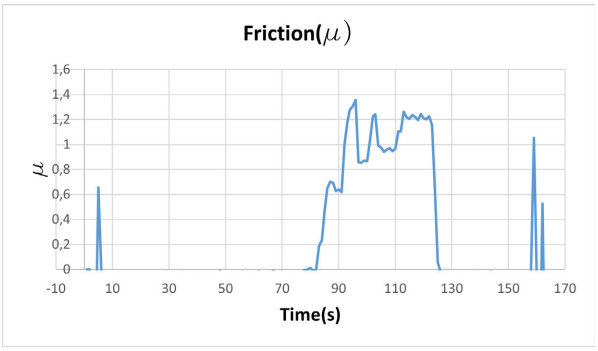

(b) Friction graph of specimen G4

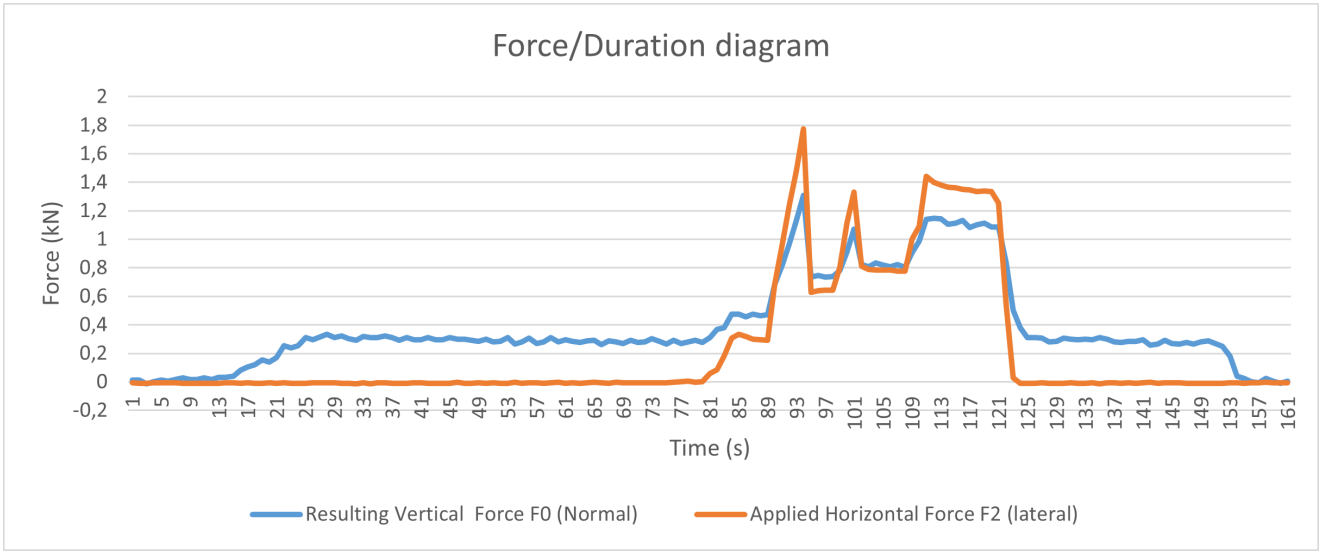

(c) Force/Time graph of specimen G4

Figure A.5: Force diagrams of testing of specimen G4

In the DIC analysis with focus on the Dx displacement of the specimens, the complete debonding of the bottom interlayer can be seen in Figure A.6b. Again, comparing Figure A.6a and A.6b, a rotation upwards is noticable in the specimen.

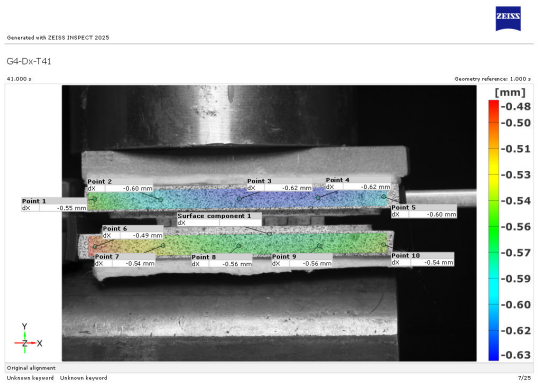

(a) DIC analysis of specimen G4: Dx displacement under 300N normal force

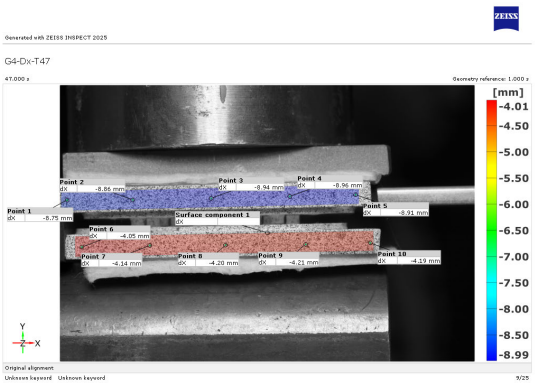

(b) DIC analysis of specimen G4: Dx displacement at moment of delamination

Figure A.6: DIC analysis of specimen G4: Dx displacements

Specimen G5

Again, specimen G5 was pre-compressed under a normal force of approximately 0.30 kN before any shear loading was applied. After loading, the peak shear force was measured at $F_{\text{shear,max}}$ = 2.58 kN with simultaneous normal load of F_{normal} = 2.03 kN. The average ratio of shear to normal force over the span from start loading to shear peak was μ = 0.990. Compared with G4, G5 delivered a substantially higher shear capacity, although still below G2 and G3. Nevertheless, its abrupt post-peak collapse again points to a sudden failure of the interlayer.

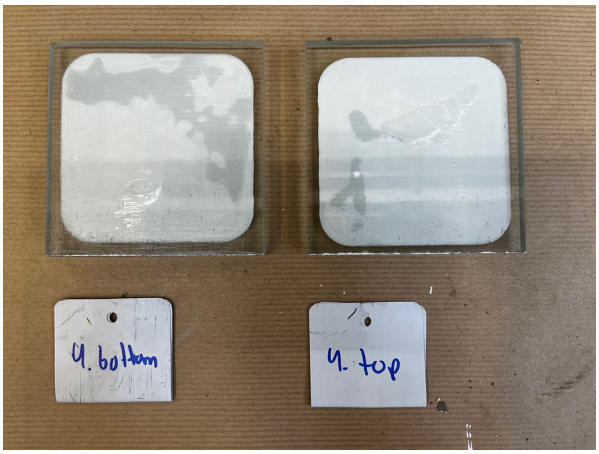

(a) Adhesion pattern on the backside of specimen G5, prior to testing

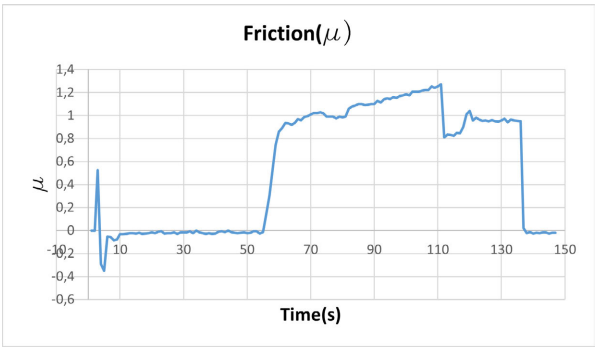

(b) Friction graph of specimen G5

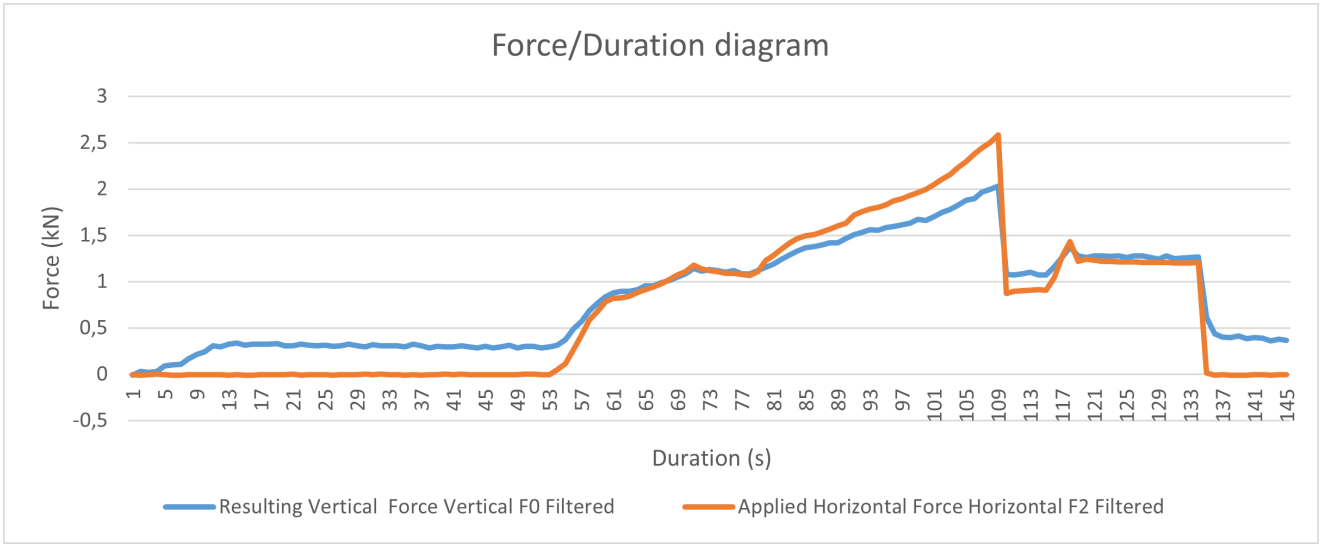

(c) Force/Time graph of specimen G5

Figure A.7: Force diagrams of testing of specimen G5

In the DIC analysis of Dx displacement, the top interlayer can be seen fully debonding from the glass. Once again, a slight rotation into the y-direction emerges between the two plates.

(a) DIC analysis of specimen G5: Dx displacement under 300N normal force

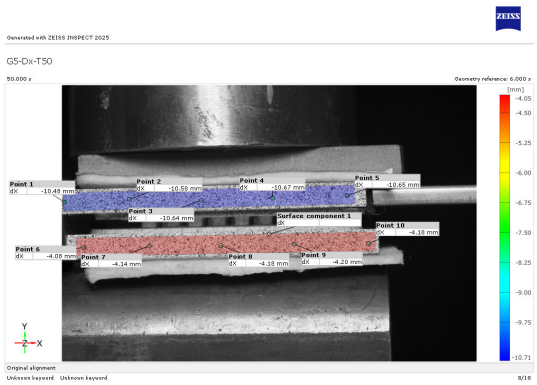

(b) DIC analysis of specimen G5: Dx displacement at moment of delamination

Figure A.8: DIC analysis of specimen G5: Dx displacements

B
Appendix B

B.1 Arduino Sketch

```
#include <math.h>
#include <AccelStepper.h>

// === HEATBLOCK CONFIG ===
const int relayPin = 10;
const int thermistorPin = A2;

const float BETA = 3950;
const float seriesResistor = 100000;
const float nominalResistance = 100000;
const float nominalTemp = 25.0;

const float targetTemp = 250.0;
const float hysteresis = 5.0;
bool heating = false;

unsigned long lastTempRead = 0;
const unsigned long tempInterval = 500;

const int numSamples = 8;
int samples[numSamples];
int sampleIndex = 0;
bool samplesFilled = false;

unsigned long lastPrintTime = 0;
const unsigned long printInterval = 2000;
bool lastReadingWasInvalid = false;

double filteredTemp = 0.0;

```

```
30
31  // === MOTOR CONFIG (A4 as input) ===
32  const int dirPin = 2;
33  const int stepPin = 3;
34  const int analogInPin = A4;
35  int sensorValue = 0;
36  int outputValue = 0;
37  const int maxSpeedValue = 6125;
38
39  #define motorInterfaceType 1
40  AccelStepper myStepper(motorInterfaceType, stepPin, dirPin);
41
42  double readTemperature(int rawADC) {
43    float resistance = seriesResistor * ((1023.0 / rawADC) - 1);  \\ Rth
44    float steinhart = resistance / nominalResistance;             \\
45    steinhart = log(steinhart);
46    steinhart /= BETA;
47    steinhart += 1.0 / (nominalTemp + 273.15);
48    steinhart = 1.0 / steinhart;
49    steinhart -= 273.15;
50    return steinhart;
51  }
52
53  void setup() {
54    Serial.begin(9600);
55
56    // Heatblock
57    pinMode(relayPin, OUTPUT);
58    digitalWrite(relayPin, HIGH); // heater off
59
60    for (int i = 0; i < numSamples; i++) {
61      samples[i] = analogRead(thermistorPin);
```

```
    samples[i] = analogRead(thermistorPin);
  }

  filteredTemp = readTemperature(analogRead(thermistorPin));

  // Stepper
  pinMode(analogInPin, INPUT);
  myStepper.setMaxSpeed(maxSpeedValue);
}

void loop() {
  unsigned long now = millis();

  // === Temperature configuration ===
  if (now - lastTempRead >= tempInterval) {
    lastTempRead = now;

    samples[sampleIndex] = analogRead(thermistorPin);
    sampleIndex = (sampleIndex + 1) % numSamples;
    if (sampleIndex == 0) samplesFilled = true;

    int total = 0;
    int count = samplesFilled ? numSamples : sampleIndex;
    for (int i = 0; i < count; i++) total += samples[i];

    int avgRaw = total / count;
    double newTemp = readTemperature(avgRaw);
    bool validReading = newTemp >= 0.0 && newTemp <= 350.0;

    if (!validReading) {
      if (!lastReadingWasInvalid) {
        Serial.println(">> Ongeldige temperatuurmeting genegeerd.");
```

```
      if (heating) {
        digitalWrite(relayPin, HIGH);
        heating = false;
        Serial.println(">> Heater uitgeschakeld wegens foute meting.");
      }
    }
    lastReadingWasInvalid = true;
  } else {
    lastReadingWasInvalid = false;
    filteredTemp = (filteredTemp * 3.0 + newTemp) / 4.0;
    double temp = filteredTemp;

    if (!heating && temp < targetTemp - hysteresis) {
      digitalWrite(relayPin, LOW);
      heating = true;
    } else if (heating && temp > targetTemp + hysteresis) {
      digitalWrite(relayPin, HIGH);
      heating = false;
    }

    if (now - lastPrintTime >= printInterval) {
      Serial.print("Temp: ");
      Serial.print(temp);
      Serial.print(" °C | Heating: ");
      Serial.print(heating ? "ON" : "OFF");
      lastPrintTime = now;
    }
  }
}
```

```


  // === Steppermotor config via analog input A4 ===
  sensorValue = analogRead(analogInPin);
  sensorValue = constrain(sensorValue, 0, 1023);
  outputValue = map(sensorValue, 0, 1023, 0, maxSpeedValue);
  myStepper.setSpeed(-outputValue); // omkeren indien nodig
  myStepper.runSpeed();



}

```

C

Appendix c

To simulate and set up the robot, offline programming in RoboDK is used. Using this software, an accurate model of the robotarm can be created. The robot arm, workbench, glass block and the casing of the glass block are modelled in Rhino3D and imported into RoboDK as .stl files. The extruder tool used is also modelled, imported and attached to the robot arm in RoboDK. Important here is the Tool Centre Point (TCP), which tells the robot arm what the central point is of the tool it uses, in this case the extruder. Next, the .gcode created with the 5-xis slicer is loaded into RoboDK and the toolpath is placed in the correct location relative to the glass block's shape. Settings and the complete RoboDK workflow will be discussed in Appendix C.

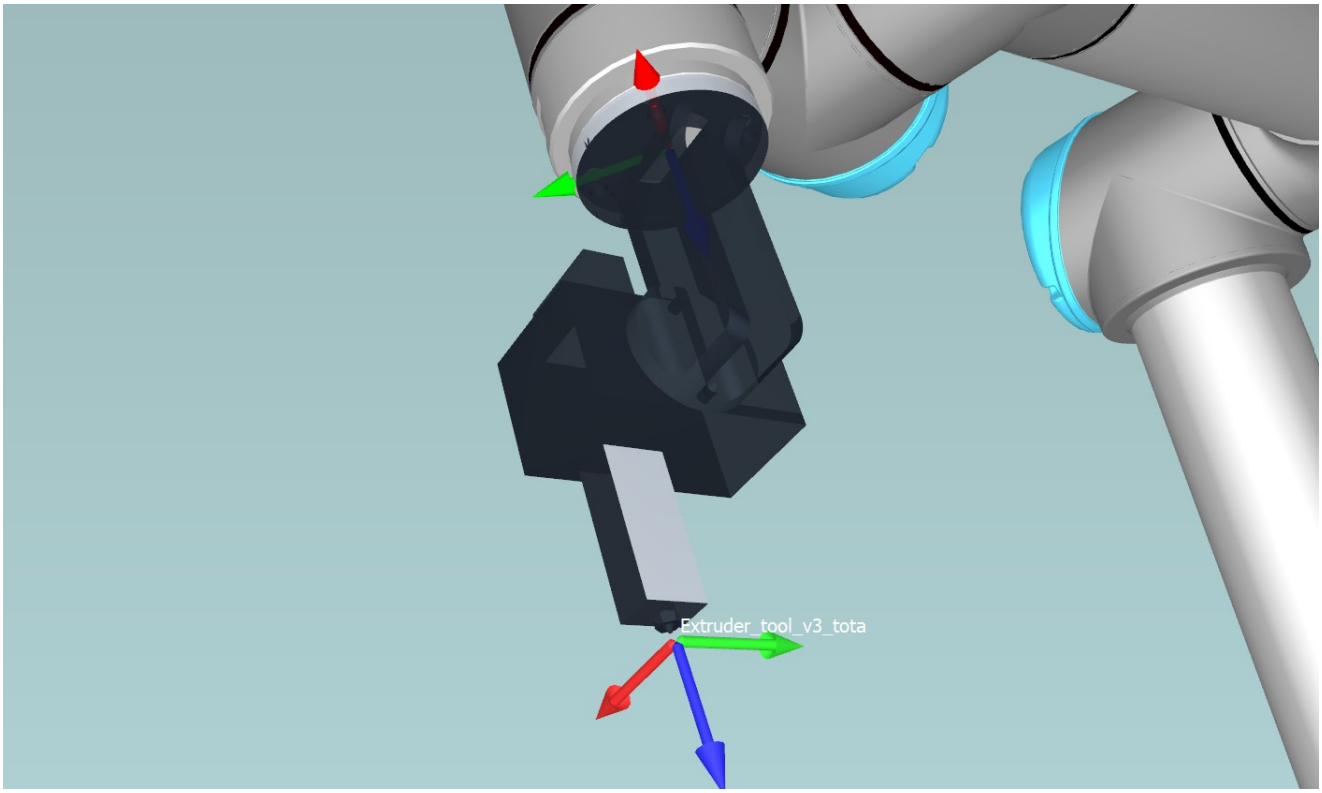

Figure C.1: Modeled Tool

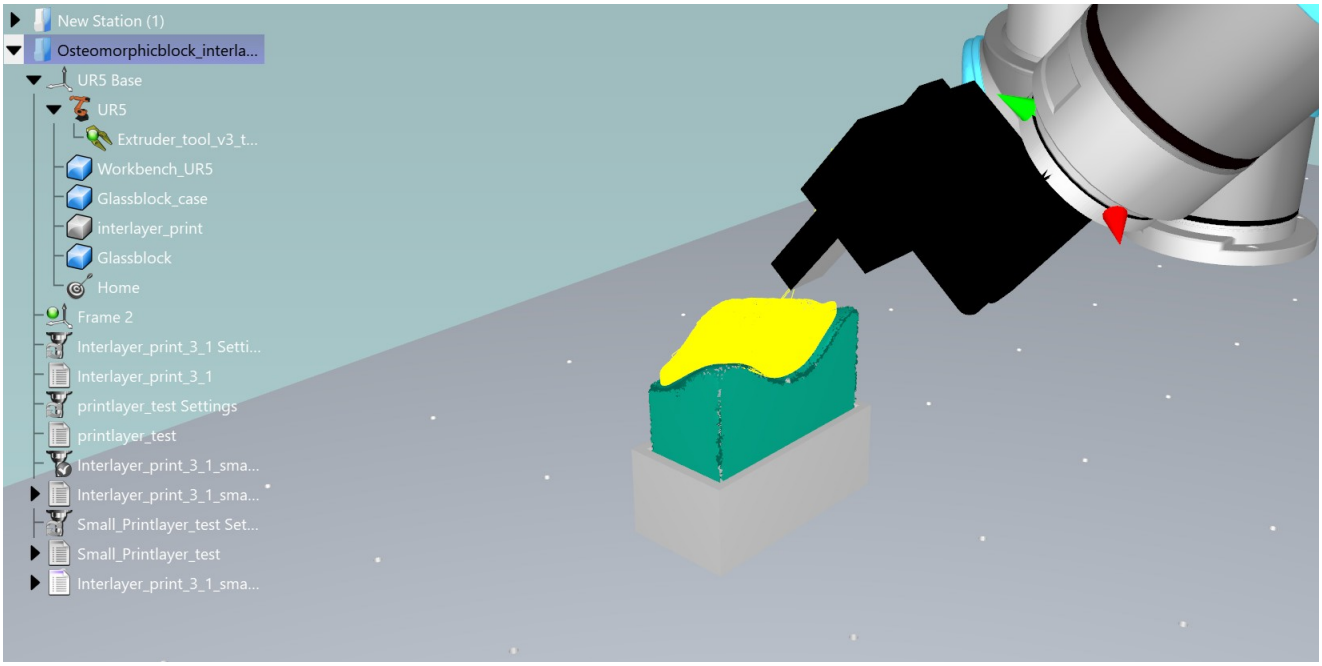

Figure C.2: Workstation modeled with .gcode imported into the correct location

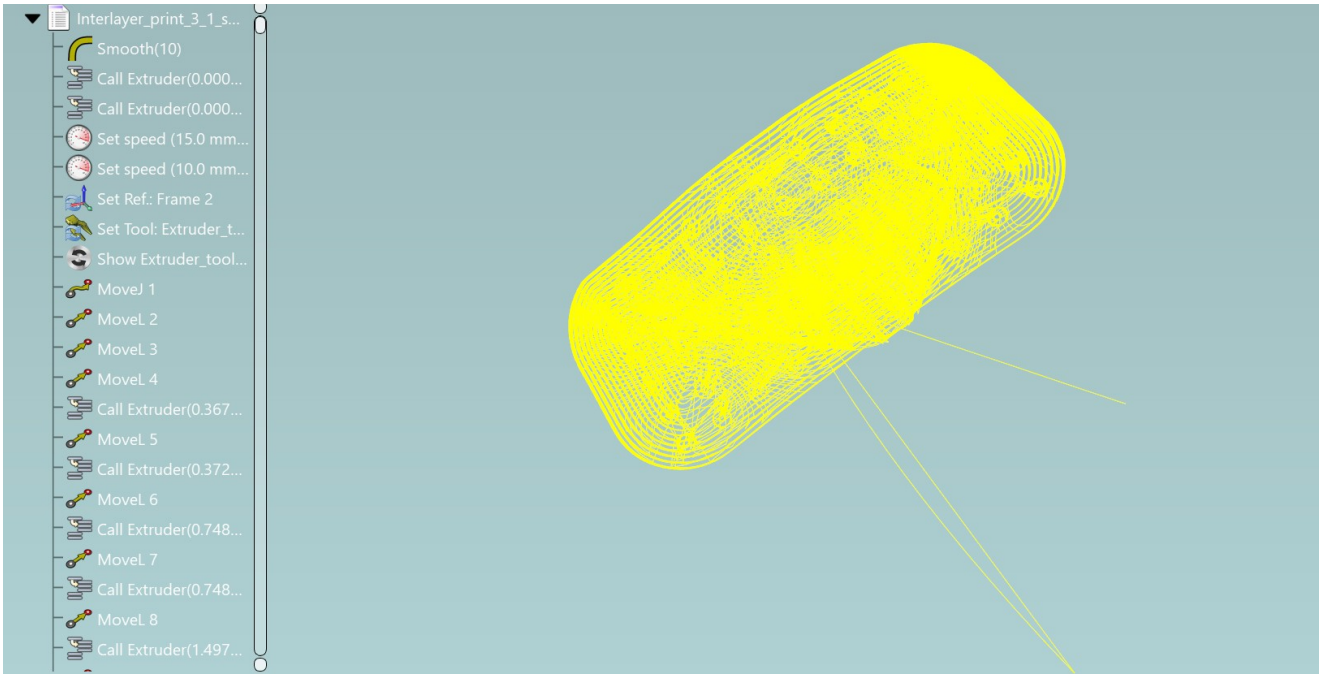

Figure C.3: .gcode imported into the correct location

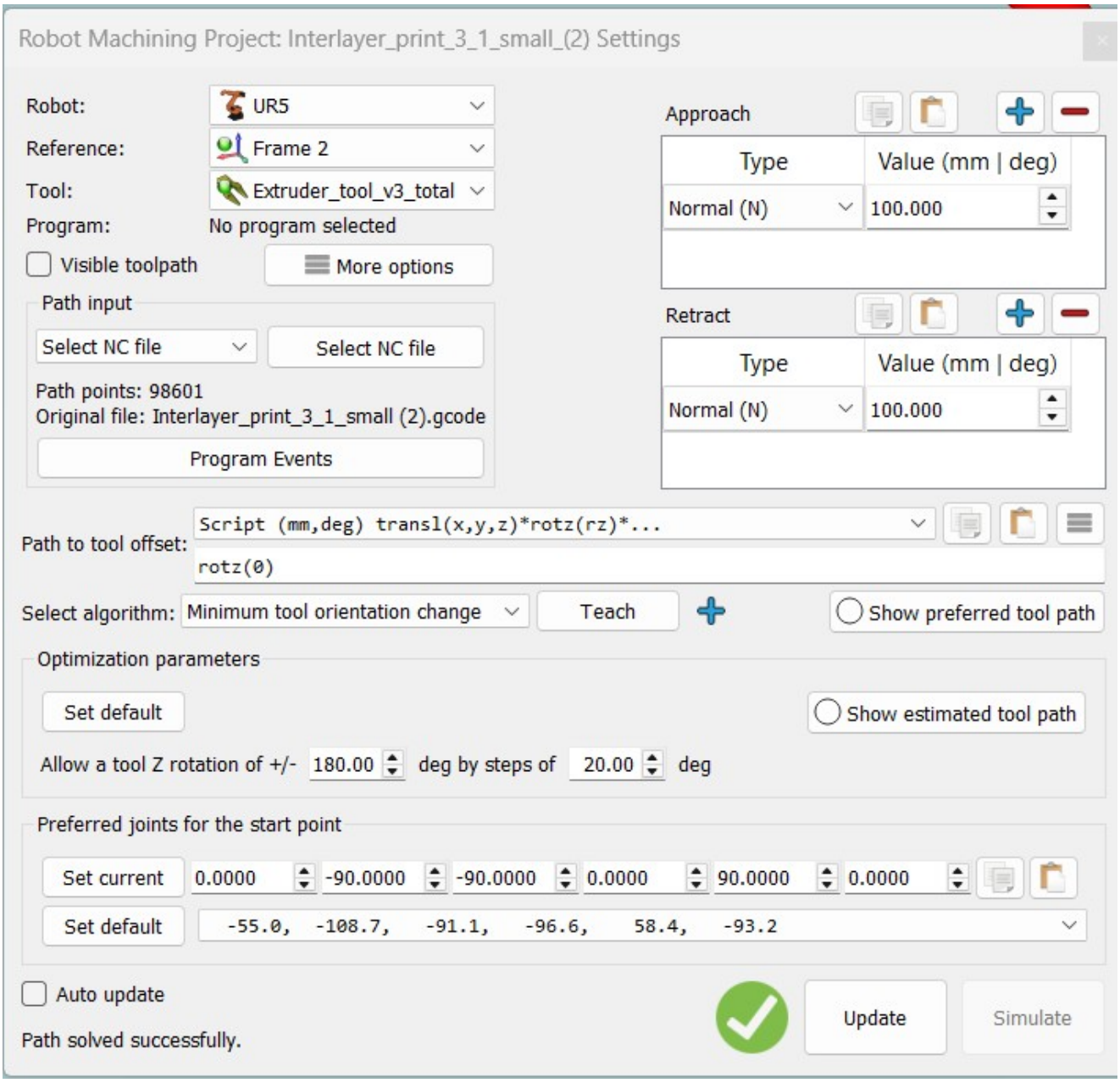

Figure C.4: Settings of the .gcode, click on program events to alter settings

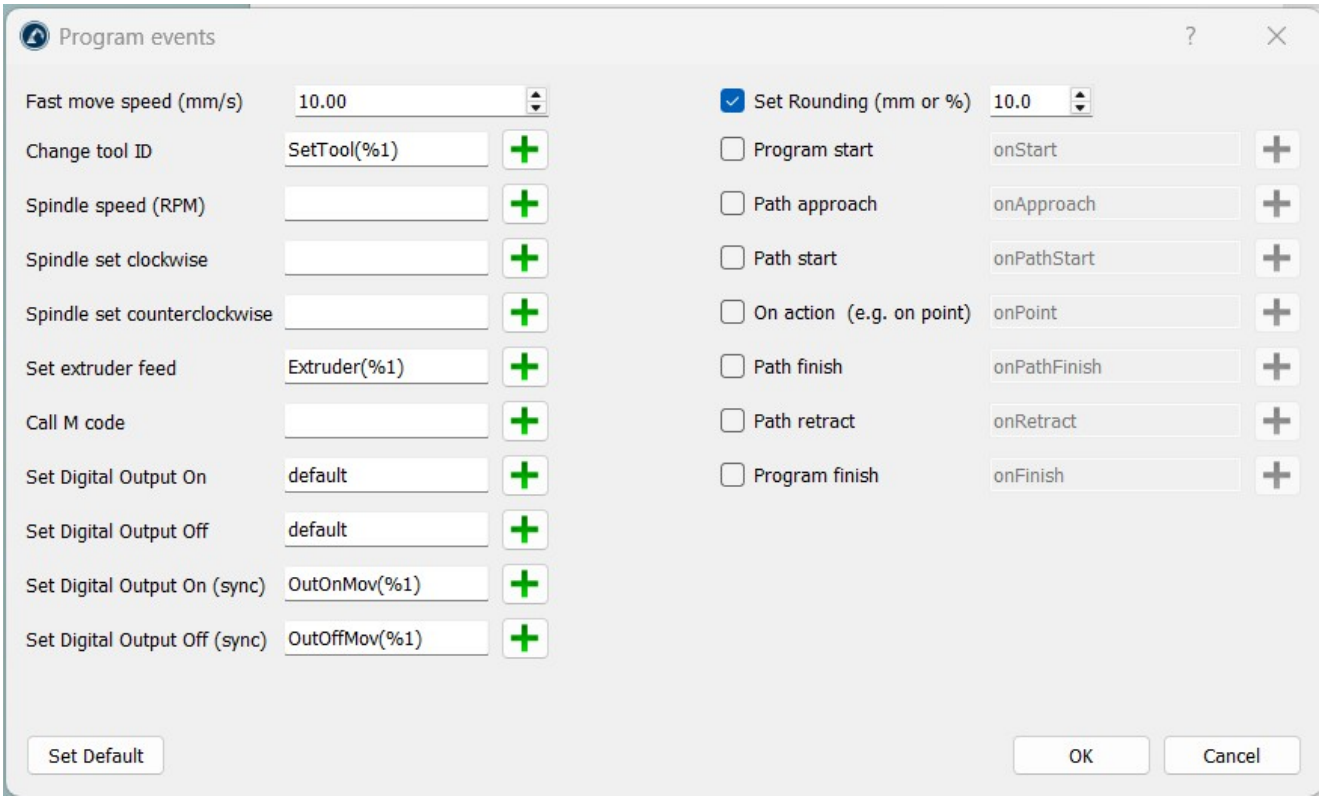

Figure C.5: Program Events of the .gcode, set move speed (mm/s), remove SetRPM(%1), set rounding to at least 1

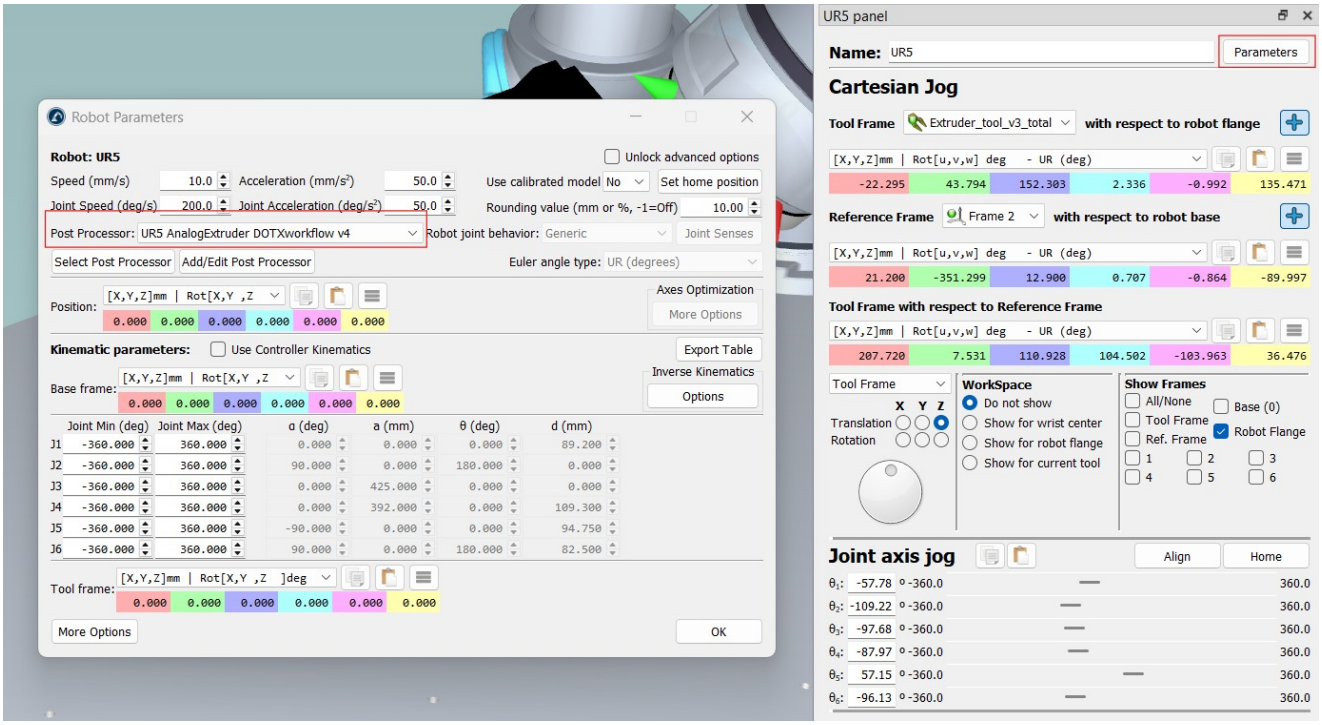

Figure C.6: In parameters on the UR5 robot, set which post-processor will be used

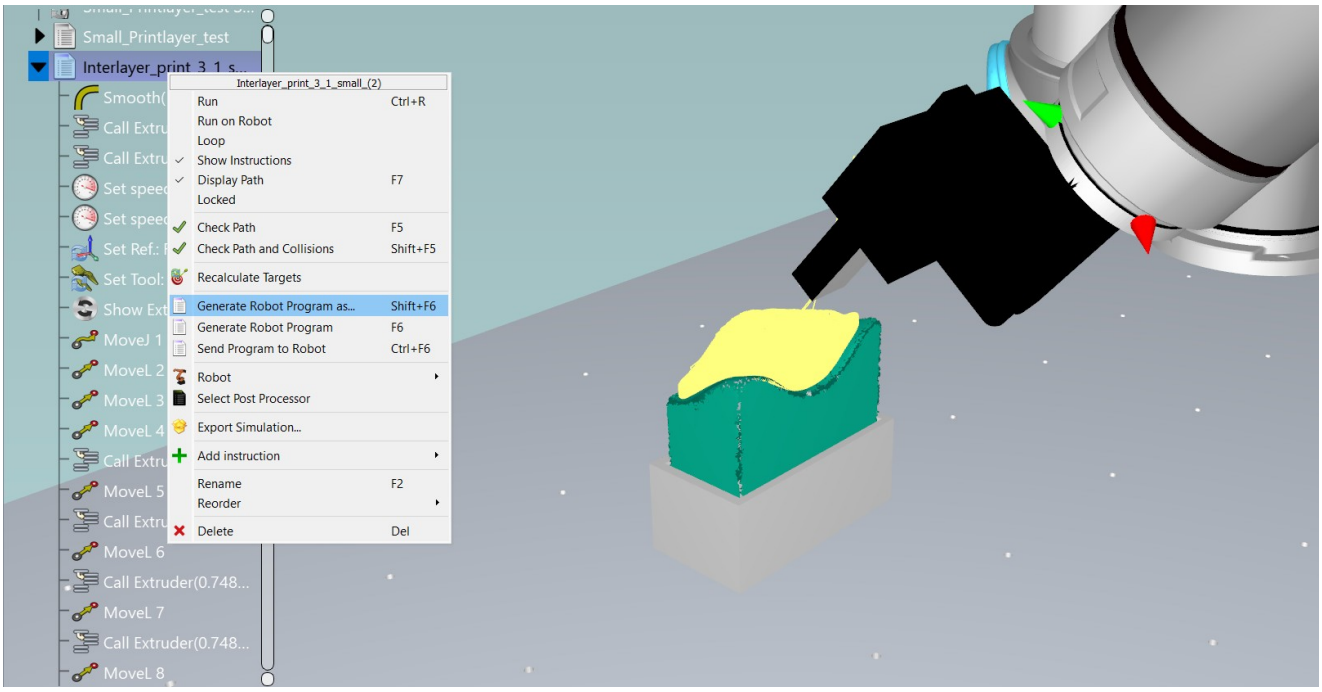

Figure C.7: Export program as.. using the correct post-processor

C: > Users > eloyv > Dropbox > Mijn pc (DESKTOP-E509UAO) > Documents > Master Building Technology > Graduation > P4 > 5 axis slicer > .gcode > Interlayer_setting.script

```
def Interlayer_print_3_1_small_2():
  # Global parameters:
  global speed_ms    = 0.300
  global speed_rads  = 0.750
  global accel_mss   = 3.000
  global accel_radss = 1.200
  global blend_radius_m = 0.001



  # Main program:
  # Program generated by RoboDK v5.9.0 for UR5 on 02/06/2025 15:51:59
  # Using nominal kinematics.
  blend_radius_m = 0.010
  set_standard_analog_out(1, 0.000)
  set_standard_analog_out(1, 0.000)
  speed_ms    = 0.010
  speed_ms    = 0.010
  # set_reference(p[0.021200, -0.351299, 0.012900, 0.012339, -0.015080, -1.570744])
  set_tcp(p[-0.022295, 0.043793, 0.152303, 0.040768, -0.017310, 2.364412])
  # Show Extruder_tool_v3_total
  movej([-0.959900, -1.896597, -1.590724, -1.686843, 1.018541, -1.625870],accel_radss,speed_rads,0,0)
  movep(p[-0.000853, -0.558356, 0.089368, 0.005771, -2.472181, -0.016618],accel_mss,speed_ms,0)
  set_standard_analog_out(1, 0.367)
  movep(p[-0.000925, -0.557056, 0.089444, 0.004998, -2.462949, -0.014149],accel_mss,speed_ms,0.001)
  set_standard_analog_out(1, 0.372)
  movep(p[-0.001158, -0.555765, 0.089648, 0.006661, -2.455857, -0.018639],accel_mss,speed_ms,0.001)
  set_standard_analog_out(1, 0.500)
```

Figure C.8: The exported .script, this script will serve as input for the UR5 robot, this can either be via a USB or for big script directly through an ethernet cable

D
Appendix D

D.1 Planning and Organisation

D.1.1 Timeline

Main tasks	Sub tasks	STATUS	ASSIGNED TO	START DATE	END DATE	DURATION in days	COMMENTS
P2 presentation	Material Selection to see which materials are compatible with 3D printing and/or injection moulding of an interlayer geometry. Print with available materials and order other materials at LAMA which could be compatible.	In Progress	Eloy	01-27	02-09	14	TU holiday incorporated
Mechanical testing of the identified materials when either additive manufactured or injection-moulded to conclude on materials. (compressive strength, creep resistance, UV resistance (thermal expansion?))	Testing of adhesion between the interlayer and the glass component and optimise with various surface treatments.	Not Started		02-10	02-23	14	
Design multiple interlayer and glass component geometries to test and argue on which material/geometry should be 3D printed or injection moulded.	Start computational model to create the geometry of the interface (Grasshopper?)	Not Started		02-24	03-09	14	
Develop the model by designing, printing and testing reversible connection mechanisms. Focus on how it connects to the glass	Develop computational model to create the geometry and create a Finite Element Analysis to optimise the geometry design	Not Started		03-10	03-23	14	
P3 Presentation	Finite Element Analysis (FEA) to optimise the geometry of both the interlayer and glass components for maximum structural efficiency and ease of disassembly.	Not Started		03-24	04-06	14	
Production and mechanical testing of the optimised (and final) interlayer/geometry design to determine their performance under different loading conditions.	Optimise the connection and the shape chosen	Not Started		04-07	04-20	14	
Experimental studies on the long-term behaviour of the interlayer material, including creep, fatigue, and environmental resistance. LCA of the system	Write thesis report	Not Started		04-21	05-04	14	
Design the prototype with the chosen geometries	Write thesis report	Not Started		05-05	05-18	14	
Report and presentation	Write thesis report	Not Started		05-19	06-01	14	
P4 Presentation	Finalize report and presentation	Not Started		06-02	06-15	14	
Print and create the prototype design. Final optimisation and validation testing of the prototype design.	Finalize report and presentation	Not Started		06-16	06-29	14	
P5 Presentation		Not Started		06-30	07-13	14	

Figure D.1: Planning thesis research

E
Appendix E

E.0.1 Stiff Adhesive Connection

Stiff adhesives include epoxies and acrylates; these adhesives boast the highest strength among all adhesive types. However, their rigidity makes them prone to cracking as a result of significant differential movements in the joints. Additionally, they necessitate a regulated environment for proper curing. Except for transparent epoxies and acrylates, these types of joints can compromise the transparency of the assembly.

Atocha Memorial, Madrid

The Atocha Memorial in Madrid is a monument commemorating the victims of the March 2004 attacks in Madrid. A cylindrical wall of borosilicate glass forms an 11 metres high and 9.5 metres diameter enclosure. This structure comprises 15.100 solid cast glass blocks weighing 8.4 kg each (Bellapart, 2007). The round glass blocks are glued together using a transparent acrylic adhesive. The curvature in the wall creates a rigid shell structure of structural glass. To create the curvature in the structure, a block geometry with two opposed concave and convex sides was developed, see figure E.1c. This form allows the irregular curved surface to be created without the use of different geometries. To gain a higher degree of precision, massive blocks of 200 mm x 300 mm x 70 mm were cast in special moulds under pressure. In this way, the tight tolerance requirements of $\pm$1 mm were achieved in order to guarantee a uniform glue thickness. Borosilicate was chosen as a material for the blocks due to its low expansion coefficient (4.3×10^{-6} 1/K). Because the structure must withstand the large temperature fluctuations in Madrid, choosing this material over conventional soda-lime glass reduces the thermal stresses in the blocks by half (Bellapart, 2007).

(a) Scaffolding at site (Göppert et al., 2004)

(b) Sealing the glass wall (Göppert et al., 2004)

(c) Cast glass blocks of the Atocha memorial (Bellapart, 2007)

(d) Distribution of adhesive on the glass blocks (Bellapart, 2007)

Figure E.1: Atocha Memorial, Madrid

The structure of the glass blocks is placed on a perimeter ring designed as a curved U-shaped profile of steel S355. To mitigate the shear forces between the steel ring and the glass structure due to thermal expansion differences, the glass blocks were placed onto 200 elastomer pads, each measuring 160 mm by 100 mm by 45 mm. These pads also help accommodate deflections in the post-tensioned concrete flooring, which could create high shear forces. The glue applied to bond the bricks required the construction to be built inside a tent which protected the construction side from the radiation of the sun, pollution, and rain water. The adhesive layer had an average thickness of 2 mm, allowing the absorbing of tolerances of the glass bricks while also providing enough structural strength. To make sure enough, but not too much, bonding area was utilised, tests were performed, and a final distribution of twelve chunks of glue per block was chosen. These chunks had different diameters, which minimised both overflow and air bubbles when the glue was splashed by the next brick. Figure E.1d shows the aluminium

template used to evenly distribute the glue on the glass bricks. After gluing the bricks, the glue was cured in 4 minutes by exposure to UVA radiation with a wavelength of 320 - 380 nm and an intensity of 15 and 30 mW / cm^2. After curing, the horizontal and vertical joints were sealed with ultra-transparent silicon to protect the adhesive from weathering and pollution (see Figure E.1b).

Atocha Memorial	
Unit	Concave/convex shaped cast glass
Material	Borosolicate
Interlayer	Stiff adhesive (Transparent acrylic adhesive)
Reason for interlayer	High strength and transparent
Reversibility	No
Structure	Self-supporting
Transparency	Medium

Table E.1: Joinery system Atocha Memorial